Theses and dissertations

1-1-2005

Experimental study on static response of prefabricated concrete bulb-tee bridge girder flange-to-flange connections

Siyin Tu
Ryerson University

Recommended Citation

EXPERIMENTAL STUDY ON STATIC RESPONSE OF PREFABRICATED CONCRETE BULB-TEE BRIDGE GIRDER FLANGE-TO-FLANGE CONNECTIONS

By

Siyin Tu

B.S. Civil, Chongqing University, China, 1992

A thesis

presented to Ryerson University

in partial fulfillment of the

requirements for the degree of

Master of Applied Science

in

Civil Engineering

Toronto, Ontario, Canada, 2005

© Siyin Tu, 2005

UMI Number: EC53770

INFORMATION TO USERS

The quality of this reproduction is dependent upon the quality of the copy submitted. Broken or indistinct print, colored or poor quality illustrations and photographs, print bleed-through, substandard margins, and improper alignment can adversely affect reproduction.

In the unlikely event that the author did not send a complete manuscript and there are missing pages, these will be noted. Also, if unauthorized copyright material had to be removed, a note will indicate the deletion.

UMI®

AUTHOR'S DECLARATION

I hereby declare that I am the sole author of this thesis.

I authorize Ryerson University to lend this thesis to other institutes or individuals for the purpose of scholarly research.

Author's signature: _   _____ Date: _____30/09/2005_____

The author authorizes Ryerson University to reproduce this thesis by photocopying or by other means, in total or in part, at a request of other institutions or individuals for the purpose of scholarly research.

Author's signature: _   _____ Date: _____30/09/2005_____

BORROWERS

Borrowers undertake to give proper credit for any use made of the thesis. Ryerson University requires the signatures of all persons using or photocopying this thesis. Please sign below and give address and date.

Name	Signature of Borrower	Address	Date

EXPERIMENTAL STUDY ON STATIC RESPONSE OF PREFABRICATED CONCRETE BULB-TEE BRIDGE GIRDER FLANGE-TO-FLANGE CONNECTIONS

By

Siyin Tu

Master of Applied Science in Civil Engineering
Department of Civil Engineering
Ryerson University
Toronto, Ontario, Canada,
September 2005

ABSTRACT

Prefabricated concrete Deck Bulb-Tee (DBT) bridge girder system requires precast girder

flanges to be connected and formed bridge deck at site. In this study, a new bridge deck

slab flange-to-flange connection system for precast DBT girders has been investigated.

Two types of moment transferring connection and another two types of intermittent bolted

connection were developed. A total of four full-scale bridge DBT girders for the developed

connection details were fabricated and then tested to collapse under simulated wheel load.

This thesis reports on an experimental study on static behavior and ultimate load carrying

capacity of bridge Deck Bulb-Tee girders jointed with proposed connection detail and

technology. Structural behavior, including stress and strain, crack formation and

propagation, deflection, failure mode, and ultimate load capacity, has been identified. Experimental results are compared to those obtained using the Yield-Line Theory and the available Punching Shear Equations.

ACKNOWLEDGEMENTS

TO MY FAMILY

TABLE OF CONTENTS

LIST OF TABLES

LIST OF FIGURES

LIST OF ABBREVIATIONS

AASHTO	American Association of State Highway Transportation Officials Specification
ACI	American Concrete Institute
ATC	Applied Technology Council
CHBDC 2000	Canadian Highway Bridge Design Code, 2000
CMA	Compressive Membrane Action
CPCI	Canadian Precast Concrete Institute
CSA	Canadian Standard Association
DBT	Deck-Bulb-Tee
IBC	Intermittent Bolted Connection
LVDT	Linear Variable Displacement Transducer
MCVT	Monotonic Concentric Vertical Loading Test
MSA	Maximum Size of Aggregate
MTC	Moment Transferring Connection
OHBDC	Ontario Highway Bridge Design Code
PCI	Precast Concrete Institute
SIP	Stay-In-Place
SP	Superplasticizer
STBC	Shear Transferring Bolted Connection
STC	Shear Transferring Connection
TCS	Test Control Software
W/C	Water-to-Cement Ratio

LIST OF SYMBOLS

a Depth of Equivalent Rectangular Stress Block

A_s Area of Non-Prestressed Tension Reinforcement

b_0 The Perimeter of The Critical Section for Slabs and Footing

$\bar{b}_0$ The Perimeter of The Critical Section for Slabs and Footing

b_1 Short Side of Concentrated Load or Reaction Area

b_2 Long Side of Concentrated Load or Reaction Area

c/c   Center to Center Distance

d Average Effective Depth of Section

$\bar{d}$ Effective Depth of Section

E Modulus of Elasticity

f'_c Average Compressive Strength of Concrete

$\bar{f'_c}$ Specified Compressive Strength of Concrete

f_{cr} The Cracking Strength of Concrete

f_t Diagonal Tensile Strength of Concrete

f_y Specified Yield Strength of Reinforcement

h The Thickness of The Deck Slab

l Distance between Two Supports

M_n Nominal Moment of Resistance of the Section

M_u Positive Moment Capacity of Section

P_u Ultimate Concentrated Load Capacity

V_c Punching-Shear Capacity

$\bar{V}_c$ Punching-Shear Capacity

V_r Factored Shear Resistance

β_c Ratio of Short Side to Long Side of Concentrated Load or Reaction Area

θ Acute Angle between the Horizontal and Assumed Failure Plane

ϕ_c The Resistance Factor for Concrete

α_1 Constant

Chapter 1

Introduction

1.1 General

In North America, road closures or traffic reductions due to maintenance of the bridge infrastructures is of major concern. According to recent survey on the status of Canada transportation infrastructure, a significant number of bridges require rehabilitation or replacement. As a result, increased emphasis is being placed on improving work zone safety and minimizing traffic disruption, while maintaining construction and reducing life-cycle costs and environment impact.

The current practice of bridge construction and maintenance is to use pre-fabricated girders with cast-in-place concrete deck, which takes a relatively long time to open the bridge to traffic. However, a complete prefabricated bridge system and connection technology needs to be investigated for bridge construction and rehabilitation that yields substantial economic and environment benefits.

1.2 The Problem

The aging highway bridge infrastructure in North American is being subject to increasing traffic volumes and must be continuously renewed while maintaining traffic flow. The traveling public is demanding that this rehabilitation and replacement be done more quickly to reduce congestion and improve safety. Conventionally, bridge reconstruction is typically

on the critical path because of the sequential, labor-intensive processes of completing the foundation, the substructure, the superstructure components (girders and decks), the railings and other accessories. Prefabricated bridge elements and systems will allow components to be precast off-site and shipped to the site for quick assembly while maintaining traffic flow. Depending on the specific site conditions, the use of prefabricated bridge systems can minimize disruption to the environment, improve constructibility, increase quality, and lower life-cycle costs.

Prefabricated bridge systems made of Deck-Bulb Tee (DBT) girders is the most attractive choice for bridge replacement. Figure 1.1 shows the proposed cross-section view of this bridge girder system with moment-transferring-connections (MTC). While, Figure 1.2 shows the proposed cross-section view of this bridge girder system with intermittent-bolted-connections (IBC). In these systems, the concrete deck slab is cast with the prestressed girder in a controlled environment at the fabrication facility and then shipped to the site for assembly. This technology is applicable and needed for both existing and new bridge construction.

This system requires that the longitudinal deck joints be provided to make it continuous for live load distribution. The longitudinal deck joints, which provide to make the deck continuous for integrity in this system, must be designed to distribute live loads laterally without distortion. Currently, the Canadian Highway Bridge Design Code, CHBDC (2000), as well as other North American bridges codes, does not provide any guidance or specification for the design of the prefabricated concrete girder/deck connections. Also, there is no information available in the literature to design such connections. Moreover,

there are no test data available to give confidence to the designer of such connections. As a result, failure modes of these prototypes of connections as well as the ultimate load capacity and fatigue behavior are not yet available.

1.3 Objectives

The Objectives of this study are:

1. To investigate and develop bridge deck connections for precast/prestressed Deck-Bulb-Tee (DBT) bridge girders. To provide continuous connection for live load distribution. The types of connections are designed in the forms of moment transferring and intermittent bolted connections.

2. To provide experimental data up-to-complete collapse on full-scale bridge connection system subjected to static loading. This includes identifying the failure mode, crack formation and propagation, deflection, ultimate load capacity.

In this thesis, a detail experimental study on the static behavior of Deck-Bulb-Tee (DBT) girder connections is presented. Results from four full-scale bridge models, two of which are moment-transferring connections and other two are intermittent-bolted connections, are reported. The key parameters considered herein are:

1. Type of connections
2. Dimension of the joints
3. Details of the reinforcement, and
4. Loading conditions.

3

1.4 Scope

The scope of this study includes the following:

1. A literature review of the experimental and theoretical research work on prefabricated bridge systems and joints, theoretical calculation for punching shear and ultimate load carrying capacity of slabs using Yield-Line theory.

2. Development of moment-transferring and intermittent-bolted connections.

3. Experimental study on four full-scale bridge deck connection models simulating the developed connections.

4. Correlation between the experimental findings and the theoretical study.

1.5 Contents and Arrangement of the Study

Chapter 2 presents the literature review on precast/prestressed concrete bridge deck connection technology as well as recent practice in North American. In chapter 3, two types of Deck-Bulb-T girder connection are proposed. Chapter 4 reports the whole experimental program on four full-scale bridge deck connection models, including specimen design, materials preparation, construction, instrumentation, test set-up, test control and data recording. In chapter 5, testing results are discussed and theory analysis is conducted. Chapter 6 concludes the significant findings of this study and the recommendations for further research.

Chapter 2

Literature Review

2.1 General

Prefabricated girders have been extensively used in highway bridges. The most frequently used elements are the precast/prestressed concrete I-beams and box beams. In prefabricated girder systems, especially in the parking garages, it is a common practice to use evenly spaced mechanical flange-to-flange connectors to join adjacent girders. These mechanical connectors serve to align the flanges in the out of-plane direction. But most important, they must resist multiple types of diaphragms forces. While millions of mechanical flange connectors are used each year, very little test information exists on how to design these connectors. Most connectors have been developed through field experience by individual precast manufacturers without standard test methods to determine the strength and deformation capacity. Some researchers worked in the development of connectors in precast units for building and parking garages. However, very few researchers worked on developing connections for the precast/prestressed bridge girders.

2.2 Prefabricated T-Beam Bridges

The involvement of the prefabrication industry in bridge construction consists primarily of providing some factory-produced elements. Through mass production of the material and reduction of on-site construction time, economic benefits are most often achieved.

Prefabricated elements commonly produced are prestressed concrete piles, I-beams, box beams, channels, hollow and solid slabs, deck panels, steel I-beams and box beams.

Various forms of precast/prestressed T-beams have evolved over the past decades to build short-span bridges (Curtis, 1967; Kwei, 1967). These include contiguously placed single-T, double-T, and multiple-T sections and are suitable for bridges in the span range of 6 to 24 m. However, some single-T bridge section can span up to 36 m. These precast sections are produced in standard widths of 1.2, 1.8 and 2.4 m. The fully precast beams are transported to the site and erected adjacent to each. V-joint between the edges of their flanges are filled with non-shrink mortor grout and are transversely post-tensioned to provide for lateral resistance and continuity for load transfer (Shahaway, 1990; Arokiasamy et al., 1992). Other means of shear transfer can be achieved through the use of grouted keyways, transverse tie rods, or weld plates (Sprinkel, 1985). Some of these beams have projecting web reinforcement that is embedded in the cast-in-place slab to develop the composite action for live load. Others may be fabricated for use with or without concrete topping (Sprinkel, 1985).

For increased span capacities, the Concrete Technology Corporation developed the bulb-T series in 1959, having a 1.2 m wide flange and several standard depths. Arthur Anderson improved this design in 1969, developing the innovative deck bulb-T series with large standard flange widths of 1.5 m and 3.0 m, each with several standard depths from 700 to 1900 mm, with span capacities up to 57 m (Anderson, 1957, 1972, 1973). Placed contiguously, these girders provide a ready-make deck, eliminating the need for a closely cast-in-place deck. Anderson also developed the Washington series 14-bulb-T, which were

standardized with some modifications in 1988 as the AASHTO-PCI bulb-T Series (Geren and Tadros, 1994).

Roller et al. (1995) have presented the results of testing a 21 m long, 1.35 m deep pretensioned high strength concrete Bulb–Tee girder having a 3 m top flange. The results showed that this girder has withstood more than 5 million cycles of fatigue loading and satisfied all serviceability requirements.

2.3 Prefabricated Bridge Deck Systems

2.3.1 Partial Depth Bridge Deck Panel System

Partial depth prefabricated deck panels act as stay-in-place forms and not only allow more controlled fabrication than fully cast-in-place decks, but also could increase the strength of the finished bridge owing to the use of pretsressed panels. This bridge deck system is shown in Figure 2.1. When panels are used, the bottom layer of the reinforcement in both transversal and longitudinal directions that is present in a conventional cast-in-place, full depth, reinforced concrete bridge deck is eliminated.

Few authors dealt with the composite action between girders and bridge deck with precast panels. Burns and Centennial (2001) carried out a full 200 mm thick precast, normal weight concrete deck and the other two specimens used 100 mm thick cast-in-place, lightweight concrete deck panels with 100 mm thick cast-in-place, normal weight concrete deck. The load deflection curves and strength for each pair of specimens are almost identical. Strain gauges placed across the width of the slab showed that the full width of the slab was effective in both cases. Based on the test results, full composite action, with the use of

precast/prestressed concrete panels, can be assumed for both service load and strength calculations.

Abendroth (1995) experimentally investigated the nominal flexure and shear strength of composite slab system with precast/prestressed concrete panels as subdeck in bridge construction. Five full-scale models of composite slab specimens were constructed and tested. Experimental results were compared with analytical results using the yield line theory and punching shear equation and concluded that full-composite behavior was maintained between the reinforced concrete topping and the precast concrete panel and punching shear mode of failure governed the nominal strength of the slabs.

2.3.2 Full Depth Bridge Deck Panel System

To rehabilitate the decks of heavily traveled bridges, full depth prestressed concrete panels are placed transversely on the supporting girders and post-tensioned longitudinally. Full depth bridge deck system is shown in Figure 2.2. Portions of a deteriorated deck can be removed during night operations and the full depth panels installed in time to open the structure to morning traffic. Other deck systems offer similar rapid construction methods with the advantages of reduced dead load and enhanced durability.

Yamane et al. (1998) developed new full depth precast prestressed concrete bridge deck panel system. The newly developed system includes stemmed precast panels, transverse grouted joints, longitudinal post-tensioning and welded threaded and headless studs. A finite element analysis was carried out to find out stresses in the deck panel and compare these stresses with experimental values. They constructed full-scale prototype of the

proposed precast panel system and tested under fatigue and ultimate loading. They concluded that the performance of the proposed system meets all the structural requirements for bridge decks and comparable to exodermic bridge deck system in weight and much less expensive. An exodermic bridge deck consists of a fabricated steel grid for the bottom portion and a reinforced concrete slab for the top portion. A part of the steel portion extends upward into the reinforced concrete in order to achieve a composite deck. Punching shear, rather than flexure, was the mode of failure for the proposed system.

In 1999, 1301.12 m² of deteriorating bridge deck of Route 7 over 50 bridges in Fairfax County, Virginia, USA, required replacement [McKeel (2002)]. Virginia's DOT opted to use full-depth prefabricated concrete deck panels to satisfy community concerns with respect to reduction in the level of service. Operating only at night, work crews saw cut sections of the existing deck, lifted and removed them by crane, and immediately installed new deck panels that matched the deck cavity. A rapid-setting concrete overlay was then placed, and after only 3 hours the bridge was able to support full traffic. The bridge was completely open to traffic during the day.

In 2001, Route 29 over Sugar Creek in Illinois required the re-decking of an existing 77.13 m-long, 11.4 m-wide five-span bridge [McKeel (2002)]. The existing steel beams were reused and made composite with the prefabricated deck panels. A total of 29 panels were laid across the length of the bridge. The panels were connected by shear keys and post-tensioned longitudinal, traffic delays were minimized as a result of the speeding up of the construction time.

Tadros et al. (2002) studied the behavior of debonded shear key system for girder and full depth deck connections. The system has the advantage of facilitating future deck removal, while protecting the top flange of the girder from damage, which is particularly significant for bridges in cold climates where deck concrete is subjected to deterioration due to freeze-thaw cycles and deicing chemicals.

2.4 Prefabricated Girder Connections

The PCI committee on connection details (1995, 1998) published typical details and its design method for standard connections for precast/prestressed concrete Double-Tee girders (see Figure 2.3). The connection included longitudinal and transversal joints. The criteria for the connection designs are strength, ductility, volume change accommodation, durability, fire resistance, constructability, aesthetics, and seismic requirement. The flange-to-flange double-tee connection is made of an inclined steel plate anchored to the concrete flange using a special shape steel rod. This connection transfers the shear through welding of plates with a rod. Also, same details were presented in Applied Technology Council Report ATC-8 (1981) for T-beam flange connection with some modifications.

This report discussed some connection details for prefabricated concrete building element connections to resist earthquake loading. In one of these details, rebar hooks extend from each panel and are connected with longitudinal rebars and the joints filled with cast-in-place concrete. Other detail shows an intermittent connection for floor panel, consisting of a steel plate embedded in the panel at intervals and welded together with a connecting rod. The report present a limited slip bolted connection for concrete floor panels. This

10

connection consists of box embedded in the concrete panels at intermediate location and connected together with slotted plate and bolts, which permit some allowance for the slip.

Pincheira et al. (1998) carried out pilot series of tests on double-tee flange-to-flange connector to examine its strength and deformation capacity when subjected to multi-axial and cyclic loading. The connector consisted of a steel plate with filet-welded reinforcing bars embedded in 50 mm thick concrete slab, which was very similar to the PCI standard details [The PCI committee on connection details (1995,1998)] and the one presented in ATC-8 report [Applied Technology Council, 1981]. They observed moderate to high levels of deformation ductility under monotonic loading, while the deformation capacity and ductility of the connector were limited under cyclic loading.

Arockiasany et al. (1991) studied fatigue strength of joints in a precast/prestressed concrete double-tee bridge. 1:3.5 scale model of a two span, transversely and longitudinally post-tensioned, continuous double-tee system was tested in static and fatigue loading. Constant amplitude fatigue loading was applied on the model at typical locations simulating HS20-44 AASHTO (1998) truck loading. Structural integrity of the bridge system was checked and experimental deflection of the system was compared with finite element analysis results. The ultimate load, computed from plastic analysis, was found to be in good agreement with the measured value. Researchers concluded that double-tee bridge system, assembled with post-tensioning in both the longitudinal and transverse directions, shows monolithic behavior under both static and fatigue loading. Bridge system was maintaining its structural integrity after 8 million cycles.

Hariatmadar (1997) studied seismic response of connection in precast concrete double-tee girders. He constructed 35 specimens of 5 types of connections and tested under monotonically increasing shear force, reversed cyclic shear and axial forces until failure using displacement control. Connections consist of angle welded with either anchor bars or headed studs or combination of both. He also developed design interaction curves and associated equation for each connection type and developed practice-oriented method to determine the connection strength under shear and axial forces and combination of these forces at joint between elements in precast system.

Hofheins et al. (2002) studied behavior of welded plate connections in precast concrete panels under simulated loads. Ten precast concrete wall panel assemblies were tested under in-plane lateral cyclic-loading for loose-plate connection located in the vertical joint between panels. Shear loads were transmitted through the embedded plate to the surrounding concrete by three mechanisms, namely: (1) friction between the embedded plate and concrete; (2) bearing of the end of the embedded plate on the concrete; and (3) interaction between studs and concrete. Tests were performed by applying a quasi-static cyclic load to three precast hollow-core wall panels connected together with two loose-plate connectors at each vertical joint. Each loading step consisted of three cyclic load increments to simulate the effect of an earthquake. They concluded that loose-plate connection can resist relatively high shear forces, the connection fails in a brittle manner when the deformed anchor bars tear free from the embedded angles, the connection is not suitable for the high seismic region, if it should be designed to remain elastic, and connection should be modified to make it ductile by providing more surface area for concrete bearing.

Bakht and Mufti (2001) carried out two field tests on shear connected plank bridges using welded shear key. After testing these bridges, they developed a reliable and rigorous method of analysis of shear forces in the welded shear key. Based on this method, they developed simplified graphical method to rapidly predict the maximum transverse shear forces in the shear keys of any of the bridges under consideration. Load distribution in shear-connected concrete plank bridges were also presented in their study. The main purpose of the testing was to determine the suitability of various methods of bridge analysis. They carried out two field tests and concluded that the articulated plate method is suitable for analyzing the bridges under consideration, but only after longitudinal torsion rigidity of the planks is reduced suitably to account for the lack of torsion resistant at their ends.

Shah, B., (2004) reported on an experimental investigation on the behavior and ultimate load carrying capacity of bridge deck slab connections between adjacent precast girders for new prefabricated bridges. In his study, three types of moment transferring connections and two types of intermittent bolted connections were developed. A total of eight experimental tests were conducted for different connection details and simulated wheel load locations. A correlation between the theoretical ultimate load capacity obtained using the Yield Line theory and the available punching shear capacity equations, and the experimental findings was achieved.

2.5 Arching Action and Punching Shear in Bridge Deck Slabs

An un-cracked bridge deck resists traffic loads primarily through one-way flexure. Before flexure cracking occur, in-plane forces remain in significant. After the deck is significantly cracked, however, it resists traffic loads through arching action, behaving like a flat dome.

Arching action is defined by a zone of membrane compression radiating out from the point of load and surrounding zone of equilibrium circumferential tension.

Bakht (1996) and Bakht and Mufti (1996) carried out research in arching action in bridge deck slabs. The compressive membrane forces increase the flexure capacity of the bridge deck; they exist even if supports are restraint, although their distribution is influenced by the degree of edge restraint. Bakht and Lam (2000) studied the behavior of transverse confining systems for steel-free deck system. Increase in flexure capacity due to arching action is the basis for the isotropically reinforced, Ontario-type bridge deck, which uses much less reinforcing steel than would be required in a traditional deck designed by procedures of the AASHTO (1998) specification. The Canadian Highway Bridge Design Code (CHBDC) 2000 considers the effect of compressive membrane action provided that certain boundary condition exists and the slab thickness is adequate. It provides empirical design of reinforced concrete decks, with four layer of isotropic reinforcement.

The arching action cannot resist the full wheel load. There remains a small flexure component for which the minimum amount of isotropic reinforcement is more than adequate. The reinforcing steel in the bridge deck slab has dual purpose, it provides for both local flexure resistance and global confinement required to develop arching effects.

Hewitt and Bachelor (1975) and Fang et al. (1990) carried out extensive finite-element analysis to verify the design of reinforced concrete decks using the concepts of internal arching action. Mufti et al. (1993) and Newhook and Mufti (1996) investigated the behavior of bridge deck without reinforcing steel.

Khanna et al. (2000) studied the role of steel reinforcement in conventionally reinforced deck slabs of girder bridges. A full-scale model was constructed in four segments. Segment A contained isotropic steel reinforcement in two layers, conforming to the requirements of the OHBDC (1992). Segment B contained only the bottom layer of steel reinforcement. Segment C contained only the bottom transverse steel bars. Segment D contained only bottom transverse glass fiber reinforced polymer (GFRP) bars having the same axial stiffness, but 8.6 times the axial tensile strength, as those of the steel bars in segment C. Each segment of the deck slab was tested to failure under a central concentrated load, simulating the dual tire footprint of 250 mm × 250 mm dimension of the typical commercial vehicle. They concluded that (i) only the bottom transverse reinforcement influences the load carrying capacity of a reinforced concrete deck slab, and (ii) the stiffness of the bottom transverse reinforcement, rather than its strength, is of paramount importance.

The enhancement of flexure strength of a deck slab in slab-girder-type bridge, which is due to in-plane compressive strength resulting from the lateral restraint provided by the girders, has been presented by Braestrap and Morley (1980). The improved flexure capacity of the deck slab due to arching action or compressive membrane action (CMA), the mode of failure of deck slab in a slab-girder bridge of conventional design is expected to be a

punching shear type failure. Azad et al. (1994) carried out studies on punching shear of the deck slab. They carried out experimental tests on 12 panels supported on the steel girder to find punching shear capacity and compared with three different approaches:

1) The American Concrete Institute (ACI) (2002) formula for the computation of shear strength of a slab under two-way action;

2) The plasticity based approach of Jiang and Shen (1986), and;

3) Finite Element Model.

Jiang and Shen's model is a plasticity based failure model proposed to determine the punching capacity for the axi-symmertic plain concrete slab using parabolic Mohr-Coulomb failure criteria and also proposed simplified formula to compute the punching shear of plain concrete slab, by taking the yield line to be straight, as follow (with change of notations);

$$P = 0.074 f_c' sh \dots\dots\dots\dots\dots\dots\dots\dots\dots\dots\dots\dots\dots\dots\dots\dots\dots(2.1)$$

Where:

$P =$ Punching shear capacity, N

$f_c' =$ Compressive strength of concrete, MPa

$h =$ The thickness of the slab, mm

$s = \pi(d_0 + h)$, with d_0 being diameter of the loaded area, mm.

They proposed modification to ACI equation based on their study and concluded that ACI formula spears to be true for low-to-moderate concrete strength. Stefanou (1993) studied the punching shear resistance of solid slab bridge decks prestressed longitudinally and

reinforced transversely. He presented current design approaches including Kinnunen-Nylander theory of punching and the plastic theory applied to punching. Empirical treatments of punching, mainly those adopted by British and American codes were presented.

Sawko and Saha (1967) presented detailed ultimate load analysis of bridge decks using yield line theory for simply-support, edge stiffened, and continuous bridge decks. They covered all possible models of collapse for different loading positions. They extended the basic yield line theory to cover the effect of edge stiffening and punching shear. They also suggested that it's possible to obtain the collapse loads of composite slab-beam bridges by transferring these to quasi-orthotropic plates and employing the yield-line approach in their analysis.

Mufti and Newhook (1998) and Kuang and Morely (1993) studied punching shear strength of restrained concrete bridge slabs. Petrou and Perdikaris (1996) studied punching shear failure in concrete decks as snap-through instability of arching action mechanism activated in the deck. They proposed two DOF three hinge strut mechanism subjected to single transverse concentrated load at its apex in bridge deck slab to find punching shear analytically and proposed a model that gives comparable results with experimental results.

Graddy et al. (2002) studied the punching shear behavior of bridge deck under fatigue loading, including the effect of the arching action, both experimentally and analytically. Full-scale cast-in-place panels and precast/prestressed panel with cast-in-place topping were constructed and tested under fatigue loading. Finite-element models were developed

and both analytical and experimental results were compared. They proposed a method to calculate punching shear capacity that includes the effect of the membrane compression. Also they compared punching shear capacity using AASHTO (1998) and ACI (2002) punching equations and the general punching shear equation proposed by Tsui et al. (1986), Whitt et al. (1993) and Kim et al. (1994) which derived from equilibrium of forces acting on the assumed plane failure planes and as follows:

$$\bar{V}_c = 2\left(b_1 + b_2 + \frac{2\bar{d}}{\tan\theta}\right)\frac{\bar{d}}{\tan\theta}f_t \quad \text{(Empirical units)} \dots\dots\dots\dots\dots\dots\dots\dots\dots\dots\dots(2.2)$$

$$f_t = \left(2 + \frac{4}{\beta_c}\right)\sqrt{\bar{f}_c'} \leq 4\sqrt{\bar{f}_c'} \quad \text{(Empirical units)} \dots\dots\dots\dots\dots\dots\dots\dots\dots(2.3)$$

Where:

$\bar{V}_c = $ Punching-shear capacity, lb

$b_1 = $ Short side of concentrated load or reaction area, in

$b_2 = $ Long side of concentrated load or reaction area, in

$\bar{d} = $ Effective depth of section, in

$\theta = $ Acute angle between the horizontal and the assumed failure plane

$f_t = $ Diagonal tensile strength of concrete, psi

$\beta_c = $ Ratio of short side to long side of concentrated load or reaction area

$\bar{f}_c' = $ Specified compressive strength of concrete, psi.

The AASHTO (1998) equation for the punching shear capacity of slabs, which is identical to ACI (2002) code equation of punching shear capacity associated with a reactangular footprint in non-prestressed slabs and only for slab prestressed in one direction. An angle of failure of 45° is considered with critical section for the two way shear lies at the distance of half the effective depth of the section. The equation is as follows:

$$\bar{V}_c = \left(2 + \frac{4}{\beta_c}\right)\sqrt{\bar{f}_c'}\, \bar{b}_0\, \bar{d} \qquad \text{(Empirical units)} \ldots\ldots\ldots\ldots\ldots\ldots\ldots\ldots\ldots\ldots (2.4)$$

Where:

$\bar{V}_c$ = Punching-shear capacity, lb

β_c = Ratio of short side to long side concentrated load or reaction area

$\bar{f}_c'$ = Specified compressive strength of concrete, psi.

$\bar{b}_0$ =   The perimeter of the critical section in slabs and footing, in

$\bar{d}$ =   Effective depth of section, in

$$\bar{V}_c = \left(0.17 + \frac{0.33}{\beta_c}\right)\sqrt{\bar{f}_c'}\, \bar{b}_0\, \bar{d} \qquad \text{(SI units)} \ldots\ldots\ldots\ldots\ldots\ldots\ldots\ldots\ldots\ldots(2.5)$$

Where:

$\bar{V}_c$ = Punching-shear capacity, N

β_c = Ratio of short side to long side concentrated load or reaction area

$\bar{f_c'}$ = Specified compressive strength of concrete, MPa.

$\bar{b_0}$ = The perimeter of the critical section in slabs and footing, mm

$\bar{d}$ = Effective depth of section, mm

The general punching shear equation reduced to AASHTO and ACI equation if the angle of failure plane equals 45°. While, a value of 38° was proposed by Tsui et al. (1986).

The CHBDC (2000) equation for the punching-shear capacity of slabs also considered a failure similar to that for the AASHTO (1998) and ACI (2002) equation of punching-shear capacity. The equation for non-prestressed member is as follows:

$$V_r = \phi_c f_{cr} b_0 d \quad \dots\dots\dots\dots\dots\dots\dots\dots\dots\dots\dots\dots\dots\dots\dots\dots\dots \quad (2.6)$$

$$f_{cr} = 0.4\sqrt{f_c'} \qquad \text{For normal density concrete} \dots\dots\dots\dots\dots\dots\dots\dots \quad (2.7)$$

Where:

V_r = Factored shear resistance, N

ϕ_c = The resistance factor for concrete

f_c' = Specified compressive strength of concrete, MPa

b_0 = The perimeter of the critical section in slabs and footing, mm

d = Average effective depth of section, mm

f_{cr} = The cracking strength of concrete, MPa

f'_c = Specified compressive strength of concrete, MPa

It should be noted that AASHTO, ACI and CHBDC do not account for any increase in the predicted punching shear capacity due to arching action with increased levels of lateral restraint.

2.6 Fatigue Behavior of Reinforced Concrete

Fatigue is a process of progressive permanent change in a material subjected to repetitive stresses. These changes may be damaging and result in progressive growth of cracks and complete fracture if the stress repeats are sufficiently large.

Most materials when subjected to cyclic loading over many thousands of repeats exhibit lower strengths compared with their static strength, depending on the rate of loading, the stress ratio (minimum/maximum cyclic stress), the maximum stress, and the number of cycles. A highway bridge on a Class A route with a design life of 50 years can experience a minimum of 73 million loading cycles of varying intensities over its service life (CHBDC 2000).

Fatigue fracture of concrete is characterized by considerably larger strains and microcracking as compared to fracture of concrete under static loading. Fatigue strength of concrete for a life of ten million cycles for compression, tension, or flexure is roughly about 55 percent of static strength. Fatigue strengths for concrete beams can be 25% lower if the number of cycles is increased from 5 to 100 million cycles (Tilly 1979).

Concrete is designed to carry compression but, in tensile zones, it does in fact carry various levels of tensile stress up to its ultimate strength, at which point it cracks and tensile force is redistributed to the steel. As fatigue progresses and cracks propagate, the stress distribution changes and fatigue failure is not necessarily by the same mechanism calculated using simplified models and this, together with the variability of materials and loads, accounts for the scatter characteristic of fatigue test results.

Failure of reinforced concrete members under fatigue can be triggered by:

1) fatigue of the concrete in compression, or,

2) fatigue of the reinforcing bars in tension, or,

3) fatigue caused by a bond failure between the concrete and reinforcement.

2.6.1 Fatigue Behavior of Plain Concrete

Plain concrete, when subjected to repeated loads, may exhibit excessive cracking and eventually fails after a sufficient number of load repetitions, even if the maximum load is less than the load strength of a similar specimen. The fatigue strength of concrete is defined as a fraction of the static strength that it can support repeatedly for a given number of cycles. Fatigue strength is influenced by range of loading, rate of loading, eccentricity of loading, load history, material properties, and environment conditions.

In the past decades, researchers have put lots of efforts on the fatigue behavior of concrete, as well as concrete with fibers or cement materials such as silica fume. The behavior of concrete under fatigue loading becomes clearer.

Concrete is not considered to be a homogeneous material, and fatigue of concrete is a progressive process of micro-crack initiation and propagation leading to macro-cracks, which can grow and determine the remaining fatigue life by causing stress to increase until failure occurs. The important characteristics of the fatigue process are the stress/strain changes under cyclic loading and the related mechanics of crack growth.

Researches at Lehigh University by Asssimacopoulos et al. (1959) have shown that fatigue failure of plain concrete tended to occur at the matrix-aggregate interface. Considering crack formation and growth under static loading, Kaplan (1962, 1965) suggested that the beginning of the failure process was marked by the formation of multiple cracks in the mortar with the aggregate forming a barrier. He associated the cracking with the release of strain energy and it is reasonable to assume repeated loading is similar. It appears that the mechanism of fatigue in concrete starts with the breakdown of bond between the cement matrix and the aggregate. This is followed by the progression of cracking through the mortar, arrested when it meets a stone until the process is repeated. When the strain energy released overcomes the remaining cohesive forces in the concrete, complete fracture results.

Byung (1991) conducted an experiment to obtain the fatigue lives of concrete at various stress levels. 14 beam specimens, with the same dimension of 100 x 100 x 500 mm, were tested under four-point flexural loading. Three different levels of applied fatigue stresses were considered in this study. The test results indicate that the probabilistic distributions of fatigue life of concrete are different for different stress levels. Byung found that the shapes

of the probabilistic fatigue-life distributions of concrete depend on the level of applied fatigue stress. He concluded that the shape parameter of the Weibull distribution for the fatigue life of concrete ranges from 2.0 to 4.0 depending on the level of applied fatigue stress.

Sun et al. (1993) studied the fatigue performance and damage mechanism of steel fiber reinforced concrete. They investigated the effects of volume fraction of steel, amount of silica fume, and their composite on fatigue performance. Test results show steel fiber reinforced concrete has excellent performance in resisting crack initiation and propagation; thus, the ability of resistance to fatigue is increased greatly. They concluded that the key to increase in fatigue resistance for high-strength concrete is the increase of cracking-arresting ability. However, resistance to crack arrest comes in two ways: i) reduction of size and amount of original crack sources; and ii) capacity of inhibiting initiation and extension of crack.

Shi et al. (1993) introduced an expression to describe the flexural fatigue strength of plain concrete, which incorporates the effects of stress ratio and stress level into the fatigue equation and allows a statistical description of fatigue life in terms of both stress level and stress ratio. Laboratory flexural fatigue experiments were carried out on 78 plain concrete beams to verify the validity of the proposed fatigue equation. They found that the proposed fatigue equation could model the laboratory fatigue data of different stress levels and stress ratios with statistical correlation values exceeding 90%, and the distribution of the equivalent life is in excellent agreement with a two-parameter Weibull distribution.

Todorka et al. (1997) investigated plain concrete and fiber-reinforced concrete under low-cycle fatigue. Several hundred 4-inch cube specimens were tested uniaxially under cyclic compression with constant amplitude. The variables studied were the concrete strength (4.5, and 7 ksi cylinder strength), type of fiber (steel and polypropylene), and fiber volume (0.00, 0.25, 0.50, 0.75 and 1.00 percent). The fatigue behavior of plain concrete was found to improve with increase in concrete strength, and the energy absorption capacity increases with strength due to the stronger bond between mortar and aggregate particles and the higher tensile strength of mortar. Fibers up to 1% have considerable beneficial effect on the fatigue behavior of concrete. At lower stress levels fibers dissipate much more additional energy than at higher stress levels.

Gao et al. (1998) studied the fatigue of concrete under uniaxial compression cyclic loading. Three series of specimens with the dimensions of 100 x 100 x 300 mm were tested under cyclic loading. During testing, irreversible strain and strain range were measured and recorded at certain fatigue cycles. Based on the experiment, they observed that fatigue of concrete can be divided into three parts: irreversible strain, strain caused by cyclic creep under the action of average stress, and fatigue strain range, respectively. A simple and practical fatigue model for concrete under uniaxial compression with constant stress range has been proposed.

2.6.2 Bond Between Concrete and Reinforcement under Cyclic Loading

The transfer of forces across the interface between concrete and steel by bond stresses is of fundamental importance to many aspects of reinforced concrete behavior. Satisfactory bond performance is an important goal in the detailing of reinforcement in the structural

components. Bond stresses in the reinforced concrete members arise from two distinct situations. The first is anchorage or development where bars are terminated. The second is flexural bond or the change of force along a bar due to a change in bending moment along the member. Bond can be considered as the shearing stress between the concrete and the reinforcing bars. It is the result of adhesion, friction, and the support of the deformations. Plain bars depend mainly on adhesion and friction, while deformed bars depend on the support of the ribs. The effects of cyclic loads on bond are (i) to reduce the bond strength at failure, and, (ii) to accelerate the rate of bond deterioration as the stress range or the number of cycles increased.

Mor. et al. (1992) studied fatigue of high-strength reinforced concrete under low-cycle high-stress magnitude of cyclic loading. Four groups of RC beams with normal-weight aggregate or light-weight concrete were tested at the stress level of 64% to 80% of the yield load as determined in the static test. They concluded that fatigue capacity of high-strength RC beams was found to be related to the bond between concrete reinforcement directly and not any other strength properties.

Research also indicates that the ultimate bond strength under fatigue loading is directly related to internal damage to the concrete. Thus, repeated loads have a similar influence on the bond strength and slip as on deformation and failure of un-reinforced concrete. In most bond fatigue tests, four separate stages are apparent. The first is a fast increase in slip due to initial crushing of concrete; the second is a rapid reduction in the slip rate due to the stabilization of process; the third is a long portion with a constant slip rate; and the fourth is

a fast increase in the slip rate as the failure approaches. Such a response is typical of a pullout failure. A splitting failure would result in a sudden drop on load carrying capacity.

2.7 Truck Loading Specified in North American Bridge Codes

To examine the load carrying capacity of the deck slab, the truck wheel load, the load factor and the dynamic load allowance need to be identified. The Canadian Highway Bridge Design Code, CHBDC (2000), specifies CL-W loading for bridge design, where CL stands for the Canadian Loading and W stands for the gross load of the CL-W Truck in kN. In Ontario, a CL-625-ONT Truck is used in the design of the bridges. The total load of the CL-625-ONT Truck remains at 625 kN, but the axle load distribution differs from that of CL-W Truck. The maximum wheel load of CL-W Truck and CL-625-ONT is 87.5 kN, which is distributed on a 0.25×0.25 m surface area of the bridge deck.

The Live Load Factor including dynamic allowance based on CL-625 Truck or lane is 1.70 for the Ultimate Limit State (ULS) combination-1. CHBDC specifies a 40% increase in live load for dynamic load allowance for slab design. The AASHTO-LRFD (1998) specification specified HS-20 Truck for bridge design. It also specifies a maximum load of 145 kN per axis i.e. 72.5 kN per wheel, which is distributed on rectangular surface area of 510 mm width. The live load factor including dynamic load allowance for limit state strength-I is 1.75, while it specified a 33% increase in Truck Load for deck slab design.

Chapter 3

Proposed Prefabricated Bulb-T Girder Connections

3.1 General

The Deck-Bulb-T (DBT) girder units are basically a combination of 4 depths and 3 flange widths. The depths available are 800, 1100, 1500 and 1800 mm. The depth varies by using different depths of side forms. Available flange widths are 1200, 1500 and 2000 mm and are set by varying the distance between the side spans on the top flanges. For exterior girders, the standard barrier section is always fabricated on a 1200 mm wide unit in order to reduce the overturning effect of the eccentric barrier load.

All the Deck-Bulb-T (DBT) girder units are constructed with normal weight concrete with the exception of the DBT 1800 series. This unit is cast with semi-light weight concrete for the bulb and the web, but normal weight concrete is used in the flange. Basically, the DBT 1800 series is designed assuming semi-light weight concrete for all design aspects. The normal weight concrete for the flange is used to increase the resistance of the top surface of the girder to the effects of salt penetration and for abrasion.

Actual girder weights, however, are calculated based on hybrid properties. One aspect that requires attention results from the relative flexibility of the DBT girders. As a result, a full-depth diaphragm between girders is required to provide transverse deck stiffness. Also, the

connection between DBT flanges should have enough strength to provide continuity for live load distribution.

Based on the information obtained from the literature review and the CHBDC (2000) code requirements for design of the deck slabs under wheel load, two moment-transferring connections (MTC) and two intermittent-bolted connections (IBC) were developed to maintain the structural integrity of the bridge cross-section and to provide local resistance of the deck slab against CHBDC wheel load.

3.2 Proposed Moment-Transferring-Connection (MTC)

3.2.1 MTC-1

The first moment transferring connection (MTC-1) has a joint width of 325mm. In this connection the rebars as well as the dowel rebars are extended 270 mm beyond the inner edge of the joint and ended with horizontal 180° hooks. Also, bottom rebars with 180° hooks are projecting from the girder flange to be embedded in the cast-in-place joint. The girder flange end is formed with 150 mm wide, 155 mm deep, closure strip grove throughout the girder length. Figure 3.1 shows cross-section of the MTC-1 girder connection with structural details.

It is assumed that the DBT girder will be aligned to provide 25 mm gap that can be filled with a 25 mm diameter Form Backer Rod.

3.2.2 MTC-2

The second moment transferring connection (MTC-2) has a joint width of 300 mm. In this connection both the bottom and top rebars are extended 270 mm beyond the inner edge of the joint. Also, the bottom rebars ended with vertical 180° hooks. The girder flange end is formed with 150 mm wide, 155 mm deep, closure strip grove throughout the girder length. Figure 3.2 shows cross-section of the MTC-2 girder connection with structural details.

3.3 Proposed Intermittent-Bolted-Connection (IBC)

3.3.1 IBC-1

The first intermittent bolted connection (IBC-1) has bolted joints repeated at the equal intervals along the length of the girder, 850mm. Each bolted joint is made of steel plates with dimensions of 245 mm (height) × 150 mm (width) × 25 mm (thickness). Each plate is embedded in the concrete deck slab using two 19 mm in diameter, 200 mm long, high strength bolts. Each steel plate accommodates two holes at its lower end for A325 bolts of 19 mm diameter. The hole of the bolt has a horizontal slot to accommodate any tolerance arising from girder alignments. A trapezoidal grove is made at the top of the girder flange ends to allow for concrete grout after connecting the steel plates. Also, the joint has a 75 mm deep, 40 mm wide, trapezoidal shape shear key throughout the girder length. Figure 3.3 shows the cross section of the IBC-1 girder connection with structural details.

3.3.2 IBC-2

The second intermittent bolted connection (IBC-2) is similar to IBC-1. The only difference is that, in IBC-2, a 12 mm thick steel plate with dimensions of 100 mm × 150 mm × 12 mm

is welded to the other end of the two dowel bolts. This additional steel plate is embeded into the concrete deck to provide extra bearing resistance for the anchor bolts. Also, the joint has a 75 mm deep, 40 mm wide, trapezoidal shape shear key throughout the girder length. Figure 3.4 shows the cross section of the IBC-2 girder connection with structural details.

Chapter 4

Experimental Study

4.1 General

Based on the information from the literature review and the CHBDC (2000) requirements for design of deck slabs under wheel load, two moment-transferring connections (MTC) and two intermittent-bolted connections (IBC) were developed. Four full-scale bridge models simulating these connections were tested to collapse under concentric loading.

The experimental program was undertaken to investigate the behavior and the ultimate load carrying capacity of the proposed moment-transferring connections (MTC) and intermittent-bolted connections (IBC) under monotonic loading. In the experimental program, full-scale bridge deck connection models were constructed and loaded up to failure under the simulated truck-wheel load. Experimental results, including deflections, concrete strains, steel strains, cracking load, crack patterns and ultimate load carrying capacity, were recorded and analyzed.

In this chapter, a detail description of the proposed bridge deck connection models is presented, including the design of the bridge models, material properties, construction of the models, instrumentation, test equipment and experiment setup.

4.2 Description of the Bridge Models

The experiment program was carried out on four full-scale bridge deck connection models. Wide-flange girders were constructed with different connection patterns at each side of each girder to maximize the use of the tested models. Then, each two girders were placed side by side and flange-to-flange connections were installed to form an integral slab-girder system. After testing, the connection between the flanges of the two girders were separated using a concrete saw and then were rotated 180° to form the other type of connection between flanges. For all of the models, the width of girder deck slab was 1800 mm, the span length was 2000 mm and the flange (deck slab) thickness was 225 mm. The girders were simply supported at 1500 mm over a neoprene bearing pads.

Two girders were placed side by side and connected with either MTC or IBC type connection. Each girder web was reinforced with 3-15M rebars at the top and bottom, and with 10M stirrups at 200 mm center to center (c/c). The bridge deck slab was reinforced with 15M rebars at 300 mm c/c at the top and bottom in both directions. This reinforcement represents 0.3% of the cross-sectional area as per CHBDC (2000). All the girders and joints were cast with high early strength concrete with a minimum specified compressive strength of 50 MPa at 7 days.

Table 4.1 shows a summary of the description of the bridge models. The description of the model contains the first three letters representing the type of the connections, i.e. MTC refers moment–transferring connection while IBC refers intermittent-bolted connection. The following number represents the number of connections developed for either MTC or IBC. The last letter represents the load location with respect to the centroid of the joint connection, i.e. C refers to concentric vertical loading. Also, the IBC connections were tested with a

simulated wheel load located at the mid-distance between the steel plate joints. As such, the last letter in the bridge models "B" represents that loading between the steel plate joints. Figures 4.1 and 4.2 show the details of moment transferring and intermittent bolted connections as well as the location of the simulated wheel load on the joint cross section.

4.2.1 Bridge Deck Connection Model M1 (MTC-1-C)

The first bridge deck connection model represented a moment transferring concrete connection with detail type 1 shown in Figure 4.3(d). It was constructed in the lab and then tested under monotonically increasing simulated wheel load. The model consisted of two girders, with concrete deck connected with cast-in-place concrete joint, also called closure strip, as shown in Figure 4.3(e). The cross-sectional dimensions and structural details are shown in Figure 4.3. In this connection, the top and dowel 15M rebars were extended 270 mm beyond the inner edge of joint from both the girder flanges and ended with 180° horizontal hooks as shown in Figure 4.3(a) and 4.3(b). Also bottom rebars with 180° vertical hook were projecting from the girder to embed into the cast-in-place joints. Each girder was cast with sides having 150 mm wide and 155 mm deep closure strip grove through out the span. Also the joint consisted of 75 mm deep and 40 mm wide trapezoidal shape shear key throughout the span for better load transfer between old (precast) and new (cast-in-place) concrete. Figure 4.3 (e) shows details of the shear key and joint opening as well as detail for the Form Backer rod. The center-to-center (c/c) distance between the girders was 1825 mm. The total width of the closure strip (joint) was 325 mm of which includes a 25 mm space between the two girders to accommodate 25 mm diameter Form Backer rod. The joints were filled with concrete grout of the same specified concrete strength as the girders. After grout hardening, the girder system was loaded at the centroid of the joint using simulated wheel load distributed

34

over an area 250 mm × 250 mm. Figure 4.4 shows plan and cross-section views of loading position.

4.2.2 Bridge Deck Connection Model M2 (MTC-2-C)

The second bridge deck connection model represented a moment transferring concrete connection with detail type 2 shown in Figure 4.5 (c). It was built and tested under monotonically increasing simulated wheel load. The model consisted of two girders, with concrete deck connected with full-depth cast-in-place concrete joint, also called closure strip, as shown in Figure 4.5 (a). The cross-sectional dimensions and structural details are shown in Figure 4.5. In this connection, 15M top rebars were extended 270 mm beyond the inner edge of joint from both the girder flanges as shown in Figure 4.5(a). Also, bottom rebars with 180° vertical hook were projecting from the girder with the same length of 270 mm to embed into the cast-in-place joints as shown in Figure 4.5(a) and 4.5(b). Each girder was cast with sides having a 150 mm wide full depth deck strip through out the span. Also the joint consisted of 75 mm deep and 50 mm wide trapezoidal shape shear key throughout the span for better load transfer between old (precast) and new (cast-in-place) concrete. Figure 4.5 (c) shows details of the shear key and joint opening. The center-to-center (c/c) distance between the girders was 1800 mm. The total width of the closure strip (joint) was 300 mm. The joint was filled with concrete grout of the same specified concrete strength as the girders. After grout hardening, the girder system was loaded at the centroid of the joint using simulated wheel load distributed over an area 250 mm × 250 mm. Figure 4.6 shows plan and cross-section views of loading position.

35

4.2.3 Bridge Deck Connection Model M3 (IBC-1-C)

The third bridge deck connection model was an intermittent bolted connection with detail type 3 shown in Figure 4.7(e). It was built and tested under monotonically increasing concentric loading located at the mid-span of the girder and at the mid-length between plated connection location as shown in Figure 4.8. This model consisted of two girders were simply supported with flanges connected by intermittent bolted connection as shown in the Figure 4.7. The connection was made of two steel plates of size 210 mm (height)×150 mm (width) × 25 mm (thickness). These plates were embedded in the bridge deck slab sides with two 200 mm long (d=19 mm) high-strength bolts conforming to ASTM A325 standards, welded to the plate as shown in Figure 4.7(e). The size of the weld was 10 mm. The steel plates were located at a spacing of 850 mm as shown in Figure 4.7(a). The girders were placed side-by-side touching each other and then the steel plates were connected by 19 mm diameter A325 bolts (one bolt at top and two bolts at bottom). A trapezoidal grove was made in the girder flanges to allow for concreting grout after connecting the steel plates by bolts. Plans and sections of this model are shown in Figures 4.7(b) to 4.7(d). The c/c distance between the girders webs was 1800 mm. Figure 4.8 shows the plan and cross-section view of the loading position, which is at the mid-distance between two IBC connections.

4.2.4 Bridge Deck Connection Model M4 (IBC-2-C)

The fourth bridge deck connection model M4 was also an intermittent bolted connection with type 2 as shown in Figure 4.9 (d). It was similar to bridge model M3 with respect to overall dimensions, cross section, rebar arrangement and joint details. The only difference in model M4 was that an additional steel plate with dimension 100 mm (height)×150 mm

(width)×12 mm (thickness) was attached and welded at the free end of the dowel bolts to embed into the concrete deck. The purpose of adding an end steel plate inside the concrete slab is to provide extra bearing resistance as well as improve the deformability of the joints. Model M4 was built and tested under monotonically increasing concentric loading located at the mid-span of the girder and at the mid-distance between the bolted joints as shown in Figure 4.10.

4.3 Materials

Local available materials were used to construct all of the proposed bridge models.

4.3.1 Concrete

Ready mix concrete was supplied for the girder and the deck slab of the bridge models. While, for the joint (closure strip) of the girders, concrete was mixed at the structural laboratory of Ryerson University.

4.3.1.1 Ready-mix concrete

Ready mix concrete with 7-day minimum strength of 50 MPa was used for all the bridge models. The cement was normal-strength Portland cement, CSA type 10, manufactured by Canadian Cement Company. The aggregate used in this concrete mix had a maximum nominal size of 10 mm for the first set of the models (M1 and M3) and 20 mm for the second set (M2 and M4). 10 mm size aggregate was used to ensure concrete spreading in very tight space for the joints.

Standard cylinders of 100 mm diameter and 200 mm height were cast concurrently while casting the bridge models. The cylinders were kept beside the models to ensure the same curing condition. The concrete cylinders were tested on the same day the bridge models was tested to determine the concrete compressive strength. An average of three cylinders was taken for each test of the bridge models. Table A.8 (Appendix A) shows the average compressive strength as well as the slump test results for the concrete used to build the girders. Figure B.1 shows various photos of the cylinders from casting to testing.

4.3.1.2 Concrete Grout for the joints

High early strength concrete mix, having a 7-day minimum specified strength of 50 MPa, was developed in the laboratory and used to fill the bridge joints. Cylinders were cast for each joint and tested on the same day the bridge model was tested. Testing of the cylinders was carried out on the MTS machine as per ASTM C 39 (2003). Table A.9 (Appendix A) shows the average compression strength of the concrete cylinders as well as slump test results for concrete used to fill the joints.

4.3.1.2.1 Cement

CSA Type 10 normal Portland cement was used in this project.

4.3.1.2.2 Aggregate

Natural gravel with nominal maximum size of aggregate (MSA) of 9.5 mm and natural sand were used as course and fine aggregate in concrete mixes. The grading or particle size distribution of coarse and fine aggregate was determined in accordance with ASTM C 316 and the results are presented in Table A.1 and A.2 (Appendix A). The specific gravity, bulk

density, moisture absorption, and surface moisture content of coarse and fine aggregates calculated as per ASTM standards are tabulated in Table A.3.

4.3.1.2.3 Water

Natural tap water was used in the concrete mix. The water-cement ratio of the mix was 0.35.

4.3.1.2.4 Superplasticizer (SP)

The poly-naphthalene sulfonic acid based SP was used for the concrete mixtures. The superpalsticizer is in accordance with ASTM C 494 type F specifications. The physical characteristics provided by manufacturer are presented in Table A.4 (Appendix A).

4.3.1.2.5 Mixture Proportion of the Concrete for Joints

The proportion of the concrete was carried out in accordance with ACI's absolute mix design method. The targeted compressive strength at 28 days was 70 MPa. The details of mix proportion of concrete are presented in Table A.7.

All concrete mixtures were prepared in 0.08 m³ batches in a concrete mixer. The batching sequence consisted of following five steps:

Step 1: Homogenizing the coarse aggregate and fine aggregate for 30 seconds;

Step 2: Then approximately 75% of the water was added and mixed for 30 seconds;

Step 3: Cement was then added and the mixing was done for another minute;

Step 4: The remaining water along with SP was added and concrete was mixed for 3 minutes;

Step 5: After 2 minutes set, the mixing was resumed for 2 more minutes.

4.3.2 Reinforcing Steel

The girder and deck slab for all the bridge models were reinforced using steel rebars. In deck slab, M15 rebars were used @300 c/c in both top and bottom directions, as per the Canadian Highway and Bridge Design Code CHBDC (2000) requirements. In girder web, 3-M15 rebars were placed at the top and bottom, with M10 stirrups @200 c/c.

4.3.3 Steel Plates

Steel plates, conforming to ASTM A325 standard, with 24 mm thickness were used to develop the connection assembly. The testing shows that the 24 mm plates had yield strength of 355 MPa, with modulus of elasticity (E) of 200 GPa. In model M4, 12 mm thick steel plates were welded to the end of the dowel bolts and embed to the concrete deck slab. (See Figure 4.9)

4.3.4 High Strength Bolts and Nuts

High strength structural bolts and nuts were used to develop bolted connection for the bridge deck joints. Nuts and bolts were conformed to ASTM A325 standard. Two different lengths of the bolts were used. 200 mm long bolts were welded to the steel plates and embedded in the concrete, and 65 mm long bolts were used to connect the steel plates to form the IBC connection.

4.3.5 Form Backer Rod

25 mm diameter Form Backer Rod was used in Model M1 to fill the aligned gap between the bottom edges of two precast deck at the cast-in-place concrete joint (See Figure 4.3(e)).

4.4 Construction of the Bridge Models

The construction of the bridge models was carried out in two phases. In the first phase, from March 2004 to July 2004, models M1 and M3 were constructed in the structural laboratory of Ryerson University located at Geary Street, Toronto. In the second phase, from September 2004 to June 2005, model M2 and M4 were constructed at the structural laboratory of Ryerson University in the new Engineering Building located at Church St., Toronto. Prior to building the bridge models, structural drawings of the models and joint details were prepared.

4.4.1 Formwork

19 mm thick plywood sheets were used to support the concrete in the webs and flanges of the girders. 35 × 50 mm size wood piece were used as main supporting members of the frame, while 35 × 35 mm size wood piece were used to brace the frame. An electrical saw available at the structural laboratory of Ryerson University was used to cut the wood and plywood. First, four wooden frames (each one represents one girder) were prepared and placed side by side. For model M3 and M4, 155 × 30 mm size rectangular openings were made in the plywood supporting deck to provide gap for locating the steel plates. Figure B.2 shows the plan and elevation view of the formwork. The wood frame formwork for each girder was placed in the structural frame before placing reinforcement. After finishing the formwork, gaps between the plywood were covered with silicon. Silicon was applied

using gun and excessive silicon was wiped out before it dried out. Before placing the reinforcement mesh, form oil, i.e. form-releasing agent, was sprayed at the inner surface of the plywood.

4.4.2 Attachment of Strain Gauges on the Steel Rebars

Strain gauges were attached to the rebars at specified locations. Small area of each rebar, about 20 mm in length and 10 mm in width, was grinded and made smooth using electrical hand grinder. Strain gauges were then attached to the rebar using M-bond 200 epoxy after cleaning the surface with acetone, conditioner and neutralizer. An electrical wire was connected to each strain gauge by soldering and extended to outside the girder, for further connecting to the recording system while testing. Each strain gauge was protected by M-coat F kit and covered with thick aluminum tape. Figure B.3 shows various photos of strain gauges attachment to the rebars.

4.4.3 Placement of the Steel Rebars

Most rebars were cut and bent at off campus facility. A few rebars for model M2 were cut and bent at the workshop of the Civil Engineering Department. Reinforcement cage for each girder web was prepared outside the formwork using 10 mm diameter stirrups and then lifted into the formwork. Wooden pieces were used as a stand chair to keep the cover of the rebars. 15M rebars were placed at 300 mm c/c in both directions. Figures B.7 and B.8 shows the rebar arrangement in various models.

4.4.4 Steel Plate Assembly

Steel plate assemblies were prepared for model M3 and M4. An electric cutter and drill machine available at the workshop of the Civil Engineering Department were used to cut and drill the plates. Bolts were welded to the plates at the laboratory of Mechanical Engineering Department of Ryerson University. The size of the weld was 10 mm. The steel plate assembly was then placed in the formwork and tied properly to the steel rebars. Figures B.4 and B.5 show views of steel plates assembly for M3 and M4, respectively.

4.4.5 Styrofoam for the Joints

To develop the joint grove and the pockets of the connection, Styrofoam insulation sheets were used. Figure B.6 shows views of Styrofoam sheet and joint grove and pockets. Styrofoam was cut in pieces to the required shape and size. After cut to size, Styrofoam pieces were jointed together using silicon and masking tape to form a required shape of the joint and place in position and hold with the side forms. After placed in position, plywood was nailed on the top of the joint to prevent uplifting of the Styrofoam during casting concrete.

4.4.6 Concreting of the Girders

High early strength concrete of a specified compressive 7-days 50 MPa was used for the girders. Ready mix concrete was ordered and poured in the girders using concrete pump or bucket. The concrete was first poured in the web of the girder and then the deck slab concrete was poured on either side of the web in a balance way to avoid overturning of the formwork. A long wooden piece was used to level the concrete surface of the deck slab.

The top surface of the concrete slab was then given smooth final finish by hand trowel. Figures B.9 and B.10 show photos of the bridge models during concreting and curing.

4.4.7 Curing the Concrete

After casting the specimens, the deck surface was covered with membrane or wet burlap as soon as the concrete was set (usually 6 to 8 hours), to prevent or minimize water evaporation. During the first 3 days, water was sprayed to the specimen for curing. Figures B.9 and B.10 show the photos of curing of the specimen. For curing the joint connection concrete, several layers of burlap, which was soaked with water, were covered on the surface during the first 7 days after casting.

4.4.8 Removing the Formwork

After 7 days, the formwork was removed. The wooden formwork was removed using crook bar. The Styrofoam was removed from the specimens and then cleaned using concrete chisel, hammer and steel brush.

4.4.9 Casting the Joints

For model M1, Foam Backer rod was used to fill the gap between the two girders as shown in Figure B.11. Small formwork was prepared to support the side of the joint before casting the joint. Longitudinal rebars were placed in position and tied with the projecting rebar. Each joint was cast with 7-day 50 MPa concrete, mixed in the structural laboratory. Figures B.11 to B.13 show photos of the construction of different joint connections.

4.4.10 Bolting the Steel Plates at the Joint

For model M3 and M4, 19 mm diameter, 65 mm long, high strength bolt, with one nut and two washers, conforming to ASTM standard A325, was used to connect the steel plates. Joints and pockets were cast with concrete of the same strength as that of the girders. Figure B.13 shows different views of the bolted connection before concreting.

4.4.11 Rotation of the Girders

After testing models M3 and M4, the tested IBC joints were broken with jacking hammer and separated. Then, the girders were rotated 180° to form another modeled MTC joint connection.

4.5 Instrumentation

4.5.1 Strain Gauges

Two types of strain gauges were used in the experimental testing. Strain gages, type KFG-10-120-C1-11, were used to record the longitudinal strain in the steel rebar at critical locations in the bridge deck slab. While, type KFG-30-120-C1-11 strain gauges were used to record the concrete strain on the top surface of the bridge deck.

4.5.1.1 Steel Strain Gauges (Type KFG-10-120-C1-11)

The length of the steel strain gage was 10 mm with a resistance of $120\pm2\%\ \Omega$, and a gauge factor of $2.11\pm1\%$. The strain gauges were mounted on the rebar and protected using M-Coat F kit, strain gauge protective coating/environmental protection kit, which contains M-

Coat b Nitrile rubber coating, M-Coat FBT soft seal protective coating and M-Coat FA aluminum tape. Figure B.3 shows views of the steel strain gauges installed on the rebars.

4.5.1.2 Concrete Strain Gauges (Type KFG-30-120-C1-11)

The concrete strain gauges had a length of 30 mm, a resistance of $120\pm2\%$ Ω, and a gauge factor of $2.11\pm1\%$. The concrete surface was prepared to mount the strain gauges using M-Bond AE-10 adhesive kit, which contained M-Bond adhesive resin type AE and M-Bond type-10 curing agent. All the strain gauges were placed at the mid-span of each bridge deck. Details of steel and concrete strain gauges for different models are shown in Appendix C.

4.5.2 Linear Variable Displacement Transducers, LVDT's

Linear variable differential transformers (LVDT's), of 50 mm electrical stroke, were used to measure the deflections of the bridge deck slab in each model. In each case of bridge model, five LVDT's were mounted under the concrete deck slab at five different mid-span locations to measure deflections during the loading stages. LVDT's locations for all bridge models are shown in Appendix C and Figures D5~D8. While, Figures D.1 (a) and D.2 (b) show views of LVDT's mounted under the bridge model.

4.5.3 Mechanical Dial Gauges

Mechanical dial gauge with travel sensitivity of 0.01 mm was used to measure the deflection of the main loading frame beam at its mid-span. Figure D.2 (d) shows the details of mechanical of dial gauges during testing. The dial gauges were manually taken at each increment of the loading throughout the test. An average loading-deflection curve of the

loading steel frame is shown in Figure D.4. The results of the LVDT's recorded from the testing were adjusted with the deflection of the loading steel frame.

4.6 Test Equipment

4.6.1 Loading Frame

A self-contain rigid portable steel frame, made of W-shape section, was used to test the bridge models. Figure D.1 shows views of the loading frame.

4.6.2 Hydraulic Jack

A hydraulic jack having a capacity of 900 kN was used to apply testing load. The jack was mounted on a W-shape monorail beam supported by a rigid portable steel frame as shown in Figure D.2 (a).

4.6.3 Load Cell

A universal flat load cell, of 900 kN (200,000 lbs) capacity, was used to measure and record the applied on bridge models M1 and M3. While, during the testing of models M2 and M4, a new load cell with a capacity of 1300 kN (300,000 lbs) was used. Figure D.1 and D.2 (a) show the load cell mounted at the bottom of the hydraulic jack.

4.6.4 Data Acquisition System (SYSTEM 6000)

During testing, the data from the LVDT's sensors and strain gages were captured by data acquisition unit (SYSTEM 6000). The test control software, TCS, is a powerful tool developed specially for data acquiring; reducing and analyzing the dynamic analog data

47

captured by SYSTEM 6000. It simplifies the process for collecting and converting data captured by strain gauges and LVDT's.

4.6.5 Elastomeric Bearing Pad

Elastomeric plain bearing pads were used to support the bridge girders over the steel beams of the testing frame. Pads were cut to rectangular shape of size of 250 × 250 mm, with 15 mm thickNess. Correction was applied to the deflection data to compensate deflection of the pads. Figure D.2 (c) shows the testing of elastomeric bearing pad, while Figure D.3 shows the average load-deflection behavior of the elastomeric bearing pads.

4.7 Experimental Setup and Testing Procedure

Each bridge model was supported at girder ends on elastomeric bearing pads to allow rotation of the girders under loading. Two 12 mm thick steel plates were inserted between bottom of the girder and top of the bearing pad to transfer the load over the entire surface area of the pad. The LVDT's were placed under the deck slab of the bridge at 5 locations to measure its deflection under increasing loading. LVDT's were connected to the data acquisition system, SYSTEM 6000, to record the readings. Both the steel and concrete strain gauges were connected to SYSTEM 6000. All the strain gauges were checked for resistance before connecting them to the data acquisition system.

Each model was tested under increasing monotonic concentric vertical load up-to-collapse. The load was applied using hydraulic jack over a 250 mm × 250 mm surface, located at the center of the joint connection, to simulate the foot print of the wheel load on deck slab as per CHDBC (2000) specifications. A load cell was connected to the SYSTEM 6000 to

measure and record the applied jacking load. Figures D.1 and D.2 show views of bridge models during testing. While, figures D.5 to D.8 show the experiment setup arrangement for the each model. Testing procedure of each model is presented in next chapter.

Chapter 5

Results and Analysis

5.1 General

The main purpose of the full-scale experimental study was to find the ultimate load capacity of the proposed connections. The experimental study was also intended to study the structural behavior of the proposed moment transferring connections and intermittent bolted connections of the bridge deck. This includes the load-deflection and load-strain histories, crack patterns and failure modes.

In order to achieve the above objectives, experimental tests were conducted on 4 full-scale bridge deck connection models. Among them, two of which were of moment transferring connections (MTC), while the other two were of intermittent bolted connections (IBC).

Each model was tested to failure using the simulated CHBDC wheel load configuration as shown in Figure 4.1 and 4.2 as was described in Chapter 4. In all of the models, the center of the simulated wheel load coincided with the center of the connection at mid-span of the bridge deck as shown in Appendix D.5~D.8. At each increment, the load was maintained constant during recording deflections and strains.

Moreover, the cracks in the bottom and top surfaces of the deck slab as well as both sides of the models were traced at different loading stages and marked with load value in Kips (1 Kip = 4.448 kN). After finishing each testing, the applied load was released slowly.

A bridge deck connection model was considered failed when it could not carry any further load. The following section summaries the results of the experimental models in the form of longitudinal strains, deflection, cracking load, and ultimate load carrying capacity. Also, the experimental ultimate load of the models was compared with the theory analysis.

5.2 Experimental Results

5.2.1 Testing of Model M1

Model M1 consists of moment transferring connection (MTC) as shown in Figure 4.1. Figure 5.1 shows a view of bridge model M1 during loading. Testing of model M1 began by applying the load in increments at a rate of approximately 22 kN, while after cracking, the loading increment was reduced to 9 kN. When the load reached approximately 116 kN, the first concrete crack line was observed extending inside the joint and along the interface between the two concretes. From that point on, as the load increased, other cracks developed until the connection reached its ultimate load. Figure 5.2 shows view of the deflected shape of the model after releasing the load, while, Figures 5.3 and 5.4 show views of the crack pattern for model M1 after failure. The test was terminated when the deflection was increasing without any increasing in applied load.

The ultimate load capacity for model M1 was recorded as 378 kN. It was observed that the form backer rod was in place at failure. A wide diagonal crack between two deck slabs was developed at the joint starting approximately from the location of the form backer rod location. Also, test shown that there were no cracks on the bottom surface of the deck on

both girders except at the interface between the two girders. This shows that failure of the model M1 was due to failure of the joint itself in flexure.

5.2.2 Testing of Model M2

Model M2 consists of moment transferring connection (MTC) as shown in Figure 4.1. Figure 5.5 shows view of bridge model M2 during loading. Testing of model M2 began by applying the load in increments at a rate of approximately 22 kN, while after cracking, the loading increment was reduced to 9 kN. When the load reached approximately 222 kN, the first concrete crack lines were observed at the four corners of the precast deck slab near the web. The crack extended to the center loading position as the loading increased. From that point on, as the load increased, other cracks developed until the connection reached its ultimate load. At the bottom of the precast deck slab, yield-lines formed gradually and could be observed clearly with the increase of the jacking load. Crack along the joint between the precast deck slab and the cast-in-place connection was small at the beginning and only developed quickly at the last stage of the loading.

Figure 5.6 shows view of the deflected shape of the model after releasing the load, while, Figures 5.7 and 5.8 show views of the crack pattern for model M2 after failure. The test was terminated when the deflection was increasing without any increasing in applied load. The ultimate load capacity for model M2 was recorded as 476 kN. During the loading, the yield-line cracks formed in layers and widened gradually from loading area to the four support corners (See Figure 5.8). After releasing the load, circular crack was also observed around the loading position on both top and bottom of the deck slab as shown in Figure 5.9.

It can be concluded that failure of the model M2 was also due to failure of deck slab in flexure.

5.2.3 Testing of Model M3

Model M3 consists of intermittent bolted connection as shown in Figure 4.2. Figure 5.10 shows view of bridge model M3 during loading. Testing of model began by applying the load in increments at a constant rate of approximately 9 kN. When the load reached approximately 89 kN, the first crack was observed on the bottom surface of the deck near the location of the steel plate in one of the girders. Also, cracks propagated locally in a fan shape very close to the location of the connecting steel plate as shown in Figure 5.11(e) and 5.11(f). From that point on, as the load increased, these cracks increasingly widened until failure due to debonding the dowel bolts near the front side of the model as shown in Figure 5.12. This may be attributed to the embedded length of the dowel bolt. This is evident when observing the crack pattern at the bolted joint near the back of the model, as shown in Figure 5.13. After testing, it was evident that the 25 mm thick steel connecting plates did not deform at all. The test was terminated when the debonding dowel bolts blew out from the deck slab and the structure could not take any more load (See Figure 5.12).

The ultimate load capacity for model M3 was recorded as 215 kN. At failure, few cracks were observed on the top of deck slab along the joint and along the interface between the concretes as shown in Figure 5.11. It can be concluded that the failure of model M3 was due to debonding failure of the dowel bolts, and a dowel bolts longer than 200 mm may increase the load capacity of this type of connection.

5.2.4 Testing of Model M4

Model M4 consists of intermittent bolted connection as shown in Figure 4.2. Figure 5.14 shows view of bridge model M4 during loading. Testing of model began by applying the load in increments at a constant rate of approximately 9 kN. When the load reached approximately 177 kN, the first concrete crack line was observed on the bottom surface of the deck near the location of the steel plate in one of the girders. Also, cracks propagated locally in a fan shape very close to the location of the connecting steel plate as shown in Figure 5.15. From that point on, as the load increased, these cracks widened until failure due to debonding the dowel steel plates near the front side of the model as shown in Figure 5.15. After testing, it was observed that the 25 mm thick steel connecting plates did not deform at all. The test was terminated when the deflection was increasing without any increase in applied load. The ultimate load capacity for model M4 was recorded as 266 kN. At failure, few cracks were observed on the top of deck slab along the joint and along the interface between the concrete. It can be concluded that M4 also failed due to debonding failure of the dowel bolts and steel plates.

5.3 Comparison Between Moment-Transferring-Connections (MTC)

5.3.1 Failure Mode

The failure mode of moment-transferring-connections (MTC), M1 and M2, was due to flexural failure of the deck slab. With the load increased, cracking at the bottom slab developed and the yield lines formed. Table 5.1 shows the cracking and ultimate load values.

In model M1, the partial-depth joint connection, the yield lines did not form along the cast-in-place concrete joint connection as expected but they formed at the precast deck slab. The gap between the two precast girders, which is located underneath the deck slab due to the alignment of the girders, did not crack until the structure reached its ultimate load capacity. Such phenomenon indicates that the connection, which contains reinforcement and a shear key at the interface, is capable to transfer the loading and makes the two precast girders work integrally together. For model M2, the full-depth joint connection, the yield lines were observed more clearly than M1 during the testing.

5.3.2 Cracking Patterns

Cracking patterns showed to be much different between models M1 (partial-depth connection) and M2 (full-depth connection).

For model M1, cracks started at the side deck at the interface of cast-in-place concrete and precast slab at loading of 116 kN. Bottom cracking was observed within the precast slab initiated at 178 kN. As shown in Figure 5.3, side cracking was developed extensively within the joint area during the loading. This is an indication that the stress concentration at the joint connection area was considerable.

For model M2, the first crack was observed to be at the bottom of the precast slab and the side of the cast-in-place connection at the loading of 222 kN. The cracking load at deck bottom was 25% higher than that of M1. Yield lines were formed at the deck slab from the loading area extending to the four support corners as the load increased. Cracks at the side of the full-depth joint area were much less than that observed from M1. This could indicate

that the stress concentration level at joint was much less for full-depth connection, M2, than that of the partial-depth connection, M1. In model M2, the joint interface between the cast-in-place concrete and precast deck slab did not crack until reaching 85% of the ultimate load capacity. Furthermore, after the testing, a circular punching shear crack around the loading area was observed on the top and bottom of the deck. This crack pattern was almost a circular around the simulated wheel loading position with a diameter of 300 mm. However, the punching shear angle observed from the testing was close to 90°, usually, this angle is about 45°.

5.3.3 Load Capacity and Deflection

Figure 5.43 shows a plot of the deflection profiles of the models at a specified load of 75 kN, while Figure 5.44 shows the deflection profiles at the ultimate load for the two models.

The cracking load at bottom slab for models M1 and M2 were 178 kN and 222 kN respectively, and the corresponding ultimate load capacities were 378 kN and 476 kN. The cracking load of M2 was 25% higher than that of M1. While, the ultimate load capacity of M2 was 26% more than that of M1. The difference of the load capacity of two models at these two stages was almost identical. A good correlation between the two models might exist and could be developed in design of these MTC connections.

At the loading stage of 75 kN, the deflection at the center point of the connection for M1 and M2 was 0.34mm and 0.15mm, respectively. However, at ultimate loading capacity, the deflection at center location of the connection was 14.69 mm for M1 and   28.75 mm for M2 (See Figure 5.43 and 5.44). At 75 kN loading stage, the deflection of M1 was about

two times larger than that of M2. However, at ultimate loading stage, the deflection of M2 was about two times larger than that of M1.

5.3.4 Strain Values Recorded from Rebars and Concrete

Maximum tensile strains were recorded under the loading in steel gauges as shown in Figures 5.24, to 5.30. Very small strains were recorded near the supports as shown in Figures 5.20, 5.23, 5.25 and 5.31.

In concrete strain gauges, maximum compressive strains were recorded at location C2 and C5 in both the models M1 and M2, as shown in Figures 5.33 and 5.36, respectively. It can be observed that at the same load increment, model M2 exhibited more compressive strain in the top surface of the concrete at the centre of the joints. Therefore, it can be concluded that the load carrying capacity of moment transferring connections, as well as stress distribution, depends on the joint profile and reinforcement details. In model M1, due to bent rebar at the joint, stresses concentrated at the center of the joint at rebars and transferred less load away from the joint as compared to model M2. Model M1 and M2 behaved monolithically and both models behaved ductile as shown in Figure 5.38.

5.4 Comparison Between Intermittent-Bolted-Connections (IBC)

The IBC models, M3 and M4, had almost identical bolted connections with a 25 mm thickness of the steel plate and one bolt at top and two bolts at the bottom of the steel plate. The only difference between these two connections is that, in model M4, an additional steel plate with dimension of 100 mm (height) ×150 mm (width) ×12 mm (thickness) was attached and welded at the end of the dowel bolts to embed into the concrete slab and work

as dowel plates. The purpose of these additional steel plates was to provide extra bearing resistance as well as improve the deformability of the joints. Table 5.2 shows the cracking and ultimate load value for model M3 and M4.

The simulated loading conditions were exactly identical for these two models. Both models were loaded concentrically with the simulated wheel load at the mid-distance between the bolted joints. Figure 5.61 shows the deflection profile of the models at the ultimate load.

5.4.1 Failure Mode

From observation made during the testing, it could be concluded that the failure of M3 was due to debonding failure of the dowel bolts. The failure mode of Model M3 shows a brittle type of failure. From design point of view, localized debond failure should be avoided. The testing results indicate that increasing the bond between the dowel bolts and the concrete deck slab is desirable.

The failure mode of M4 was also resulted from debonding failure of the dowel bolts and plates. However, with an extra steel plate attached at the end of dowel bolts, the structure behavior, not only on ultimate load capacity but also on ductility, has been improved apparently.

In model M4, the strain of BS5 and BS8, which were embedded at the bottom rebars near the end of dowel bolts, were recorded as high as 2000 μm/m as shown in Figure 5.49 and 5.51. It could indicate that

   i) The bottom rebars at the end area of dowel bolts had yielded at the ultimate loading stage;

ii) The bond strength of this type connection is strong enough to transfer the load to deck slab and make the bridge structure work integrally;

5.4.2 Cracking Patterns

For IBC connection, cracking was observed starting from the side of the deck slab. Small cracking was initiated at the side of grout area.

For model M3, cracking at the bottom of deck slab initiated from the end of the dowel bolts after reaching a jacking load of 133 kN. For model M4, bottom cracking started at the end of the dowel bolts, the same location as that of M3, but the cracking load was 178 kN, which was 34% higher than that of M3.

The development of the bottom cracking did not show much difference between the two IBC connections with the load increasing. For both models, cracking developed along the arc of the end dowel bolts and widened until failure.

For model M3, a longitudinal cracking was observed on the top of the joint grout at the ultimate load. While, no crack was observed on the top of the surface of model M4 after testing.

5.4.3 Load Capacity and Deflection at Different Stages

The ultimate load capacity of model M3 and M4 was 215 kN and 266 kN, respectively. The ultimate load capacity for model M4 was 24 % higher than that of M3.

Small cracking at the side of joint grout portion started at 89 kN for both models. This load value, which was far less than the ultimate load capacity, indicates that the concrete property for this small-amount grout should be improved. For example, steel fiber concrete can be a solution to delay or arrest the initiation of the crack of the grout.

At the ultimate load capacity, the deflection at the joint center was 7.50 mm for model M3, while it was 11.88 mm for model M4. This also indicates that the deformability of the joint connection was improved significantly.

5.4.4 Strain Values Recorded from Rebars and Concrete

Strains in the rebar near the loading area and near the girder webs were observed to be very small as shown in Figures 5.47, 5.48, 5.50 and 5.52. Concrete strain gauges at the load location were relatively of high magnitudes as shown in Figures 5.54 and 5.57, but did not show any sign of concrete crushing. Compression strains in most of the top and bottom rebars at the girder web locations, as shown in Figures 5.45, 5.47, 5.50 and 5.52, were very small and showed that arching action is not significant in this type of connections. It can be concluded that the load carrying capacity of the intermittent bolted connections depends on:

1) The bond strength between the dowel bolts (plates) and the concrete, and,

2) The level of restraint in the steel plates in tension.

Also, models M3 and M4 behaved monolithically but model M4 was observed to be more ductile than model M3 as shown in Figure 5.64.

5.5 Theoretical Study of Load Carrying Capacity of MTC Connections

5.5.1 Punching Shear Capacity

Punching shear capacity of M1 and M2 were calculated using different North American codes [AASHTO-LRFD (1998), ACI (2002), CHBDC (2000)] and the General punching equation given by Tsui et al. (1986), whitt et al. (1993) and Kim et al. (1994). The AASHTO-LRFD and ACI punching shear equations are the same. In the General punching shear equation, a 38° value is used for the angle of failure plane with horizontal surface, which was proposed by Tsui et al. (1986), in calculation of punching shear capacity.

The punching shear equations as described above and used in this study are presented in SI units as follows:

5.5.1.1 AASHTO and ACI Punching Shear Equation

$$V_c = \left(0.17 + \frac{0.33}{\beta_c}\right)\sqrt{f_c'} \, b_0 d \dots\dots\dots\dots\dots\dots\dots\dots\dots\dots\dots(5.1)$$

Where:

V_c = Punching-shear capacity, N

β_c = Ratio of short side to long side of concentrated load or reaction area

f_c' = Specified compressive strength of concrete, MPa

b_0 = The perimeter of the critical section for slabs and footing, mm

d = Average effective depth of section, mm

61

5.5.1.2 CHBDC Shear Resistance Equation

$$V_r = \phi_c f_{cr} b_0 d \quad \dots\dots\dots\dots\dots\dots\dots\dots\dots\dots\dots\dots\dots\dots\dots\dots\dots\dots\dots(5.2)$$

$$f_{cr} = 0.4\sqrt{f_c'} \quad \text{for normal density of concrete} \dots\dots\dots\dots\dots\dots\dots\dots\dots\dots\dots(5.3)$$

Where:

$V_r =$ Factored shear resistance, N

$\phi_c =$ The resistance factor for concrete

$f_c' =$ Specified compressive strength of concrete, MPa

$b_0 =$ The perimeter of the critical section for slabs and footing, mm

$d =$ Average effective depth of section, mm

$f_{cr} =$ The cracking strength of concrete, MPa

5.5.1.3   General Punching Shear Equation

$$V_c = 2\left(b_1 + b_2 + \frac{2d}{\tan\theta} \right)\frac{d}{\tan\theta} f_t \quad \dots\dots\dots\dots\dots\dots\dots\dots\dots\dots\dots\dots\dots(5.4)$$

$$f_t = \left(0.17 + \frac{0.33}{\beta_c} \right)\sqrt{f_c'} \quad \dots\dots\dots\dots\dots\dots\dots\dots\dots\dots\dots\dots\dots\dots(5.5)$$

Where:

$V_c =$ Punching shear capacity, N

$b_1 =$ Short side of concentrated load or reaction area, mm

b_2 = Long side of concentrated load or reaction area, mm

d = Effective depth of section, mm

θ = Acute angle between the horizontal and the assumed failure plane

f_t = Diagonal tensile strength of concrete, MPa

β_c = Ratio of short side to long side of concentrated load or reaction area

f_c' = Specified compressive strength of concrete, MPa

It should be noted that the nominal shear capacity was calculated by setting the value of the resistance factor ϕ_c = 1.0. Also, the average compressive strength of the concrete in the joint from different cylinders and the effective depth of the joint, which is different from depth of deck slab, were used to get the lower bound values. The following are the parameters used in the calculation of the punching shear:

For model M1, the partial-depth connection,

f_c' = Average compressive strength values for joint, MPa

$d = 132.5$ mm

$\beta_c = \dfrac{250}{250} = 1$

$b_0 = 2(250 + 250 + 2 \times 132.5) = 1530$ mm

$b_1 = 250$ mm

$b_2 = 250$ mm

$\theta = 38°$

For model M2, the full-depth connection,

f_c' = Average compressive strength values for joint, MPa

$d = 225$ mm

$$\beta_c = \frac{250}{250} = 1$$

$b_0 = 2(250 + 250 + 2 \times 225) = 1900$ mm

$b_1 = \quad 250$ mm

$b_2 = \quad 250$ mm

$\theta = \quad 38°$

Table 5.3 shows the values of the punching shear capacity of model M1 and M2. As shown in this table, the experimental ultimate capacity of model M1 and M2 was far less than the ultimate punching shear capacity calculated using AASHTO-LRFD, CHBDC 2000, and General punching shear equations.

5.5.2   Flexural Strength Using Yield-Line Theory

The method for the limit analysis of reinforced concrete slabs known as Yield Line theory was considered in this study. This method is an upper bound approach [MacGregor and Barlett (2000), Park and Gamble (1980)] to determine the collapse load of reinforced concrete slabs. In this method, the ultimate load of the slab system is estimated by postulating a collapse mechanism compatible with the boundary conditions. The moments at the plastic hinge lines are the ultimate moments of the resistance of the sections, and the ultimate load is determined using the principle of the virtual work or the equation of the equilibrium.

To find out the ultimate concentrated load (P_u) for the models M1 and M2 using Yield Line theory, the experimental crack pattern was observed for each model and yield lines were approximated as shown in Figure 5.17. Boundary conditions for the models were selected based on the cracking patterns. The Canadian Standard CSA.A.23.3 (1994) was used to calculate the moment capacity of the sections at different locations. Internal and external work done were calculated for each model and equated with each other to get he value of the collapse load, P_u, on the bridge deck slab.

Following are the equations used in calculation of the moments for the Yield Line theory.

$$\alpha = \frac{A_s f_y}{\alpha_1 f_c' b} \quad \text{..(5.6)}$$

$$\alpha_1 = 0.85 - 0.0015 f_c' \geq 0.67 \quad \text{.................................. (5.7)}$$

$$M_n = A_s f_y \left(d - \frac{a}{2} \right) \quad \text{..(5.8)}$$

Where:

α = Depth of equivalent rectangular stress block, mm

A_s = Tensile reinforcement area per unit width, mm²/m

f_y = Specified yield strength of the reinforcement, MPa

α_1 = Constant

f_c' = Average compressive strength of concrete, MPa

b = Unit width of section, mm

M_n = Nominal moment of resistance of the section, N·mm

d = Effective depth of the section, mm

Also, following are the parameters used in calculation of the moments for Yield Line theory:

f_c' = Average compressive strength of concrete from Table A.8 and A.9, MPa

A_s = 667 mm²/m

f_y = 400 MPa

b = 1000 mm

d = 132.5 mm for positive moment (+) at joint

d = 177.5 mm for positive moment (+) at deck slab

d = 147.5 mm for negative moment (-) at support

Table 5.4 shows the ultimate load capacity (P_u) for flexure failure for models M1 and M2 using the Yield Line theory. The flexural capacity of the models with full depth deck slab by neglecting the presence of the joint was also calculated for model M1 and M2 and summarized in Table 5.5. To calculate flexure capacity of the model with full depth deck slab, two types of failure pattern were selected, as shown in Figure 5.19, and named case I and case II, and the equations for these patterns were taken from Park and Gamble (1980), which were derived using the virtual work method. The equations used are as follows:

$$P_u = \frac{4M_u b}{l} \quad \text{for case I} \quad \dots\dots\dots\dots\dots\dots\dots\dots\dots\dots\dots\dots\dots\dots\dots\dots\dots\dots\dots(5.9)$$

$$P_u = 8M_u \quad \text{for case II} \dots\dots\dots\dots\dots\dots\dots\dots\dots(5.10)$$

Where

M_u = Positive moment capacity of section, N·mm or kN·m

l = Distance between two supports, mm or m

P_u = Ultimate concentrated load on deck slab, N or kN

Table 5.6 shows the comparison of the experimental ultimate load and theoretical load values using the yield line theory and the CHDBC punching equation. From the values shown in this table, it can be observed that in models M1 and M2, failure is governed by flexure instead of punching shear.

Table 5.7 shows the experimentally specified safe wheel load using CHBDC (2000) and AASHTO–LRFD (1998) specifications, respectively, while live load and dynamic load allowance (DLA) factors were applied to the experimental ultimate wheel load to obtain the experimental specified wheel load. Live load factors of 1.7 and 1.75 and DLA factors of 0.4 and 0.33 were used for CHBDC and AASHTO calculations, respectively. The ratio of the experimental wheel load to the specified is considered satisfactory when this value is greater than 1.0. This was the case for bridge models M1, M2 M3 and M4 for both CHBDC and AASHTO specifications.

5.6   Summary of Findings

The structural behavior of the bridge connections was examined experimentally and theoretically through yield-line method and punching-shear equations. Also, experimental wheel load capacity was compared with code specified wheel load. From the comparison

between the theoretical and experimental results in this chapter, the following conclusion can be drown:

1. Good agreement between the theoretical ultimate wheel load using the yield line method and experimental ultimate wheel load was found. This results support the reliability of using the yield line theory to predict the ultimate load of moment transferring connections of the bridge.

2. Flexure failure governs in all models with moment transferring connection other than punching shear failure.

3. Ultimate load carrying capacity of the moment transferring joint depends on:
   (1)   Profile of the connection;
   (2)   Reinforcement details at joint; and
   (3)   Effective depth of the deck at joint.

4. For intermittent bolted connections, capacity of the connection depends on the thickness of the steel plate, length of the stud embedded in the concrete and distance of the connection from the edge.

Chapter 6

Conclusions and Recommendations

6.1 General

In this research project, experimental and theoretical studies were conducted to investigate the behavior of the precast/prestressed concrete Deck-Bulb-Tee (DBT) bridge girder system under monotonic loading on both moment-transferring-connections (MTC) or intermittent-bolted-connections (IBC).

A literature review was conducted in order to establish the foundation for this study. It was observed that there is a lack of information regarding precast bridge connections. Only a few researchers have conducted studies to develop flange-to-flange connections in double tee girders. The current design practice in North American has no specific recommendations on the analysis and design of these types of connections in bridge girders.

A practical and simplified design process is desirable for such bridge deck connections. Four full-scale bridge models, representing two moment transferring connections (models M1 and M2), and other two intermittent bolted connections (models M3 and M4), were constructed and tested up-to-collapse under concentric vertical loading. The experimental specified wheel load capacity was compared with CHBDC (2000) and AASHTO-LRFD (1998) specified wheel load.

6.2 Conclusions

The most important conclusions drawn from the theoretical and experimental results in this study are summarized below. They are presented in the following two aspects: (i) failure mode of specimens; and, (ii) factors affecting the load carrying capacity of connections.

1. The failure mode of bridge models M1 and M2 was due to flexure, while, for bridge models M3 and M4, the connections failed as a result of local bond failure between concrete and the dowel bolts holding the connection steel plates. None of the models failed due to punching shear of the bridge deck.

2. The failure mode of the intermittent bolted connection depends on the position of the connection from the edge of the specimens and the length of the stud embedded in the concrete.

3. The ultimate capacity of the moment transferring connection depends on the profile at the joint connection and reinforcement details in the joint. Ultimate load capacity of M2, the full-depth connection, was 25% higher than that of M1, the partial-depth connection.

4. The ultimate capacity of the intermittent bolted connection depends on the bond strength between the dowel bolts (plates) and the concrete slab, considering that the steel plate connector is rigid enough. The ultimate load capacity of M4 was 24%

higher than that of M3, due to adding a steel plate at the end of dowel bolts to embed into the deck slab.

5. Design of moment transferring connections can be done safely by using yield-line theory for the slab, ignoring capacity of the bridge deck slab due to arching action.

6. Due to arching action, the load carrying capacity of the moment transferring connections increased, but due to less-section at the joint of deck slab for M1, connections failed in flexure before they reached to the ultimate punching shear capacity.

7. All of the proposed models satisfied the CHBDC wheel load requirements of 87.5 kN.

8. All of the proposed models also satisfied the AASHTO wheel load requirements of 72.5 kN.

6.3 Significance of Research

The tested bridge models represent one panel of a typical bridge prototype, with girder spacing of 1.8 m and deck slab thickness of 225 mm. The results from this experimental testing of these bridge models can be applied with confidence to the design of multi-girder bridge prototypes with cross-sections shown in Figures 1.1 and 1.2, given the following comments:

1. In bridge prototypes shown in Figures 1.1 and 1.2, the presence of more than two bulb tee girders would increase the rotational restraints of the girders close to the wheel load location and thus, increase the load carrying capacity of the deck slab loaded locally.

2. The presence of more than two bulb tee girders as shown in Figures 1.1 and 1.2 would significantly enhance the load distribution characteristic in such a way that they will assist in resisting the wheel load located locally over the deck slab connection.

3. Bridge prototypes are expected to have transverse diaphragms at the abutments and piers as well as at intermediate locations between the support lines. This would enhance girder rotational restraints against local deck slab deformation, magnify arching action effects and force the deck slab to fail due to punching shear rather than flexure.

4. The experimental simulated wheel load was applied over a surface area of 250 × 250 mm as specified in the CHBDC. However, the presence of the wearing surface of approximately 75 mm thickness would increase the dispersion area of the wheel load, thus increasing the load carrying of the deck slab at the joint location.

5. In case of the intermittent bolted connections tested in the laboratory, only two intermittent bolted connections were considered. However, numerous connectors are used to connect the girders. This would allow the wheel load to be shared by

more than two connectors in the longitudinal direction of the bridge, thus, increase the connection load carrying capacity more than those obtained experimentally.

6. In case of the moment transferring connections, the length of the girder in the bridge models was 2 m, making the aspect ratio of the deck slab slightly more than 2. However, in bridge prototype, the slab aspect ratio is large enough to make the wheel load transferred to the nearest girder webs over longer length.

7. The quality of the casting in the laboratory is very much similar to that in the fabrication plant, on which a controlled environment is maintained.

8. In bridge models, the joints were filled with concrete material of the same strength as that of the deck slab. In practice, non-shrink rapid-set grout will be used to reduce curing time for the joint. It is expected that the strength of the grout be higher than, or at least the same as, that of the concrete deck slab.

6.4 Recommendations of the Future Research

It is recommended that further research efforts be directed towards the following aspects:

1. The experimental study of multi-load behavior on these connections can be done on full-scale bridge models to obtain the distribution of load through connections using CHBDC and AASHTO truck loading.

2. Simplified method of connection design in terms of mathematical formula can be developed.

3. Theoretical study of these connections using Finite Element Method (FEM) can be done.

4. Fatigue study of these connections can be done on full-scale connection models.

5. New connection types can be developed and tested using stainless steel dowels.

REFERENCES

1. AASHTO, 1998, "LRFD Bridge Design Specifications", 2nd Ed., American Association of State Highway and Transportation Officials, Washington, D. C., USA.

2. Abendroth, R. E., 1995, "Nominal Strength of Composite Prestressed Concrete Bridge Deck Panels", Journal of Structural Engineering, ASCE, Vol. 121, No. 2, pp. 307-318.

3. ACI, 2002, "Building Code Requirements for Reinforced Concrete (ACI 318-89) (Revised 1992) and Commentary- ACI 318R-89 (Revised 1992)", American Concrete Institute, Detroit, Michigan, USA.

4. ACI Report, 1992, "State-of-the-Art Report on Bond Under Cyclic Loads", ACI 408.2R-92 (Reapproved 1999), Reported by ACI Committee 408.

5. ACI Report, 1992, "Considerations for Design of Concrete Structures Subjected to Fatigue Loading", ACI 215-74 (Revised 1992/Reapproved 1997), Reported by ACI Committee 215.

6. Aidoo, J., Harries, K. A., and Petrou, M. F., 2004, "Fatigue Behavior of Carbon Fiber Reinforced Polymer-Strengthened Reinforced Concrete Bridge Girders", Journal of Composites for Construction, ASCE/November/December 2004, pp 501-509.

7. Anderson, A. R., 1957, "How Beam Design Affects Prestressed Concrete Bridge Costs", Eng. News-Record, October, pp. 326-328.

8. Anderson, A. R., 1971, "Lateral Stability of Long Prestressed Concrete Beams", PCI Journal, Vol. 16, No. 3, pp. 7-9.

9. Anderson, A. R., 1972, "Systems Concepts for Precast Prestressed Concrete Bridge Construction", Special Report 132, Highway Research Board, Washington, DC, PP. 9-21.

10. Applied Technology Council, 1981, "Proceedings of a Workshop on Design of Prefabricated Concrete Buildings for Earthquake Loads", ATC-8, Applied Technology Council, Berkeley, California.

11. Arockiasamy, M., Badve, A. P., Rao, B. V. and Reddy, D. V., 1991, "Fatigue Strength of Joints in a Precast Prestressed Concrete Double Tee Bridge", PCI Journal, Vol. 36, No. 1, pp. 84-96.

12. ASTM, 2003, "ASTM Standards", American Society for Testing and Materials", West Conshohocken, PA, USA.

13. Azad, A. K., Baluch, M. H., Abbasi, M. S. A. and Kareem, K., 1994, "Punching Capacity of Deck Slabs in Girder-Slab Bridges", ACI Structural Journal, Vol. 91, No. 6, pp. 656-662.

14. Bakht, B., 1996, "Revisiting Arching in Deck Slabs", Canadian Journal of Civil Engineering, Vol. 23, No. 4, pp. 973–981.

15. Bakht, B. and Mufti, A. A., 1996, "Arching in Deck Slabs", Journal of the Institute of Engineers (India), Vol. 77, pp. 123–128.

16. Bakht, B. and Lam, C., 2000, "Behavior of Transverse Confining System for Steel-Free Deck Slabs", Journal of Bridge Engineering, ASCE, Vol. 5, No. 2, 2000, pp. 139-147.

17. Bakht, B. and Mufti, A. A., 2001, "Load Distribution in Shear-Connected Concrete Plank Bridges", 29th Annual Conference of the Canadian Society for Civil Engineering, Victoria, British Columbia, Canada.

18. Braestrap, M. W. and Morley, C. T., 1980, "Dome Effect in R/C Slabs: Rigid Plastic Analysis", Journal of Structural Division, ASCE, Vol. 106, No. ST6, pp. 1255-1262.

19. Burns, N. H. and Centennial, Z., 2001, "Composite Action between Girder and Bridge Deck with Precast Panels", PCI Journal, Vol. 46, No. 1, pp. 85.

20. Byung Hwan Oh, 1991, "Fatigue-Life Distributions of Concrete for Various Stress Levels", ACI Material Journal, Vol. 88, No.2, pp. 122-128.

21. Canadian Standard Association, 2000, "Canadian Highway Bridge Design Code CAN/CSA-S6-00", CSA International, Toronto, Ontario, Canada.

22. Canadian Standard Association, 2000, "Commentary on the Canadian Highway Bridge Design Code", 1st edition, CSA International, Toronto, Ontario, Canada.

23. Canadian Standard Association, 1994, "Design of Concrete Structures (A23.3-94)", CSA International, Toronto, Ontario, Canada.

24. Curtis, R. B., 1967, "Single-T Bridges", PCI Journal, Vol. 12, No. 2, pp. 76-81.

25. Dolan, C. W. and Pessiki, S. P., 1989, "Model Testing of Precast Concrete Connections", PCI Journal, Vol. 34, No. 2, pp. 84-103.

26. Fang, K. I., Worley, J., Burns, N. H. and Klinger, R. E., 1990, "Behavior of Isotropic Reinforced Concrete Bridge Decks on Steel Girders", Journal of Structural Engineering, ASCE, V.116, No. 3, pp. 659-678.

27. Gao, L., and Hsu, C.T.T. 1998, "Fatigue of Concrete under Uniaxial Compression Cyclic Loading ", ACI Material Journal, Vol. 95, No. 5, pp575-581.

28. Geren, K. Y., and Tadros, M. K., 1994, "The NU Precast Prestressed Concrete Bridge I-Girder Series", PCI Journal, Vol. 39, No. 3, pp. 26-39.

29. Graddy, J. C., Kim, J., Whitt, J. H., Burns, N. H. and Klinger, R. E., 2002, "Punching-Shear Behavior of Bridge Decks under Fatigue Loading", ACI Structural Journal, V. 99, No. 3, pp. 257-266.

30. Hariatmadar, H., 1997, "Seismic Response of Connections in Precast Concrete Double Tees", PhD Dissertation, Department of Civil Engineering, McGill University, Quebec, Canada.

31. Hewitt, B E., and Batchelor, B., 1975, "Punching Shear Strength of Restraint Slabs", Journal of Structural Engineering, ASCE, Vol. 101, No. ST9, pp. 1837-1853.

32. Hofheins, C. L., Reaveley, L. D. and Pantelides, C. P., 2002, "Behavior of Welded Plate Connections in Precast Concrete Panels under Simulated Seismic Loads", PCI journal, Vol. 47, No. 4, pp. 122-133.

33. Jennifer Hallowell Gross, Richard E. Klingner, and Herman L. Graves, III, 2001, "Dynamic Behavior of Single and Double Near-Edge Anchors Loaded in Shear", ACI Structural Journal, Vol. 98, No. 5, P665-676.

34. Jiang, D. H., and Shen, J. H., 1986, "Strength of Concrete Slabs in Punching Shear", Journal of Structural Engineering, ASCE, Vol. 112, No. 12, pp. 2578-2591.

35. Khanna, O. S., Mufti, A. A. and Bakht, B., 2000, "Experimental Investigation of the Role of Reinforcement in the Strength of Concrete Deck Slabs", Canadian Journal of Civil Engineering, Vol. 27, No. 3, pp. 475-480.

36. Kim, J., Burns, N. H. and Kingner, R. E., 1994, "Factors Affecting the Design Thickness of Bridge Slabs: Results of Static and Fatigue Test", Research Report 1305-2, Center for Transportation Research, University of Texas at Austin, Austin, Texas, USA.

37. Kuang, J. S. and Morely, C. T., 1993, "Punching Shear Behavior of Restrained Reinforced Concrete Slabs", ACI Structural Journal, Vol. 89, No. 1, pp. 13-19.

38. Kwei, G. C. S., 1967, "Discussion of 'Single T-Beam Bridges,' by R. B. Curtis", PCI Journal, Vol. 12, No. 5, pp. 82-83.

39. MacGregor, J. G. and Bartlett, F. M., 2000, "Reinforced Concrete: Mechanics and Design", 1st Canadian ed., Prentice-Hall Inc., Scarborough, Ontario, Canada.

40. Maekawa, K., and El-Kashif, K. F., 2004, "Cyclic Cumulative Damaging of Reinforced Concrete in Post-Peak Regions", Journal of Advanced Concreet Technology, Vol. 2, No.2, P257-271.

41. McKeel, W. T., 2002, "Bridge Maintenance and Management: A Look to the Future", A3C06: Committee on Structures Maintenance and Management, Transportation Research Board, National Research Council, Washington, D.C., USA.

42. Mor, A., Gerwick, B. C., and Hester, W. T., 1992, "Fatigue of High-Strength Reinforced Concrete", ACI Material Journal, Vol. 89, No. 2, pp 197-207.

43. Mufti, A. A., and Newhook, J. P., 1998, "Punching Shear Strength of Restrained Concrete Bridge Deck Slabs", ACI Structural Journal, Vol. 95, No. 4, pp. 375–381.

44. Mufti, A., Jaeger, L., Bakht, B. and Wegner, L., 1993, "Experimental Investigation of Fiber-Reinforced Concrete Deck Slabs Without Internal Steel Reinforcement", Canadian Journal of Civil Engineering, Vol. 20, pp. 398-406.

45. Newhook, J. and Mufti, A., 1996, "A Reinforcing Steel-Free Concrete Deck Slab for the Salmon River Bridge", Concrete International, Vol. 18, No. 6, pp. 30-34.

46. OHBDC, 1992, "Ontario Highway Bridge Design Code", 3rd ed., Ministry of Transportation of Ontario, Downsview, Ontario, Canada.

47. Park, R. and Gamble, W. L., 1980, "Reinforced Concrete Slabs", John Wiley & Sons, Inc., New York, USA.

48. Patric J. H., Marie_anne Erki, and david L. D., 2004, "Stress Redistribution in Cyclically Loaded Reinforced Concrete Beams", ACI Structural Journal, Vol. 101, No.2, P261-268.

49. PCI Committee on Connection Details, 1995, "Addendum to Design and Typical Details of Connections for Precast and Prestressed Concrete", PCI journal, Vol. 40, No. 5, pp. 46-57.

50. PCI Committee on Connection Details, 1998, "Standard Precast Connections", PCI Journal, Vol. 43, No. 4, pp. 42-58.

51. Petrou, M. F. and Perdikaris, P. C., 1996, "Punching Shear Failure in Concrete Decks as Snap-Through Instability", Journal of Structural Engineering, ASCE, Vol. 122, No. 9, pp. 998-1005.

52. Pincheira, J. A., Oliva, M. G. and Kusumo-Rahardjo, F. I., 1998, "Tests on Double Tee Flange Connectors Subjected to Monotonic and Cyclic Loading", PCI Journal, Vol. 43, No. 3, pp. 82-96.

53. Ralls, M. L., Medlock, R. D., Slagle, S., 2002, "Prefabricated Bridge National Implementation Inititive", Concrete Bridge Conference.

54. Rodriguez, M., Lotze, D., Gross, J. H., Zhang, Y.G., Klingner, R. E., and Graves, H.L., III, 2001, "Dynamic Behavior of Tensile Anchors to Concrete", ACI Structural Journal, Vol. 98, No. 4, P511-524.

55. Roller, J. J., Russell, H. G., Bruce, R. N. and Martin, B. T., 1995, "Long-Term Performance of Prestressed, Pretensioned High Strength Concrete Bridge Girders", PCI journal, Vol. 40, No. 6, pp. 48-59.

56. Roper, N. J., 2002, "Prefabricated Bridge Elements and Systems", Virginia Department of Transportation, [Online]. Available: http://www.aashtotig.org/ focus_technologies/ prefab_elements/elements.stm.

57. Sawko, F. and Saha, G. P., 1967, "Ultimate Load Analysis of Bridge Decks", Building Science, Vol. 2, pp. 223-237, Pergamon press, Printed in Great Britain

58. Shah, B., 2004, "Experimental Study on Prefabricated Concrete Bridge Girder-to-Girder Connections", Thesis Report, Ryerson University, pp1-82.

59. Shahaway, M. E., 1990, "Feasibility Study of Transversely Prestressed Double-T Bridges", PCI Journal, Vol. 35, No. 5, pp. 56-69.

60. Shahaway, M. E., and Issa, M., 1992, "Load Testing of Transversely Prestressed Double-T Bridges, "PCI Journal, Vol. 37, No. 2, pp. 86-99.

61. Shi, X. P., Fwa, T. F. And Tan, S.A. 1993, "Flexural Fatigue Strength of Plain Concrete", ACI Material Journal, Vol. 90, No. 5, pp 435-440

62. Soudki, K. A., West, J. S., Rizkalla, S. H. and Blackett, B., 1996, "Horizontal Connections for Precast Concrete Shear Wall Panels under Cyclic Shear Loading", PCI Journal, Vol. 41, No. 3, pp. 64-80.

63. Stefanou, D., 1993, "Punching Shear Resistance of Prestressed Concrete Slab", Engineering Fracture Mechanics, Vol. 44, No. 1, pp. 137-153, Printed in Great Britain

64. Sucuoglu, H., 1995, "Effect of Connection Rigidity on Seismic Response of Precast Concrete Frames", PCI Journal, Vol. 40, No. 1, pp 94-103.

65. Sun, W., Gao, J.,and Yan, Y., 1996, "Study of the Fatigue Performance and Damage Mechanism of Steel Fiber Reinforced Concrete ", ACI Material Journal, Vol. 93, No. 3, pp. 206-212.

66. Tadros, M. K., Badie, S. S. and Kamel, M. R., 2002, "Girder/Deck Connection for Rapid Removal of Bridge Decks", PCI journal, Vol. 47, No. 3, pp. 58-68.

67. Todorka P., and Kristian M., 1997, "Low-cycle Fatigue of Plain and Fiber-Reinforced Concrete ", ACI Material Journal, Vol. 94, No. 4, pp273-285

68. Tsui, C. K. T, Burns, N. H. and Klingner, R. E., 1986, "Behavior of Ontario-Type Bridge Decks on Steel Girders: Negative Moment Region and Load Capacity", Research Report 350-3, Center for Transportation Research, University of Texas at Austin, Austin, Texas, USA.

69. Whitt, J., Kim, J., Burns, N. H. and Klingner, R. E., 1993, "Factors Affecting the Design Thickness of Bridge Slabs: Test Setup", Research Report 1305-1, Center for Transportation Research, University of Texas at Austin, Austin, Texas, USA.

70. Shi, X. P., Fwa, T. F. And Tan, S.A. 1993, "Flexural Fatigue Strength of Plain Concrete", ACI Material Journal, Vol. 90, No. 5, pp 435-440

71. Yamane, T., Tadros, M. K., Badie, S. S. and Baishya, M. C., 1998, "Full Depth Precast, Prestressed Concrete Bridge Deck System", PCI journal, Vol. 43, No. 3, pp. 50-66.

72. Yasuo K., Amjad J. A., and George C. Lee, 2004, "Static and Fatigue Testing of Hybrid Fiber-Reinforced Polymer-Concrete Bridge Superstructure", Journal of Composites for Construction, Vol. 8, No.2, pp182-190.

Table 4.1- Description of Tested Models

Model	Symbols	Description of Symbols
M1	MTC-1-C	Moment-Transferring-Connection No-1 with concentric loading
M2	MTC-2-C	Moment-Transferring-Connection No-2 with concentric loading
M3	IBC-1-C-B	Intermittent-Bolted-Connection No-1 with concentric loading, Located between the pockets
M4	IBC-2-C-B	Intermittent-Bolted-Connection No-2 with concentric loading, Located between the pockets

Table 5.1 Cracking and Ultimate Load Values for Model M1 and M2

Model	Description	Cracking Load (At Side) (kN)	Cracking Load (At Bottom) (kN)	Ultimate Load (kN)	Remarks
M1	MTC-1-C	116	178	378	Partial–Depth Connection
M2	MTC-2-C	222	222	476	Full–Depth Connection

Table 5.2 Cracking and Ultimate Load Values for Model M3 and M4

Model	Description	Cracking Load At Side Corner (kN)	Bottom Cracking Load At Bottom (kN)	Ultimate Load (kN)
M3	IBC-1-C	89	133	215
M4	IBC-2-C	89	178	266

Table 5.3 Summary of Calculated Punching Shear Capacity of Models M1 and M2

Model	Description	Punching Shear Capacity			Remarks
		AASHTO and ACI Equation (kN)	CHBDC Equation (kN)	General Shear Equation (kN)	
M1	MTC-1-C	738	884	1040	
M2	MTC-2-C	1511	1209	2191	Full Depth of Deck Slab at Joint

Table 5.4 Ultimate Load Capacity of Models M1 and M2 using Yield Line Theory

Model	Description	Ultimate Load capacity Calculated by Yield Line Theory (kN)	Remarks
M1	MTC-1-C	411	
M2	MTC-2-C	561	Full Depth Deck Joint

Table 5.5 Ultimate Load Capacity for Full depth Deck Slab Using Yield Line Theory

Model	Description	Ultimate Load capacity Calculated by Yield Line Theory (kN)	
		Case (i)	Case (ii)
M1	MTC-1-C	229	372
M2	MTC-2-C	291	371

Table 5.6 Experimental Ultimate Load and Load Values Using Yield Line Theory and CHBDC Punching Equation

Model	Description	Ultimate Load (kN)			Failure Mode
		Experimental Value	Yield Line Theory	CHBDC Punching Shear Equation	
M1	MTC-1-C	378	411	884	Flexure
M2	MTC-2-C	476	561	1209	Flexure

Table 5.7 Ratio of the Experimental Specified Wheel Load to Code Specified Wheel Load

Model	Description	Experimental Ultimate Wheel Load (Pu) (kN)	CHBDC (2000)		AASHTO-LRFD (1998)	
			Experimental Specified Wheel Load= Pu/(1.7*1.4) (kN)	Ratio = Col. 4/87.5	Experimental Specified Wheel Load= Pu/(1.75*1.33) (kN)	Ratio = Col. 6/72.5
Col. 1	Col. 2	Col. 3	Col. 4	Col. 5	Col. 6	Col. 7
M1	MTC-1-C	378	159	1.82	162	2.24
M2	MTC-2-C	476	200	2.29	205	2.82
M3	IBC-1-C	215	90	1.03	92	1.27
M4	IBC-2-C	266	112	1.28	114	1.57
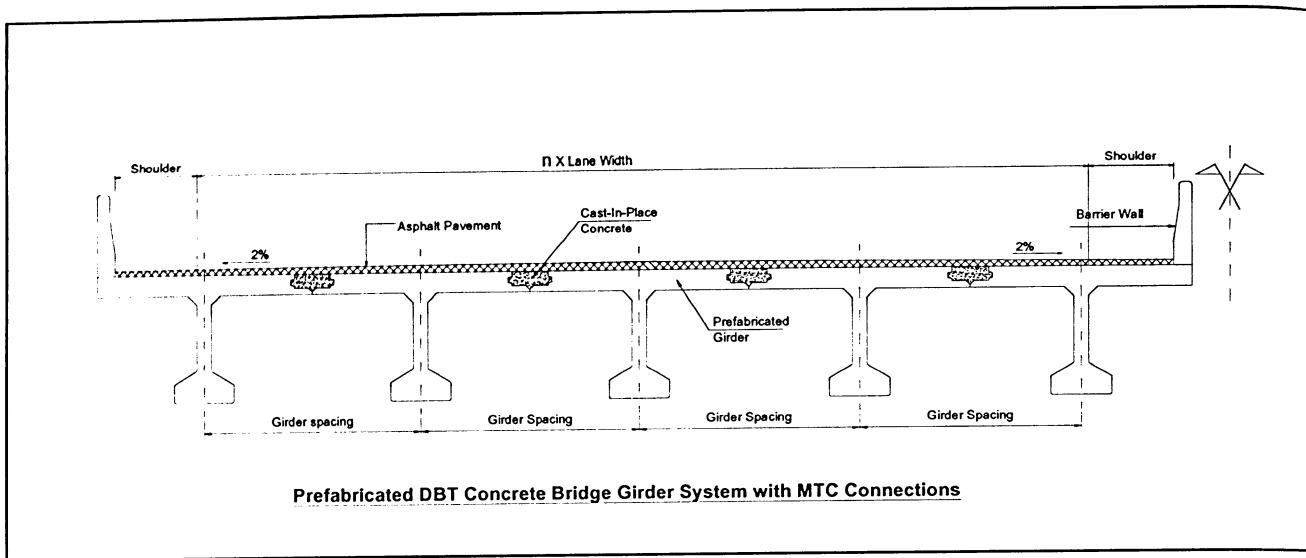
Figure 1.1 Cross-Section of Prefabricated DBT Bridge Girder System with MTC Connection
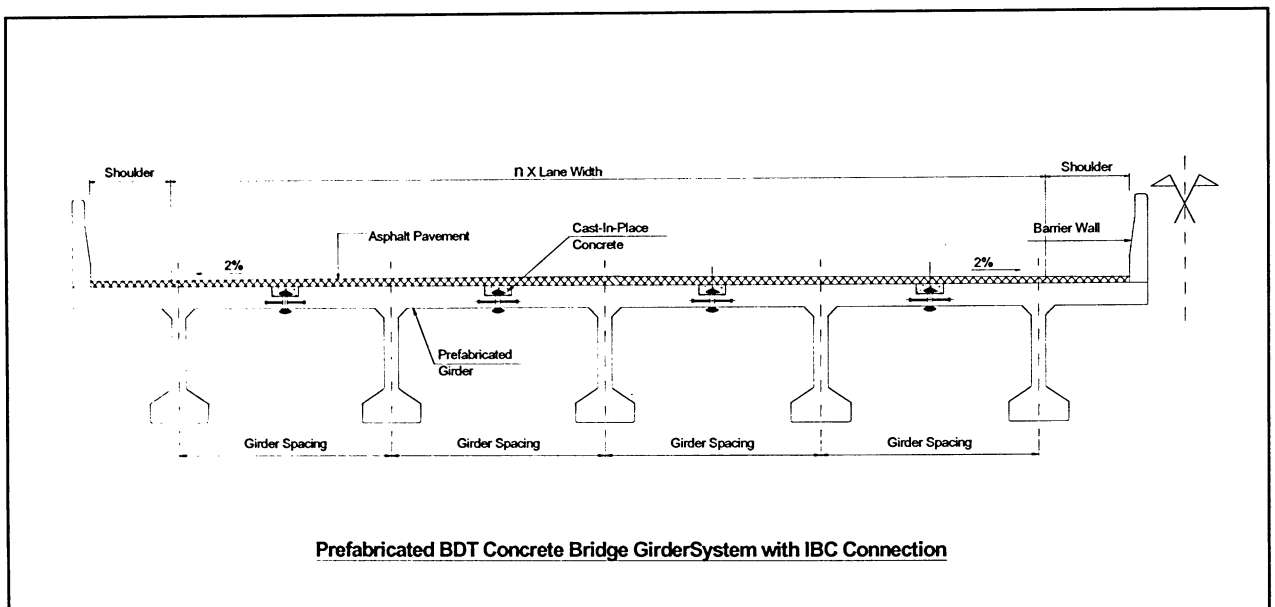
Figure 1.2 Cross-Section of Prefabricated DBT Bridge Girder System with IBC Connection
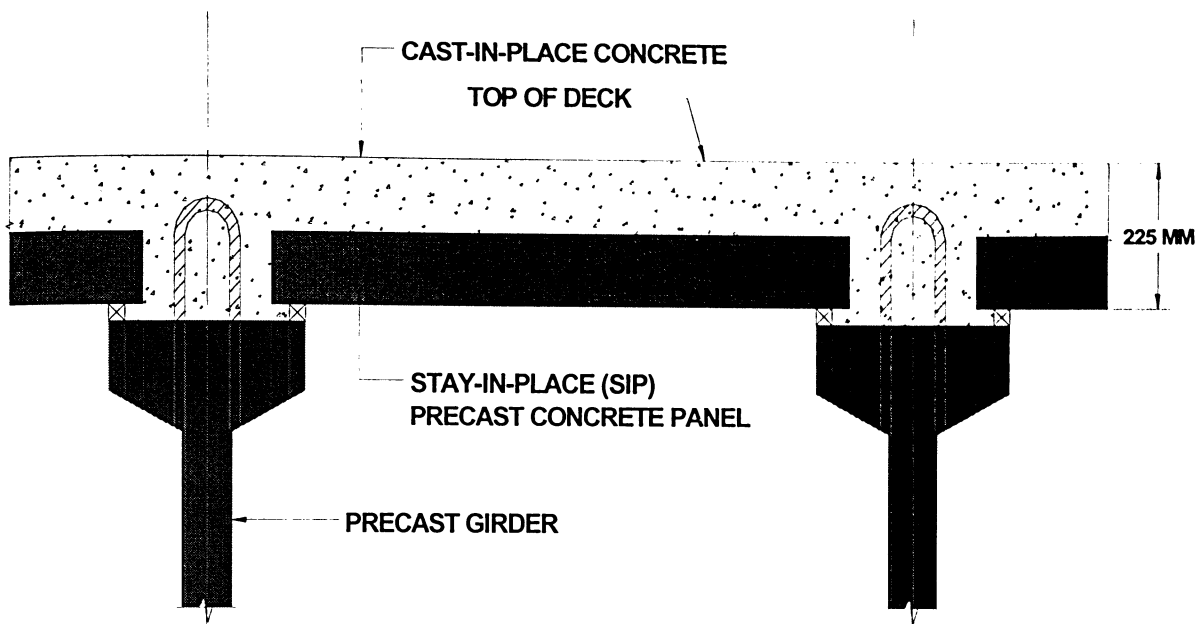
Figure 2.1 Partial-depth Prefabricated Bridge Deck Panels System
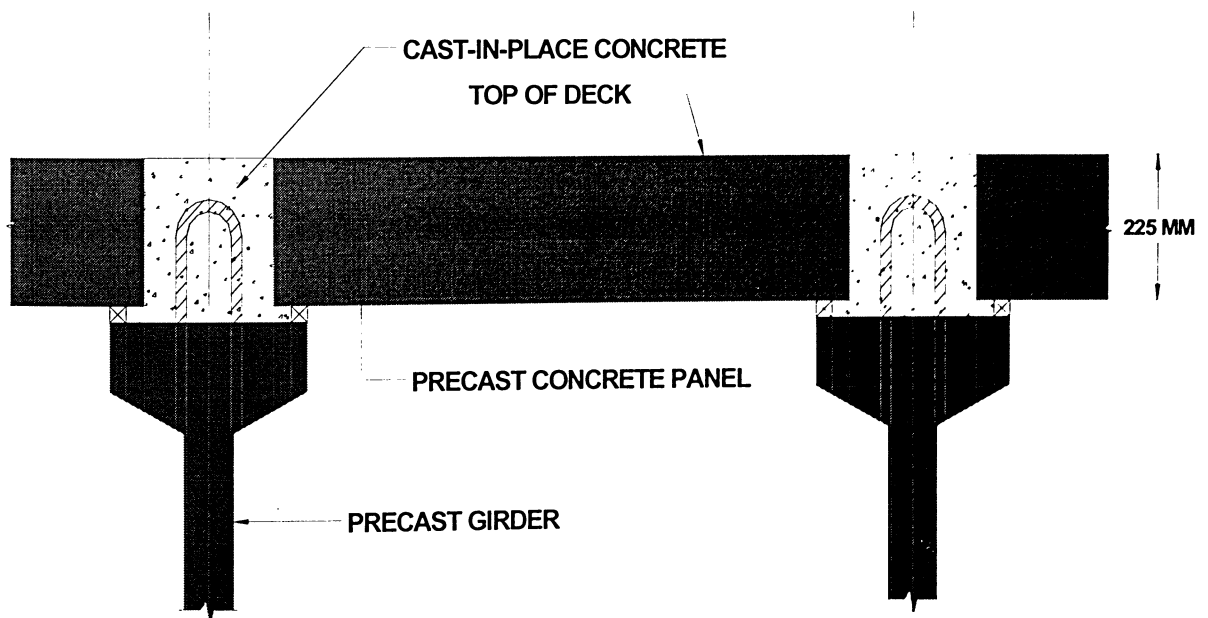
Figure 2.2 Full-depth Prefabricated Bridge Deck Panels System
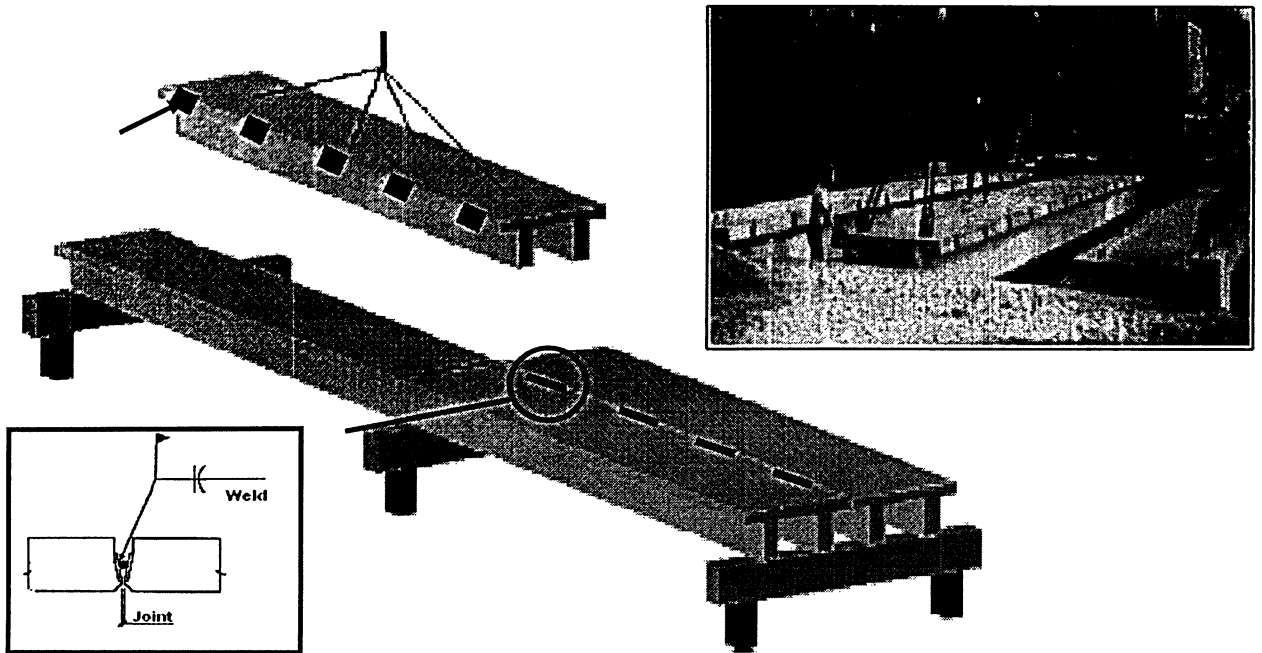
Figure 2.3 Double-Tee Girder Flange Connections [PCI (1995), (1998)]
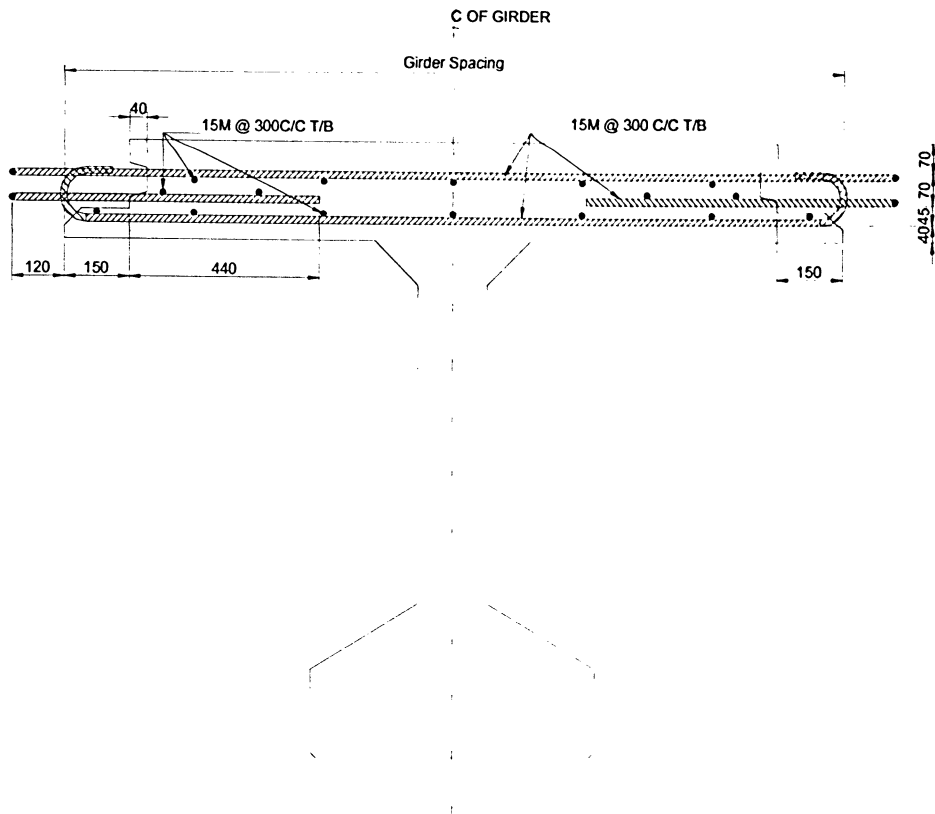
Figure 3.1 Cross-Section of the MTC-1 girder Connection with Structural Details
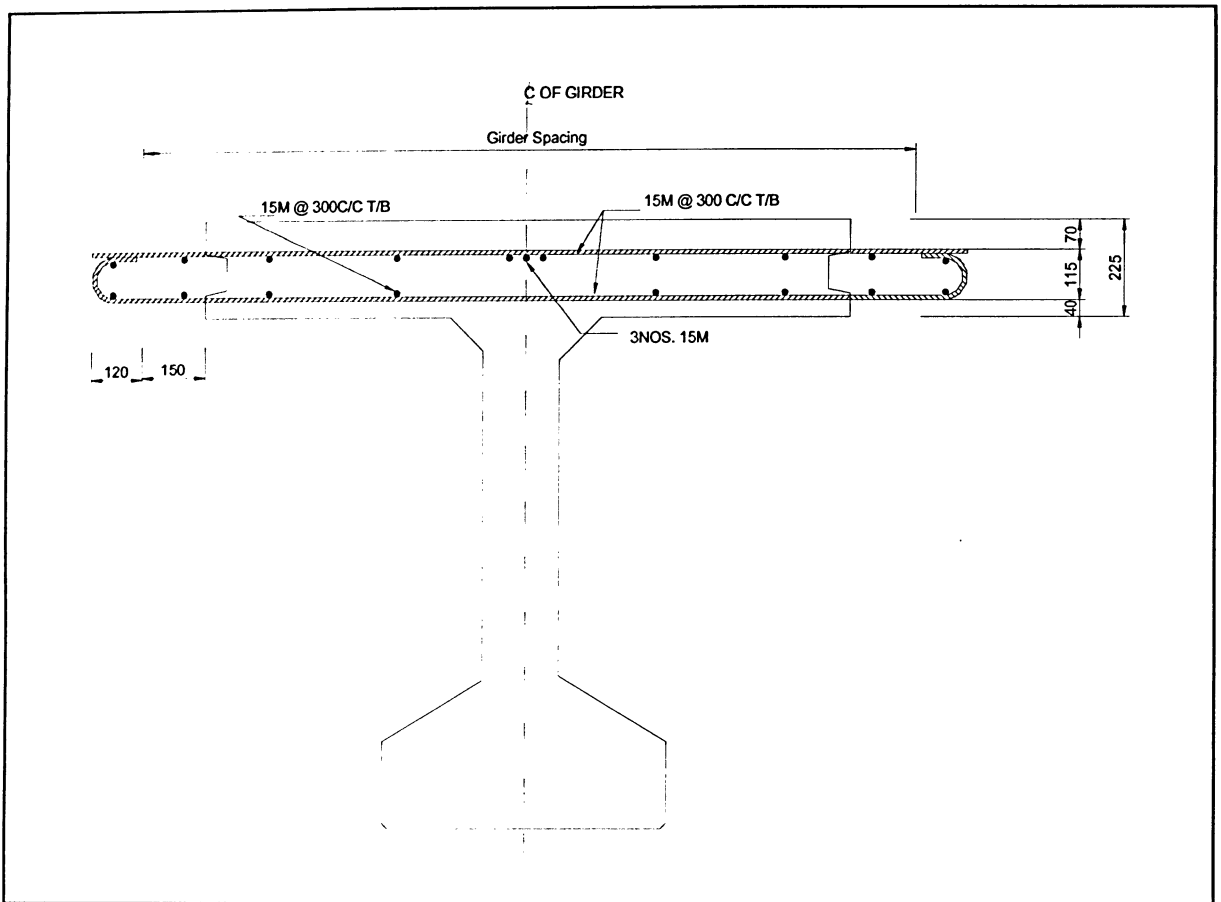
Figure 3.2 Cross-Section of the MTC-2 girder Connection with Structural Details
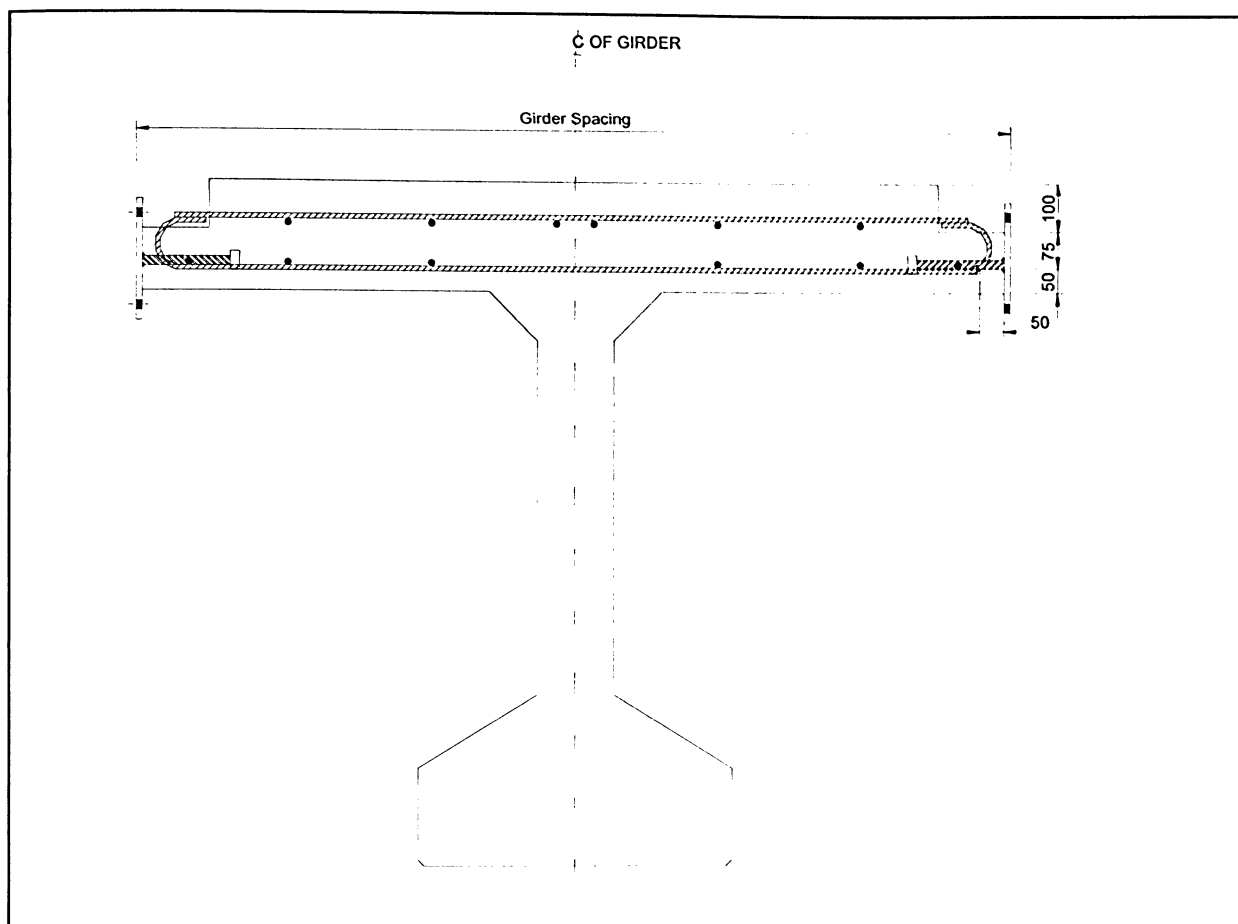
Figure 3.3 Cross-Section of the IBC-1 girder Connection with Structural Details
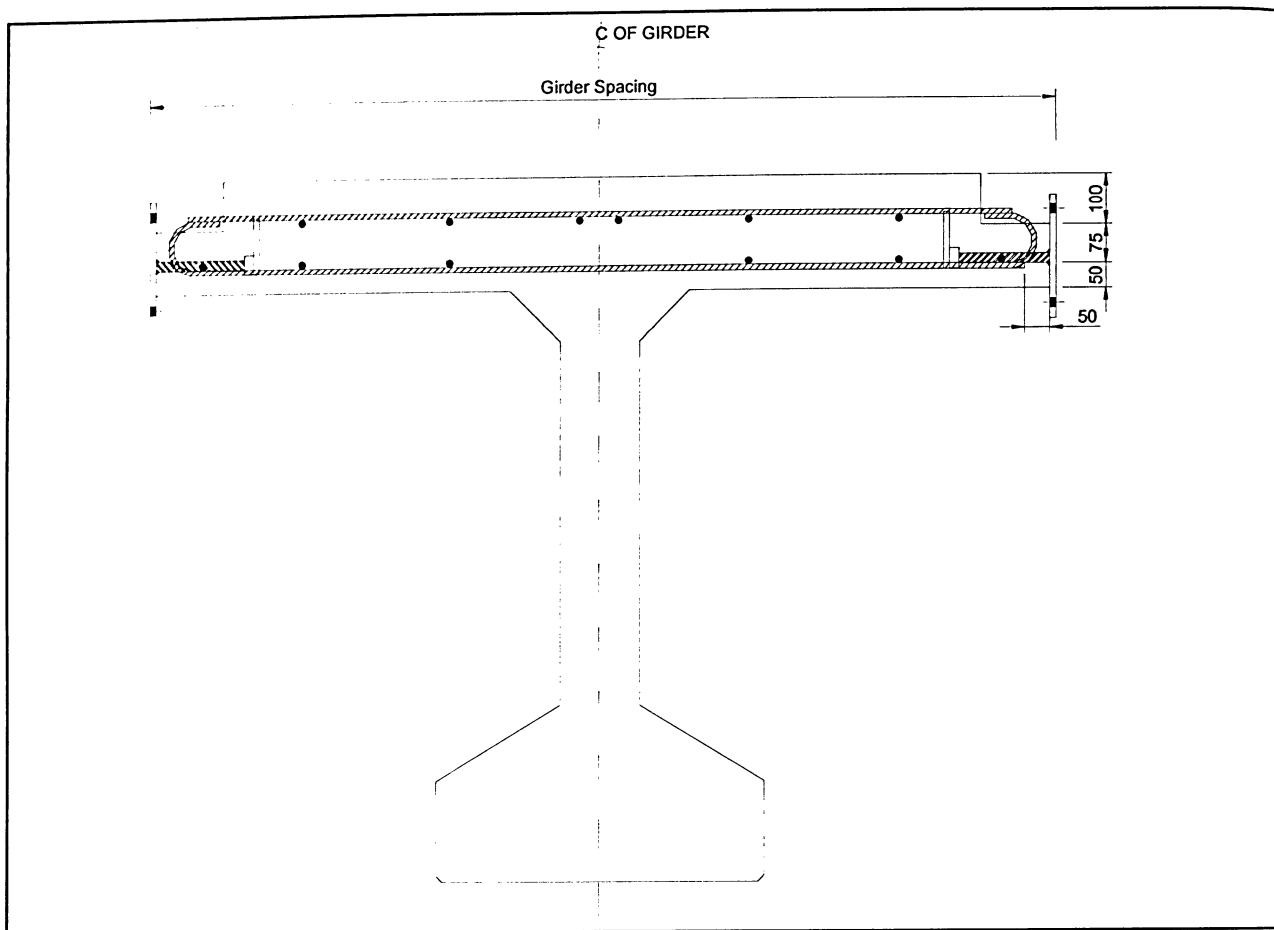
Figure 3.4 Cross-Section of the IBC-2 Girder Connection with Structural Details
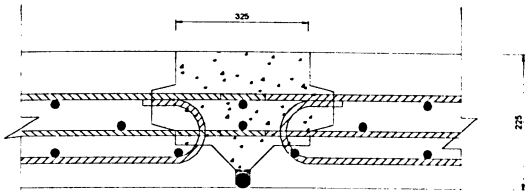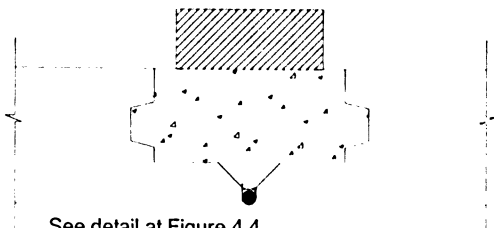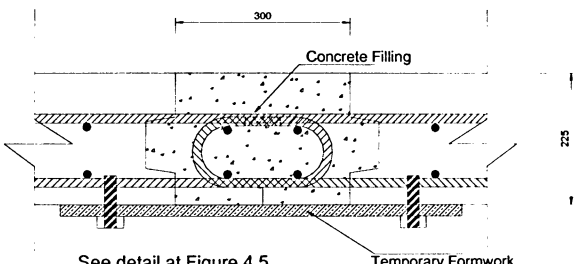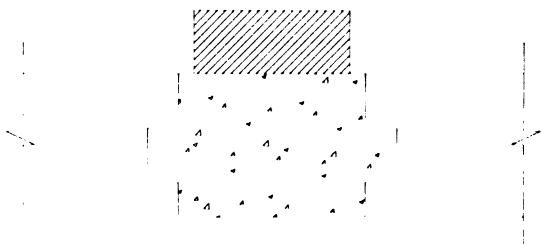
CONNECTION TYPE	LOADING TYPE
MODEL M1 – MTC-1-C	
See detail at Figure 4.3	See detail at Figure 4.4
MODEL M2 – MTC-2-C	
See detail at Figure 4.5 Temporary Formwork	See detail at Figure 4.6

Figure 4.1 Details of Moment Transferring Connections (MTC) For Models M1 and M2
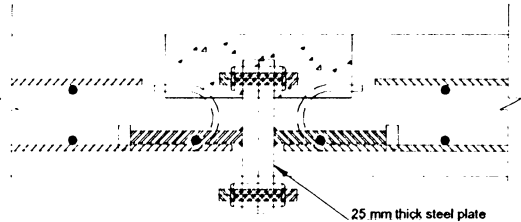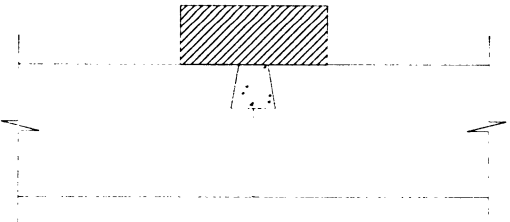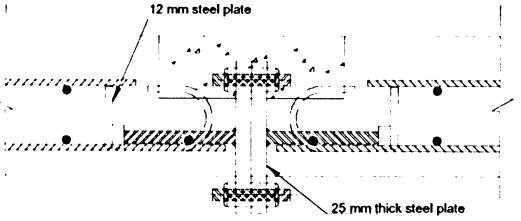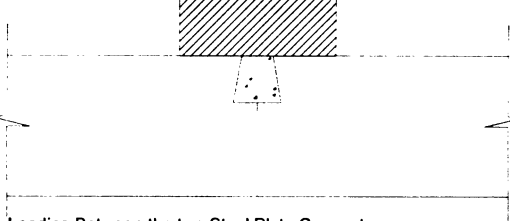
CONNECTION TYPE	LOADING TYPE
MODEL M3 – IBC-1-C	
 See detail at Figure 4.7 (e)	 Loading between the two steel plate connectors See detail at Figure 4.8
MODEL M4 – IBC-2-C	
 See detail at Figure 4.9 (e)	 Loading Between the two Steel Plate Connectors See detail at Figure 4.10

Figure 4.2 Details of the Intermittent Bolted Connections (IBC) Models M3 and M4

15M@300 C/C **15M@300 C/C** **15M@300 C/C**

100 · 200 · 300 · 300 · 300 · 300 · 150 150 150 150 · 300 · 300 · 300 · 300 · 200 · 100

250

100

B   B

A C   C   A

250

100

1800   1800

Note: All dimensions are in mm
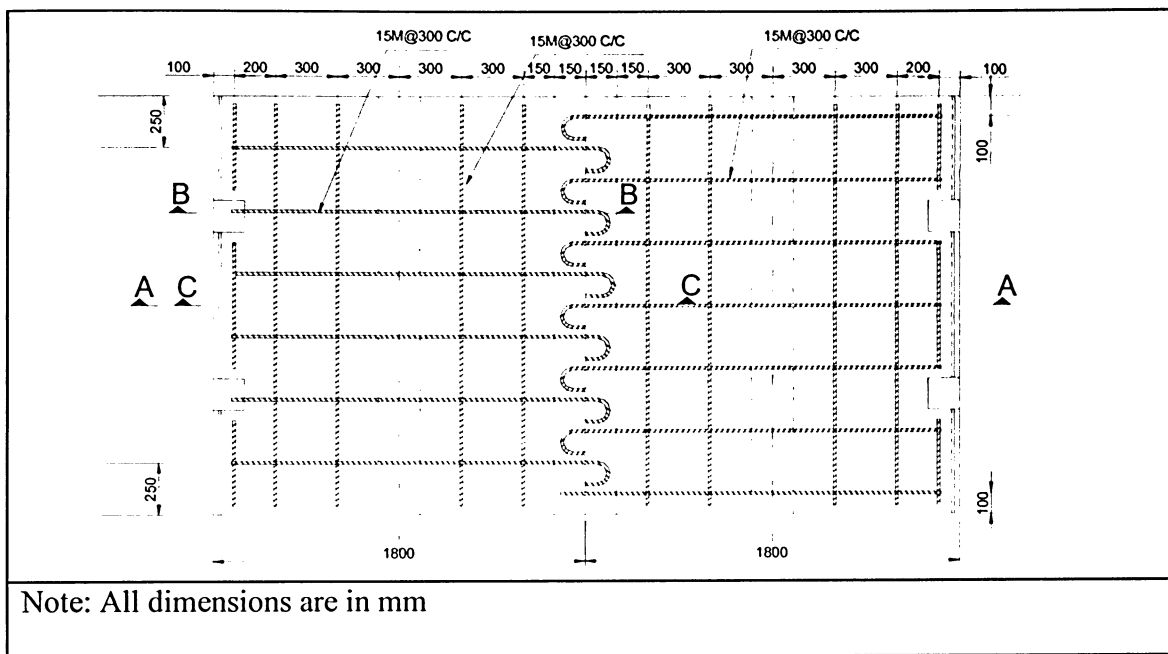
Figure 4.3 (a) Plan of Top Rebar Arrangement for Model M1

15M @300 C/C   **15M @300 C/C**

900   ·   450   · 260 · 190 · 190 · 260 ·   450   ·   900

250

100

B   B

A C   C   A   2000

15M   15M

100

250

1800   150 150   1800

Note: All dimensions are in mm
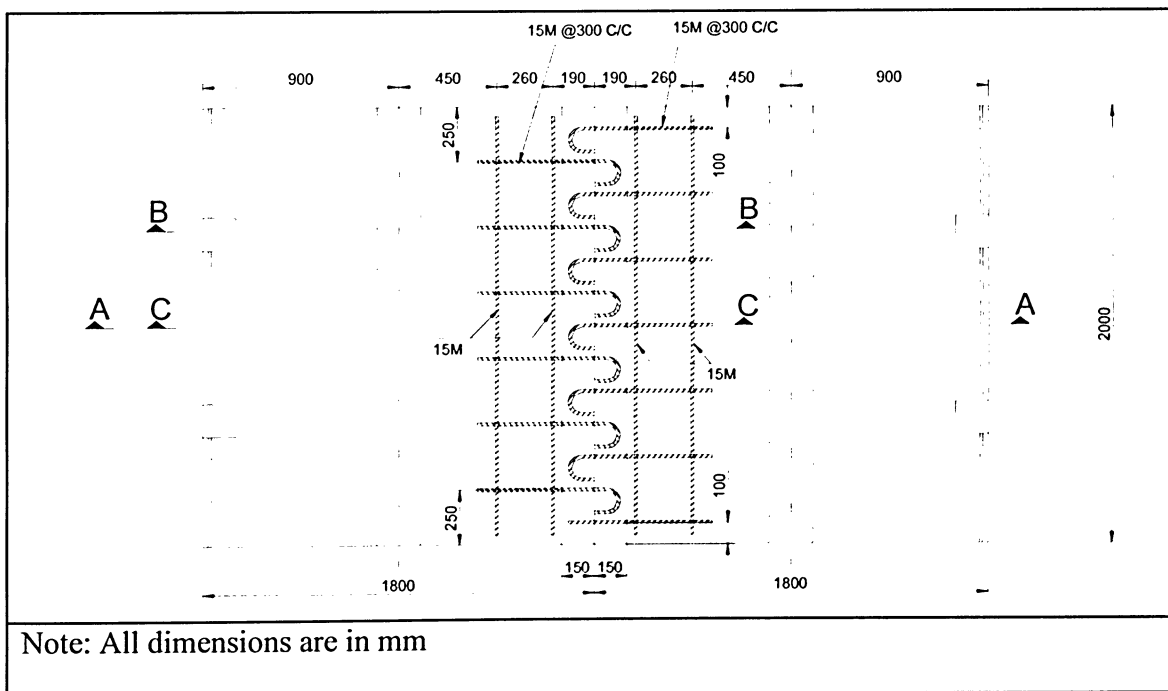
Figure 4.3 (b) Plan of Dowel Rebar Arrangement at Joint for Model M1

94
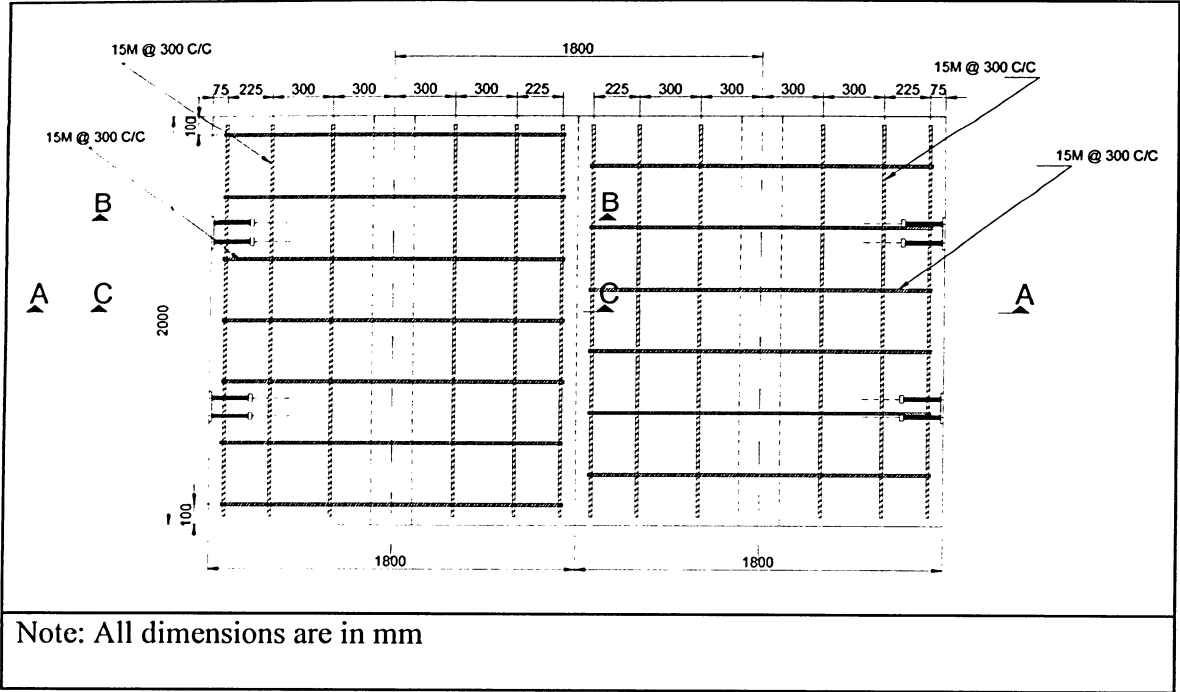
Figure 4.3(c) Plan of Bottom Rebar Arrangement for Model M1
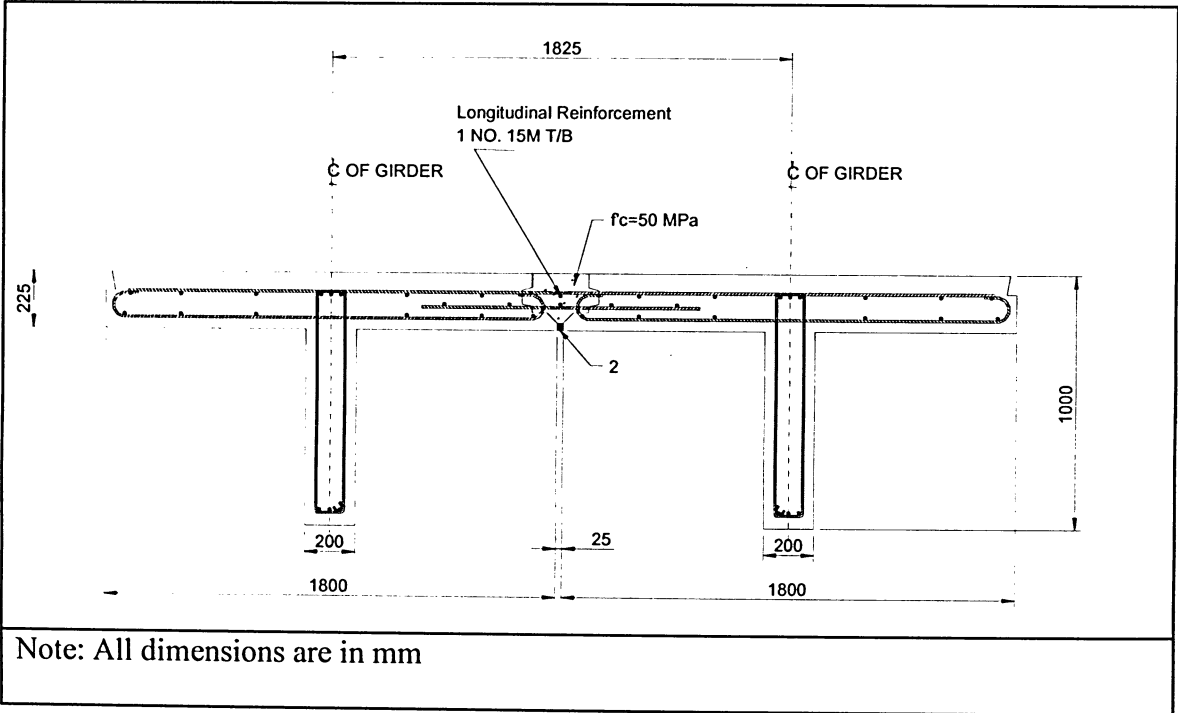
Figure 4.3 (d) Cross Section of Model M1 After Grouting

95
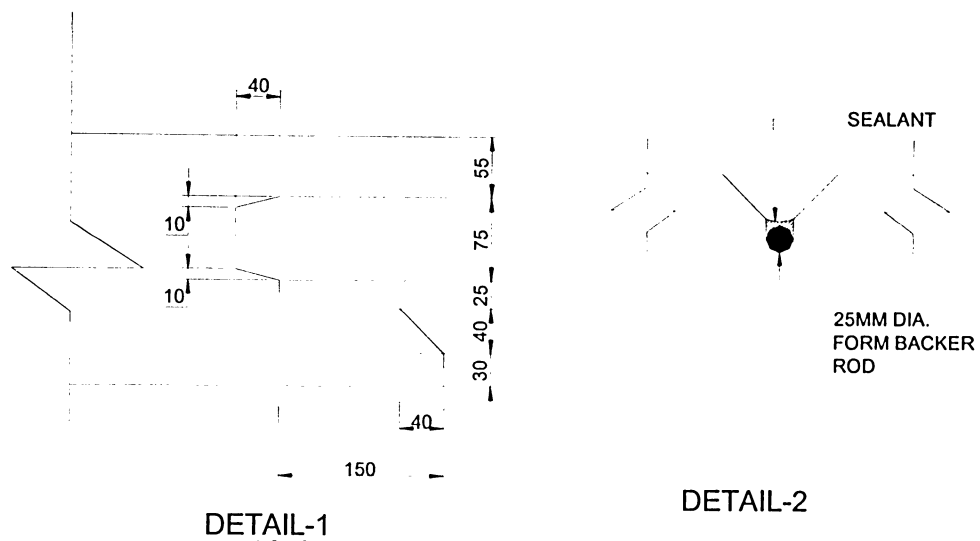
Figure 4.3 (e) Details of Shear Key and Form Backer Rod for Models M1

Figure 4.3 Plan and Cross-Section Details of Model M1
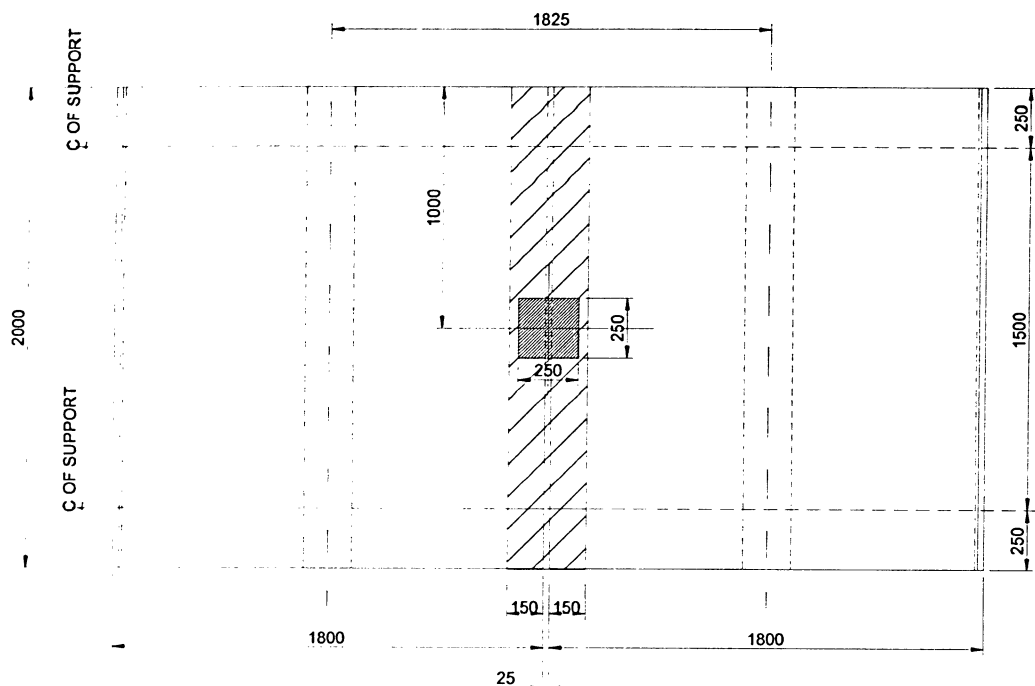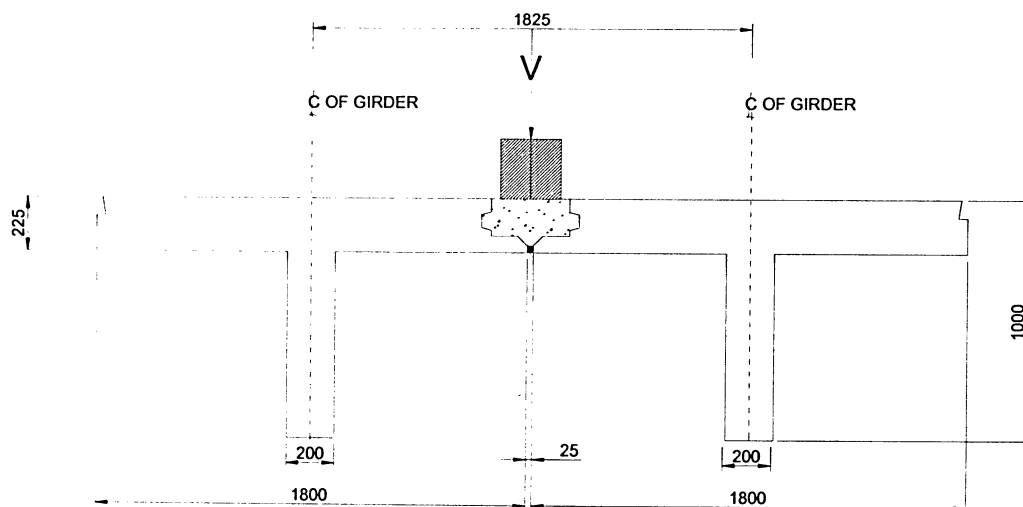
Figure 4.4 Plan and Cross-Section View of the Location of the Simulated Wheel Load for Model M1

Note: 1) All dimensions are in mm;
2) Bottom Rebars are U-hook, Top Rebars are straight, See Deatil-1
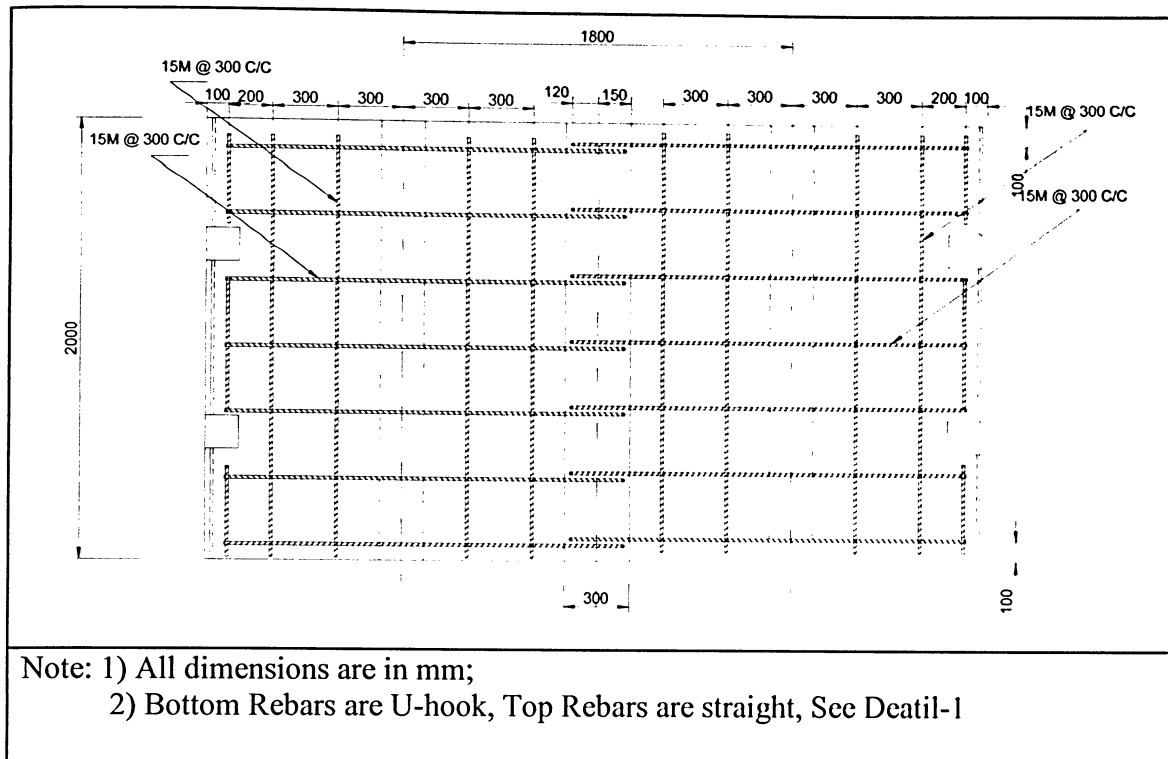
Figure 4.5 (a) Plan of Top and Bottom Rebar Arrangement for Models M2

Note: All dimensions are in mm
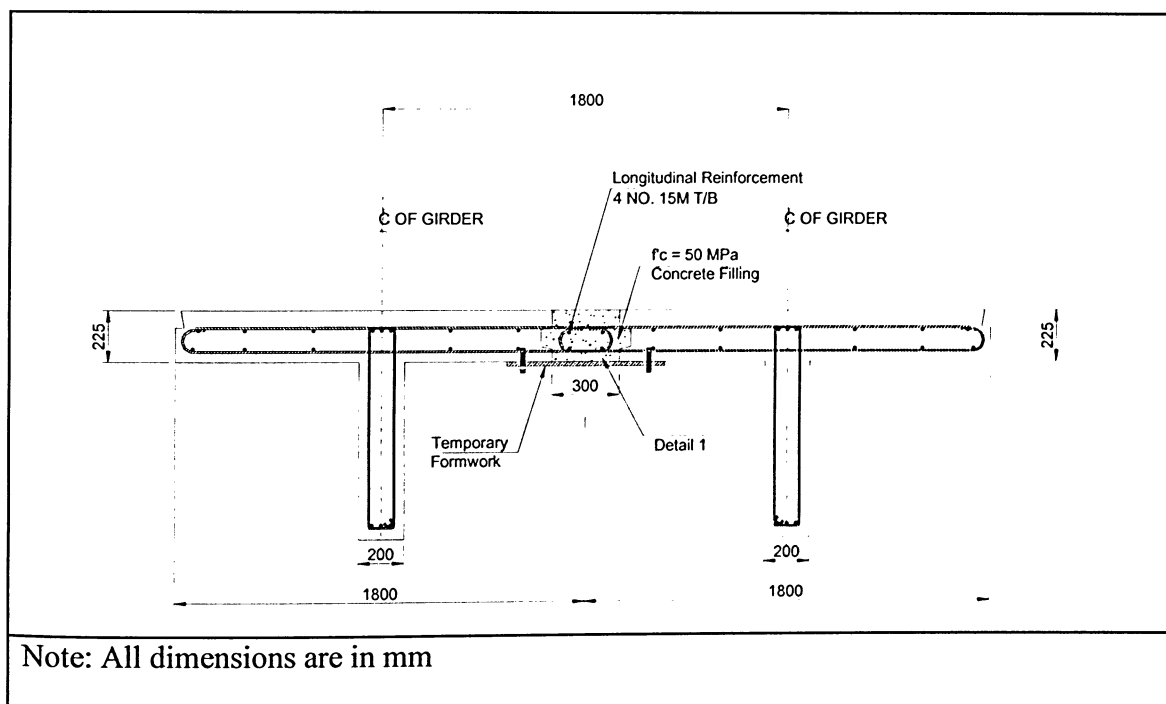
Figure 4.5 (b) Cross Section of Model M2 after Grouting
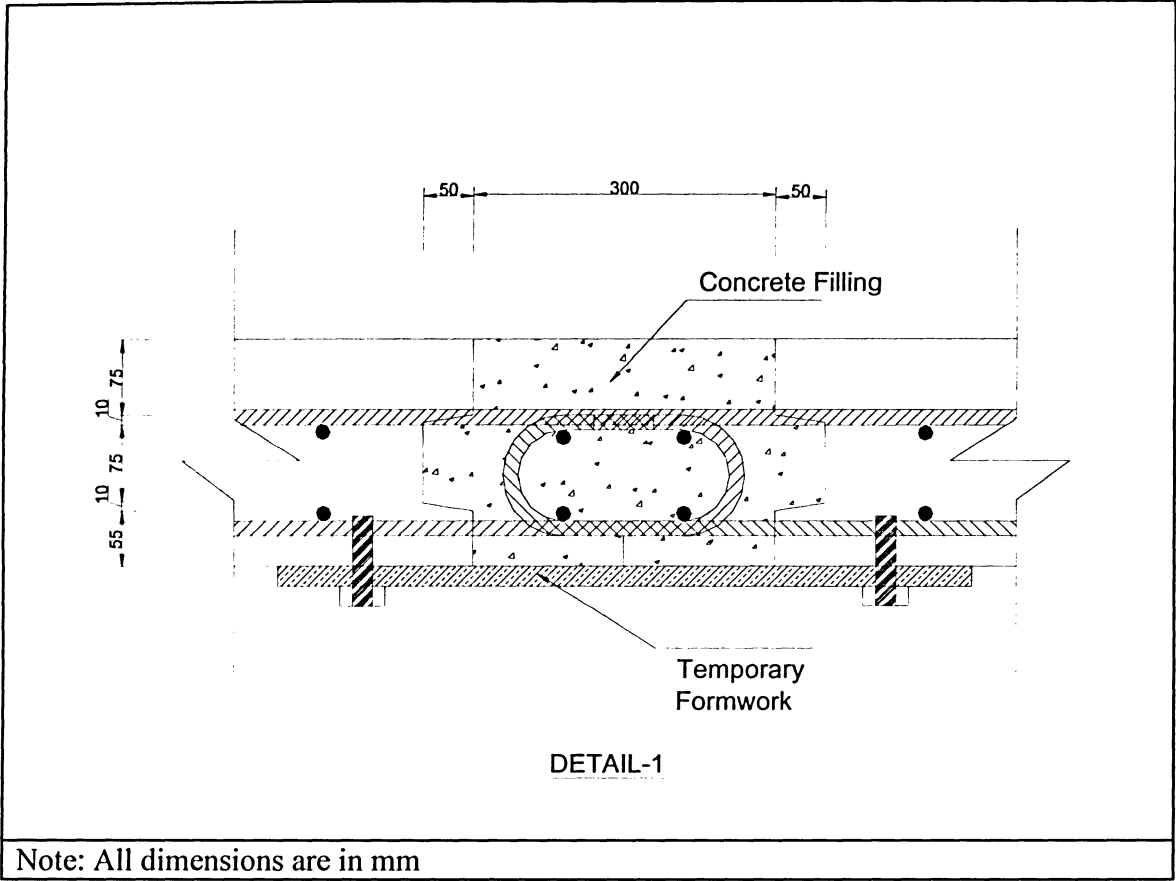
Figure 4.5 (c) Details of Shear Key and Joint Opening for Model M2

Figure 4.5 Plan and Cross-Sectional Details of Model M2
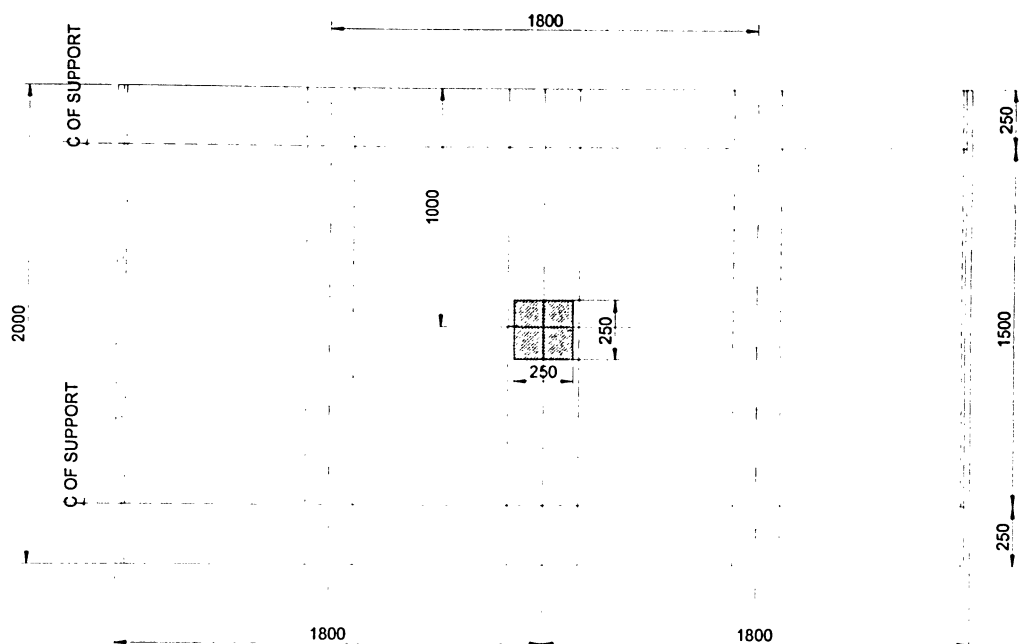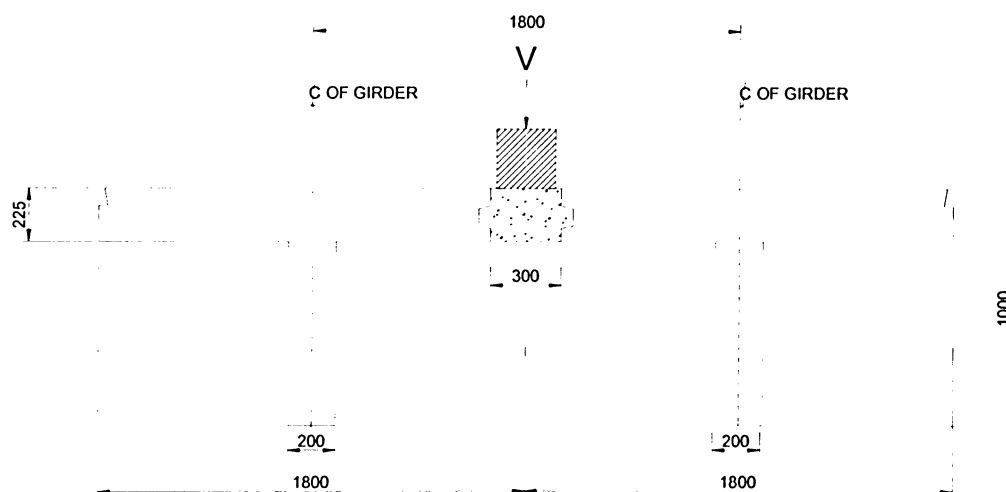
Figure 4.6 Plan and Cross-Section View of the Location of the Simulated Wheel Load for Model M2

Note: All dimensions are in mm
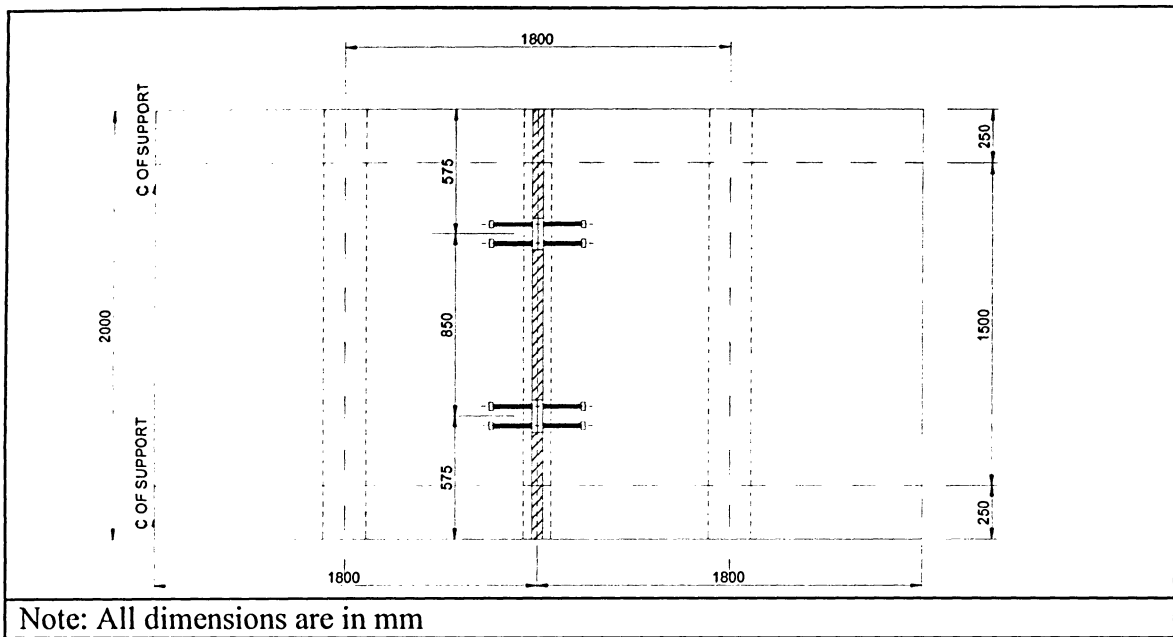
Figure 4.7 (a) Plan of Location of Bolted Connection for Model M3

Note: All dimensions are in mm
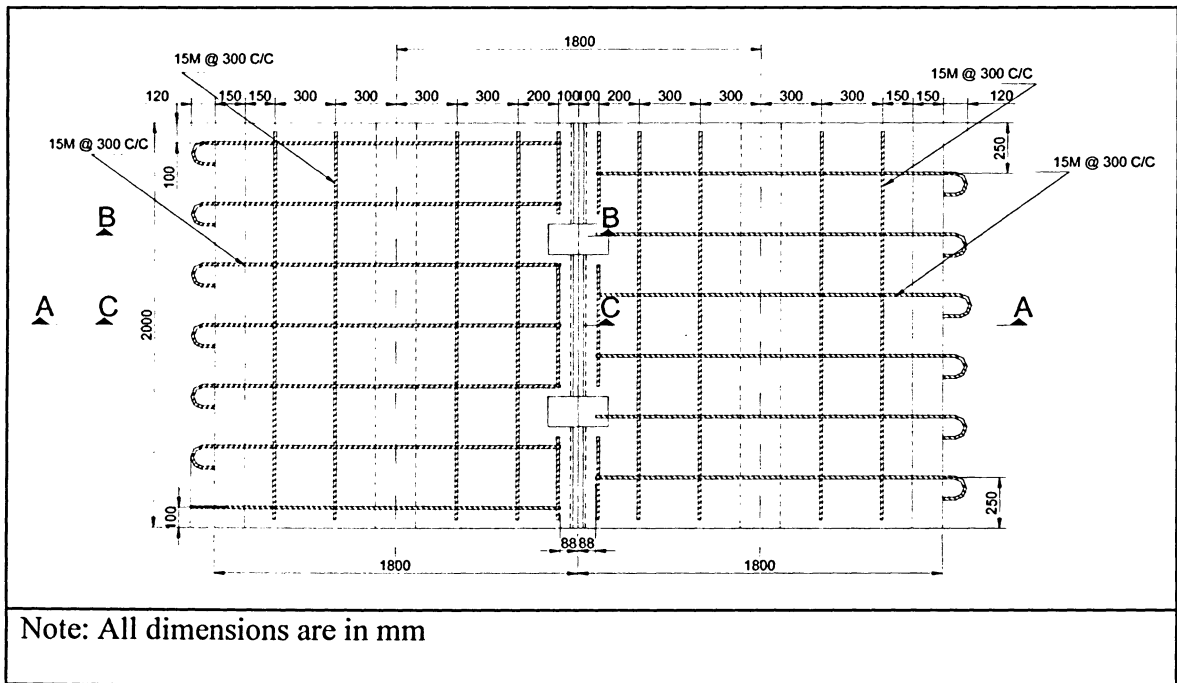
Figure 4.7 (b) Plan of Top Rebar Arrangement for Model M3

Figure 4.7 (c) Plan of Bottom Rebar Arrangement for Model M3

Figure 4.7 (d) Cross Section of Model M3 after Grouting
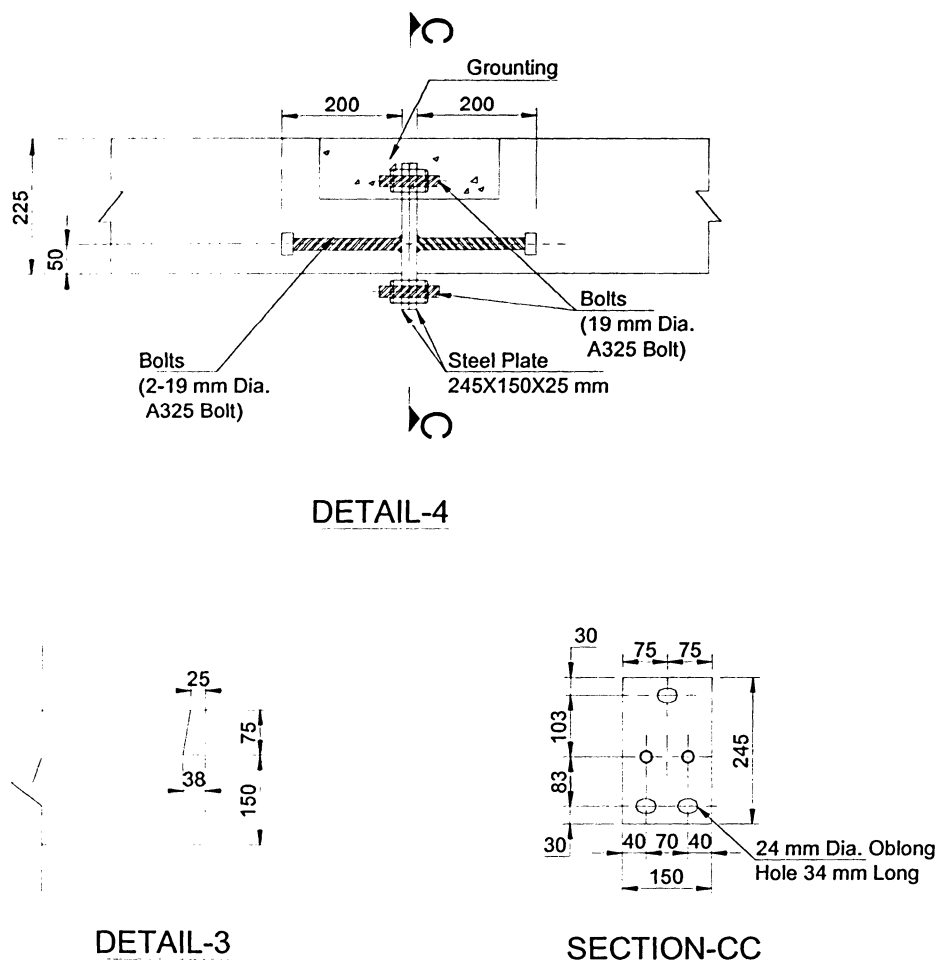
Figure 4.7 (e) Details of the Bolted Connection for Model M3

Figure 4.7 Plan and Cross-Section Details of Model M3
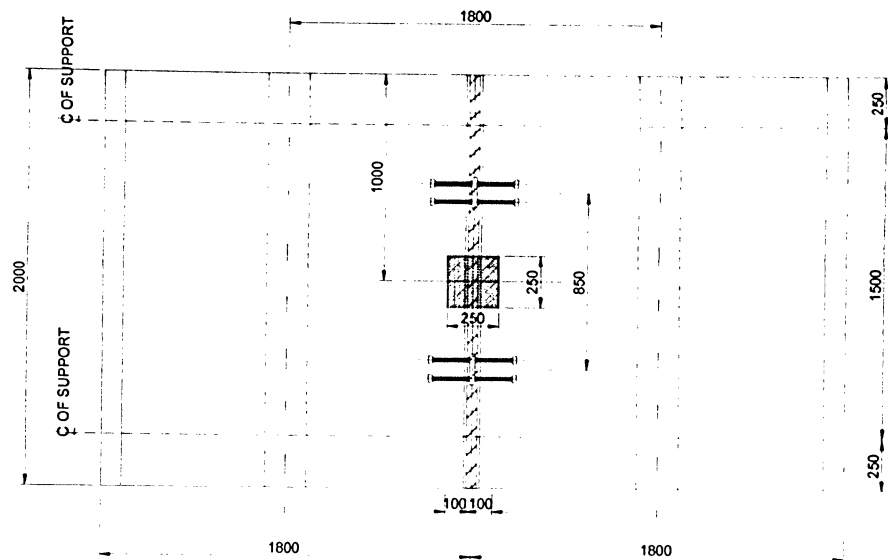
A) Plan
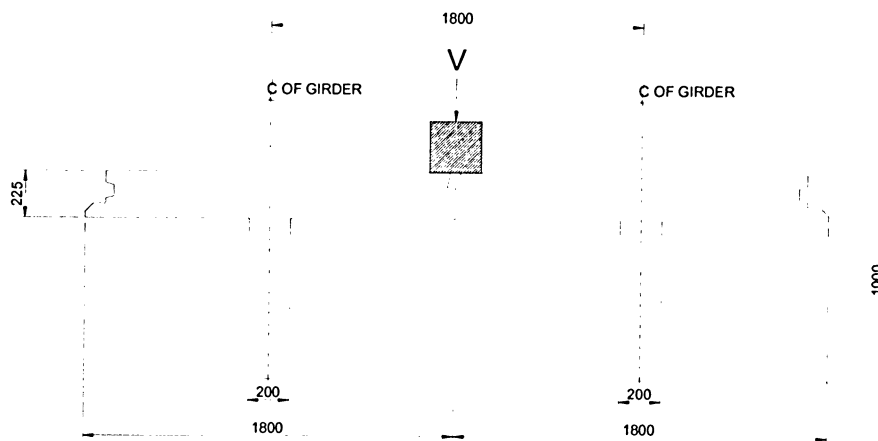
B) Cross Section

Note: All dimensions are in mm

Figure 4.8 Plan and Cross-Section View of the Location of the Simulated Wheel Load for Model M3

Note: All dimensions are in mm
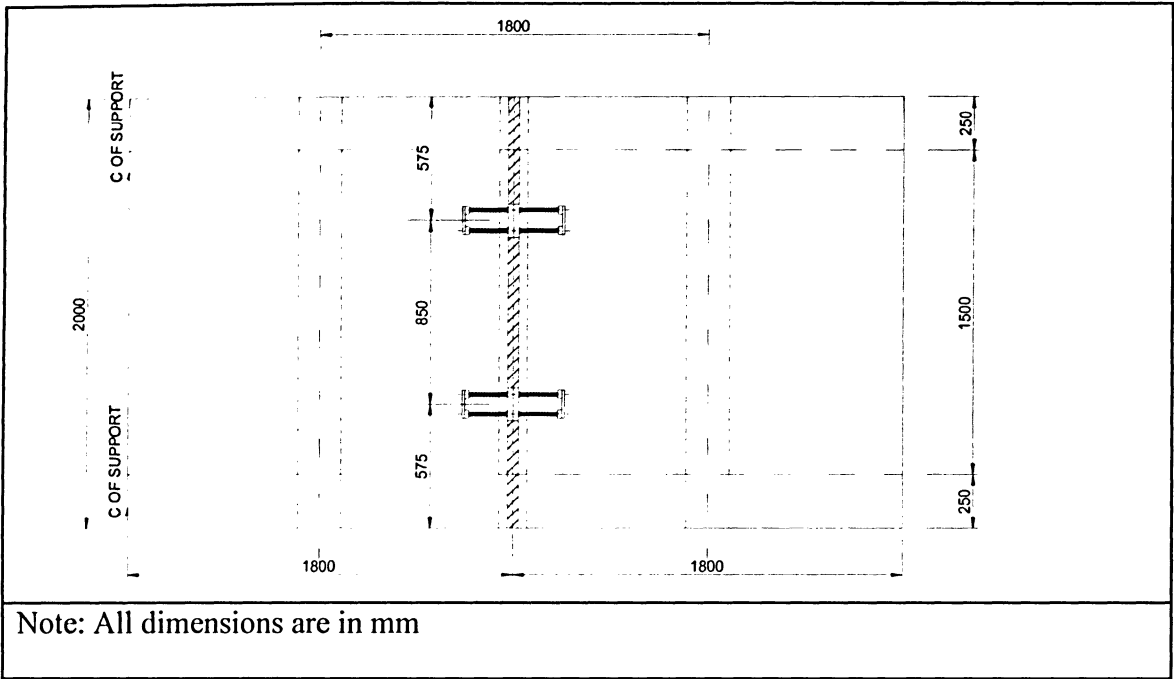
Figure 4.9 (a) Plan of Location of Bolted Connection for Model M4

Note: All dimensions are in mm
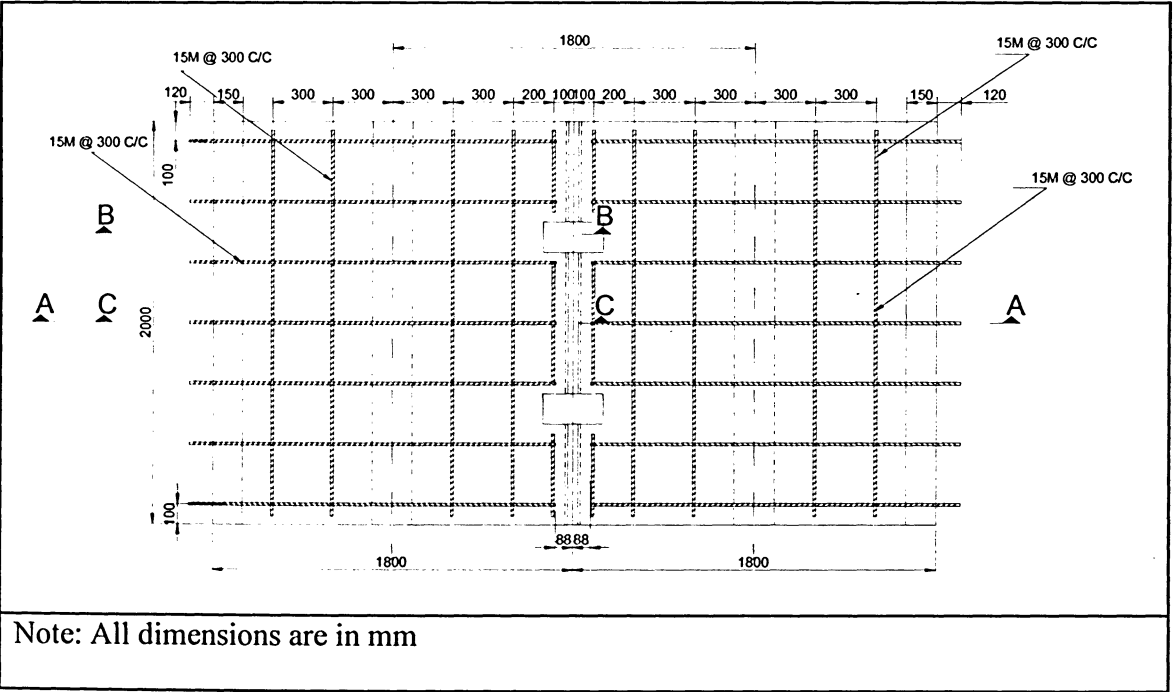
Figure 4.9 (b) Plan of Top Rebar Arrangement for Model M4

Note: All dimensions are in mm
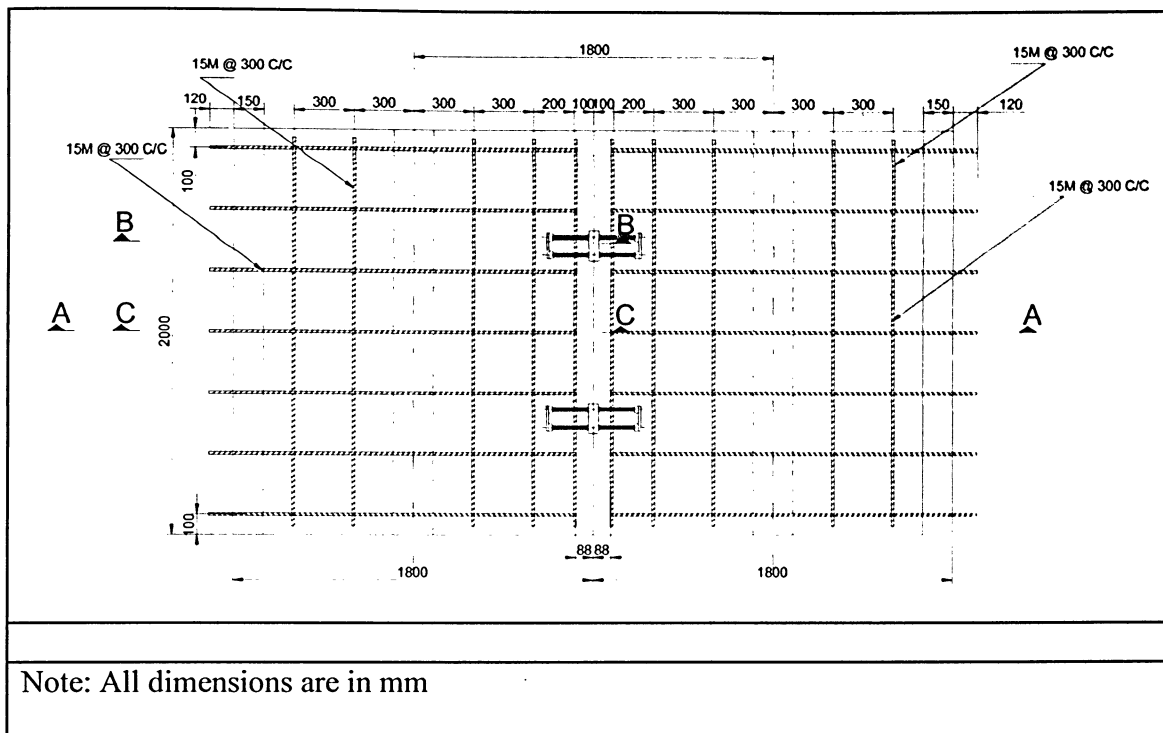
Figure 4.9 (c) Plan of Bottom Rebar Arrangement for Model M4

Note: All dimensions are in mm
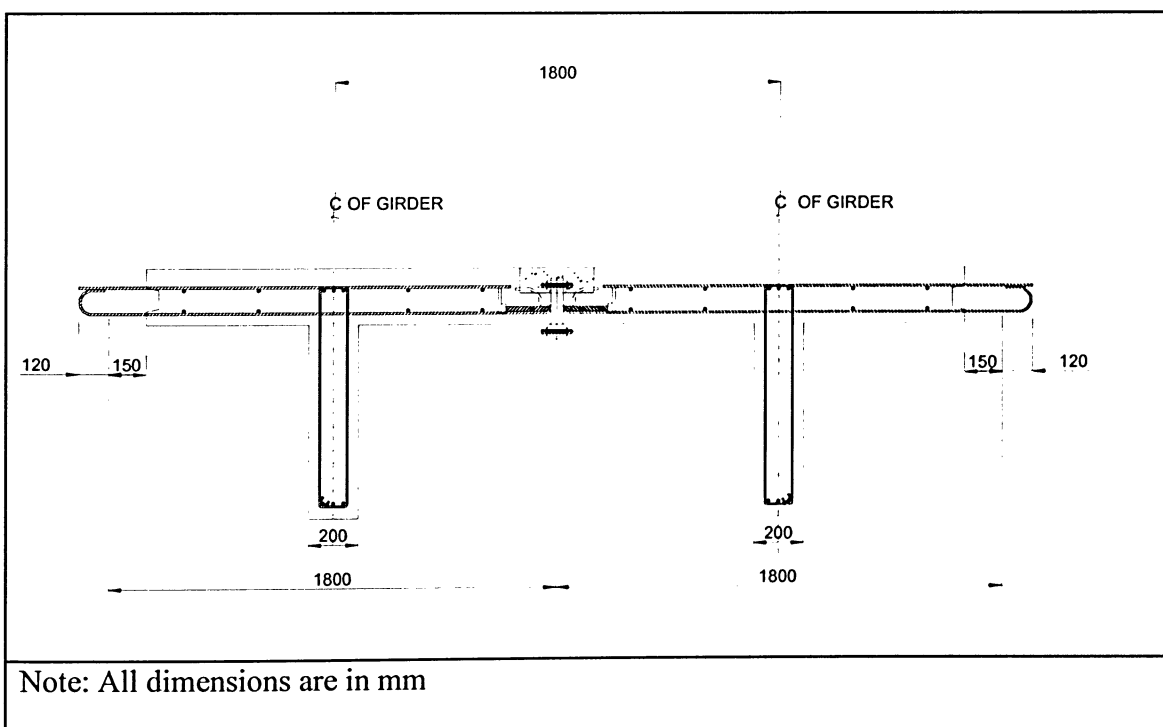
Figure 4.9 (d) Cross Section of Model M4 after Grouting

106

Figure 4.9 (e) Details of the Bolted Connection for Model M4

Figure 4.9 Plan and Cross-Section Details of Model M4
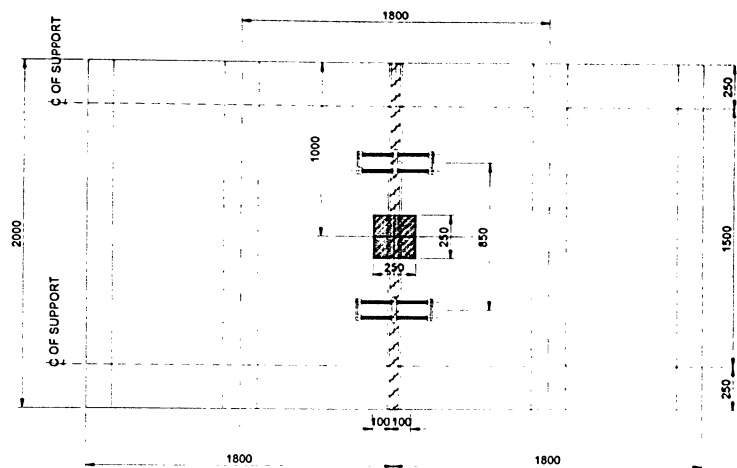
A) Plan
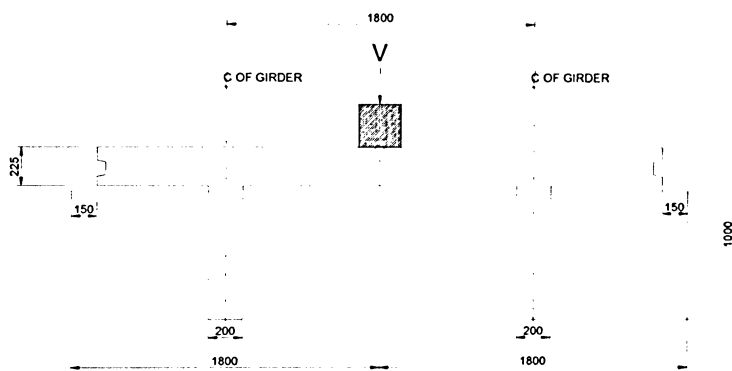
B) Cross Section

Note: All dimensions are in mm

Figure 4.10 Plan and Cross-Section View of the Location of the Simulated Wheel Load for Model M4

108

Figure 5.1 View of Model M1 During Testing
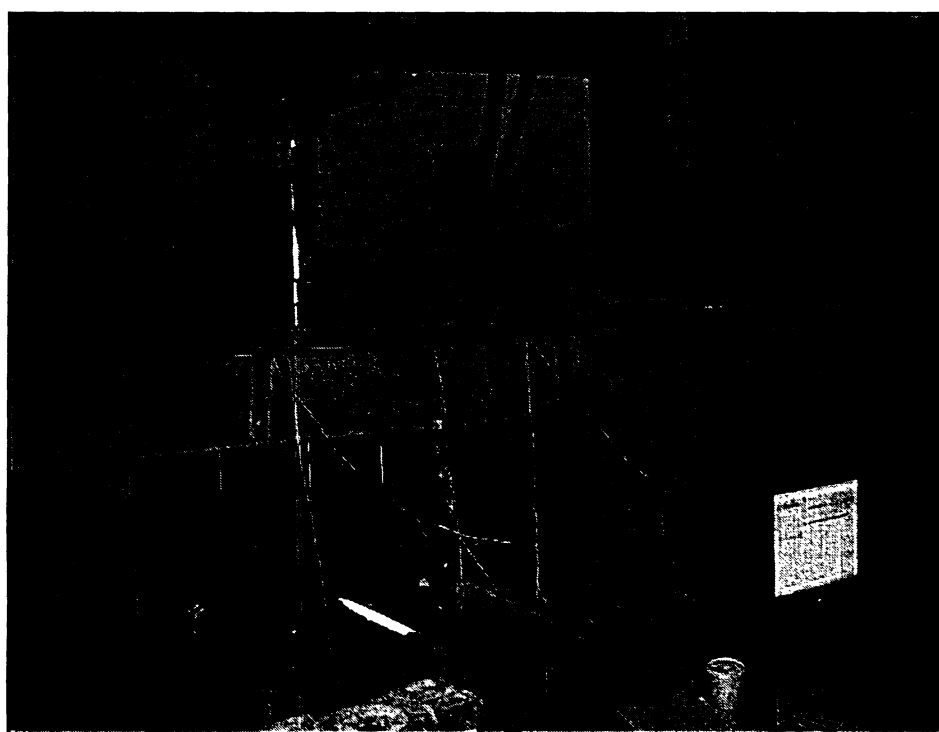
Figure 5.2 View of Deflected Shape of Model M1 After Releasing of Load
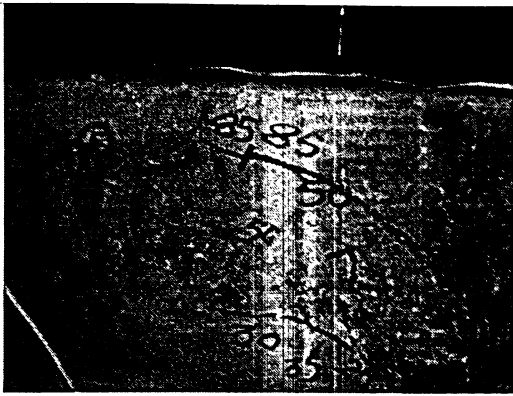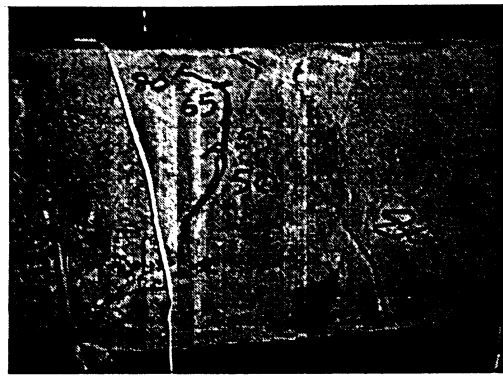
(a) Front Close-Up
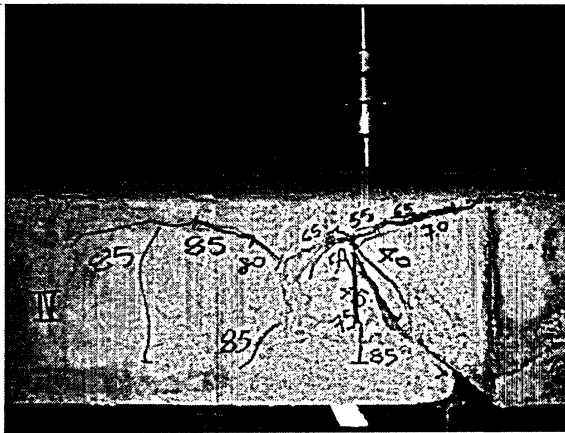
(b) Front Close-UP
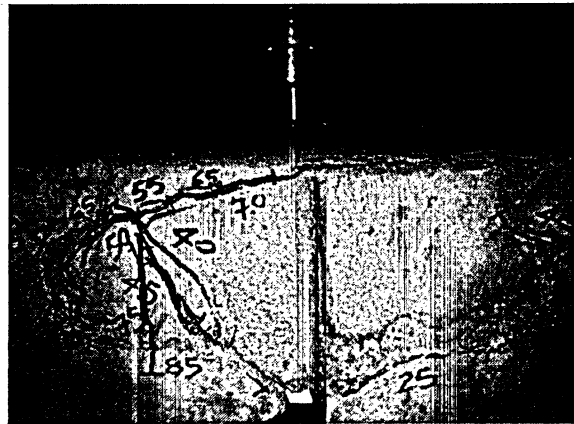
(c) Back Close-Up

(d) Back Close-Up

Figure 5.3 Views of Crack Patterns on Front and Back Side of the Joint for Model M1
After Testing
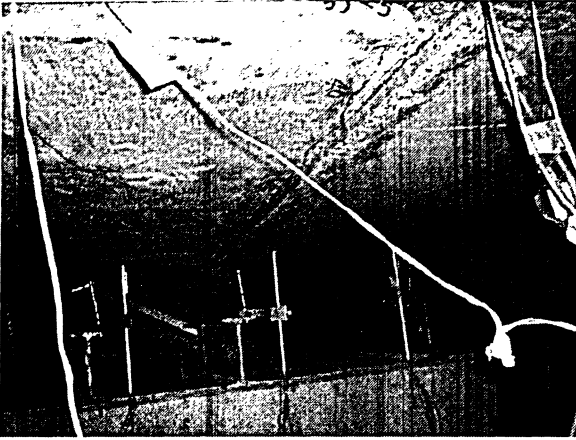
(a) From Bottom (Front Portion)

(b) From Bottom (Central Portion)
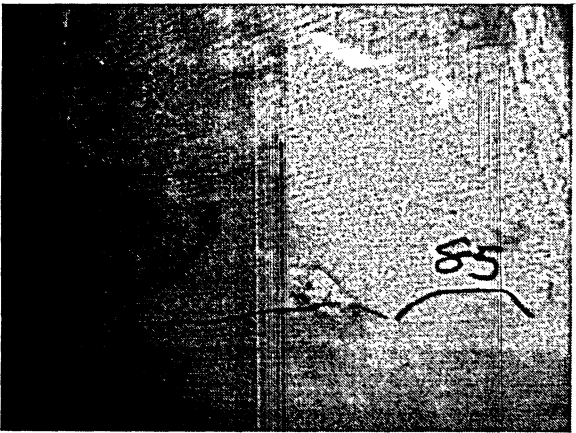
(c) Central Portion
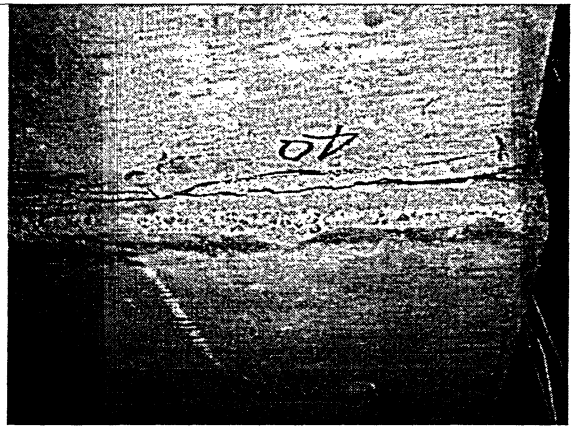
(d) From Front Side

Figure 5.4 Views of Crack Patterns at the Bottom of the Deck for Model M1 After Testing
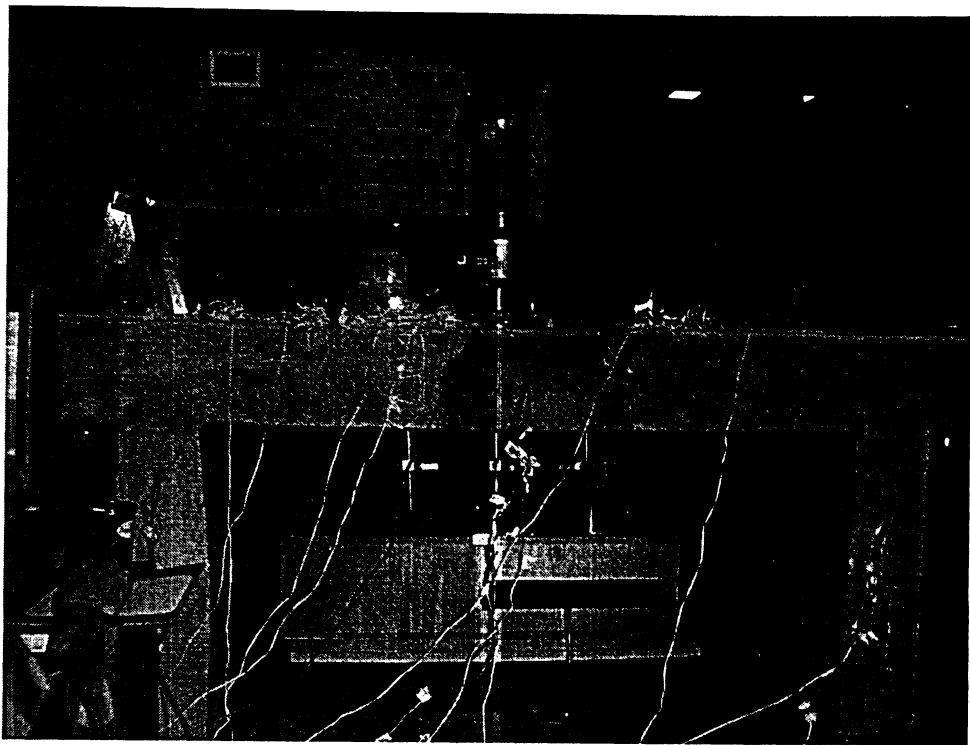
Figure 5.5 View of Model M2 During Testing
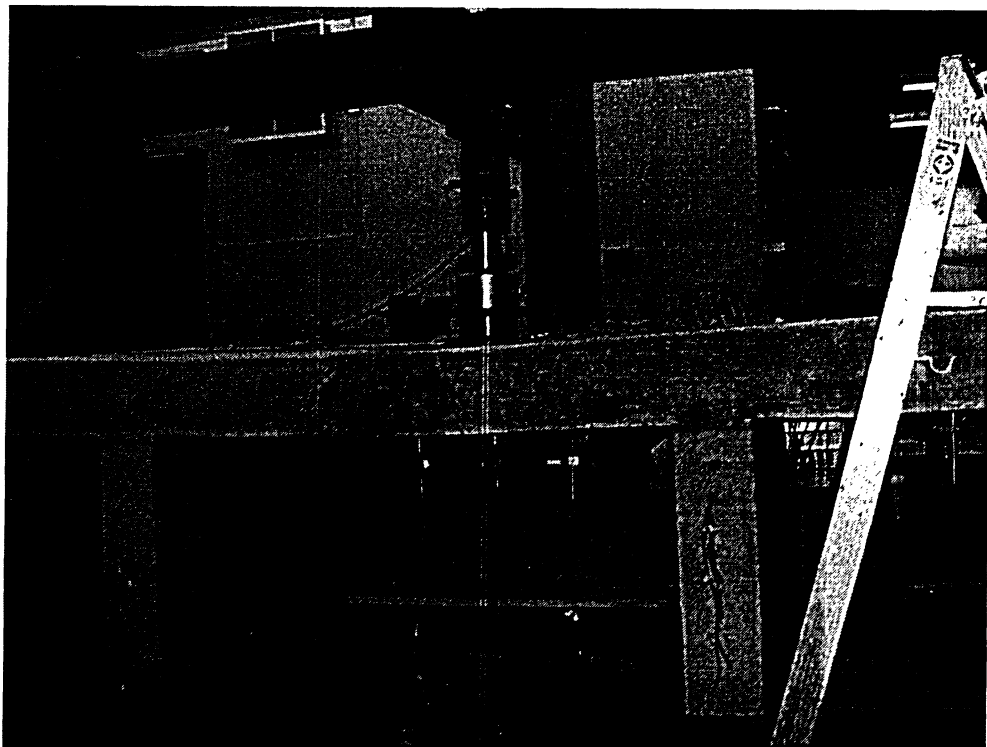
Figure 5.6 View of Deflected Shape of Model M2 After Releasing of Load
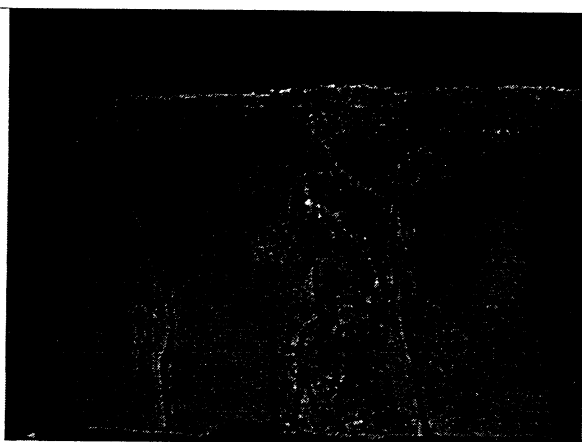
(a) Front Close-Up
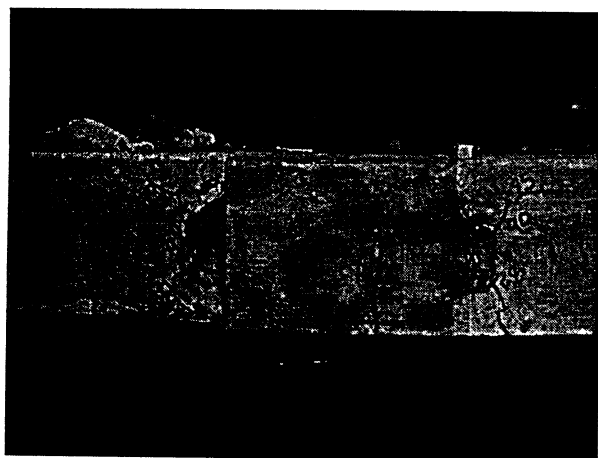
(b) Front Close-UP
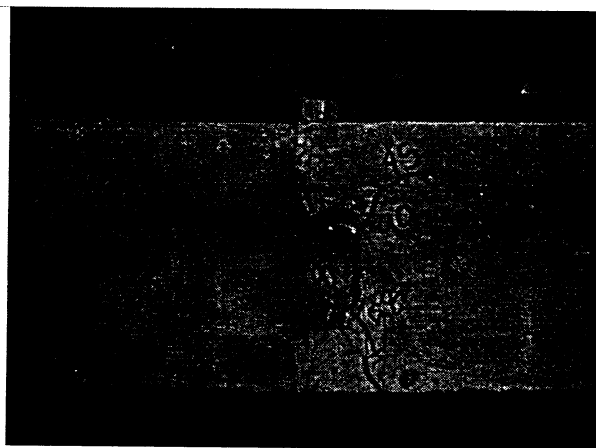
(c) Back Close-Up

(d) Back Close-Up

Figure 5.7 Views of Crack Patterns on Front and Back Side of the Joint for Model M2 After Testing

(a) From Bottom (Slab Deck Corner)
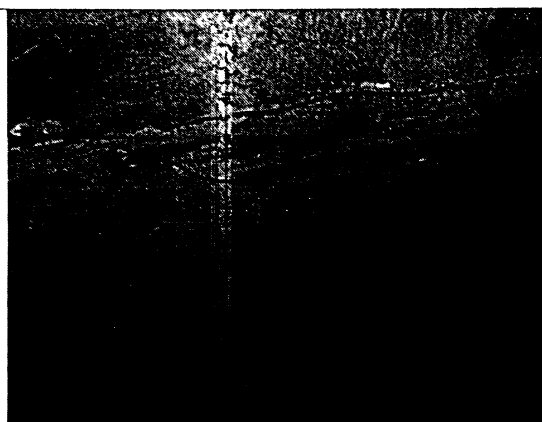
(b) From Bottom (Slab Deck Corner)

(c) From Bottom (Joint connection)

(d) From Bottom (Joint connection)

Figure 5.8 Views of Crack Patterns at the Bottom of the Deck for Model M2 After Testing
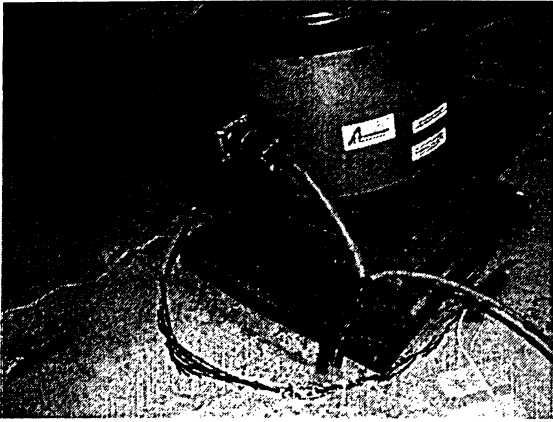
(a) From Top (Loading Area)
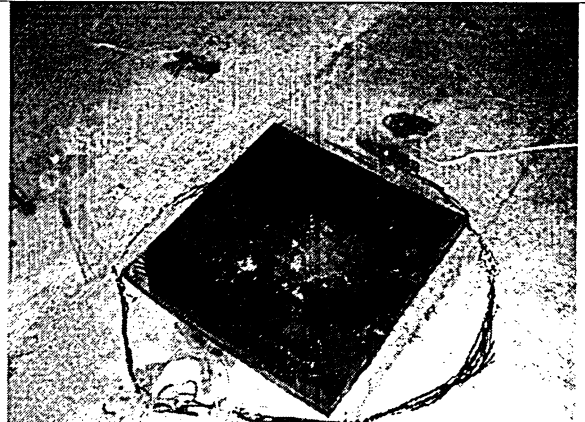
(b) From Top (Loading Area)
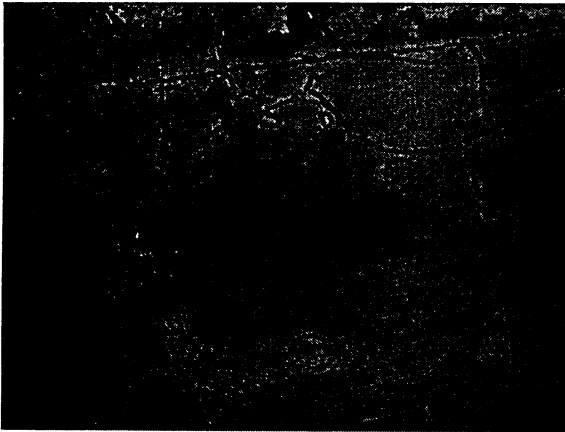
(c) From Bottom (Loading Area)
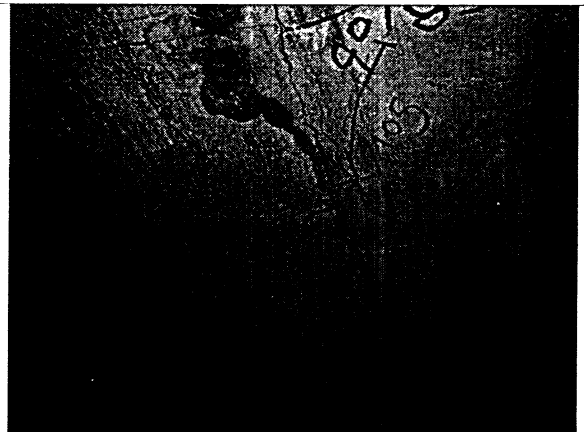
(d) From Bottom (Loading Area)

Figure 5.9 Views of Crack Patterns at loading position for Model M2 After Testing

Figure 5.10 View of Model M3 During Testing
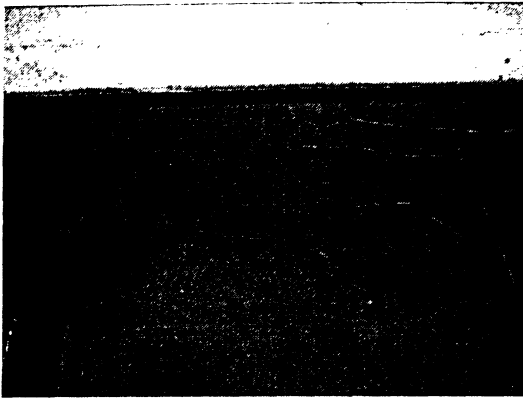
(a) Front Side (Top)
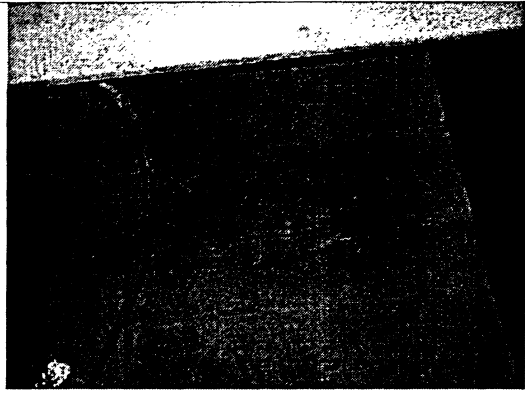
(b) Back Side (Top)
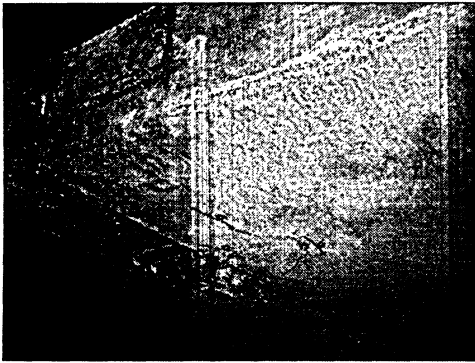
(c) From Bottom (Front)
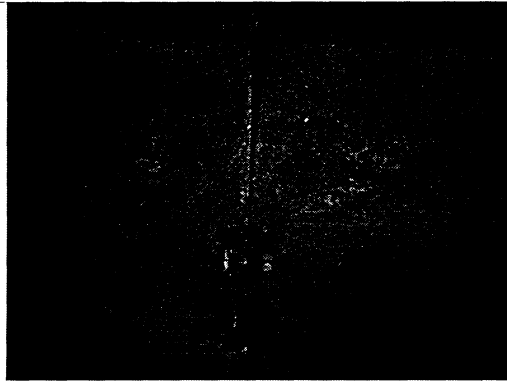
(d) Bottom Close-Up
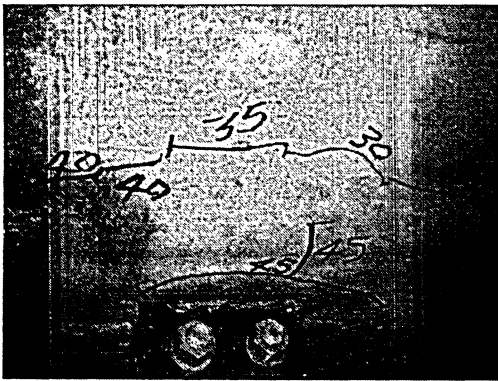
(e) Back Bolted Joint Close-Up
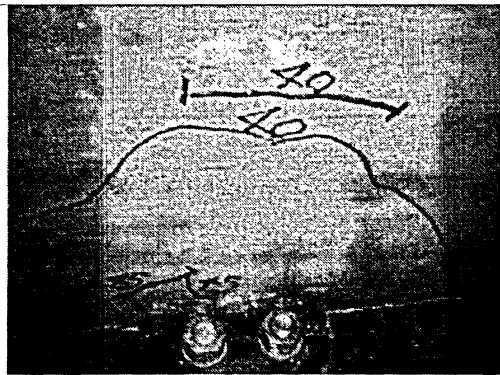
(f) Front Bolted Joint Close-Up

Figure 5.11 Views of Crack Pattern on Top and Bottom of Deck for M3 After testing
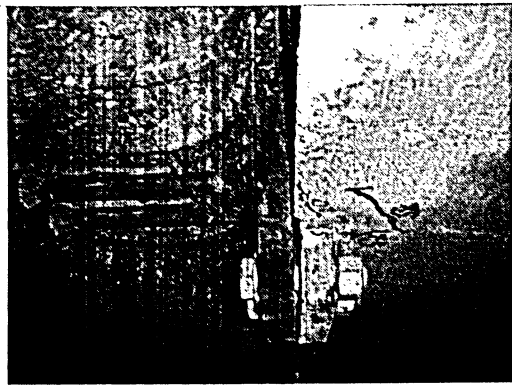
(a) From Bottom

(b) Bottom Close-Up
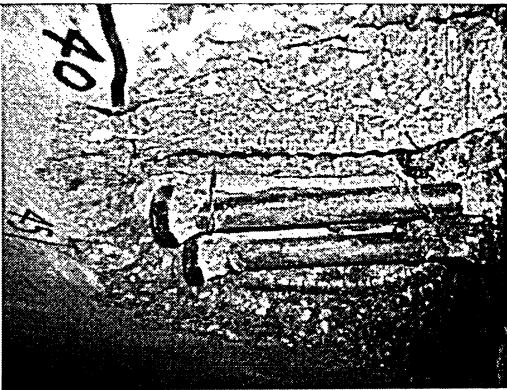
(c) Bottom Front Close-Up
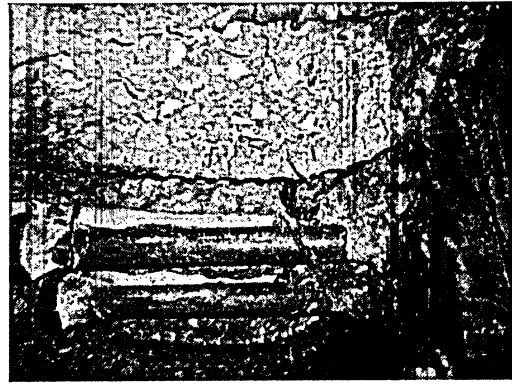
(d) Bottom Close-Up

(e) From Front Side
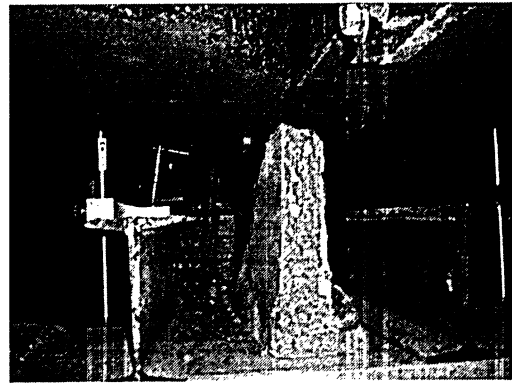
(f) Concrete Split from anchor bolts

Figure 5.12 Views of the Front Bolted Joint for M3 After testing

(a) From Bottom (Back)

(b) Bottom Close-Up

Concrete split at the end of the anchor bolts
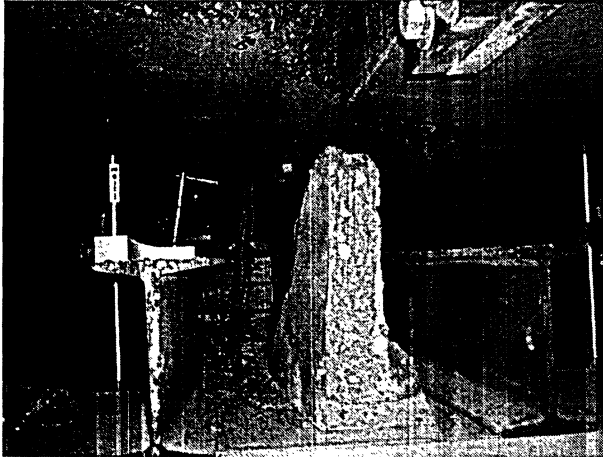
(c) Bottom Back Close-Up
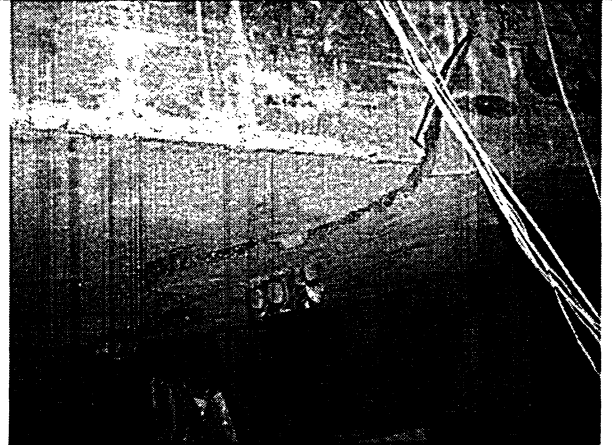
(d) Bottom Close-Up

Concrete split extending to the side of the deck

Figure 5.13 Views of the Back Bolted Joint for M3 After testing
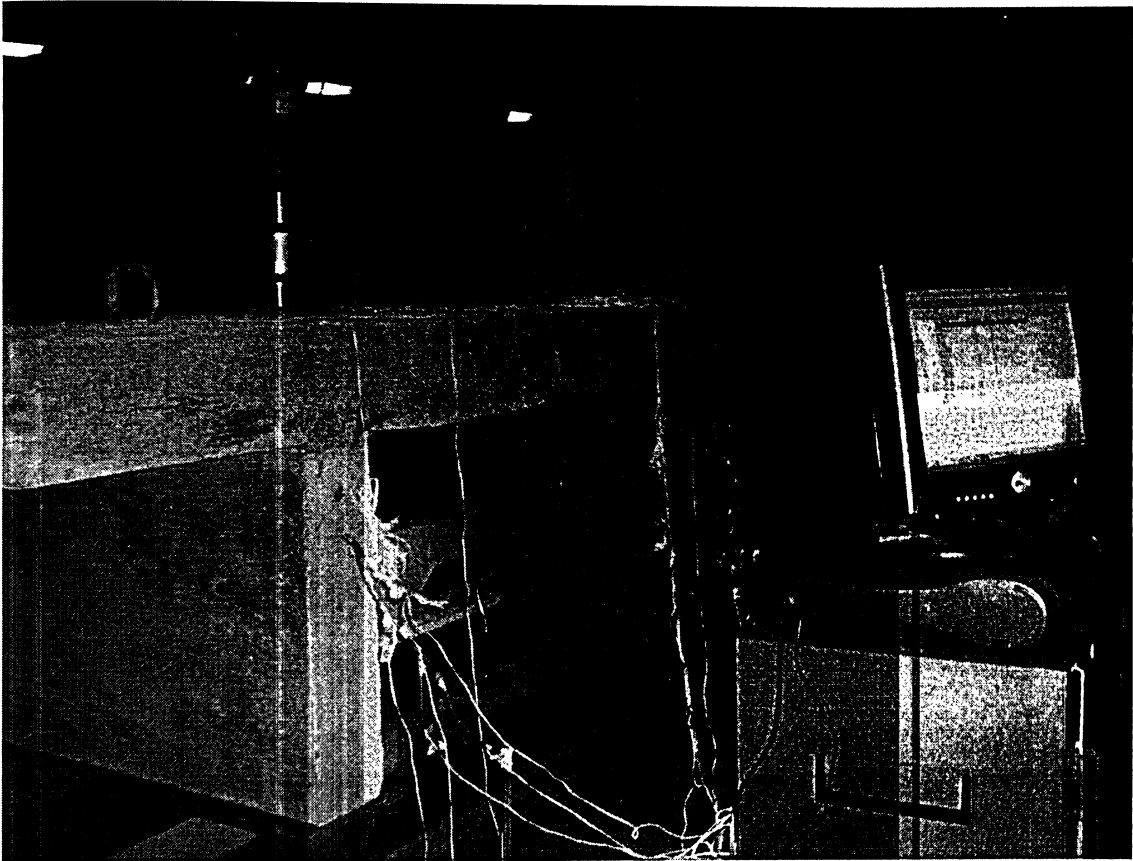
Figure 5.14 View of Model M4 During Testing
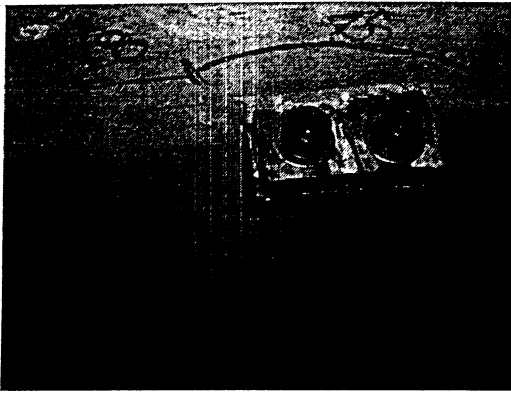
(a) Bottom Close-Up
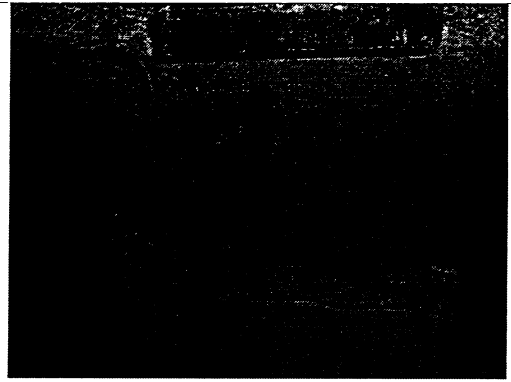
(b) Bottom Close-Up
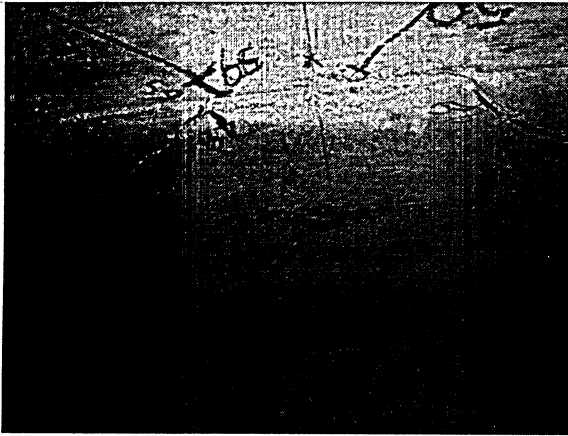
(c) Bottom Center Area

(d) Bottom Center Area
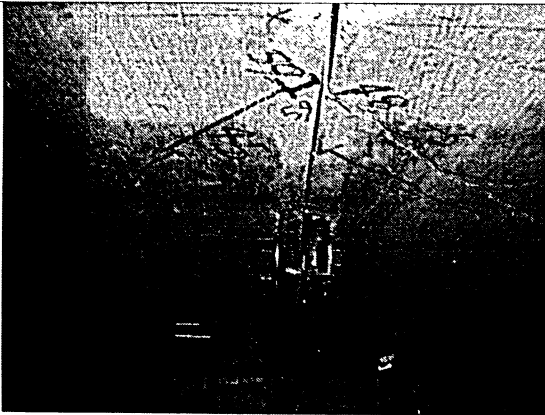
(e) Bottom Back Connector

(f) Bottom Front Connector

Figure 5.15 Crack Pattern at the Bottom of Model M4 After Testing
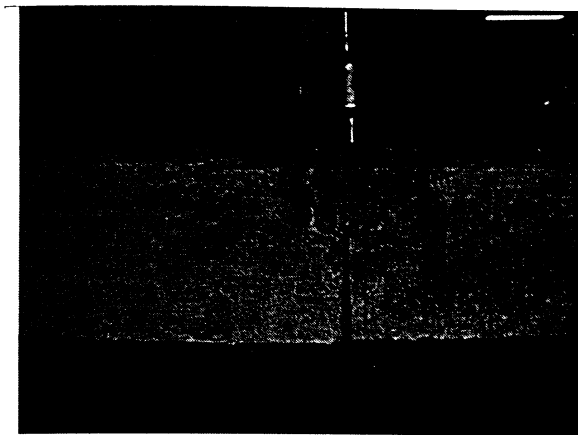
(a) Side Front
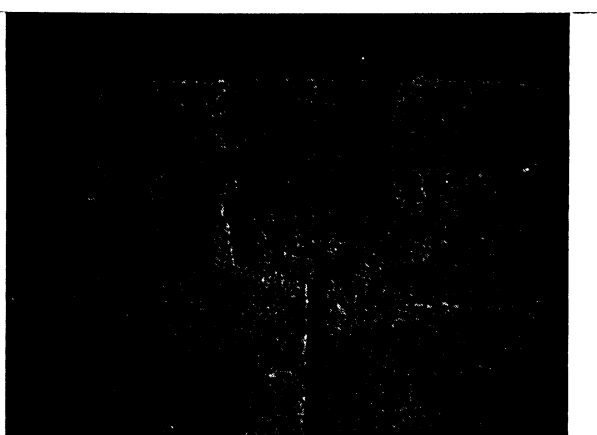
(b) Side Close-Up
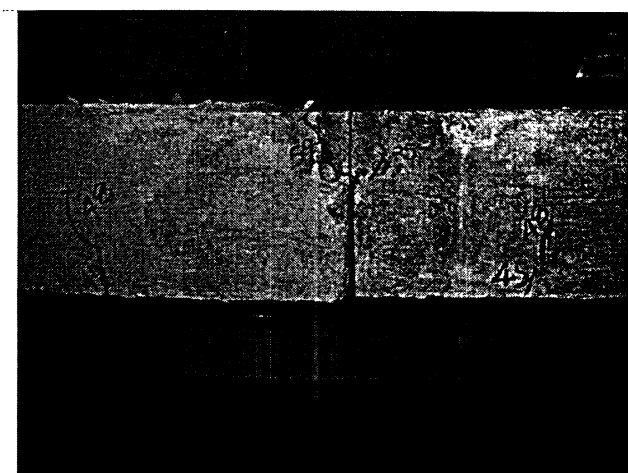
(b) Side Front
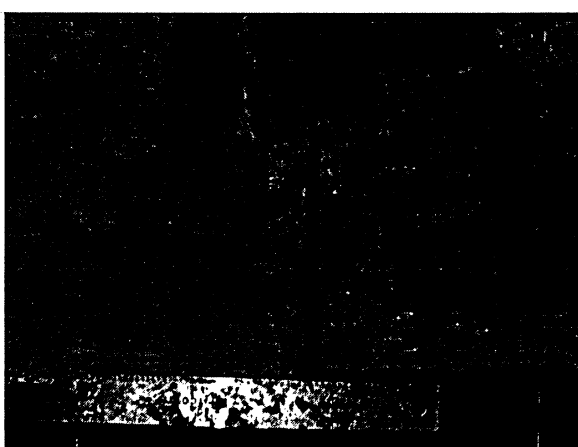
(d) Side Back

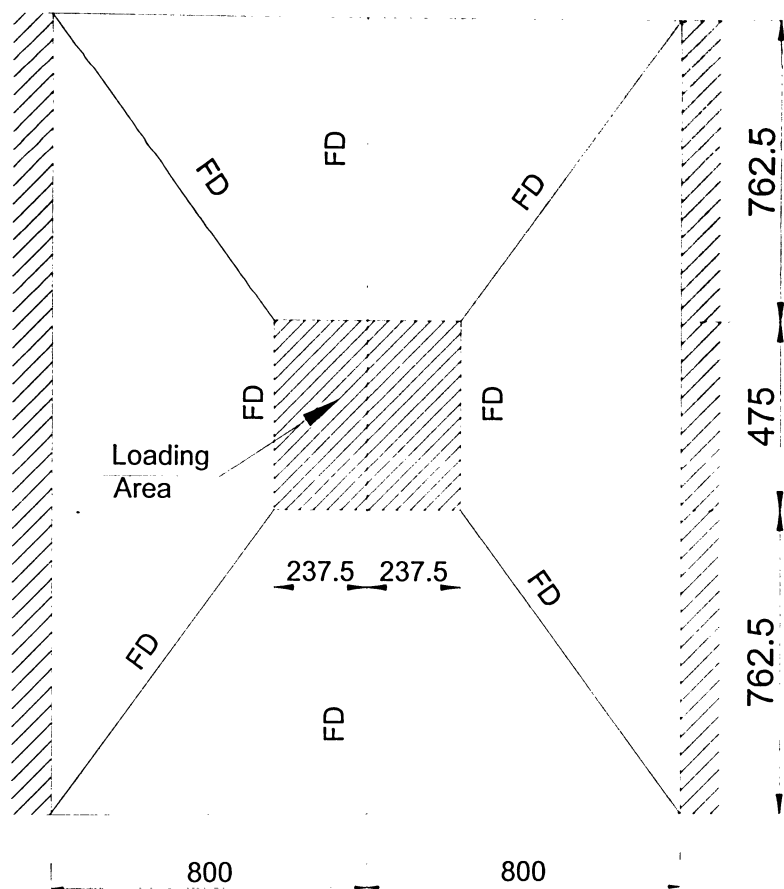Figure 5.16 Crack Pattern at the side of Model M4 After Testing
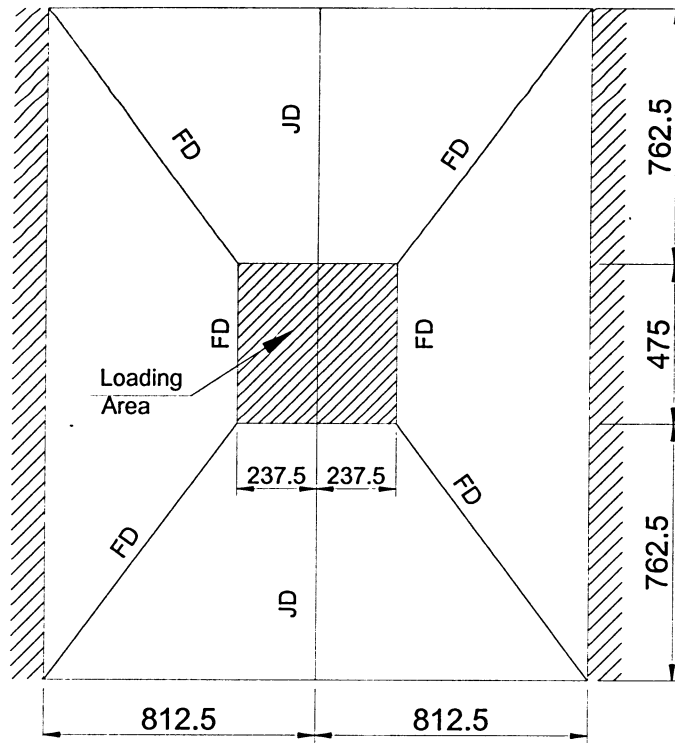
Model M1

CONVENTION

FD   FULL DEPTH OF THE DECK SLAB
JD   DEPTH AT JOINT

/////////   SIMPLY SUPPORTED EDGE

....   POSITIVE MOMENT YIELD LINE

Note: All Dimensions are in mm

Figure 5.17 Yield Line Patterns Used to Calculate Flexure Capacity of Model M1

123

Figure 5.18 Yield Line Patterns to Calculate the Flexure Capacity of Model M2

The figure contains the following labels and dimensions:

- Loading Area
- FD (Full depth of the deck slab) — labeled at multiple positions
- 762.5
- 475
- 762.5
- 237.5   237.5
- 800   800
- Model M2

CONVENTION

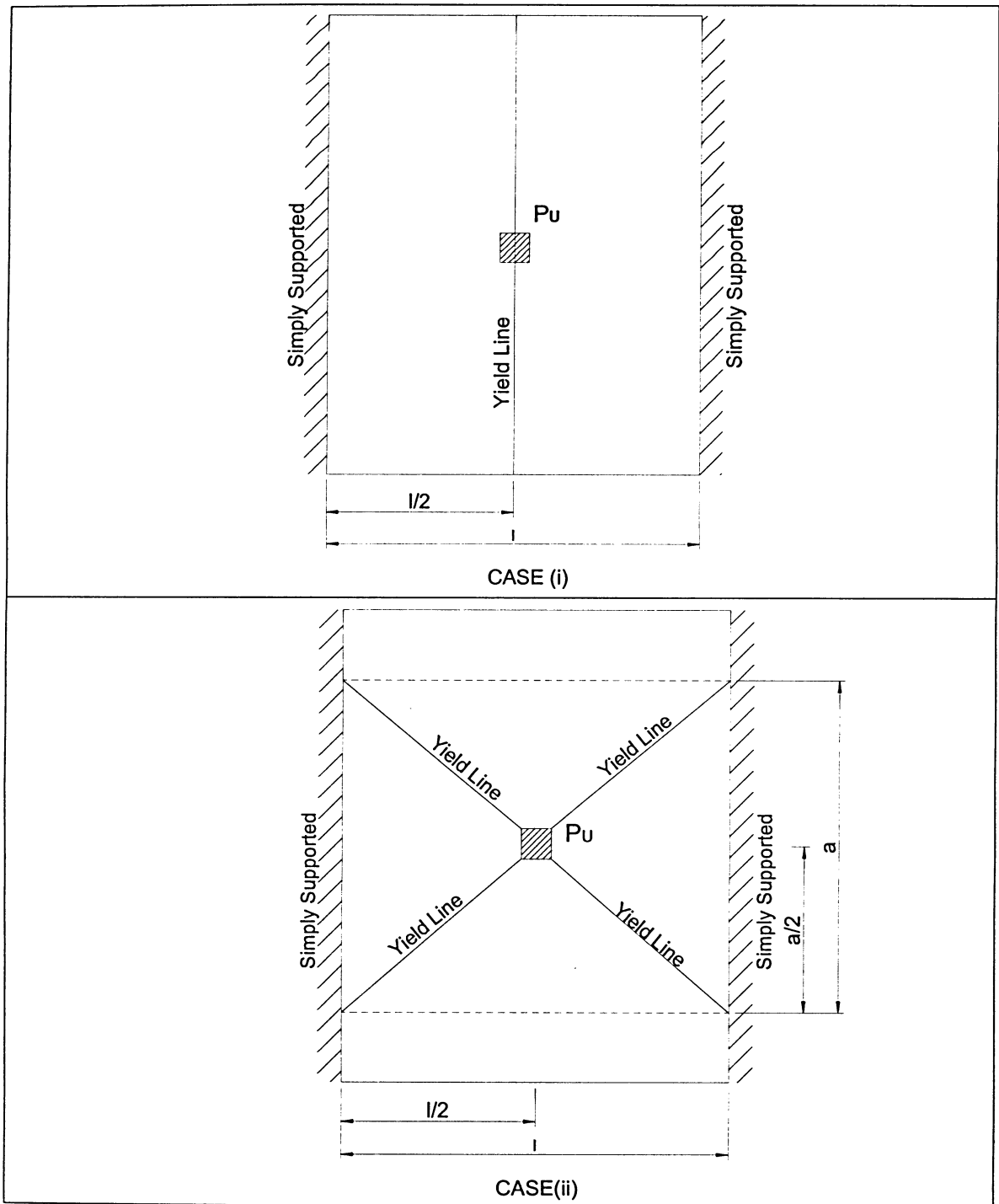|	
FD	FULL DEPTH OF THE DECK SLAB
JD	DEPTH AT JOINT
//////////	SIMPLY SUPPORTED EDGE
————	POSITIVE MOMENT YIELD LINE

Note: All Dimensions are in mm

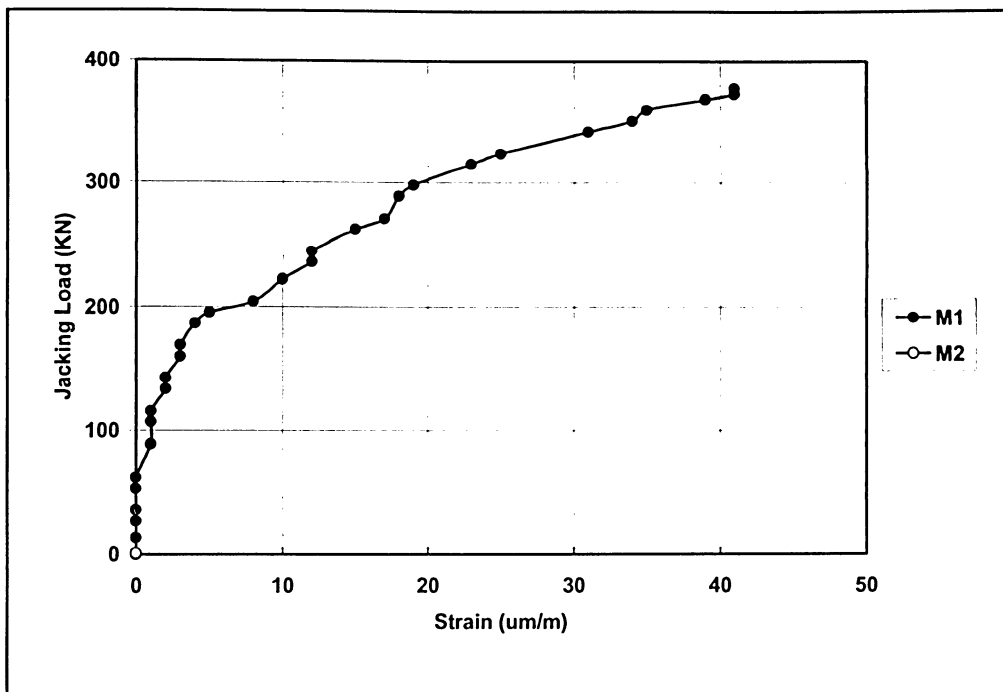Figure 5.19 Yield Line Patterns for Full Depth Deck Slab Flexure Capacity of Models M1 and M2

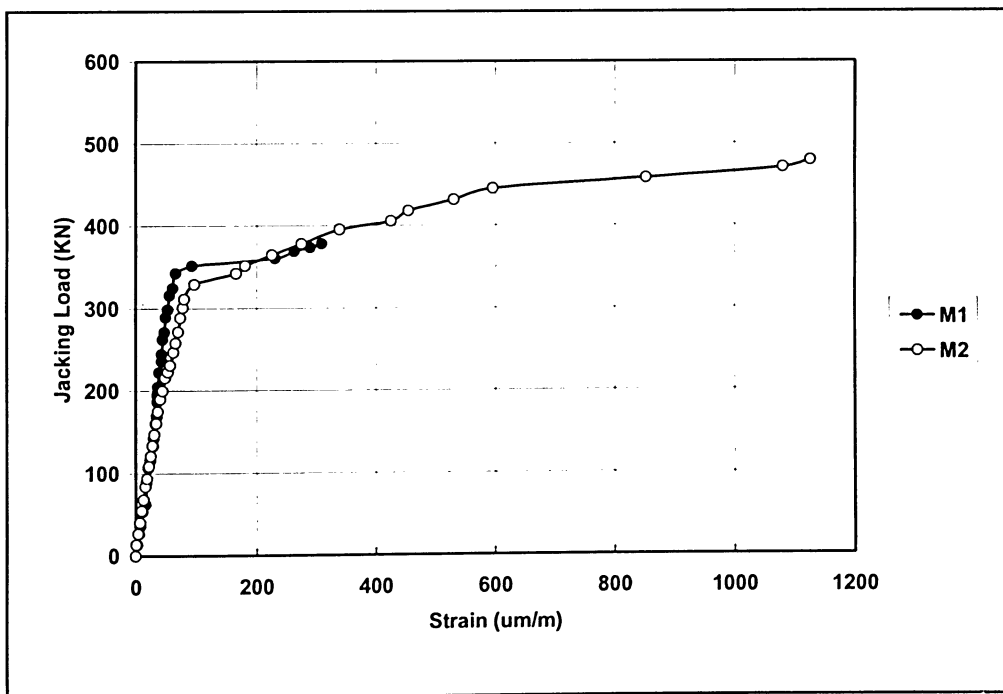Figure 5.20 Load-Strain Curves for TS1 Strain Gauges for Models M1 and M2

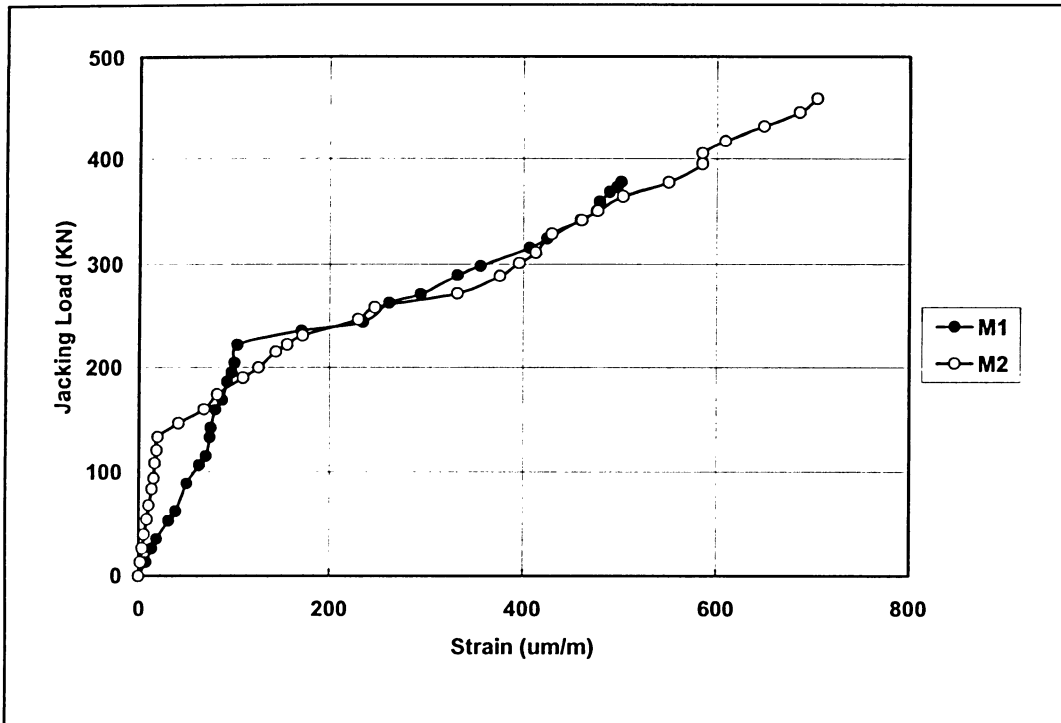Figure 5.21 Load-Strain Curves for TS2 Strain Gauges for Models M1 and M2

126

Figure 5.22 Load-Strain Curves for TS3 Strain Gauges for Models M1 and M2

Note: BS1 reading of Model M2 was keeping "0" during testing.
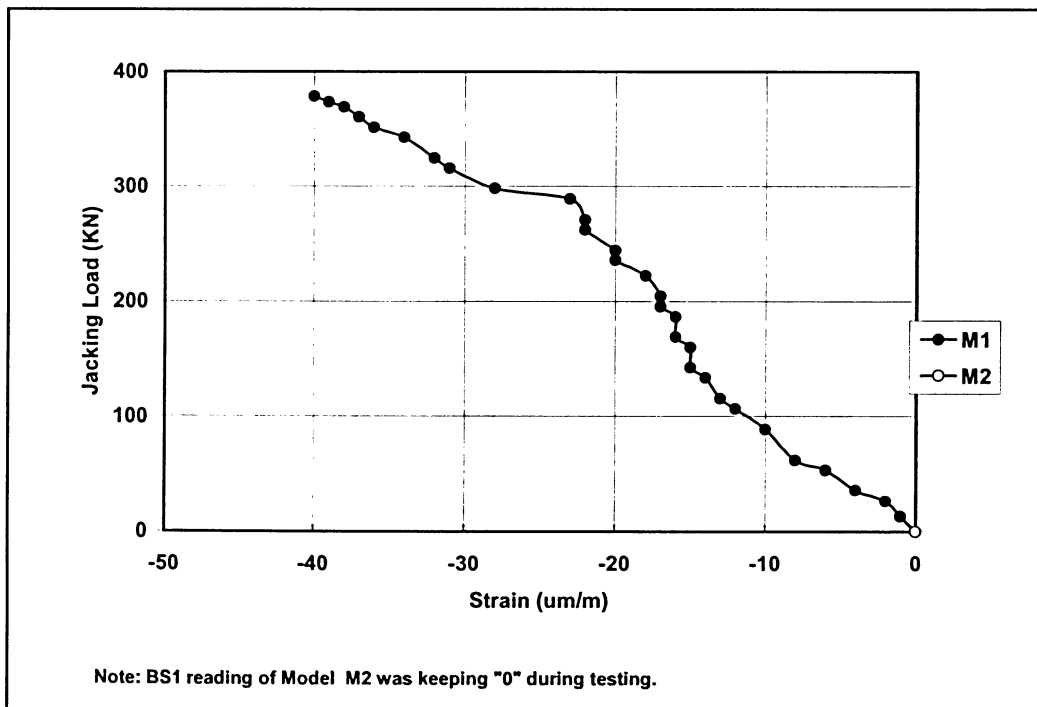
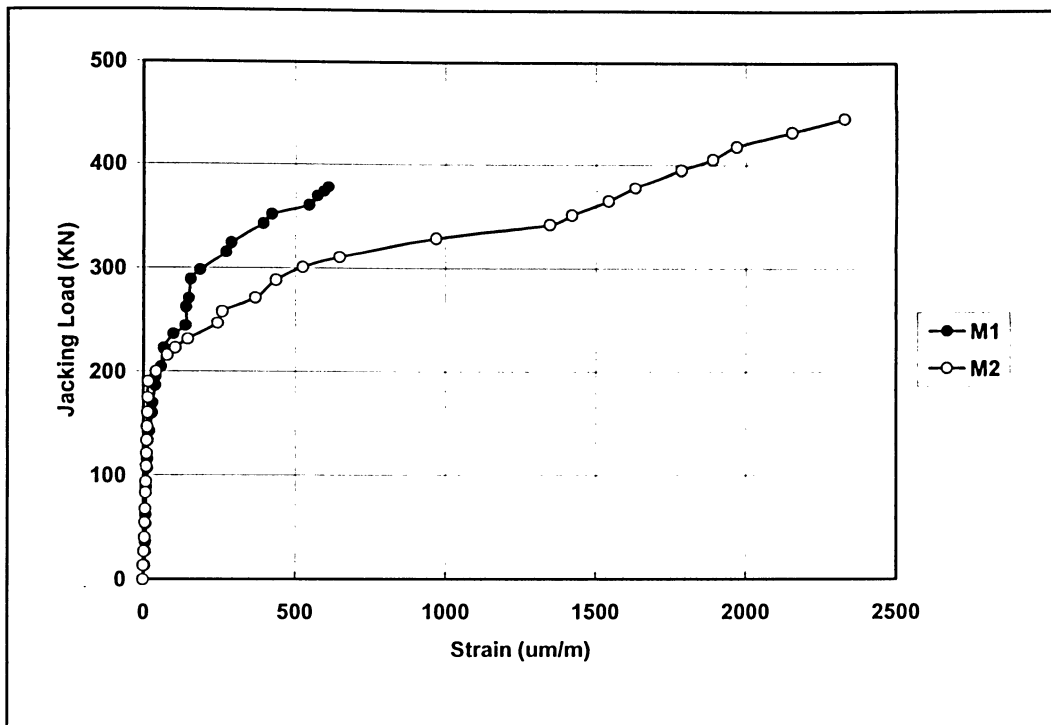Figure 5.23 Load-Strain Curves for BS1 Strain Gauges for Models M1 and M2

127

Figure 5.24 Load-Strain Curves for BS2 Strain Gauges for Models M1 and M2

Figure 5.25 Load-Strain Curves for BS3 Strain Gauges for Models M1 and M2

128

Figure 5.26 Load-Strain Curves for BS4 Strain Gauges for Models M1 and M2

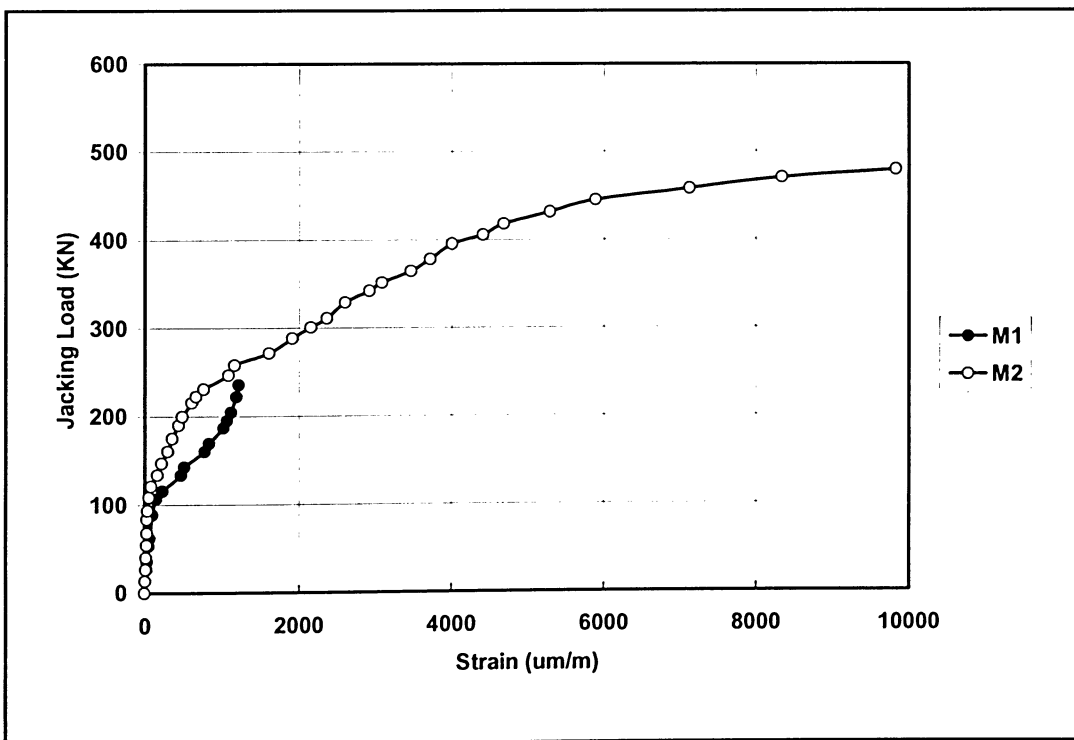Figure 5.27 Load-Strain Curves for BS5 Strain Gauges for Models M1 and M2

129
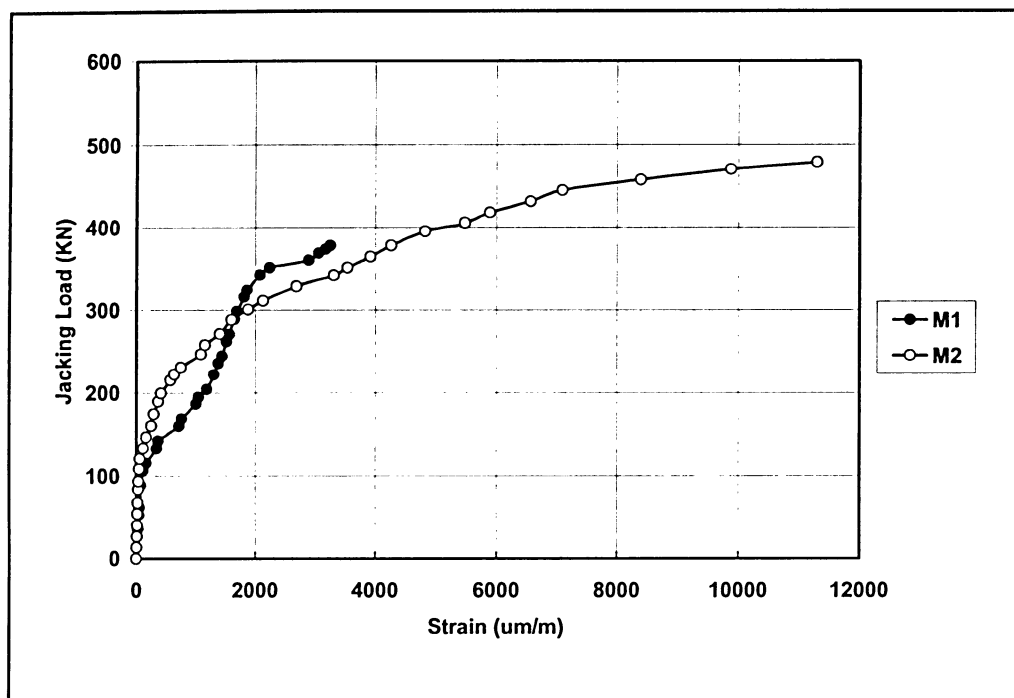
Figure 5.28 Load-Strain Curves for BS6 Strain Gauges for Models M1 and M2
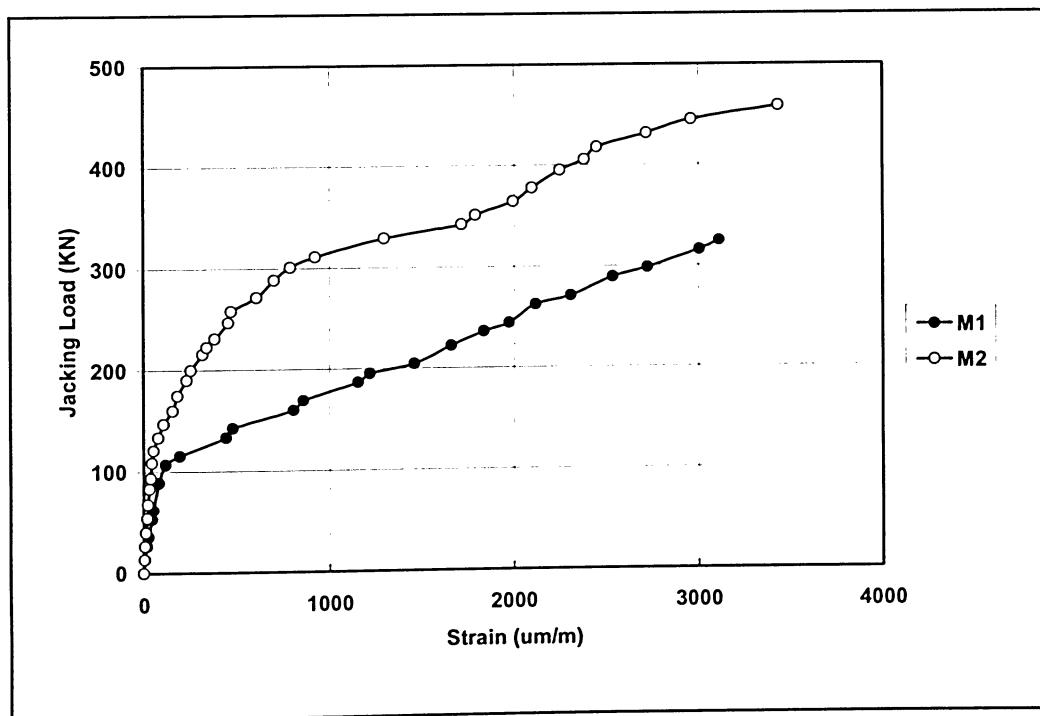
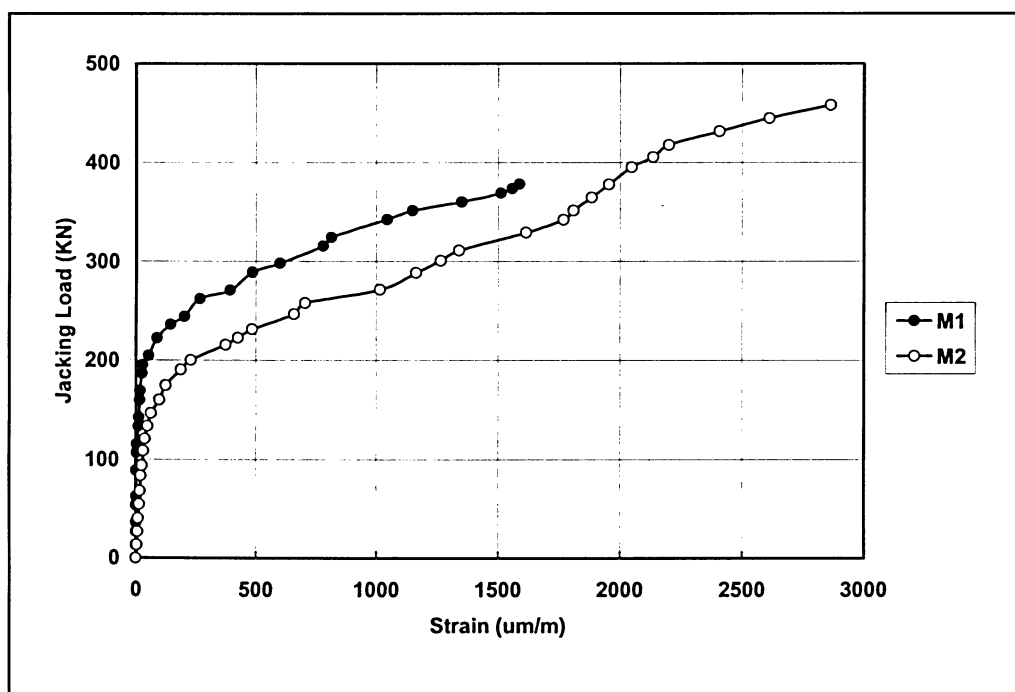Figure 5.29 Load-Strain Curves for BS7 Strain Gauges for Models M1 and M2

130

Figure 5.30 Load-Strain Curves for BS8 Strain Gauges for Models M1 and M2

Figure 5.31 Load-Strain Curves for BS9 Strain Gauges for Models M1 and M2

131

Figure 5.32 Load-Strain Curves for C1 Strain Gauges for Models M1 and M2
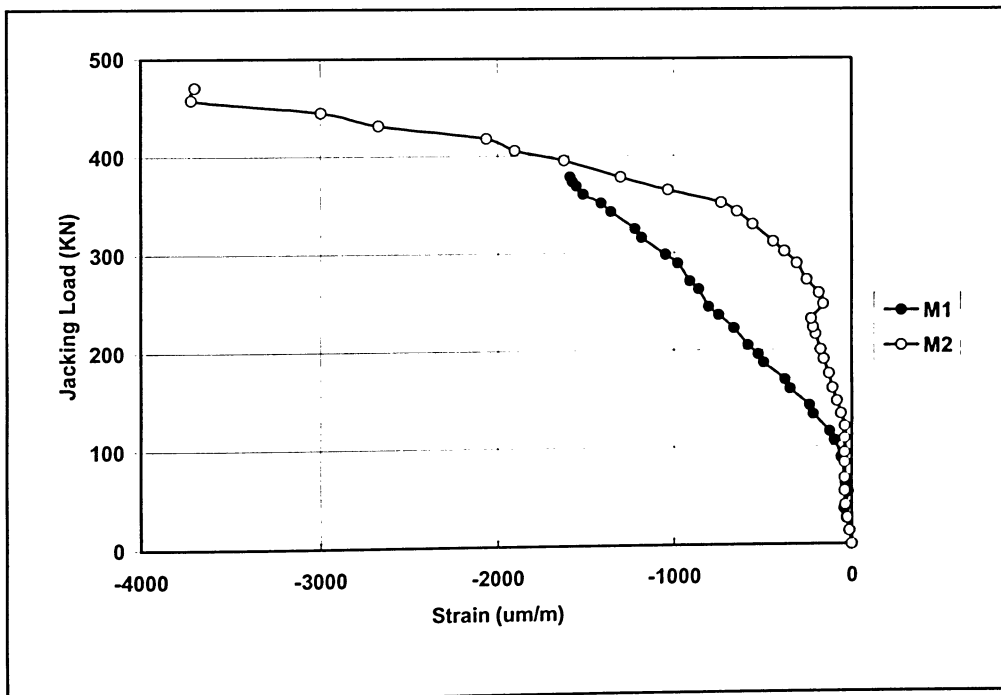
Figure 5.33 Load-Strain Curves for C2 Strain Gauges for Models M1 and M2

132

Figure 5.34 Load-Strain Curves for C3 Strain Gauges for Models M1 and M2

Figure 5.35 Load-Strain Curves for C4 Strain Gauges for Models M1 and M2
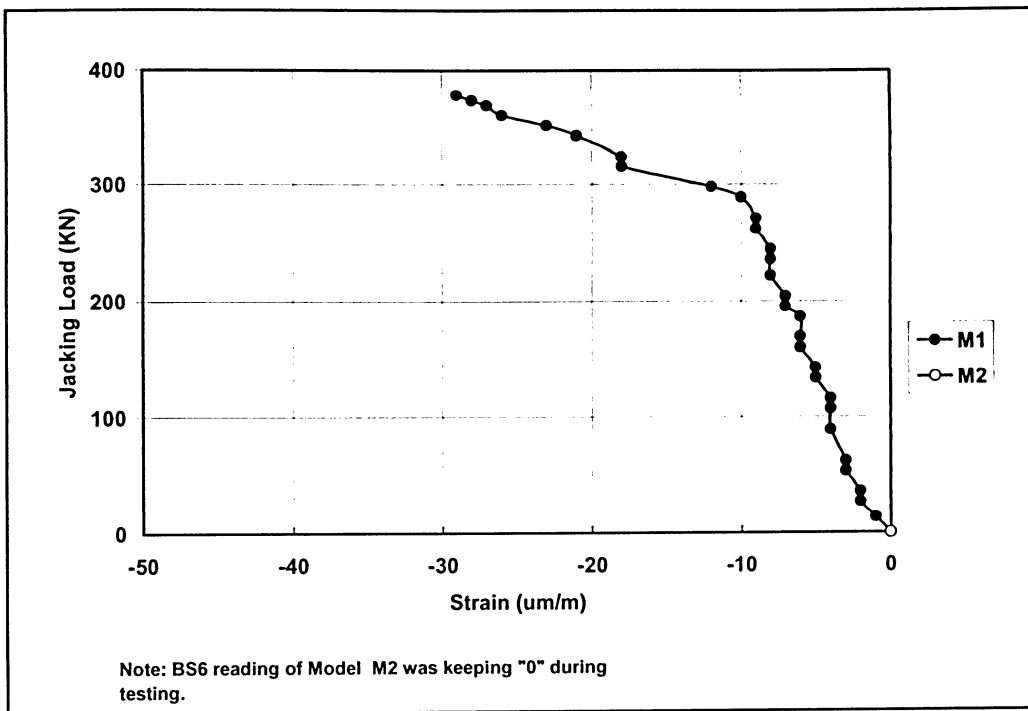
133

Figure 5.36 Load-Strain Curves for C5 Strain Gauges for Models M1 and M2

Figure 5.37 Load-Strain Curves for C6 Strain Gauges for Models M1 and M2

134

Figure 5.38 Load-Deflection Curves for LVDT #1 for Models M1 and M2

Figure 5.39 Load-Deflection Curves for LVDT #2 for Models M1 and M2

Figure 5.40 Load-Deflection Curves for LVDT #3 for Models M1 and M2

Figure 5.41 Load-Deflection Curves for LVDT #4 for Models M1 and M2

Figure 5.42 Load-Deflection Curves for LVDT #5 for Models M1 and M2
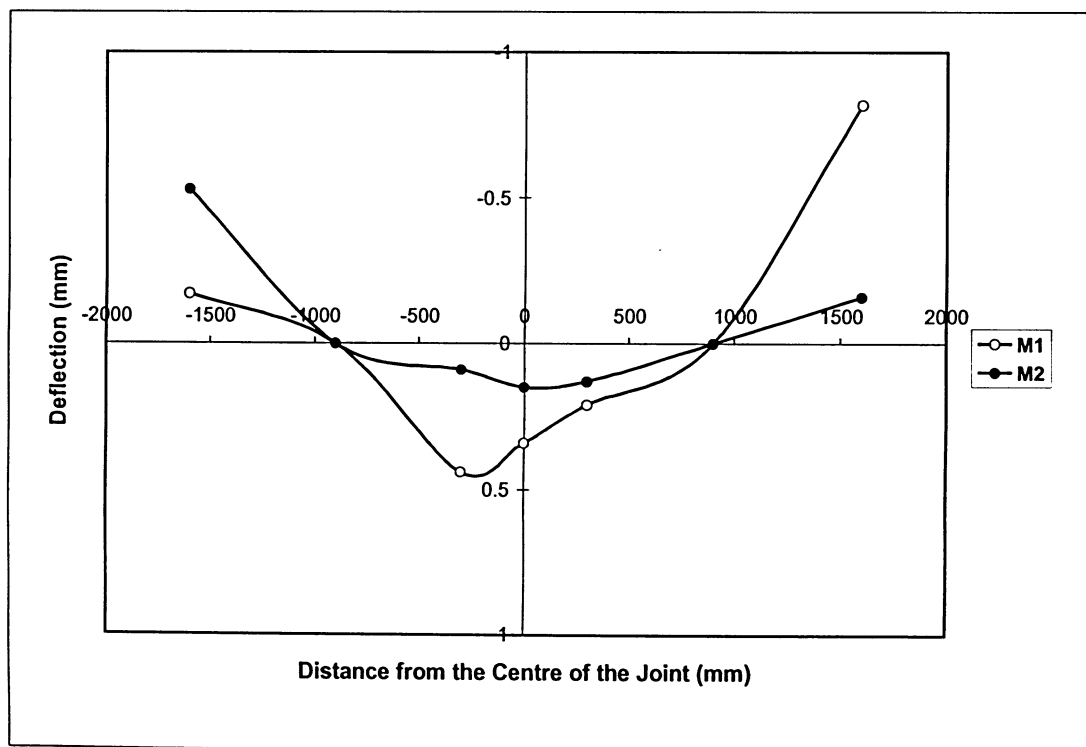
Figure 5.43 Deflection of Deck Slab of Models M1 and M2 at Load 75KN

Figure 5.44 Deflection of Deck Slab of Models M1 and M2 at Ultimate Load
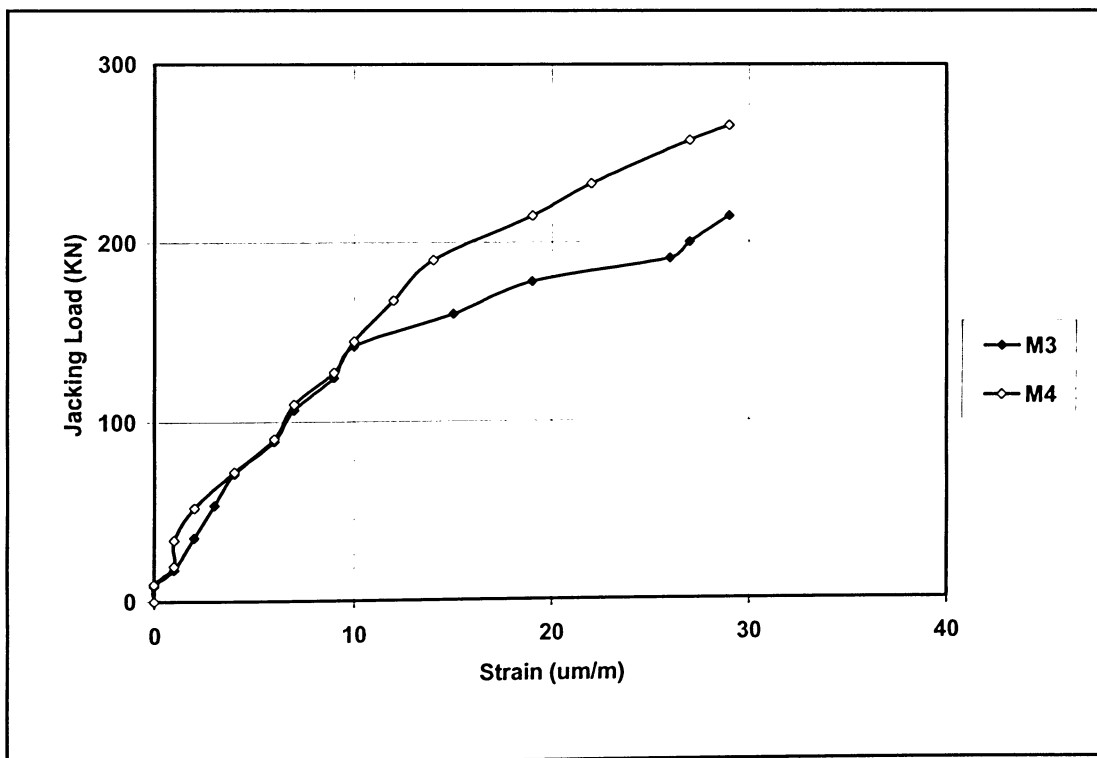
Figure 5.45 Load-Strain Curves for TS1 Strain Gauges for Models M3 and M4
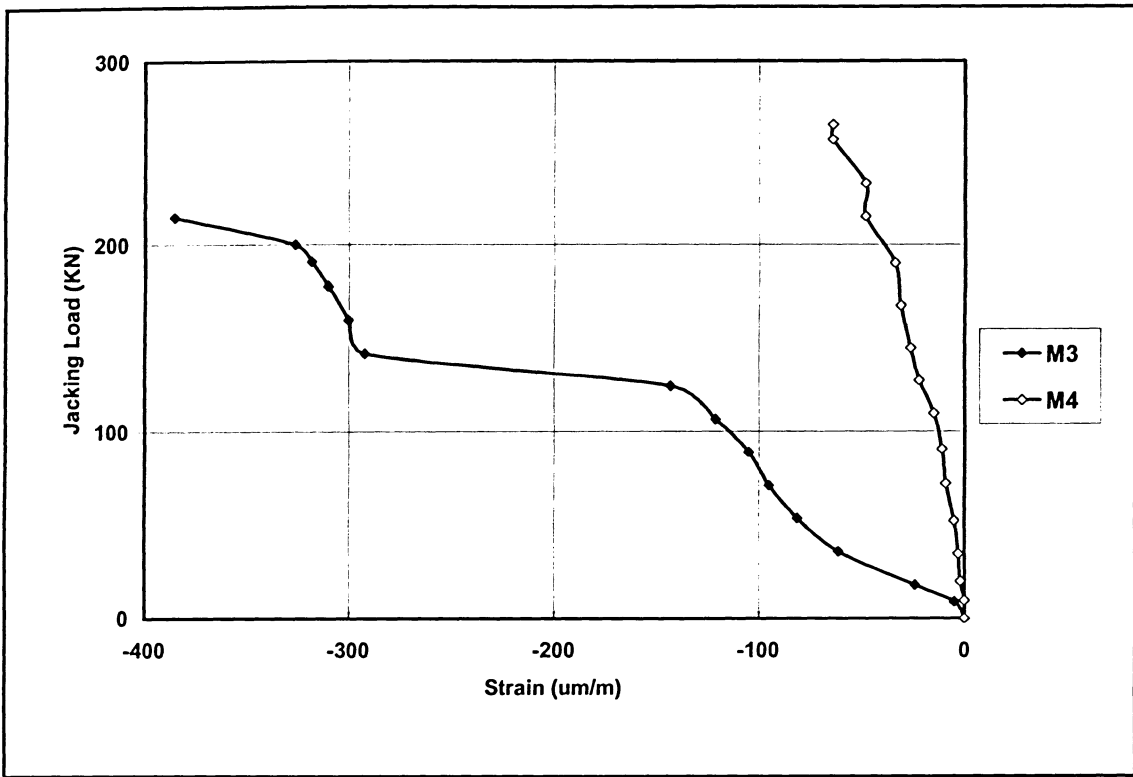
Figure 5.46 Load-Strain Curves for TS2 Strain Gauges for Models M3 and M4
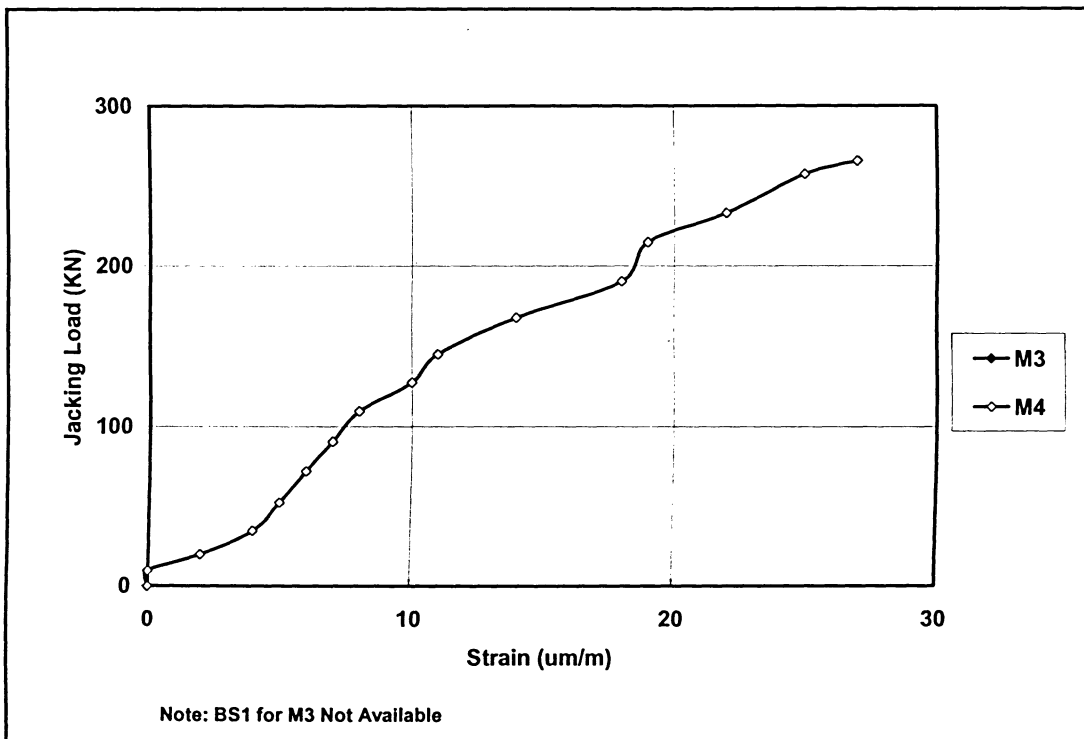
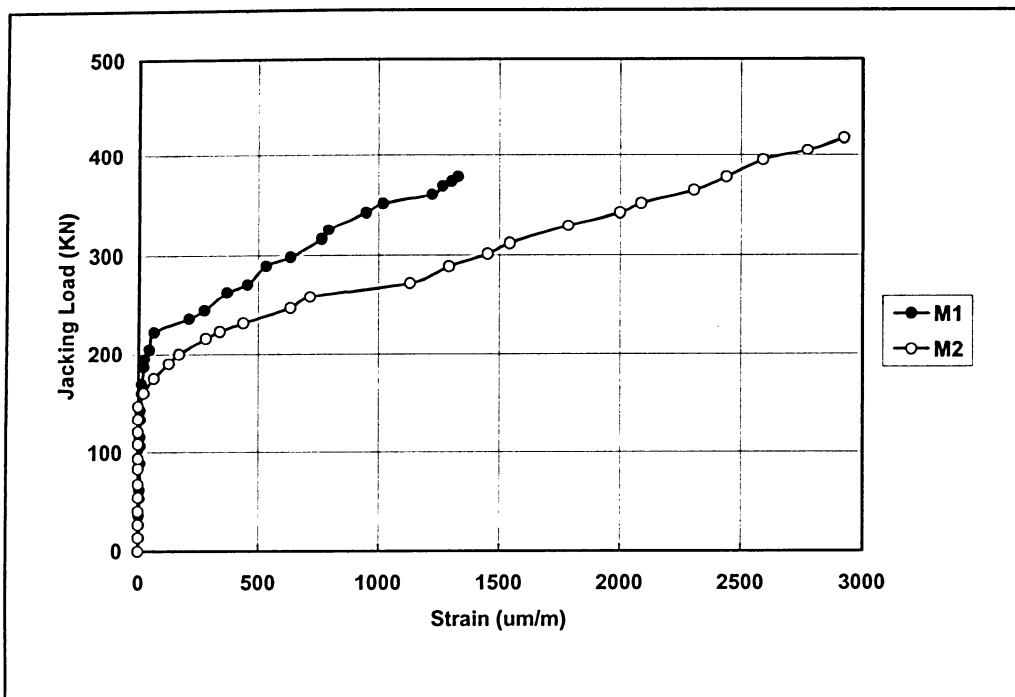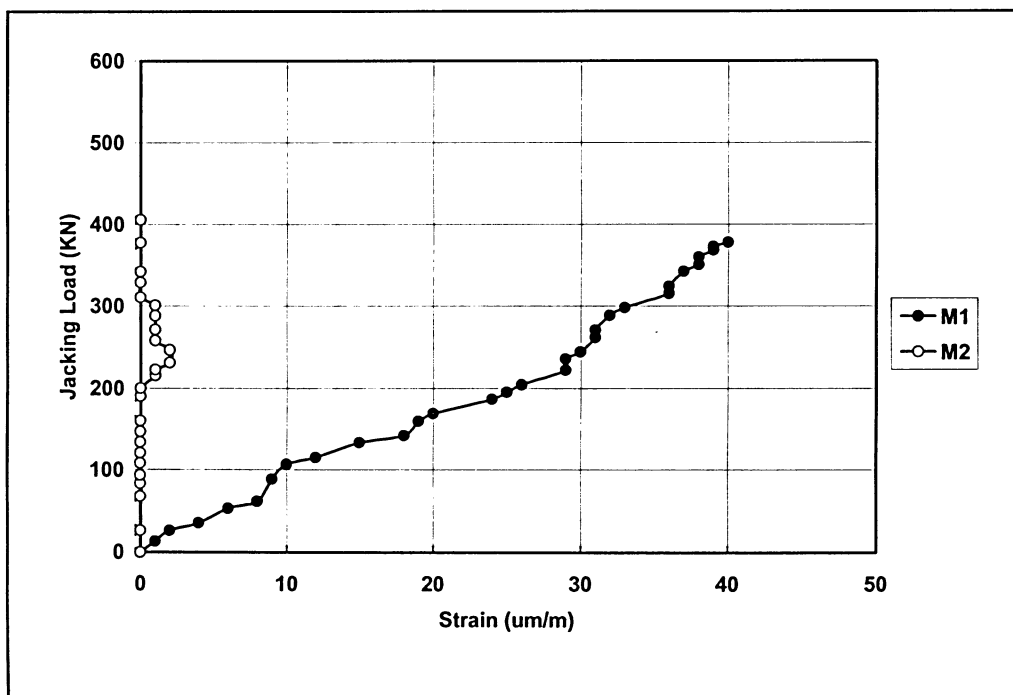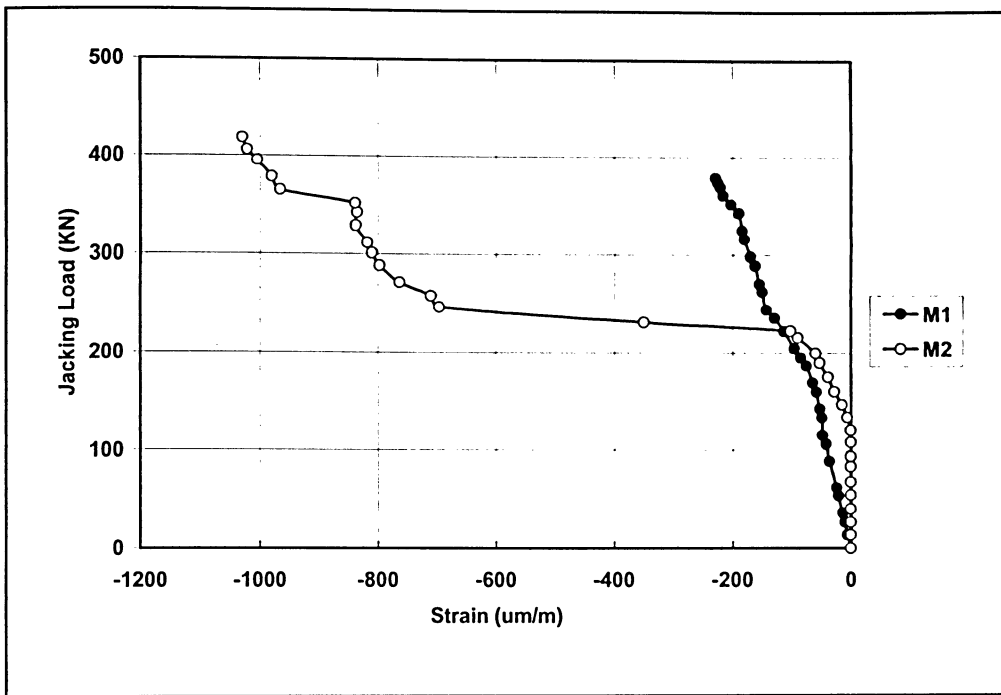Figure 5.47 Load-Strain Curves for BS1 Strain Gauges for Models M3 and M4

139
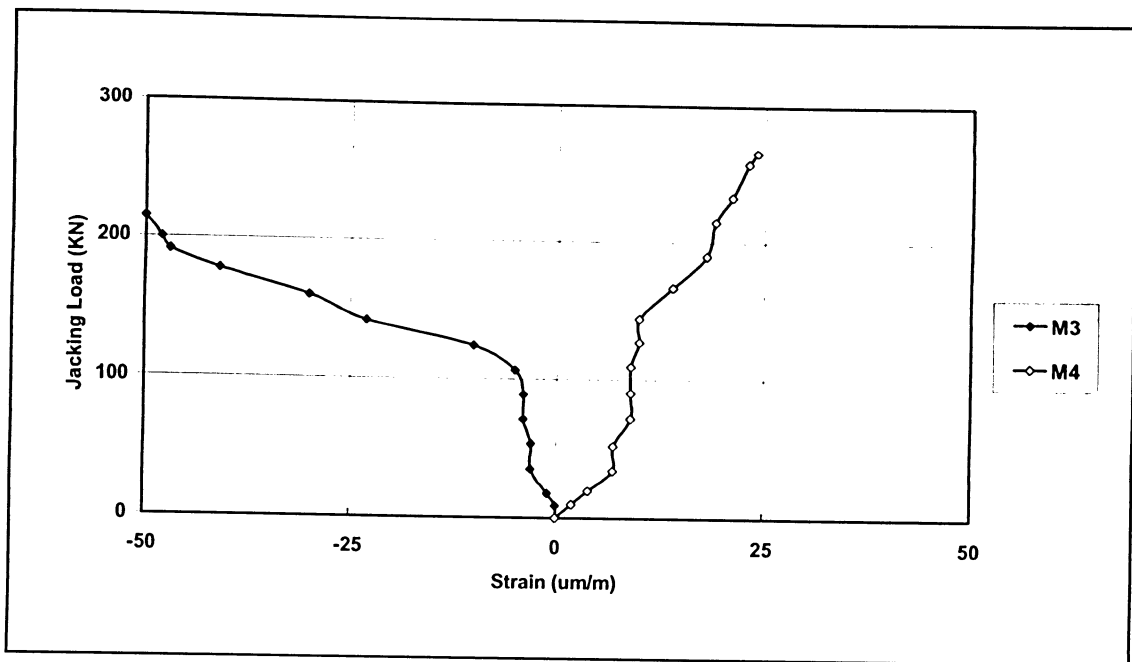
Figure 5.48 Load-Strain Curves for BS2 Strain Gauges for Models M3 and M4
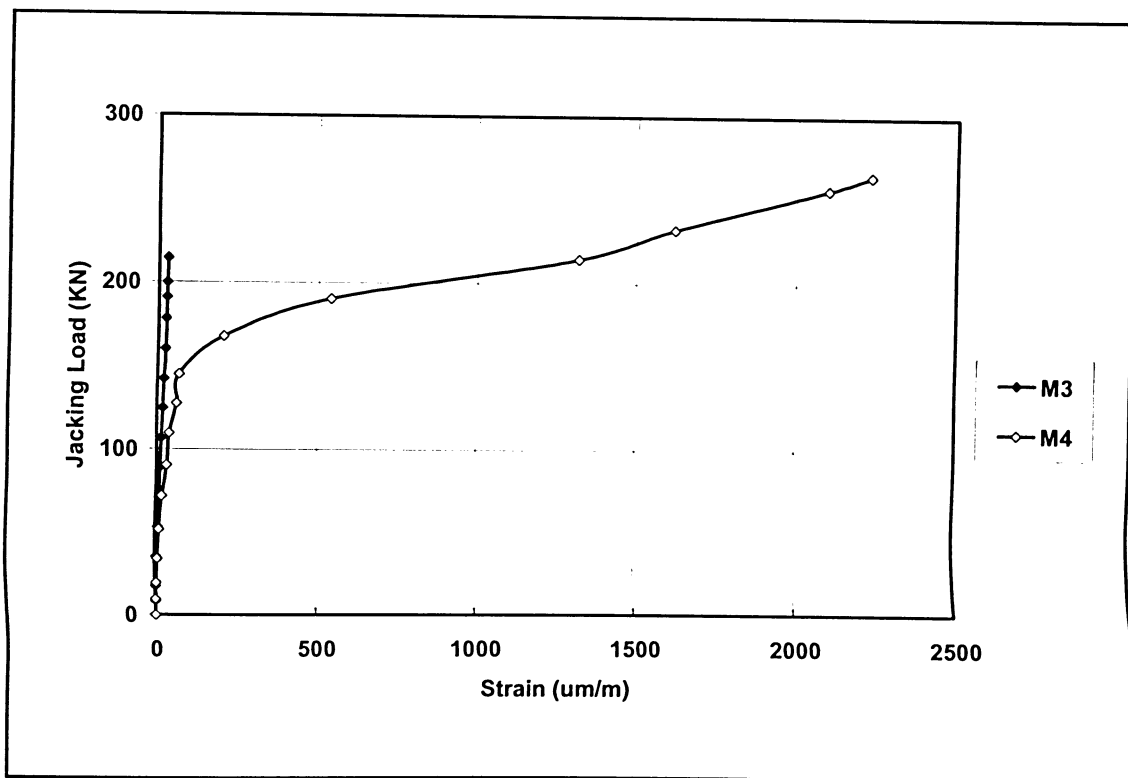
Figure 5.49 Load-Strain Curves for BS5 Strain Gauges for Models M3 and M4
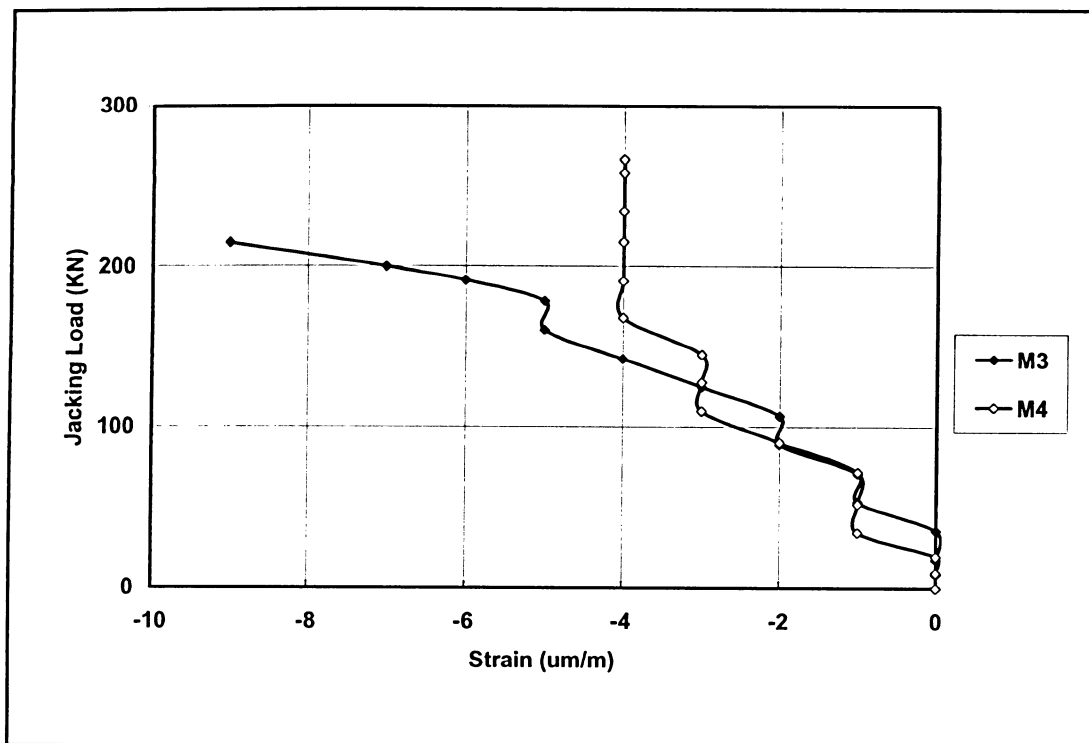
Figure 5.50 Load-Strain Curves for BS6 Strain Gauges for Models M3 and M4
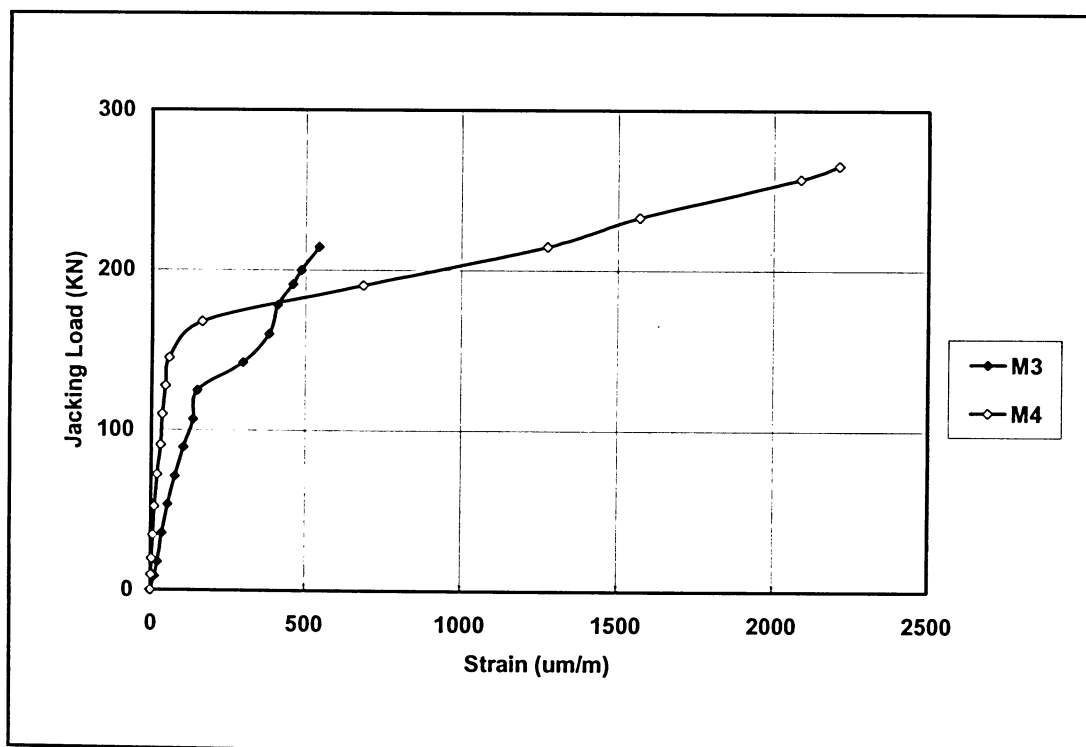
Figure 5.51 Load-Strain Curves for BS8 Strain Gauges for Models M3 and M4

141
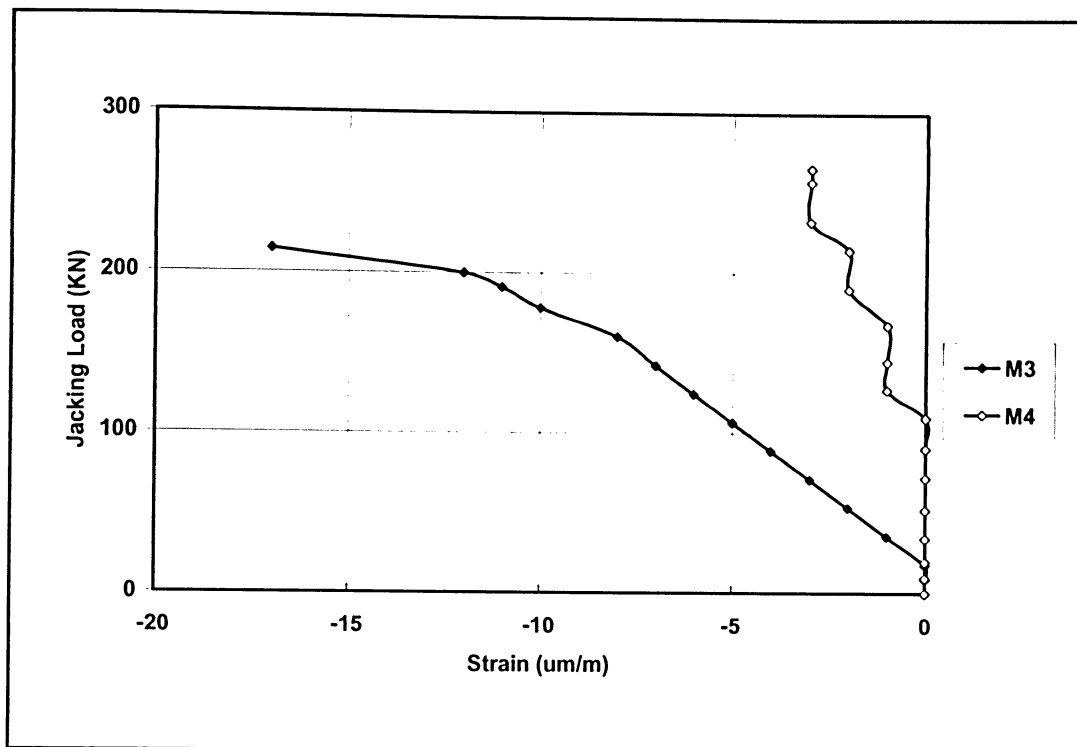
Figure 5.52 Load-Strain Curves for BS9 Strain Gauges for Models M3 and M4
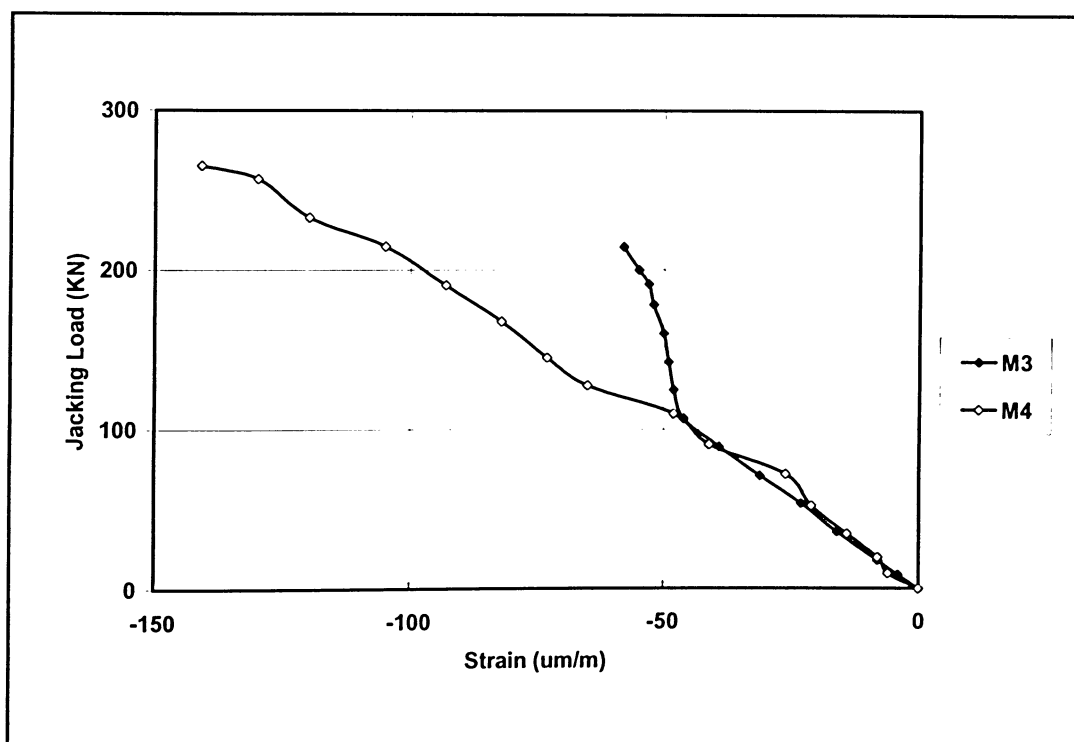
Figure 5.53 Load-Strain Curves for C1 Strain Gauges for Models M3 and M4
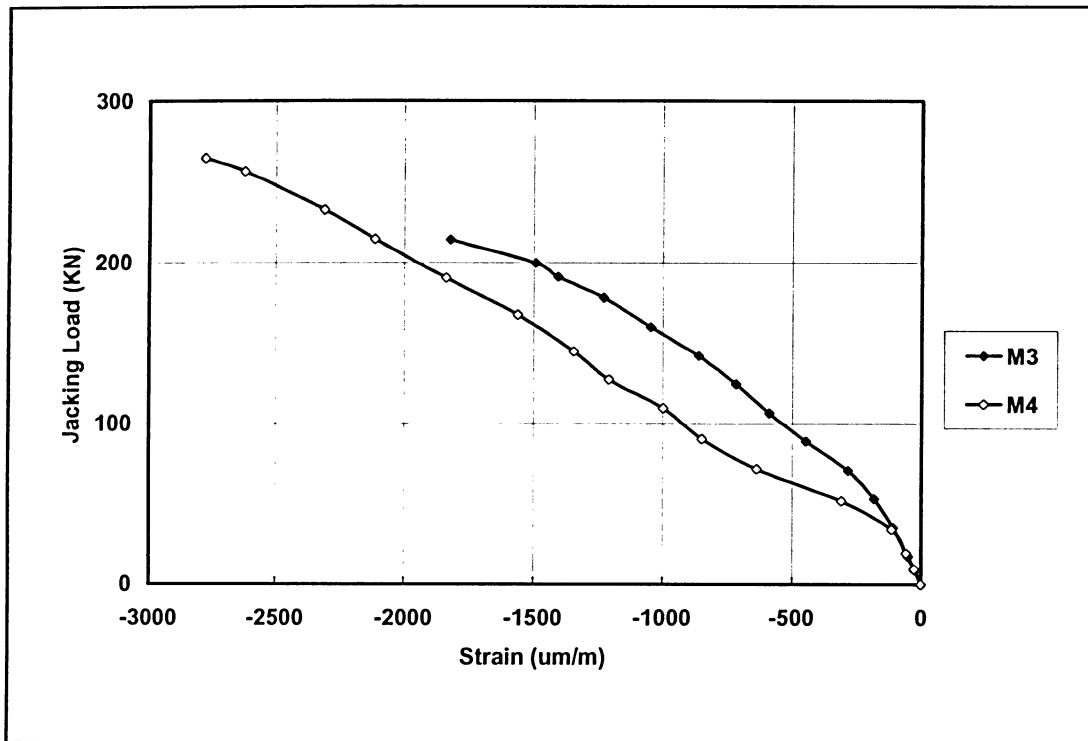
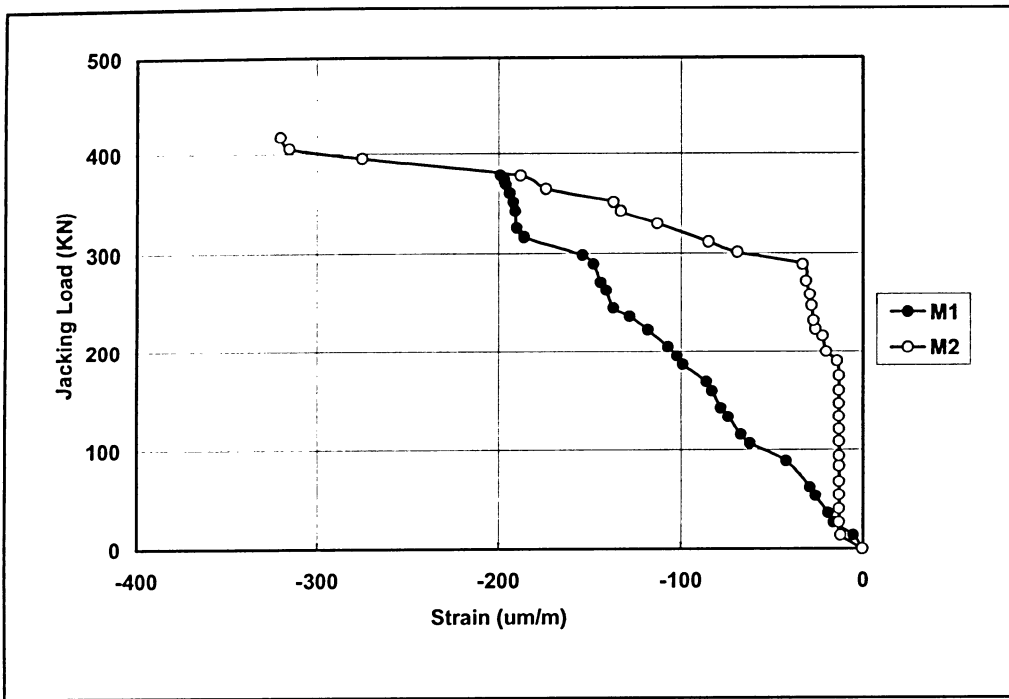Figure 5.54 Load-Strain Curves for C2 Strain Gauges for Models M3 and M4
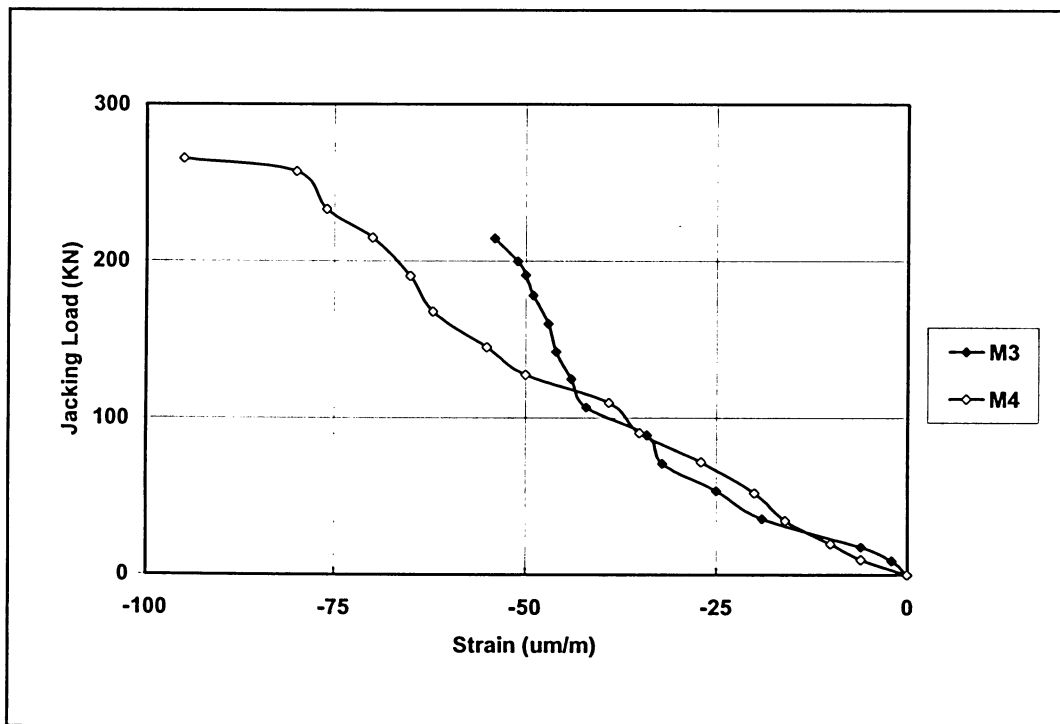
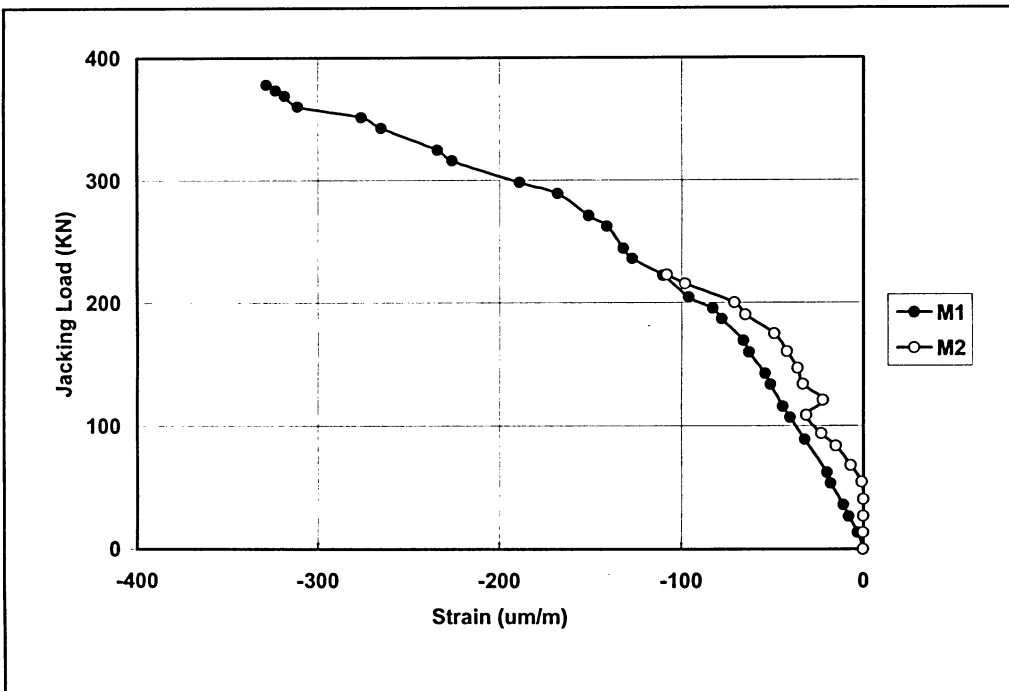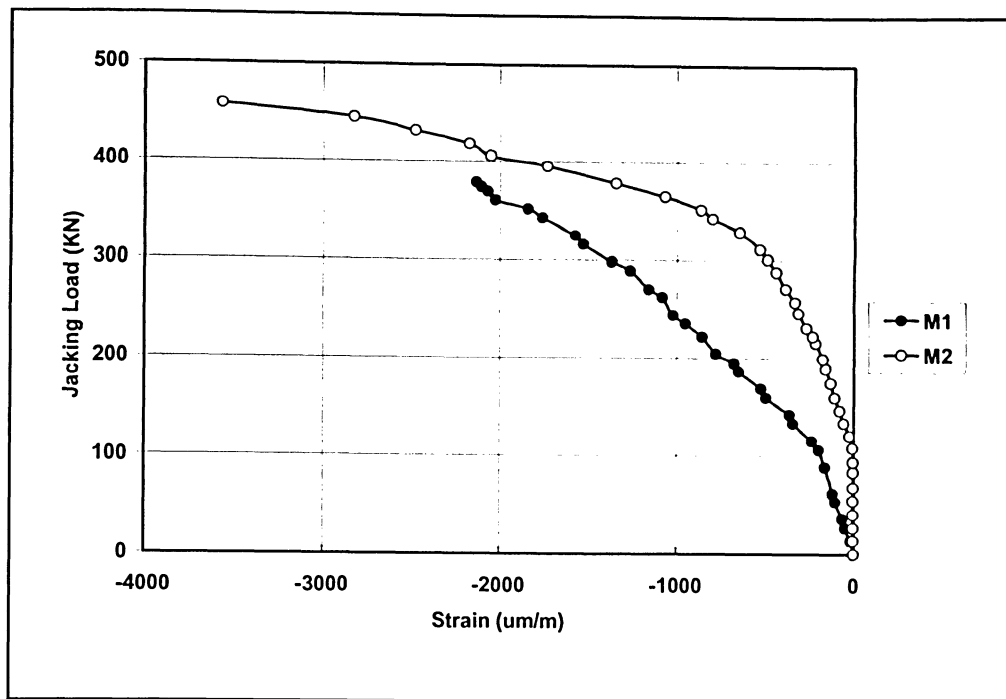Figure 5.55 Load-Strain Curves for C3 Strain Gauges for Models M3 and M4

143
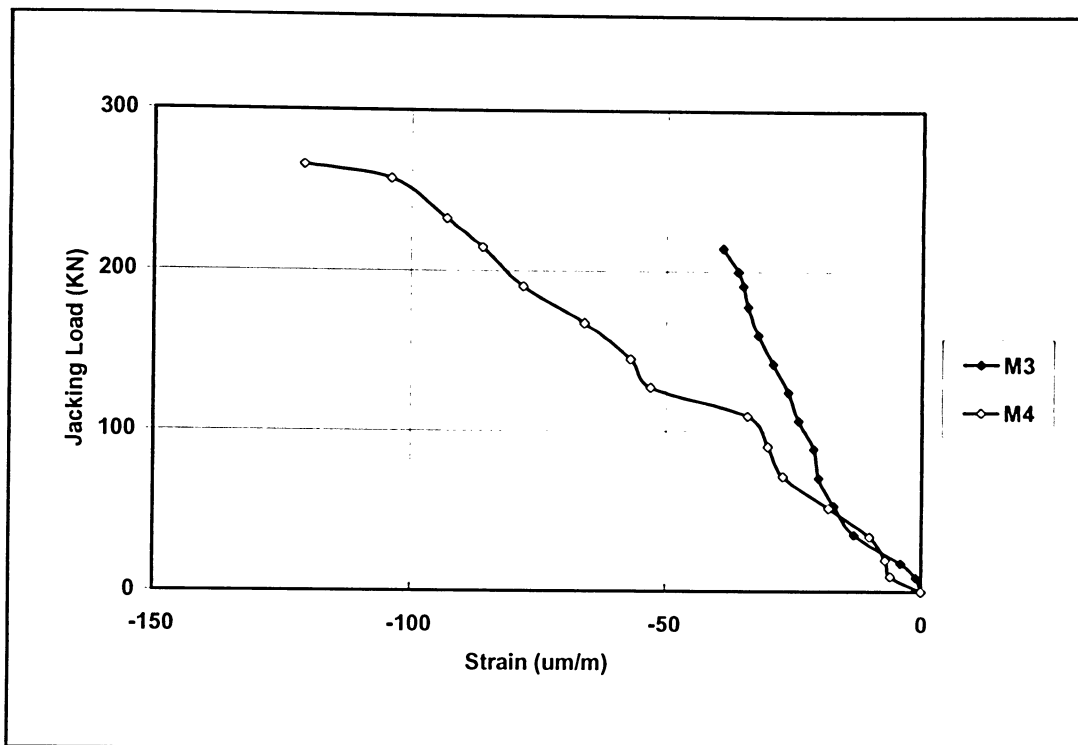
Figure 5.56 Load-Strain Curves for C4 Strain Gauges for Models M3 and M4
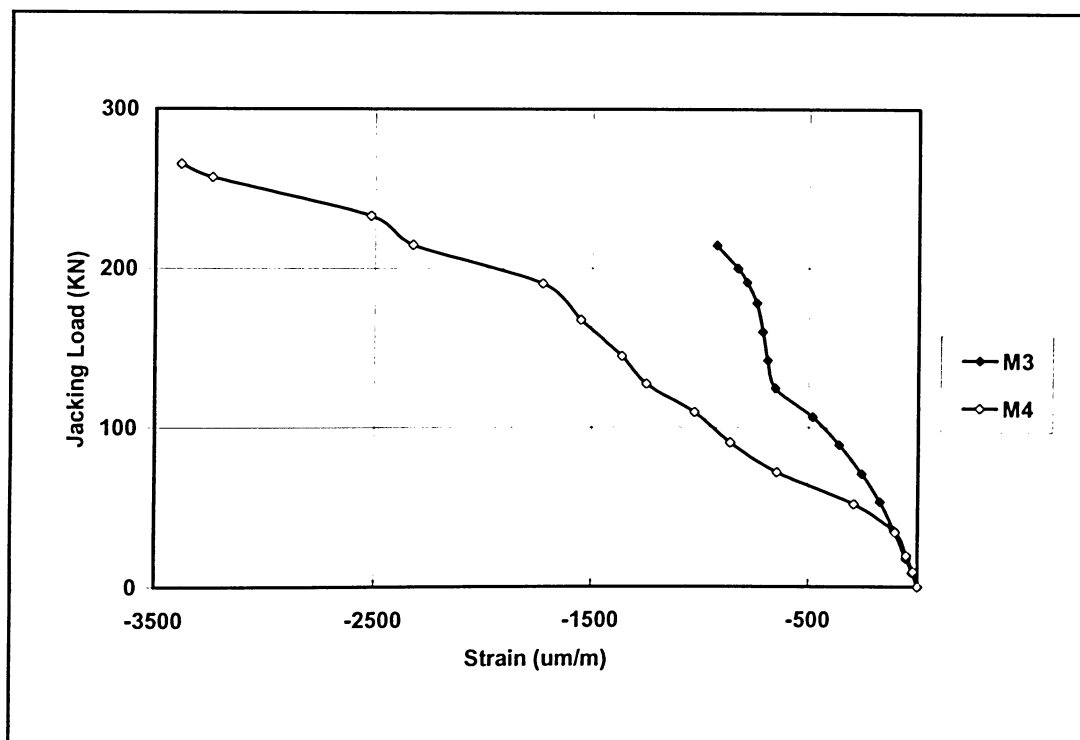
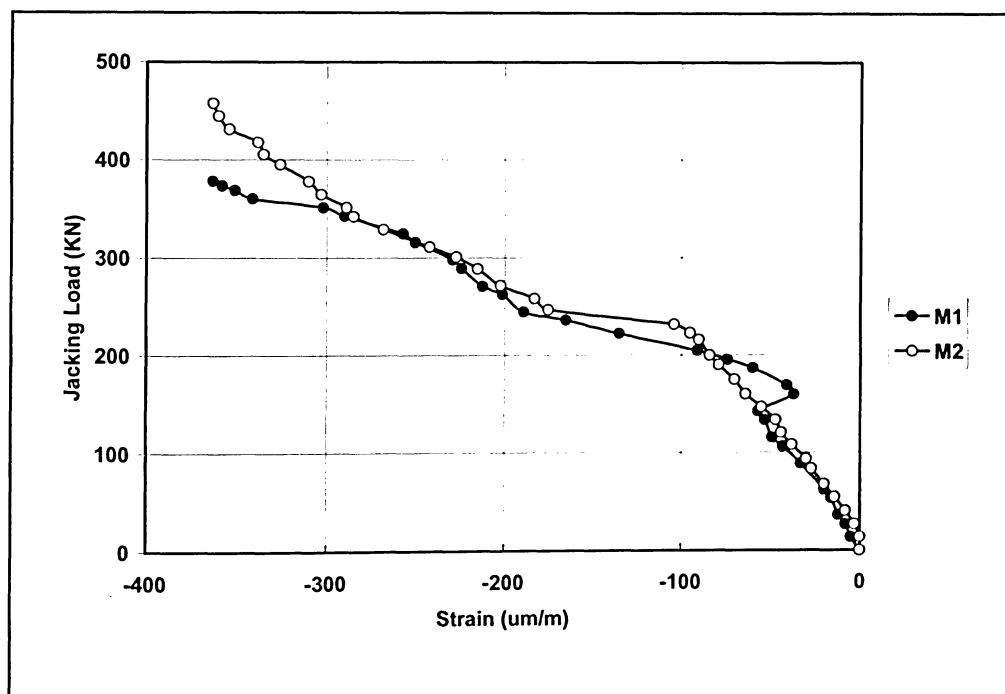Figure 5.57 Load-Strain Curves for C5 Strain Gauges for Models M3 and M4

144
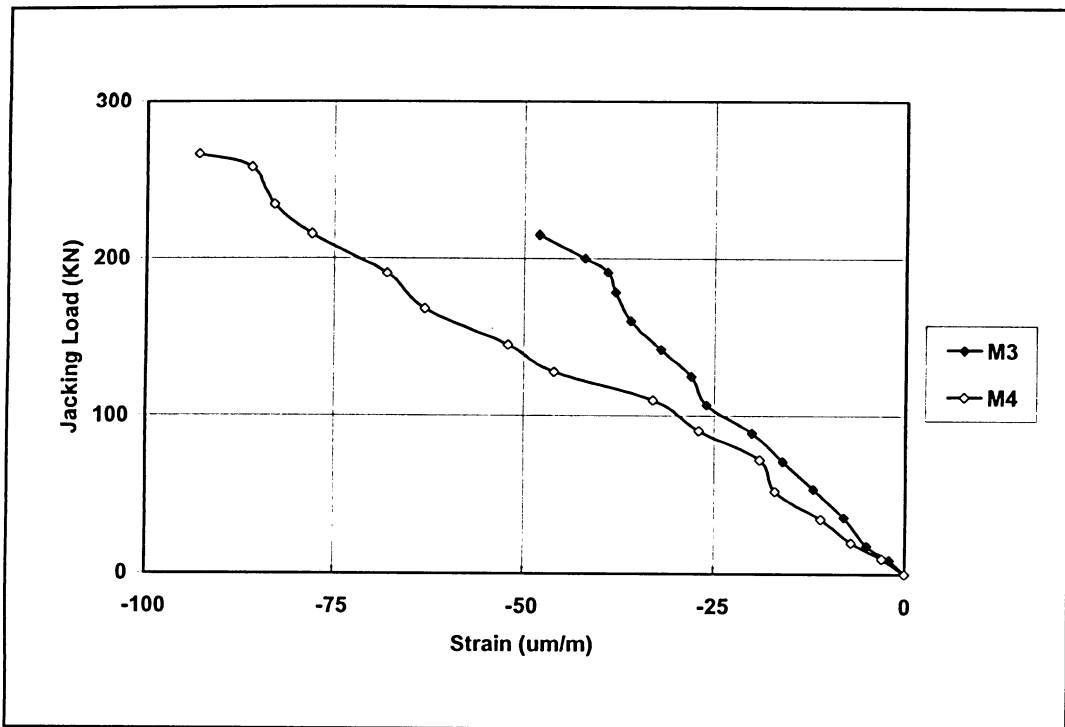
Figure 5.58 Load-Strain Curves for C6 Strain Gauges for Models M3 and M4
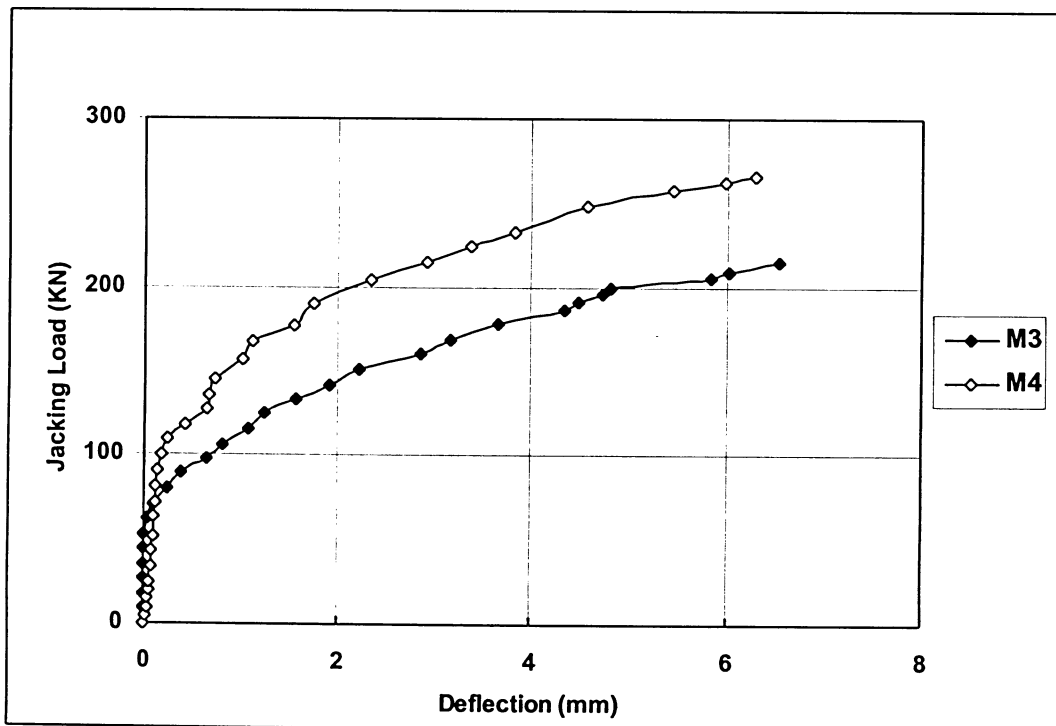
Figure 5.59 Load-Deflection Curves for LVDT #1 for Models M3 and M4
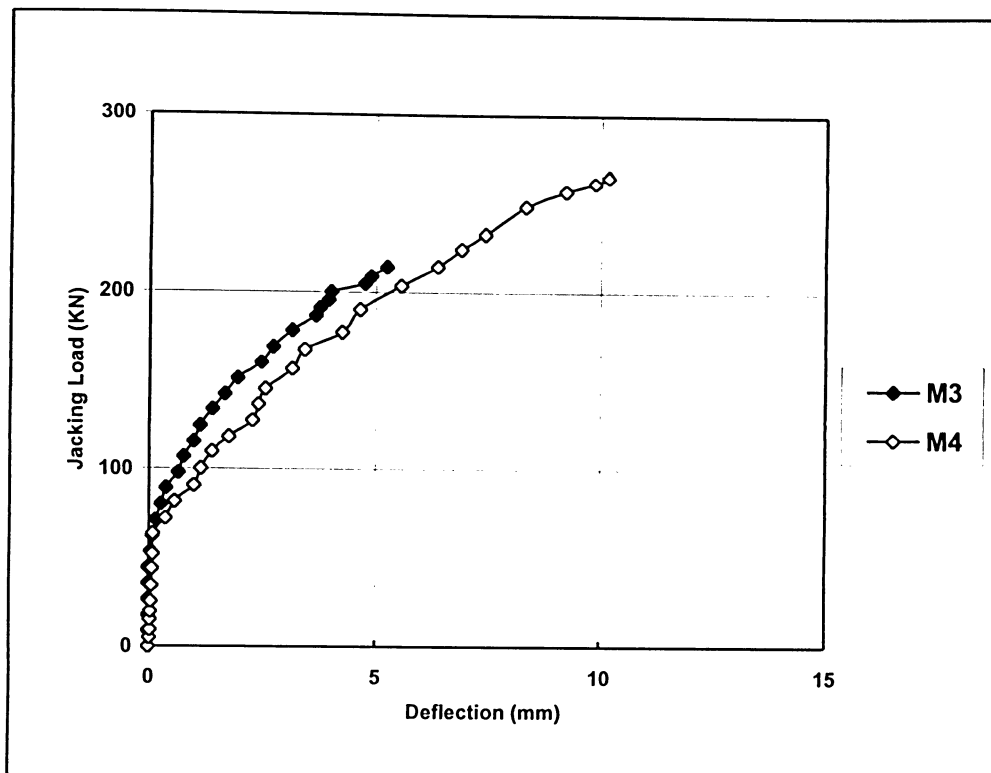
Figure 5.60 Load-Deflection Curves for LVDT #2 for Models M3 and M4
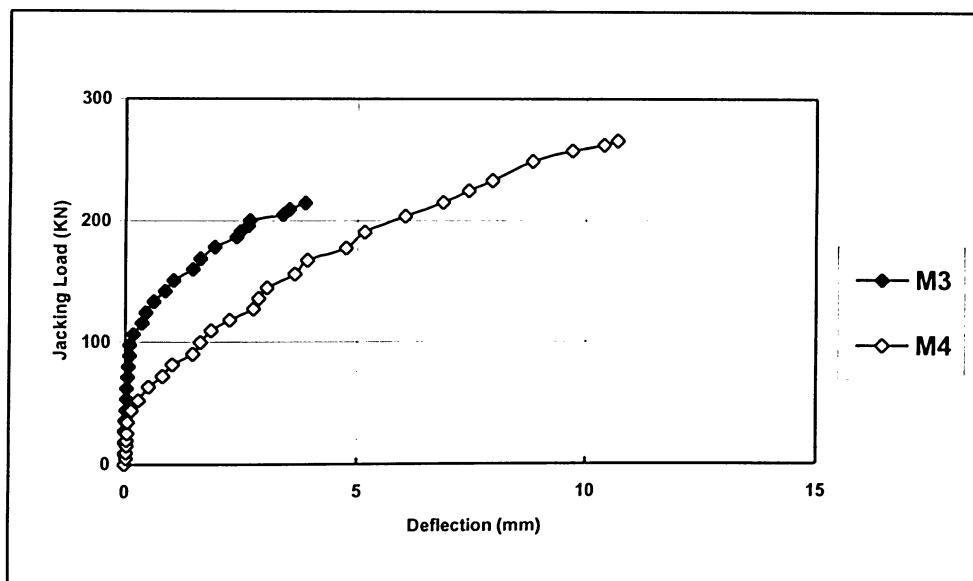
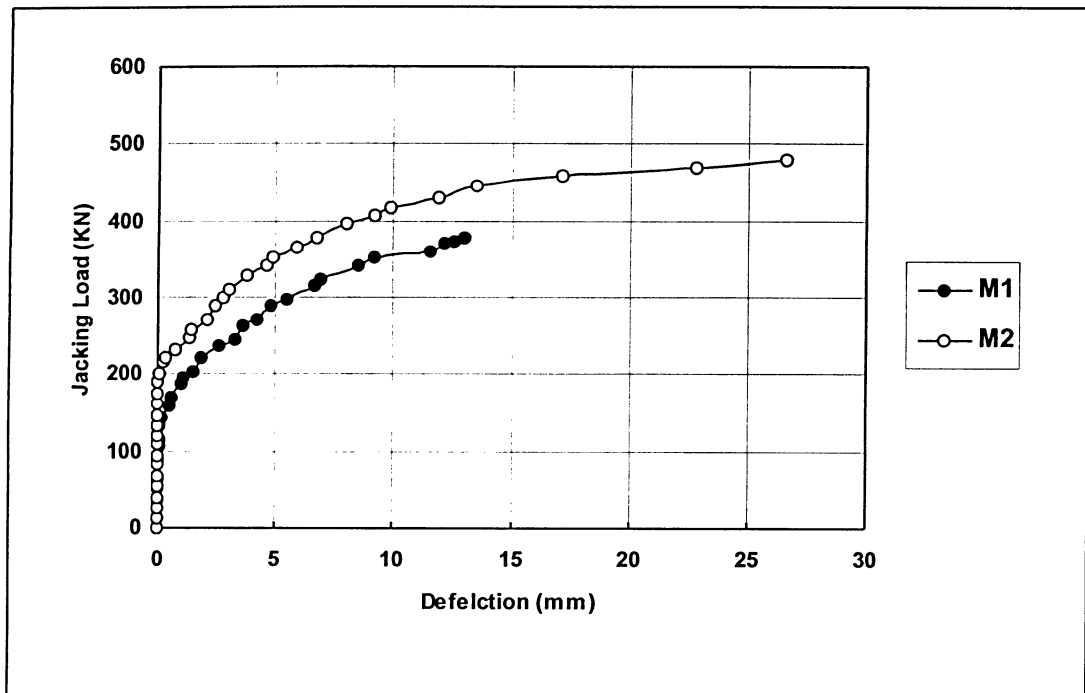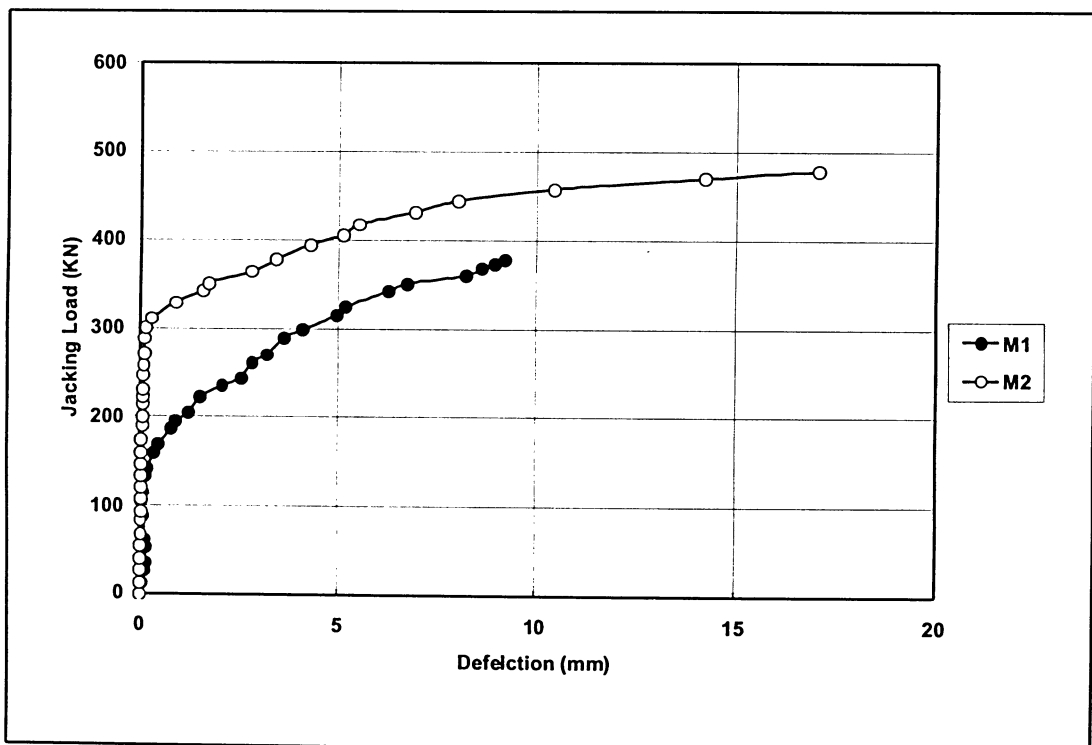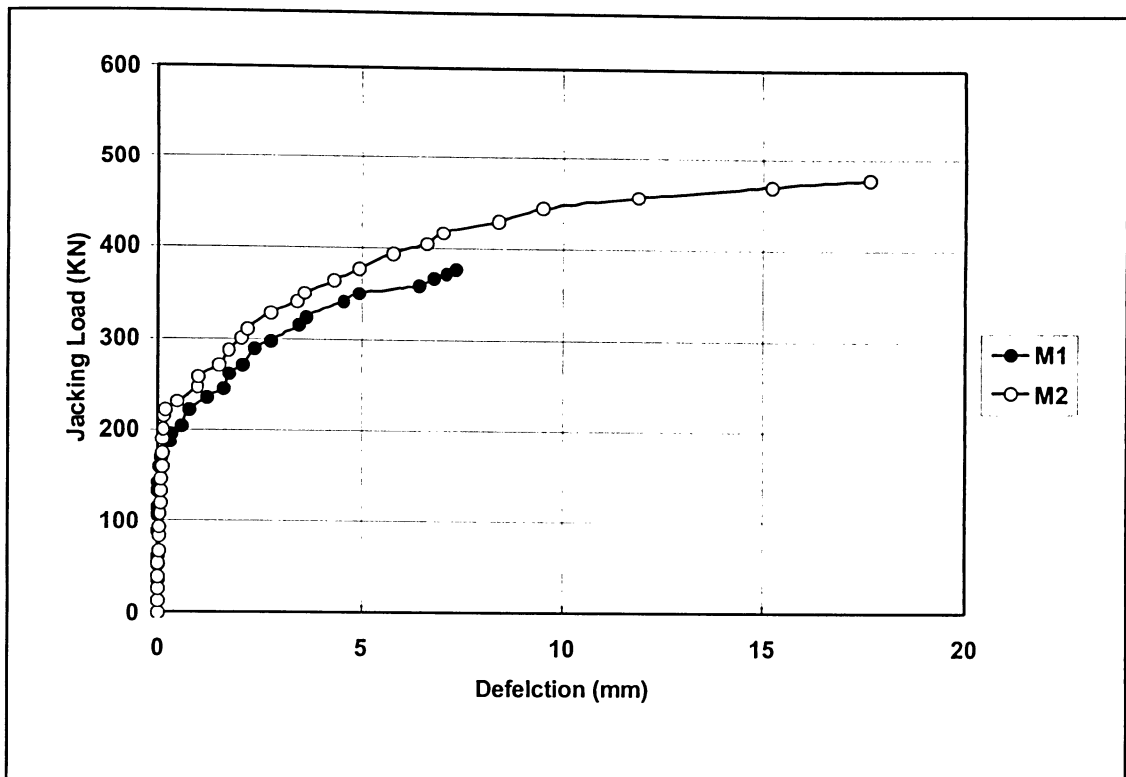Figure 5.61 Load-Deflection Curves for LVDT #3 for Models M3 and M4
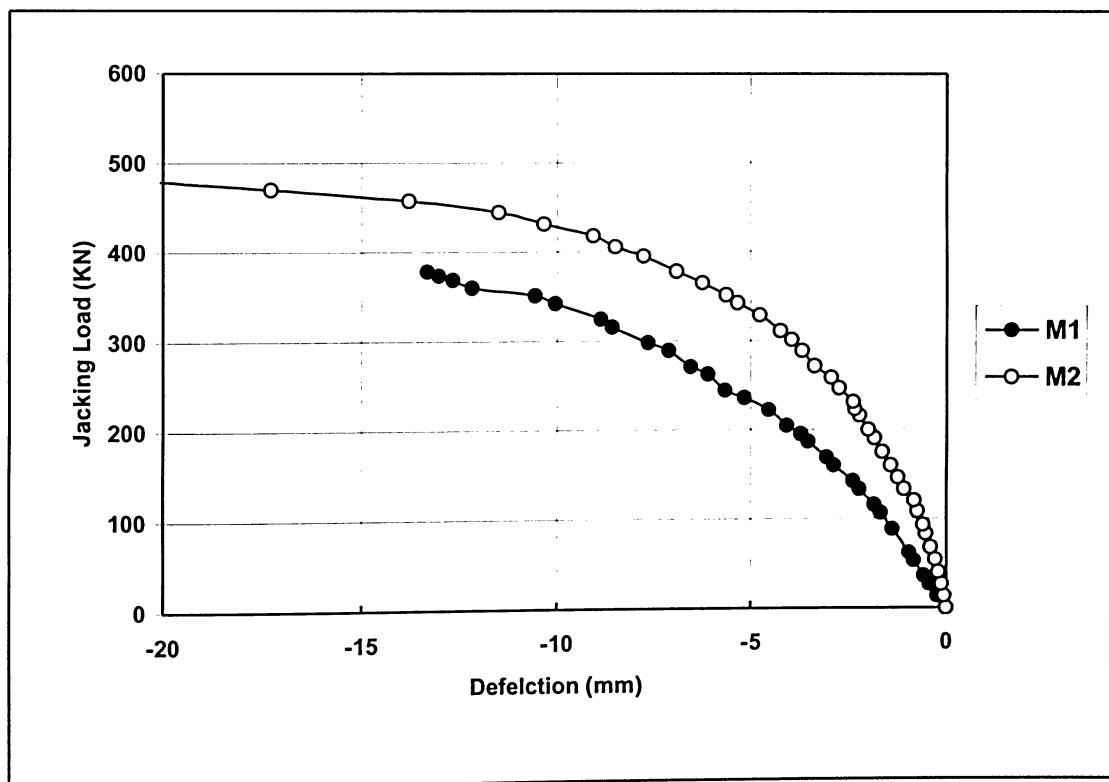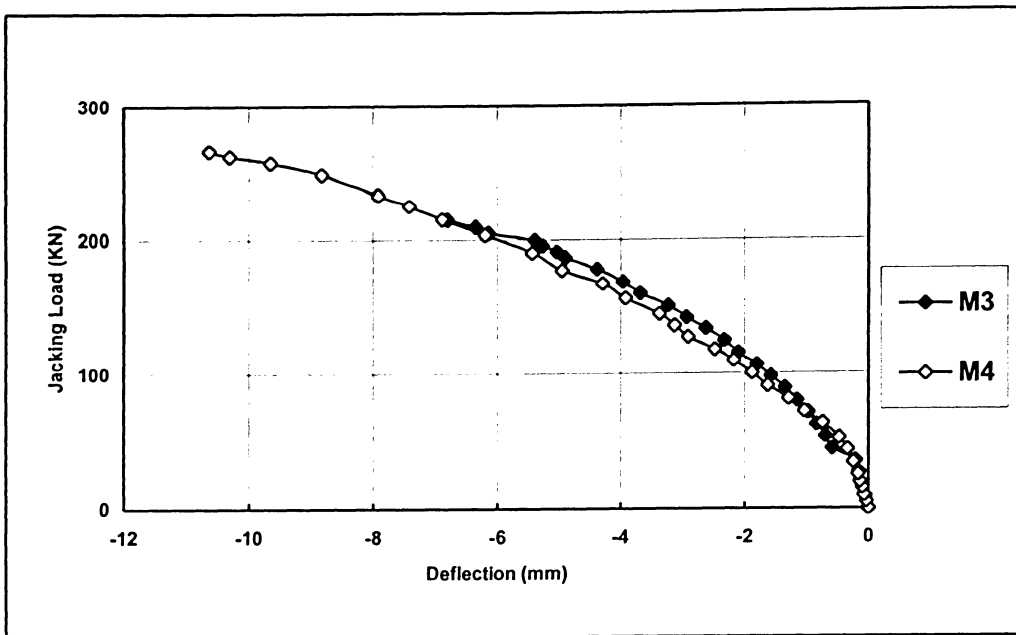
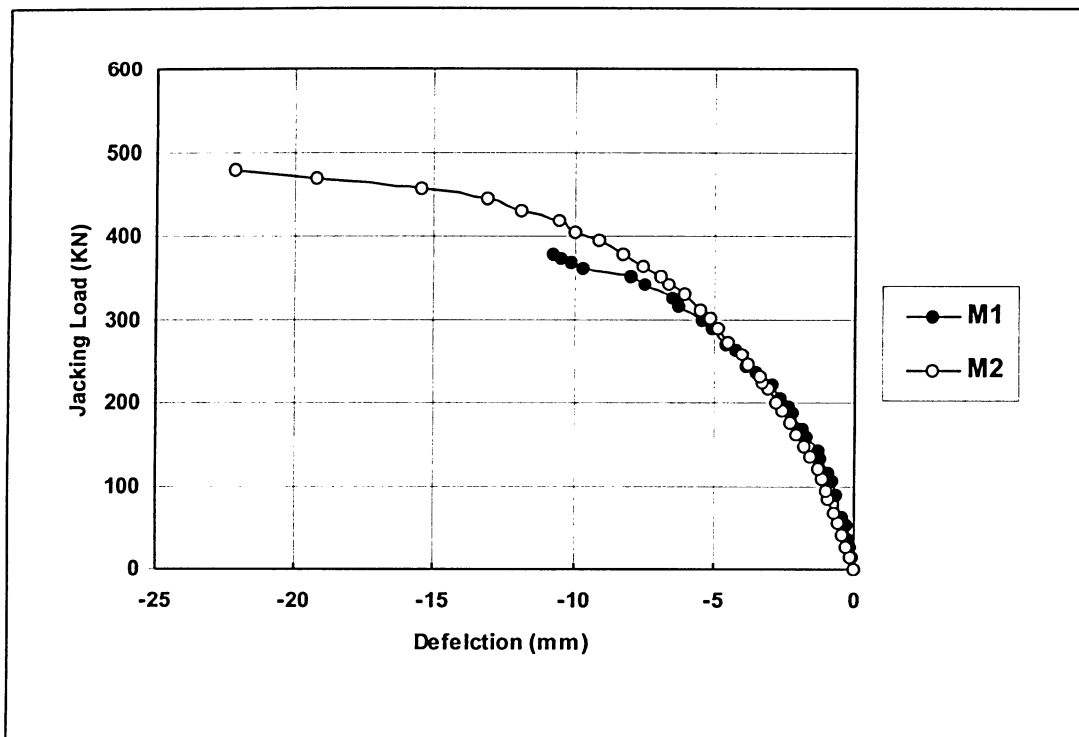Figure 5.62 Load-Deflection Curves for LVDT #4 for Models M3 and M4
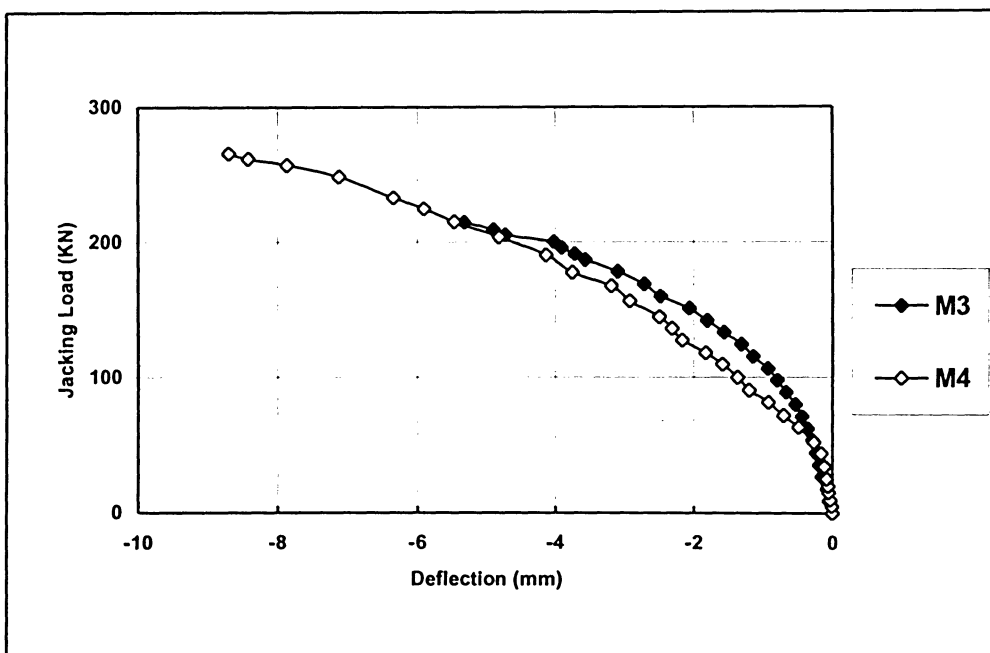
Figure 5.63 Load-Deflection Curves for LVDT #5 for Models M3 and M4

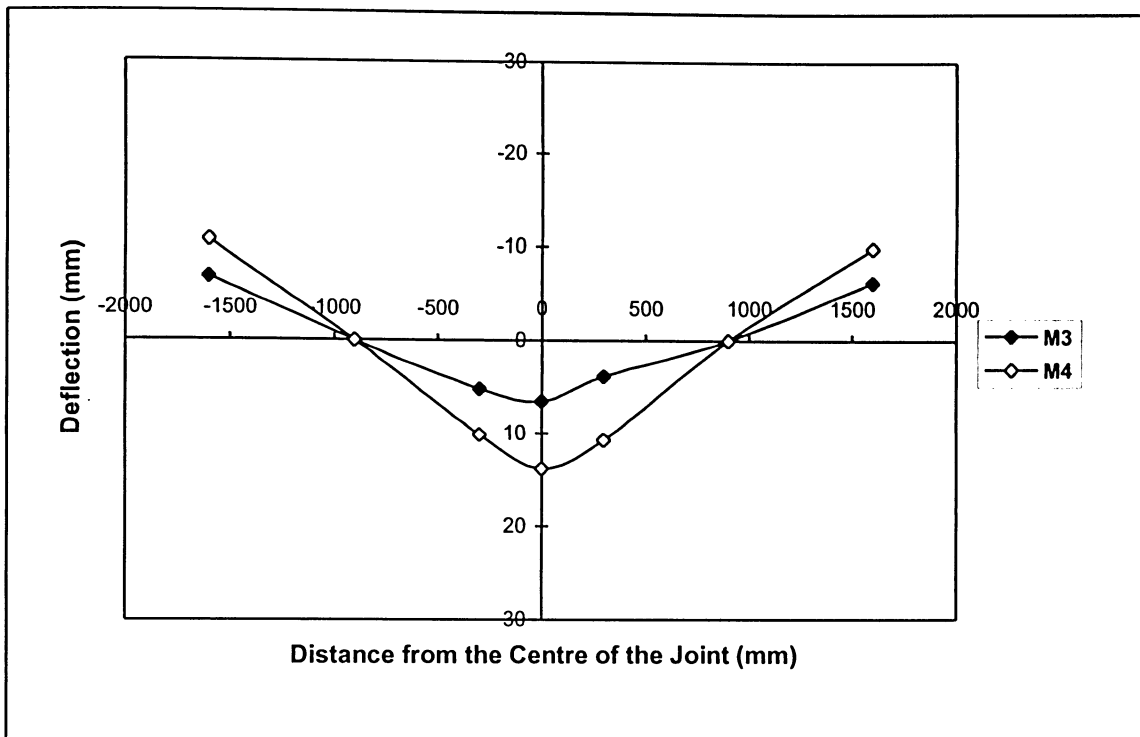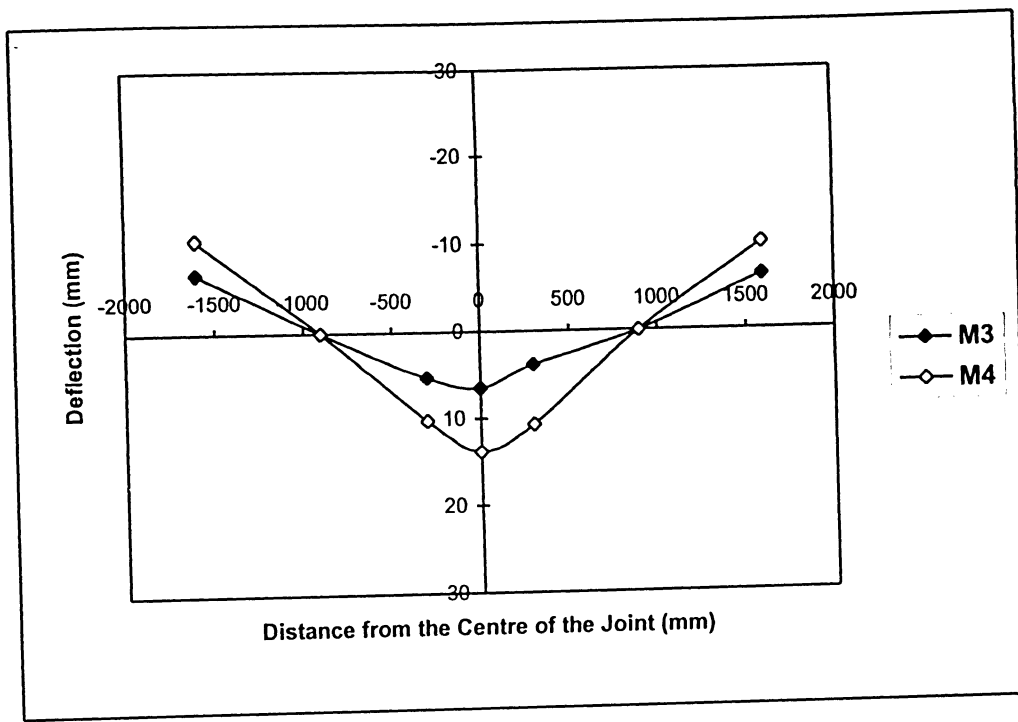Figure 5.64 Deflection of Deck Slab of Models M3 and M4 at Ultimate Load

APPENDIX A

MATERIAL PROPERTIES

Table A.1 Grading and MSA of Coarse Aggregate

Sieve size	Percentage retained by mass	Cumulative percentage retained by mass
19 mm (3/4-in.)	0	0
12.5 mm (1/2-in.)	0	0
9.5 mm (3/8-in.)	9.66	9.66
4.75 mm (No.4)	87.57	97.23
Total		106.89
Nominal MSA	9.5 mm	

Table A.2 Grading and Fineness Modulus of Fine Aggregate

Sieve size	Percentage retained by mass	Cumulative percentage retained by mass
9.5 mm (3/8-in.)	0	0
4.75 mm (No.4)	1.66	1.66
2.36 mm (No. 8)	9.56	11.22
1.18 mm (No. 16)	13.51	24.74
600 micron (No.30)	23.70	48.44
300 micron (No. 50)	27.86	76.30
150 micron (No.100)	16.84	93.14
Total		255.49
Fineness Modulus	2.55	

Table A.3 Physical Test Results of Aggregates

Test	Coarse Aggregate	Fine aggregate
Specific gravity- (Saturated Surface-Dry Basis)	2.54	2.57
Specific gravity- Bulk	2.50	2.52
Absorption %	1.58	1.35
Surface water %	1.28	2.56

Table A.4 Physical Characteristics of Superplasticizer

Characteristic	Result
Physical test	Liquid
Specific gravity at 25^0 C	1.21
% of solid by weight	40.5
PH	8.5
Color	Dark brown
Sulphates, %	1.2

Table A.5 Properties of Nut, Bolt and Washer

Properties	Bolt	Nut	Washer
Hardness	31.6	92.3	41.1
Proof Load (kN)	126	214	-
Tensile Strength (kN)	216	-	-

Table A.6 Mix Design for Models M2 and M4 (Specimens for 2nd Testing)

Material	Quantity (per M³)	Remark
Cement (Type 10)	366 KG	
Slag	123 KG	
Sand	670 KG	
20 MM Lime Coarse Aggregate	1130 KG	
Water	102 KG	
Superplasticizer (SP)	7.2 LITER	

Table A.7 Mix Design for Joint Grout

Material	Quantity (per M³)	Remark
Cement (Type 10)	457 KG	
Fine Aggregate (Sand)	683 KG	
Coarse Aggregate	1050 KG	
Water	160 KG	
Superplasticizer (SP)	4.1 LITER	

Table A.8 Concrete Compressive Strength of Bridge Model at the Time of Testing

Model	Symbols	Average Compressive Strength (MPa)	Slump Value (mm)	Remarks
M1	MTC-1-C	56	155	
M2	MTC-2-C	45	155	
M3	IBC-1-C	59	90	
M4	IBC-2-C	48	90	

Table A.9 Concrete Compressive Strength of Joint Grout at the Time of Testing

Model	Symbols	Average Compressive Strength (MPa)	Slump Value (mm)	Remarks
M1	MTC-1-C	53	120	
M2	MTC-2-C	53	85	
M3	IBC-1-C	51	135	
M4	IBC-2-C	45	95	

152

Table A.10 Concrete Compressive Strength Development of Models M2 and M4
(Specimen for 2nd Testing)

Cylinder No.	Weight (Kg)	Concrete Strength (MPa)	Number of Days After Casting	Remarks
1	4.009	25.1	1-day	
2	4.026	23.6	1-day	
3	4.041	38.2	3-days	
5	4.008	37.3	3-days	
6	4.030	44.8	7-days	
7	3.999	45.6	7-days	
8	4.002	43.5	16-days	1st Testing
9	4.022	45.9	16-days	1st Testing
10	4.015	45.1	16-days	1st Testing
11	4.000	51.7	25-dyas	2nd Testing
12	4.005	49.8	25-days	2nd Testing
13	3.980	48.0	25-days	2nd Testing
14	4.008	55.7	28-days	
15	4.001	50.4	28-days	
16	3.999	53.4	28-days	

APPENDIX B

EXPERIMENTAL PHOTOS

AND SECONDARY FIGURES
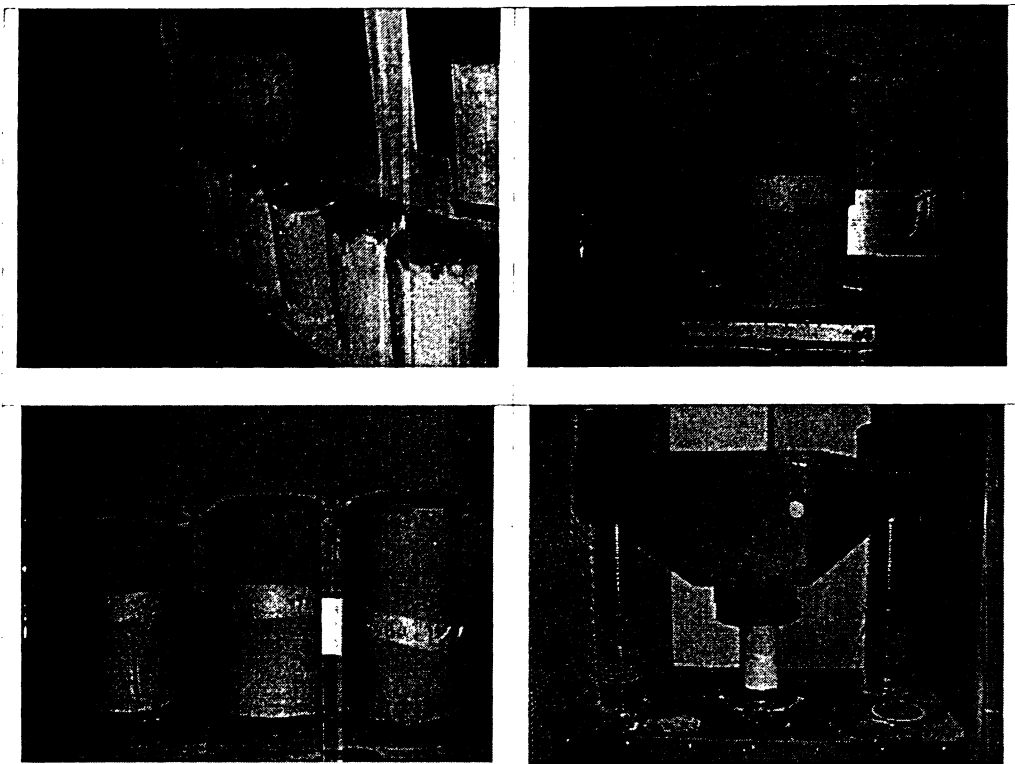
Figure B.1 Cylinders During Casting, Capping and Testing
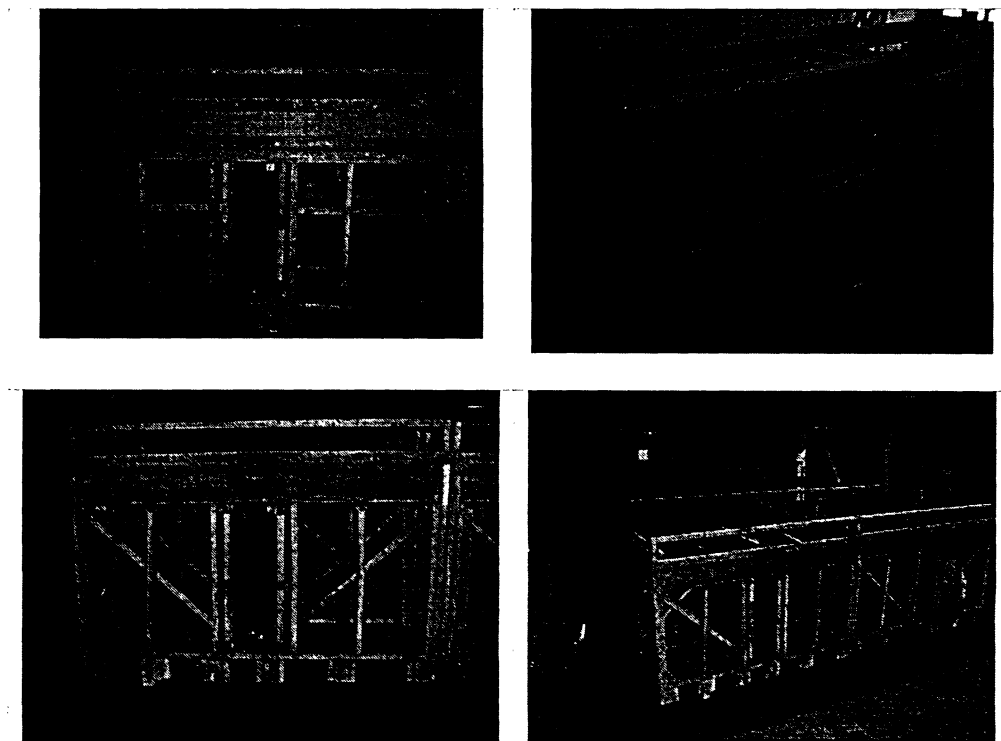
Figure B.2 Different Views of Formwork

155
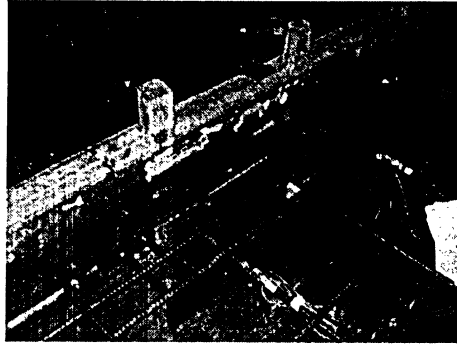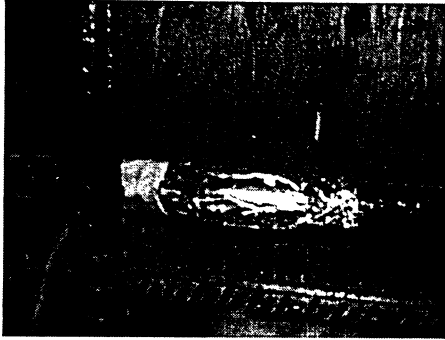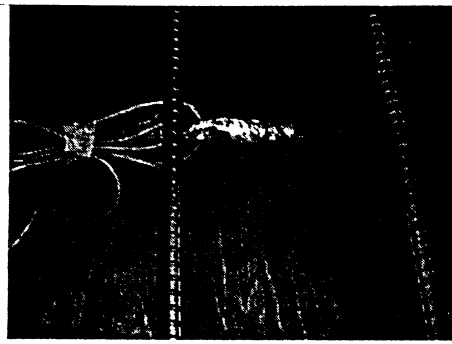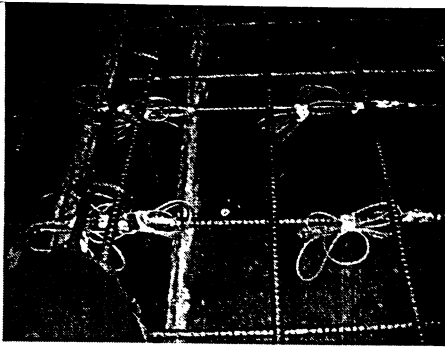
Figure B.3 Different photos of Strain Gauges
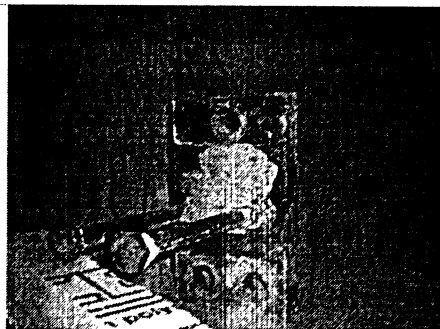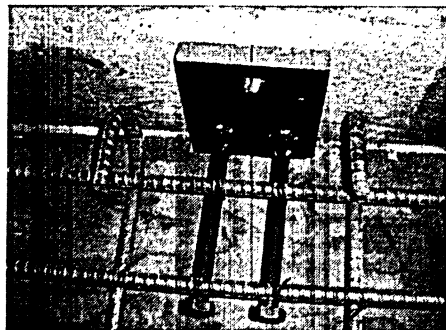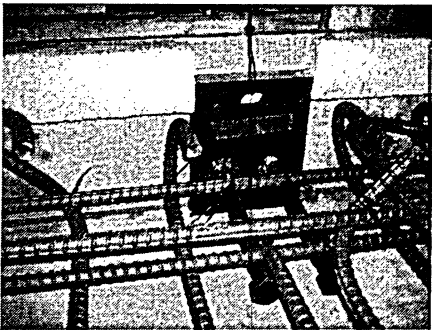
Figure B.4 Views of Steel Plate For Model M3
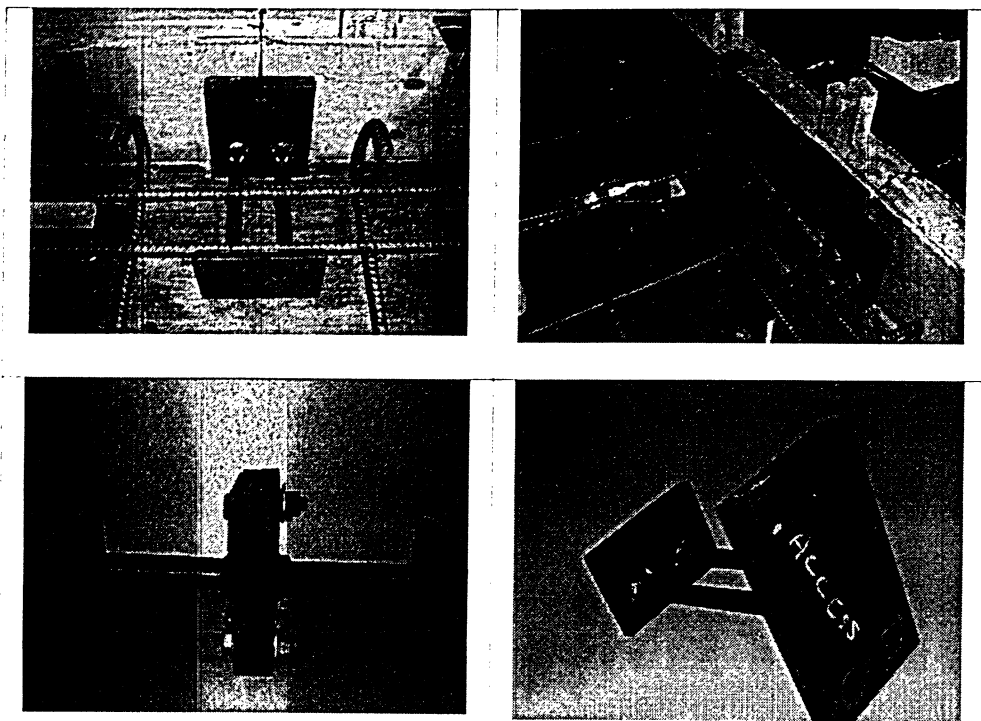
Figure B.5 Views of Steel Plate For Model M4
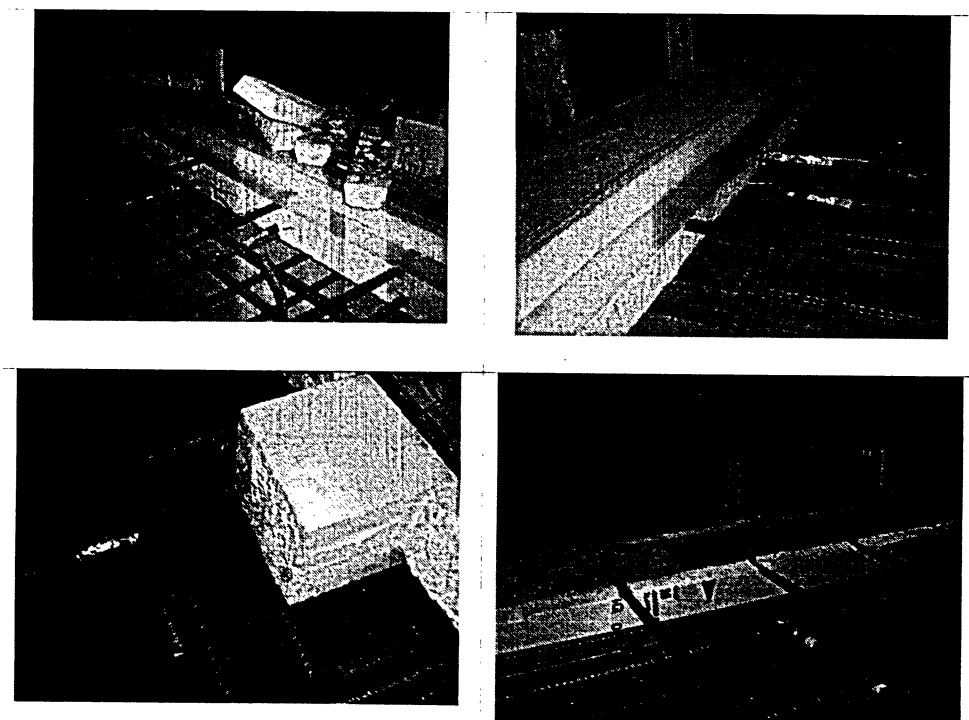
Figure B.6 Views of Styrofoam for Joint Section, Joint Grove and Pockets
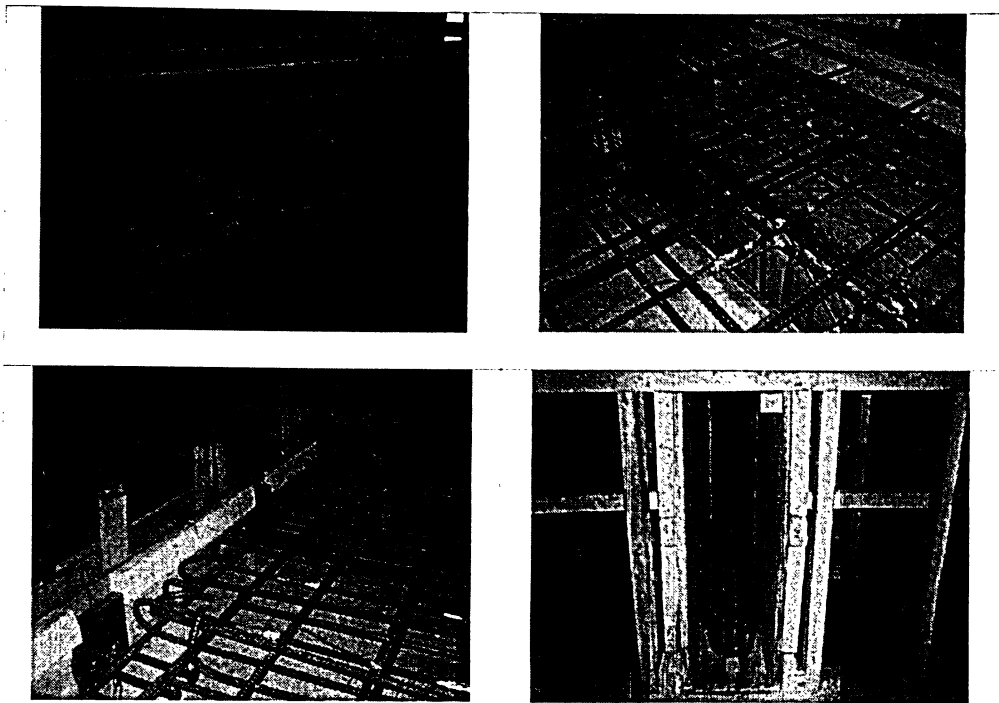
Figure B.7 Slab and Girder Reinforcement for Models M1 and M3
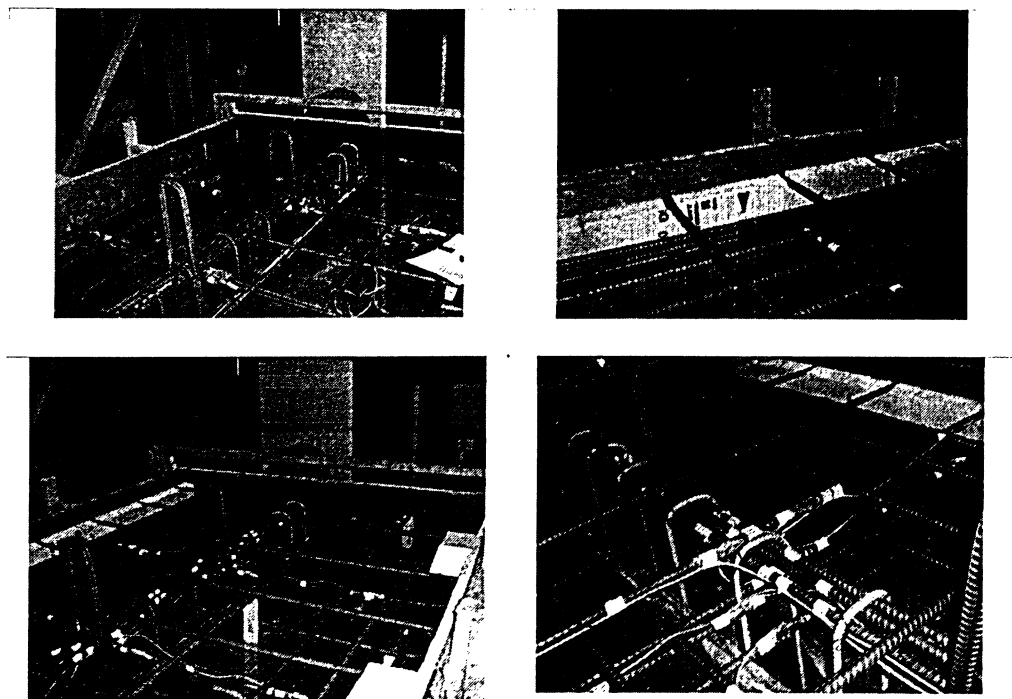
Figure B.8 Slab and Girder Reinforcement for Models M2 and M4
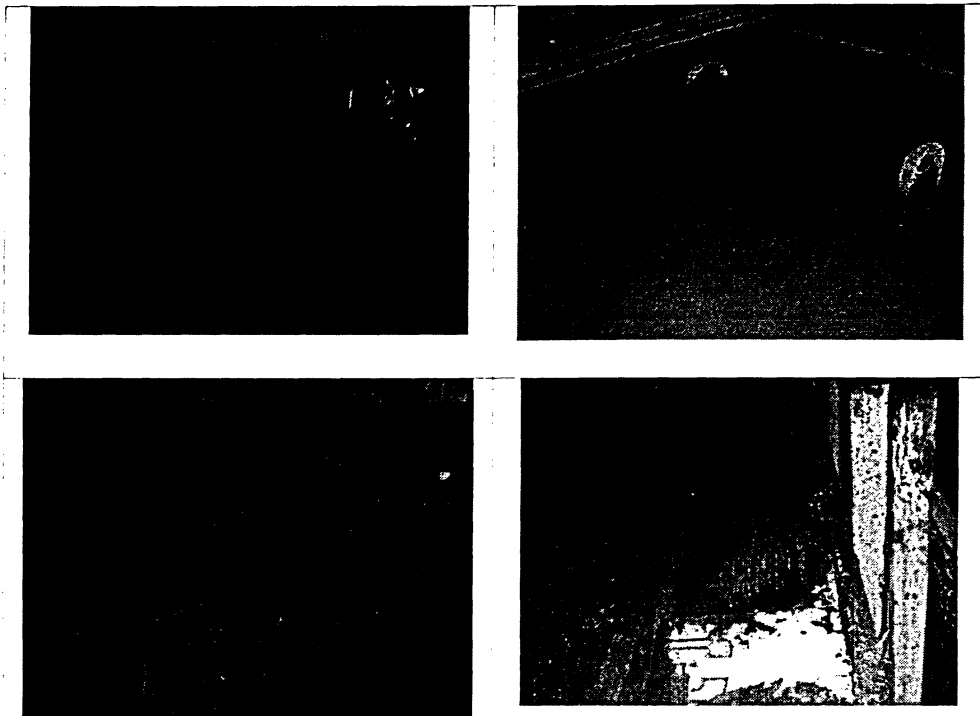
Figure B.9 Concreting and Curing of Bridges Models M1 and M3
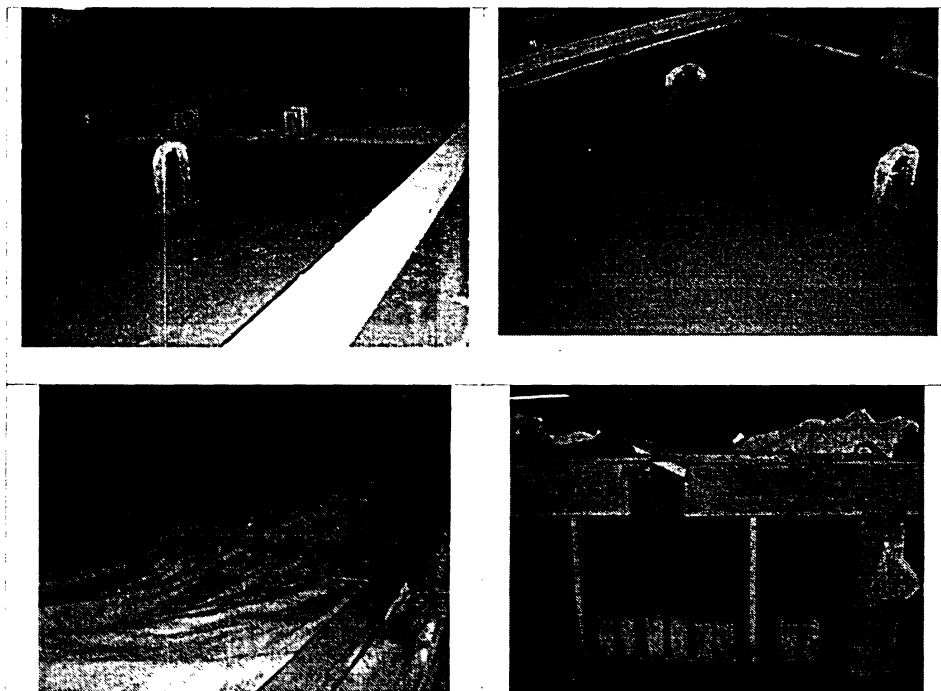
Figure B.10 Concreting and Curing of Bridges Models M2 and M4
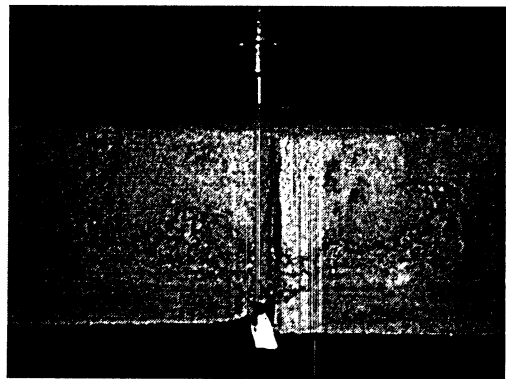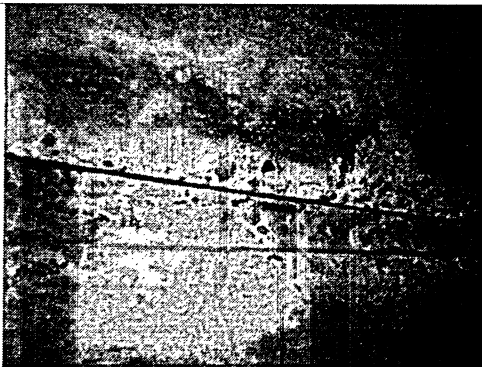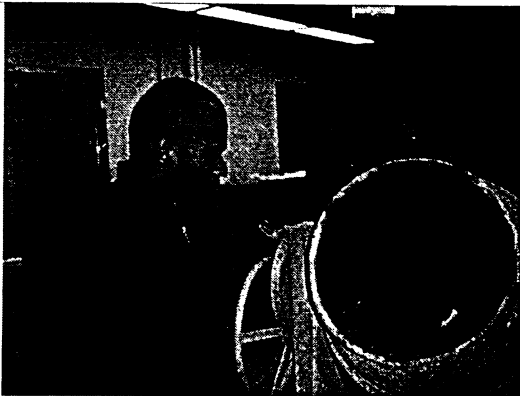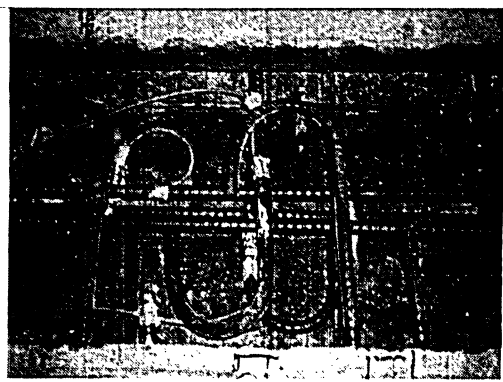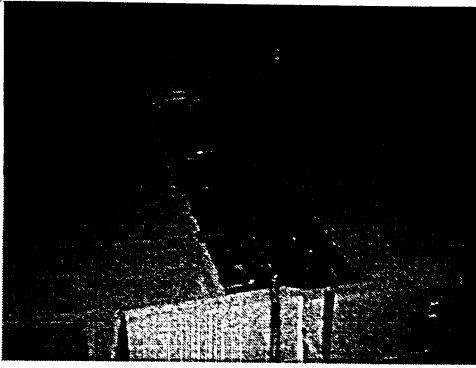
Figure B.11 Construction of Joint M1
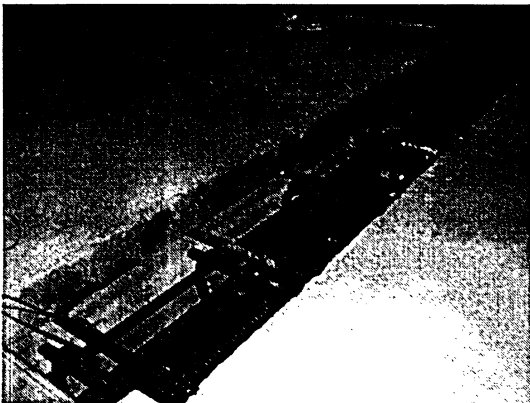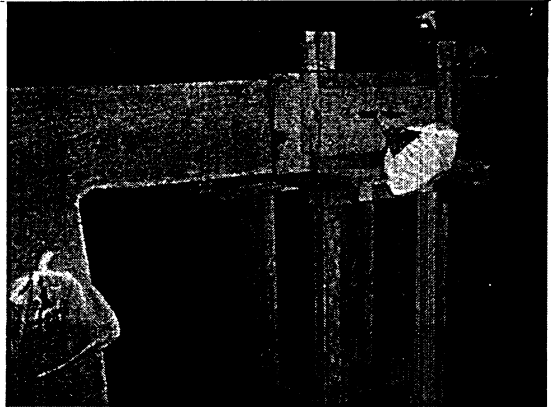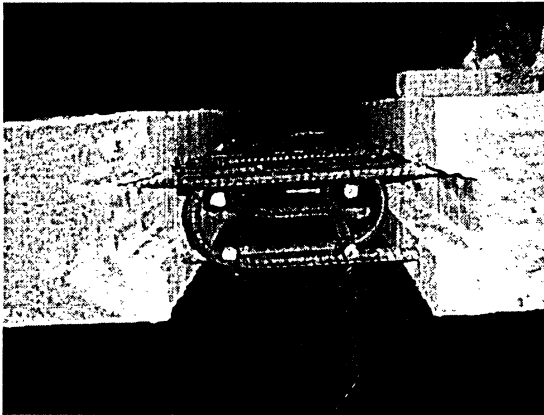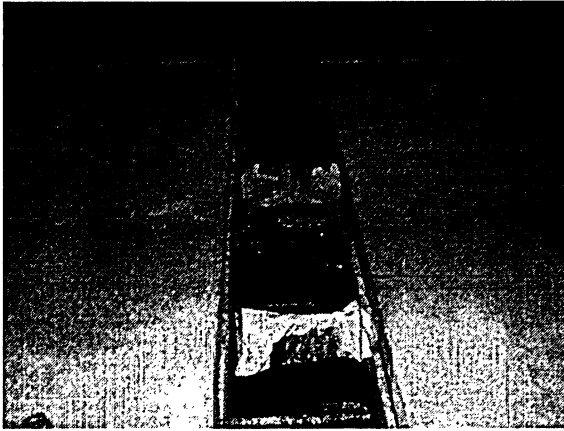
Figure B.12 Construction of Joint M2
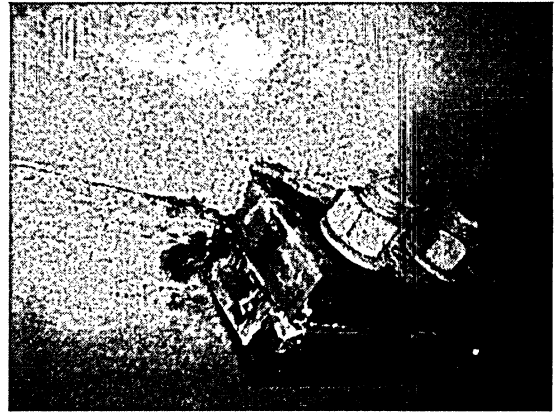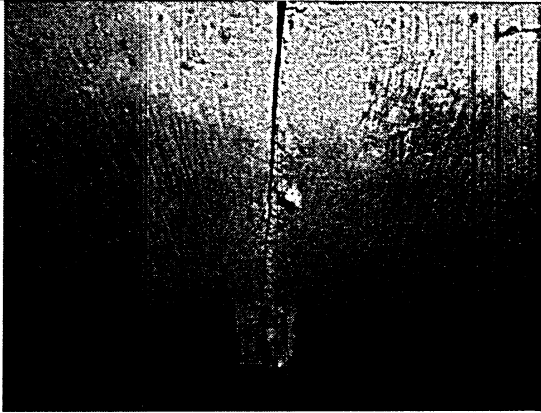
Figure B.13 Construction of Joint M3 and M4

APPENDIX C

DETAILS OF STRAIN GAUGES AND LVDT's
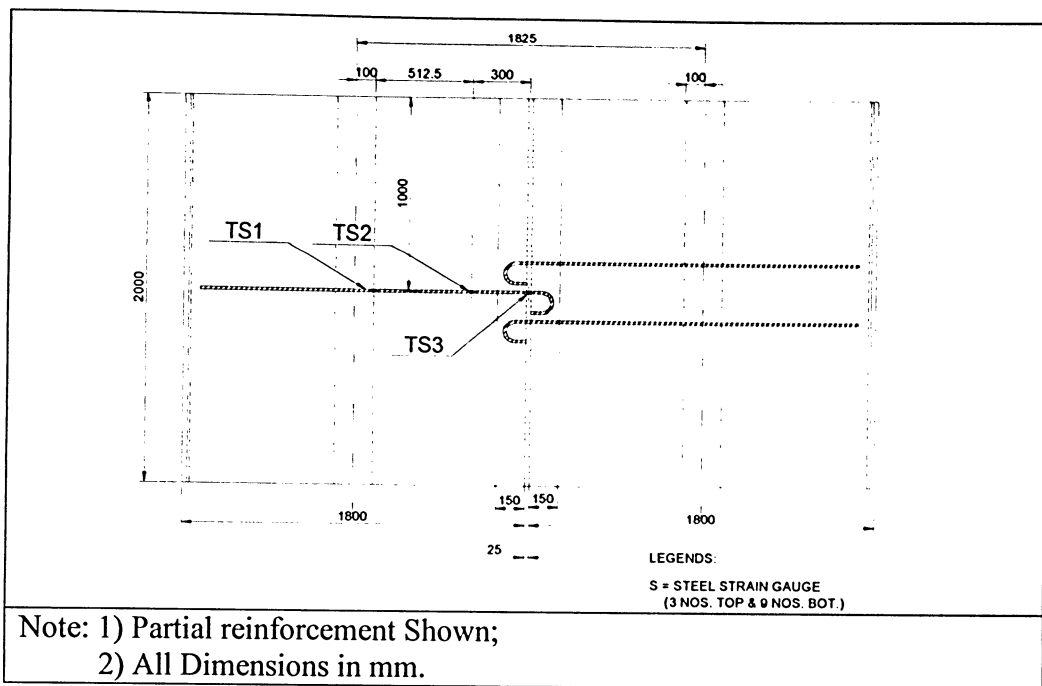
Figure C.1 Plan of Top Steel Strain Gauges Location For Model M1
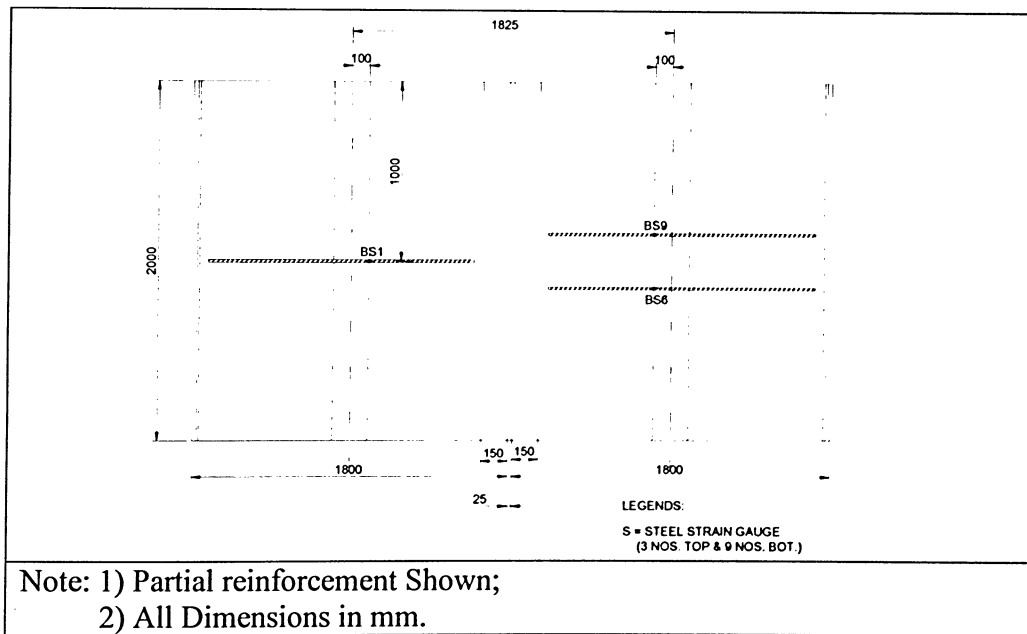
Figure C.2 Plan of Bottom Steel Strain Gauges Location For Model M1

164

Note: 1) Partial reinforcement Shown;
2) All Dimensions in mm.
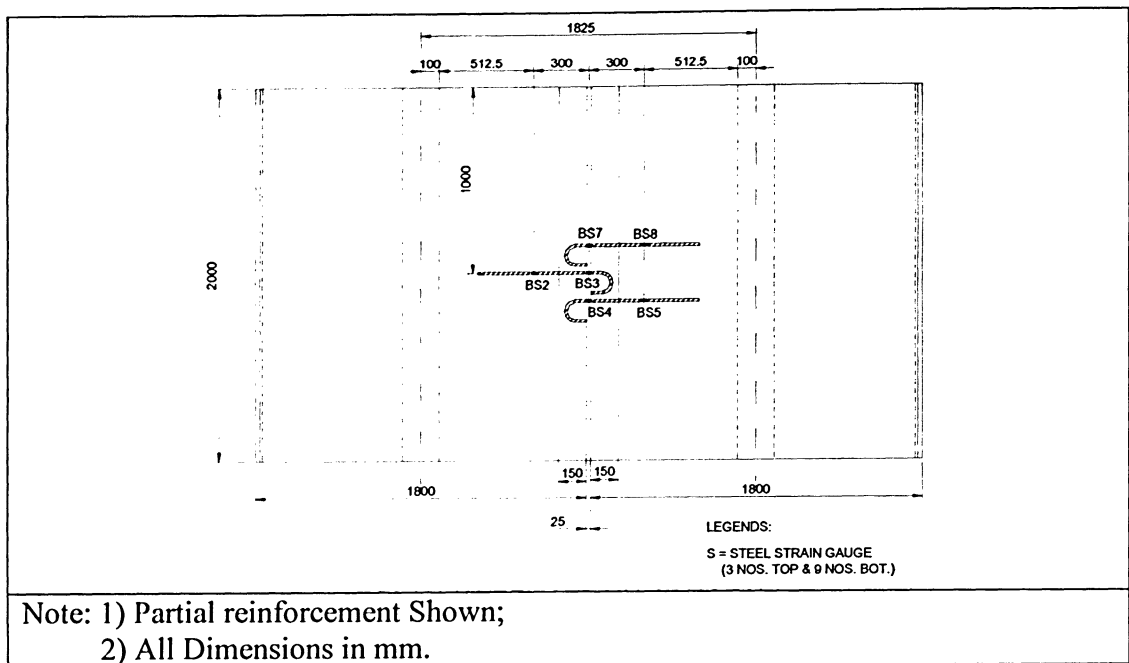
Figure C.3 Plan of Steel Strain Gauges at the Dowel Rebars For Model M1

Note: All Dimensions in mm.
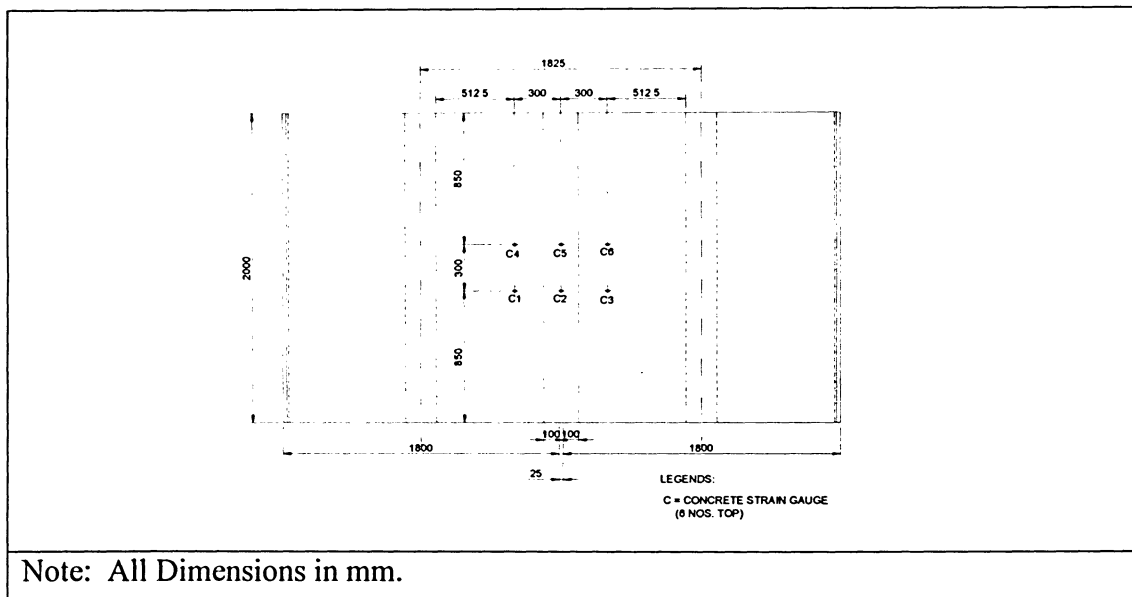
Figure C.4 Plan of Concrete Strain Gauges Location on Top Slab For Model M1
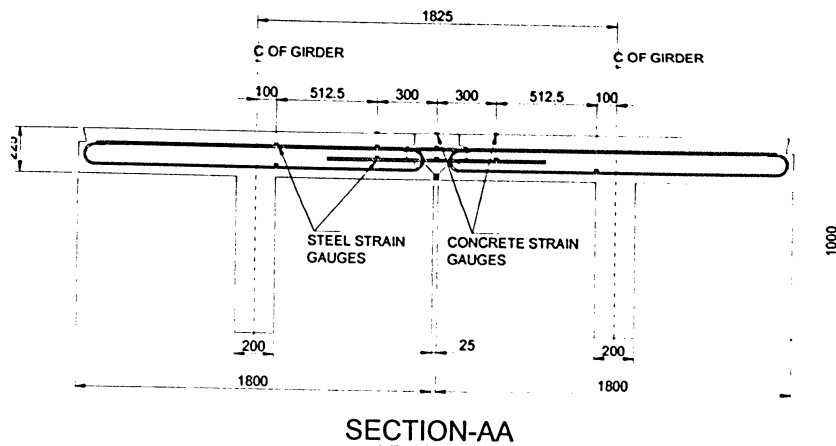
Figure C.5 Cross Section of the Strain Gauges Location for Model M1
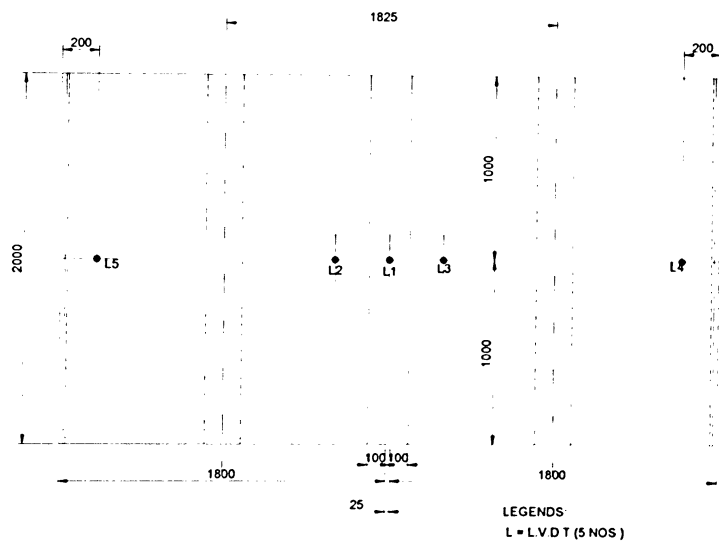
Figure C.6 Plan of LVDT's Location for Model M1

Note: All Dimensions in mm.
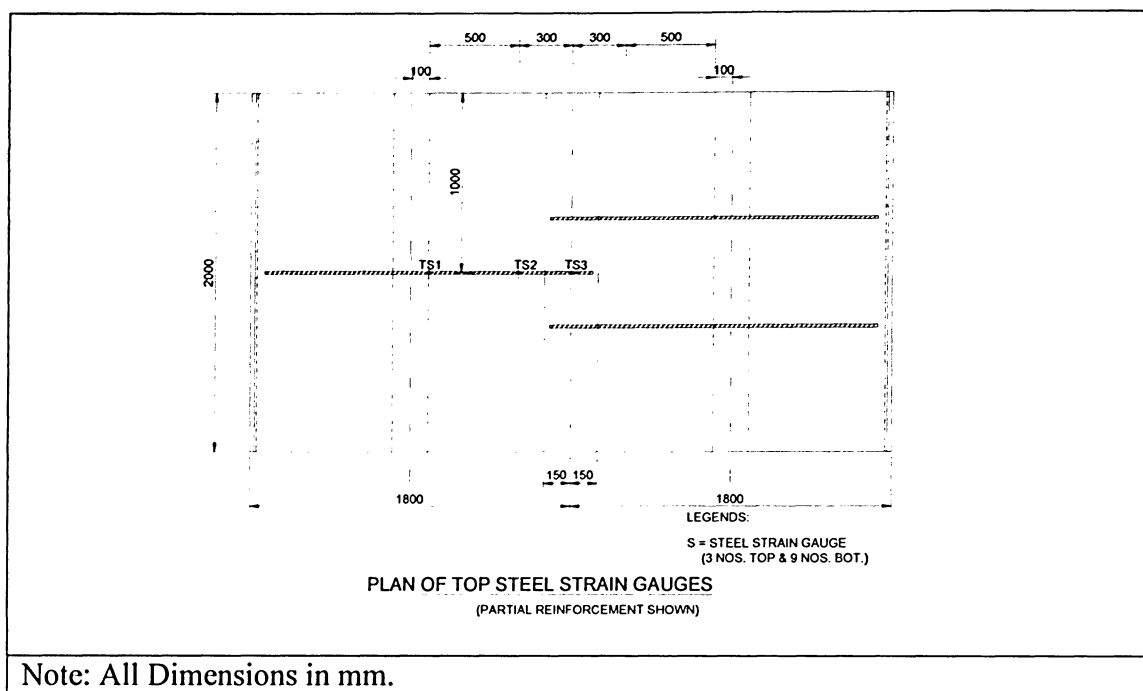
Figure C.7 Plan of Top Steel Strain Gauges Location For Model M2

Note: All Dimensions in mm.
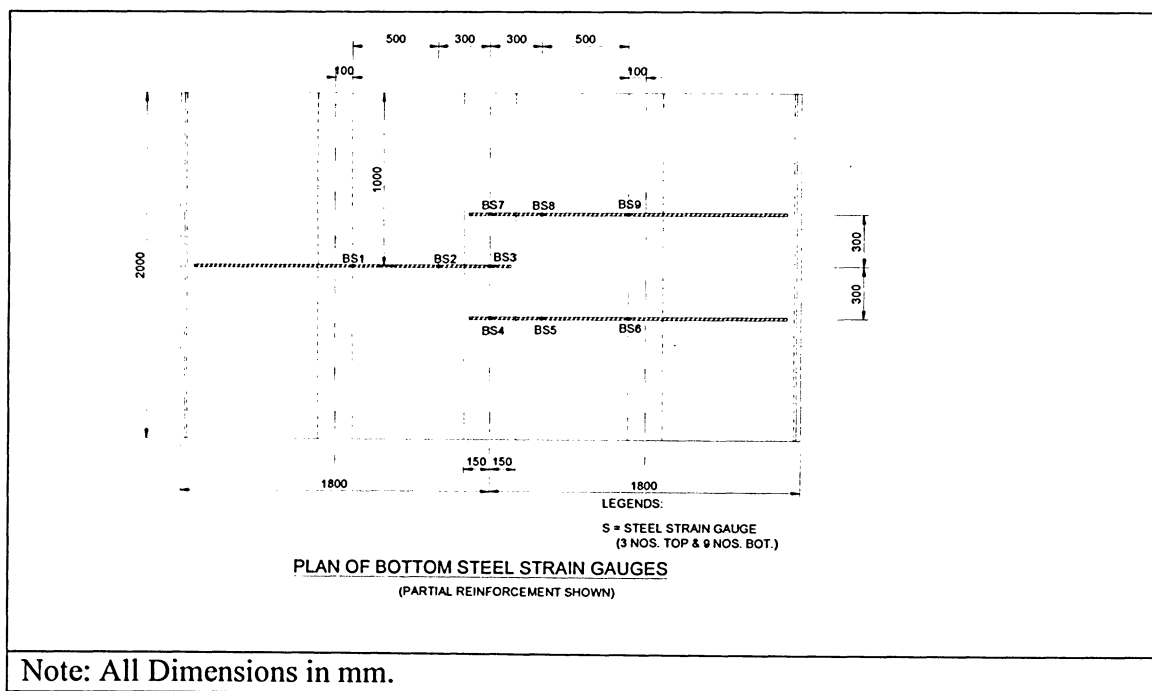
Figure C.8 Plan of Bottom Steel Strain Gauges Location For Model M2

167

PLAN OF CONCRETE STRAIN GAUGES

LEGENDS

C = CONCRETE STRAIN GAUGE
(6 NOS TOP)

Note: All Dimensions in mm.

Figure C.9 Plan of Concrete Strain Gauges Location For Model M2

Ç OF GIRDER   Ç OF GIRDER

STEEL STRAIN
GAUGES

CONCRETE STRAIN
GAUGES
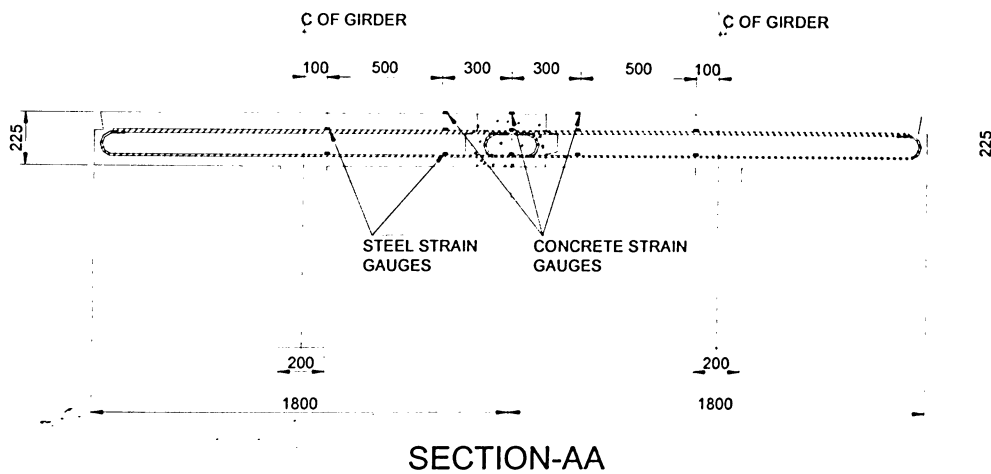
SECTION-AA

Note: All Dimensions in mm.

Figure C.10 Cross Section of the Strain Gauges Location for Model M2

168
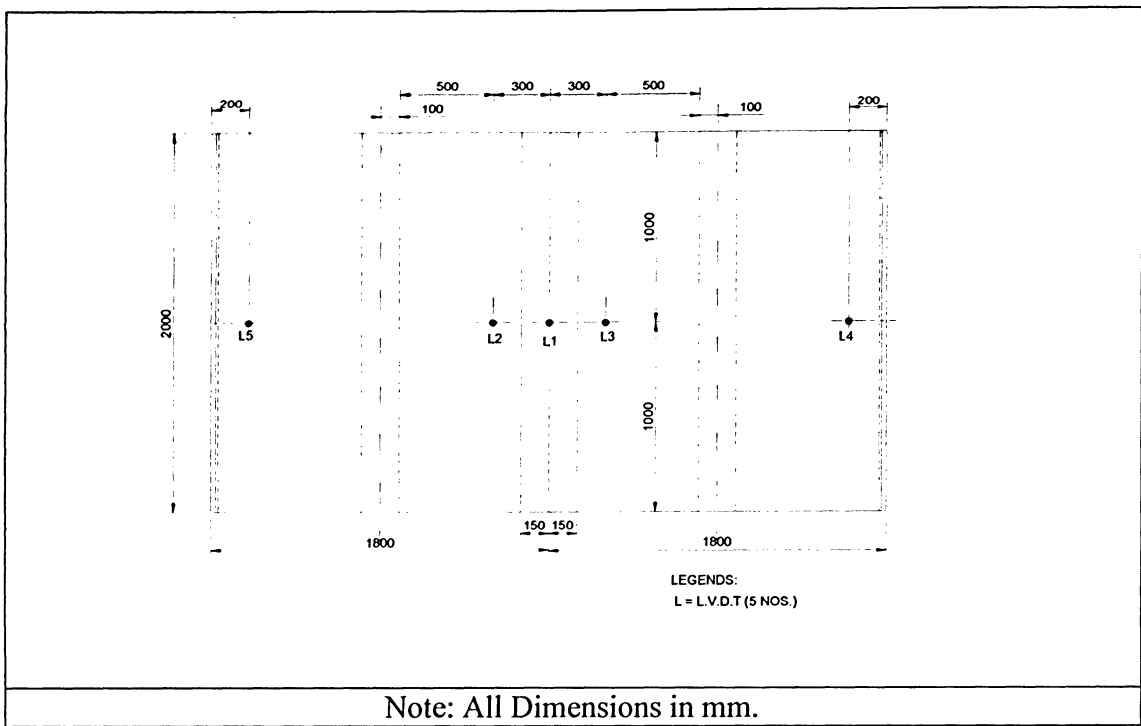
Figure C.11 Plan of LVDT's Location For Model M2

PLAN (BOTTOM STEEL STRAIN GAUGES)
(PARTIAL REINFORCEMENT SHOWN)

LEGENDS
BS = BOTTOM STEEL STRAIN GAUGES

PLAN (TOP STEEL STRAIN GAUGES)
(PARTIAL REINFORCEMENT SHOWN)

LEGENDS:
TS = TOP STEEL STRAIN GAUGES
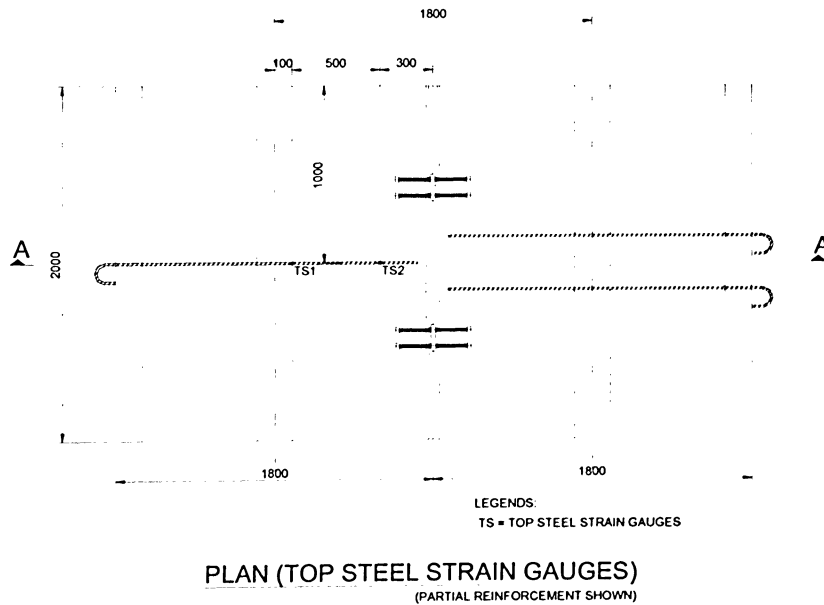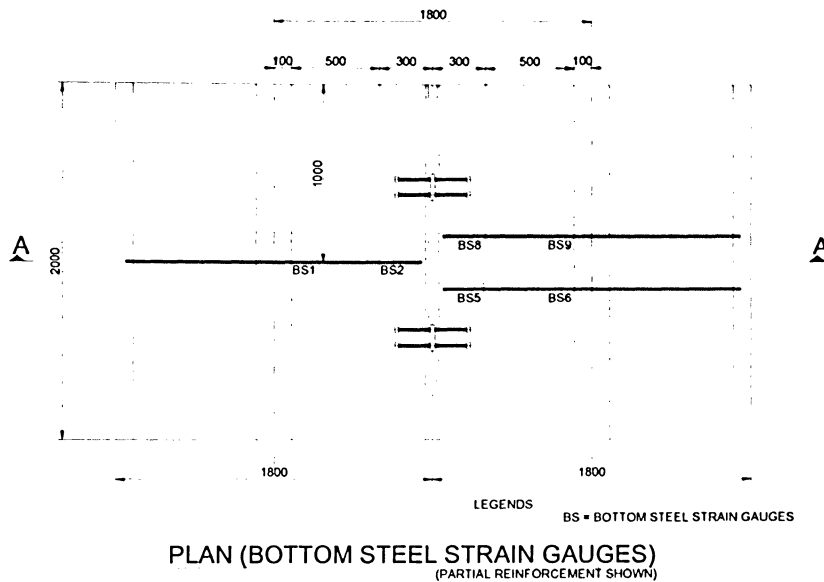
Note: 1) Partial reinforcement Shown;
2) All Dimensions in mm.

Figure C.12 Plan of Steel Strain Gauges Location For Model M3

170

Note: 1) Partial reinforcement Shown;
2) All Dimensions in mm.

Figure C.13 Plan of Concrete Strain Gauges Location on Top Slab For Model M3

SECTION-AA

Note: All Dimensions in mm.

Figure C.14 Cross Section of the Strain Gauges Location for Model M3

171
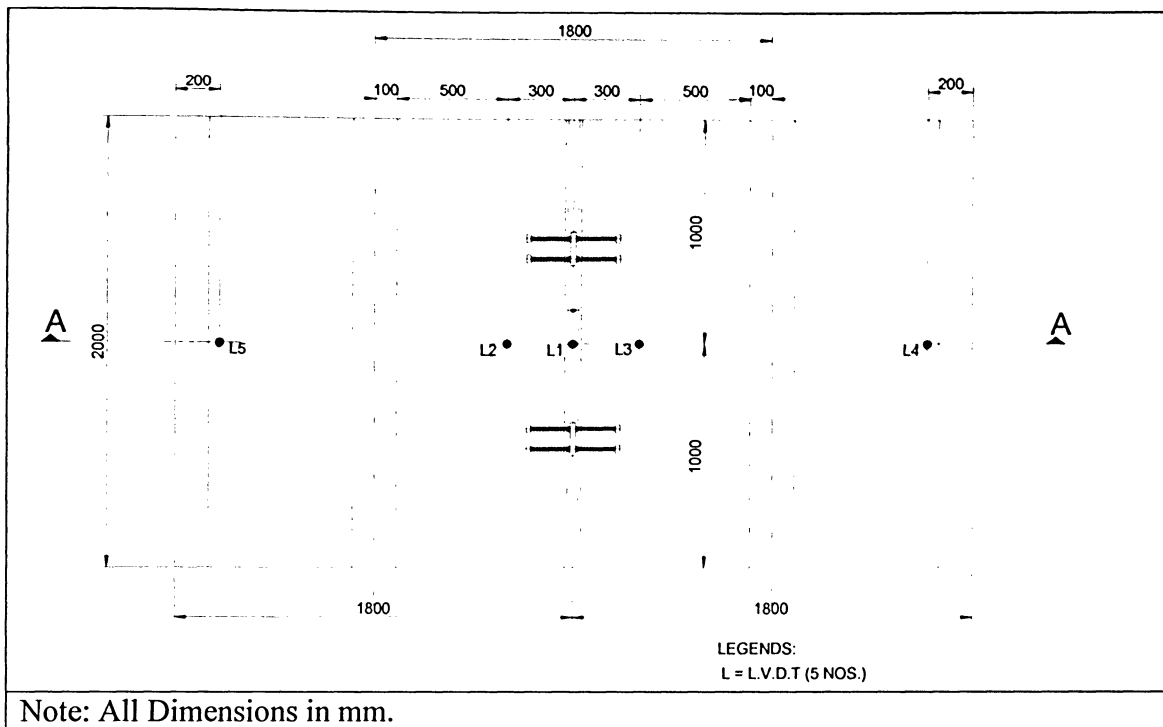
Figure C.15 Plan of LVDT's Location for Model M3

LEGENDS:
BS = BOTTOM STEEL STRAIN GAUGES

PLAN OF BOTTOM STEEL STRAIN GAUGES
(PARTIAL REINFORCEMENT SHOWN)

LEGENDS:
BS = BOTTOM STEEL STRAIN GAUGES

PLAN OF TOP STEEL STRAIN GAUGES
(PARTIAL REINFORCEMENT SHOWN)
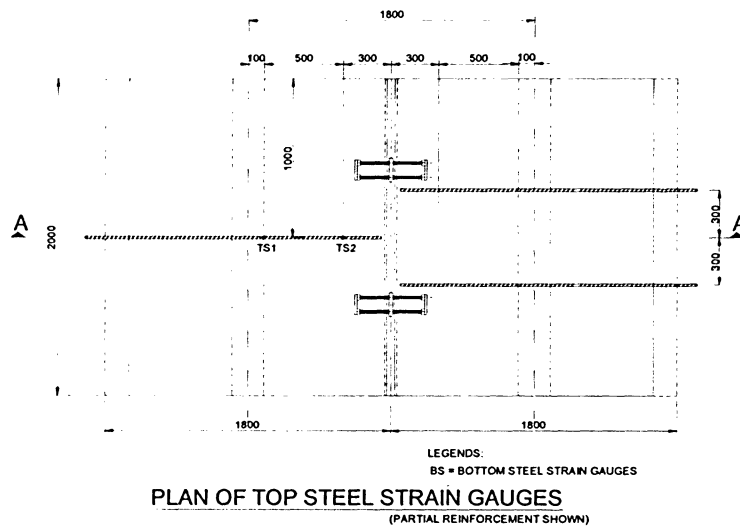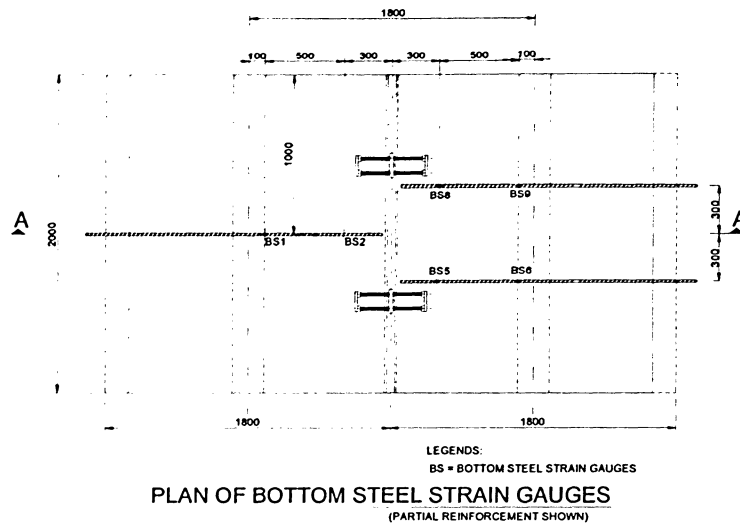
Note: 1) Partial reinforcement Shown;
    2) All Dimensions in mm.

Figure C.16 Plan of Steel Strain Gauges Location For Model M4
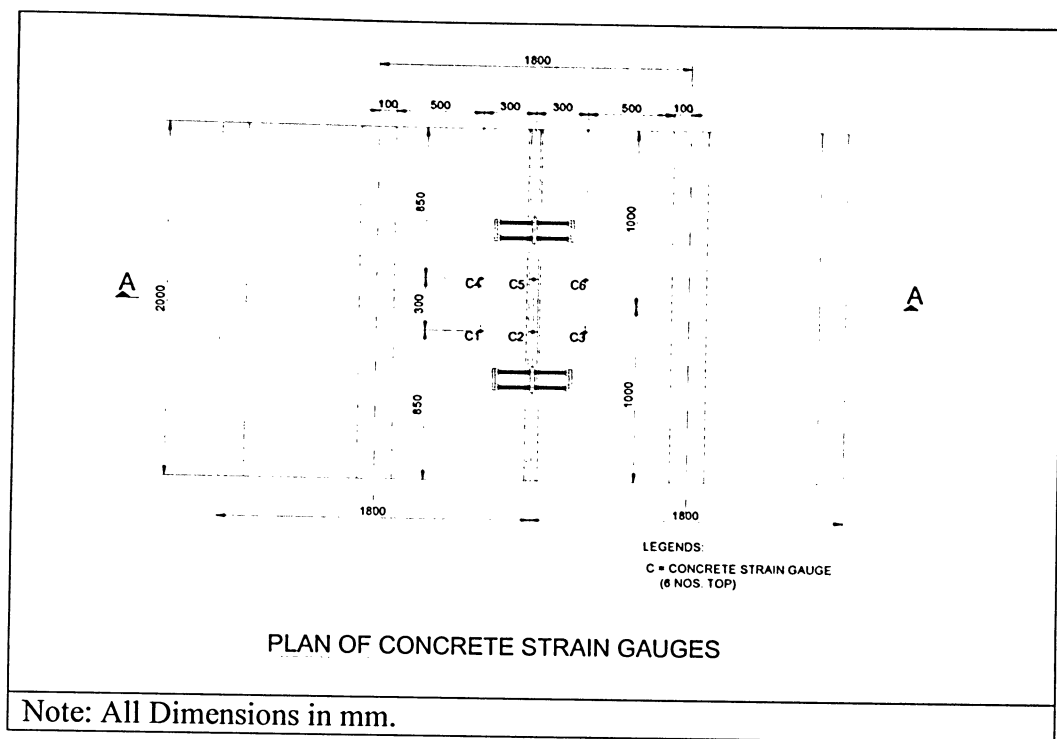
Figure C.17 Plan of Concrete Strain Gauges Location For Model M4
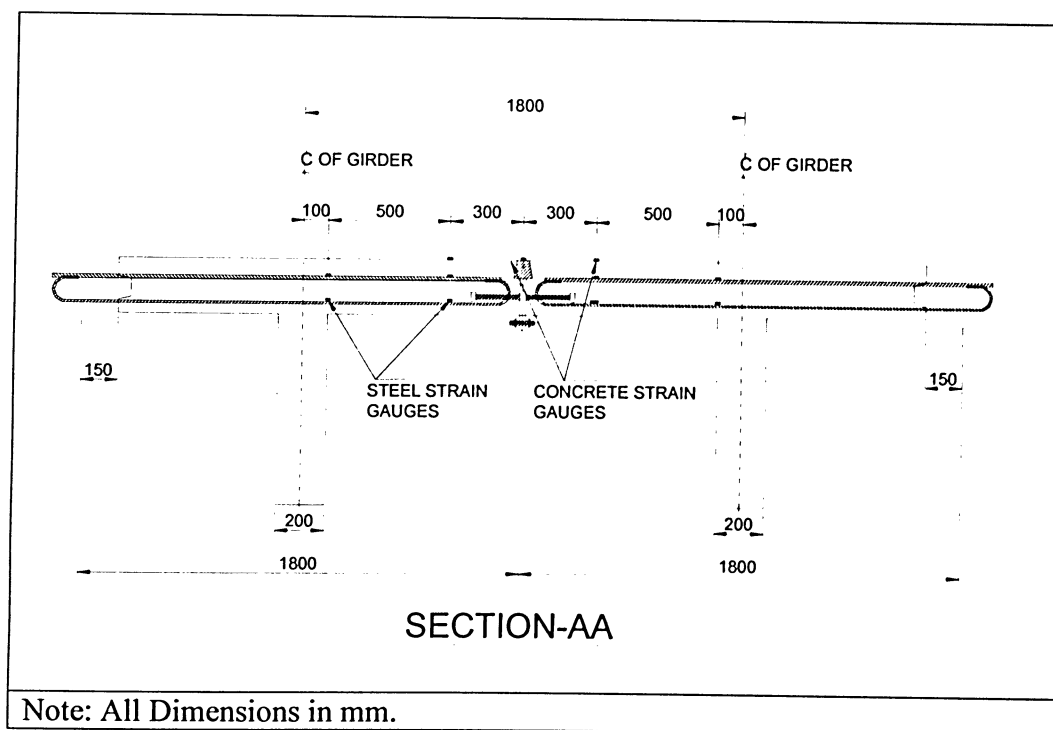
Figure C.18 Cross Section of the Strain Gauges Location for Model M4

174
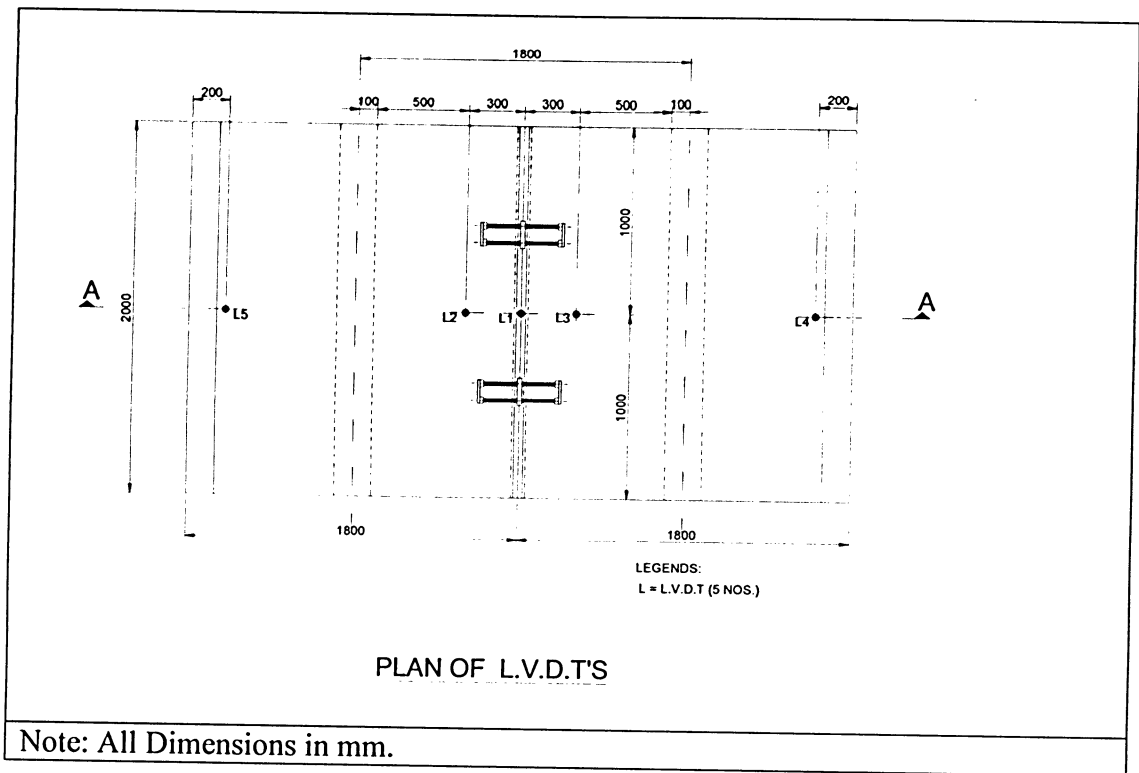
Figure C.19 Plan of LVDT's Location for Model M4

APPENDIX D

DETAILS OF TEST EQUIPMENT

AND EXPERIMENTAL SETUP
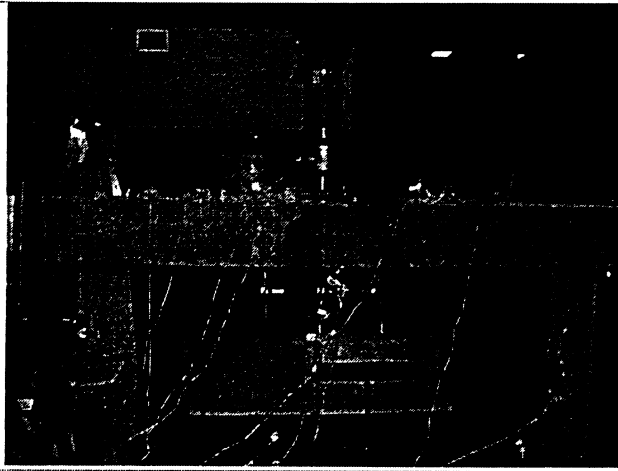
(a) Test Setup
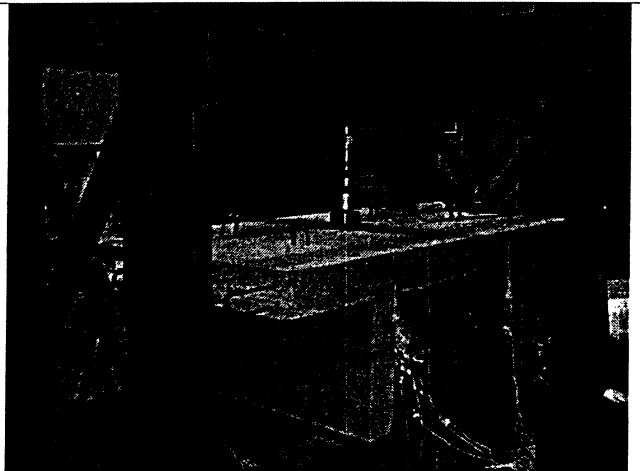
(b) Test Setup
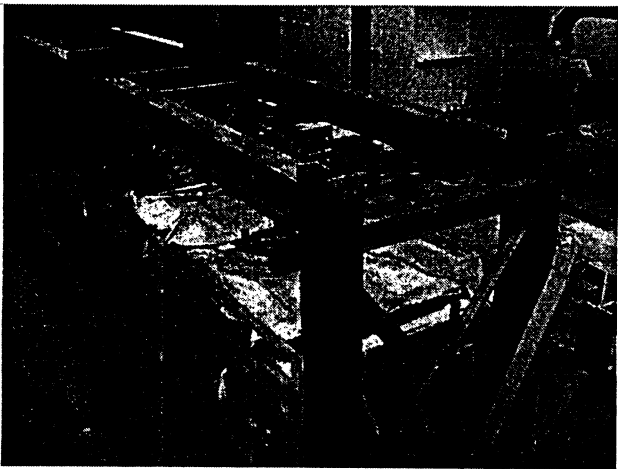
(c) Loading Frame
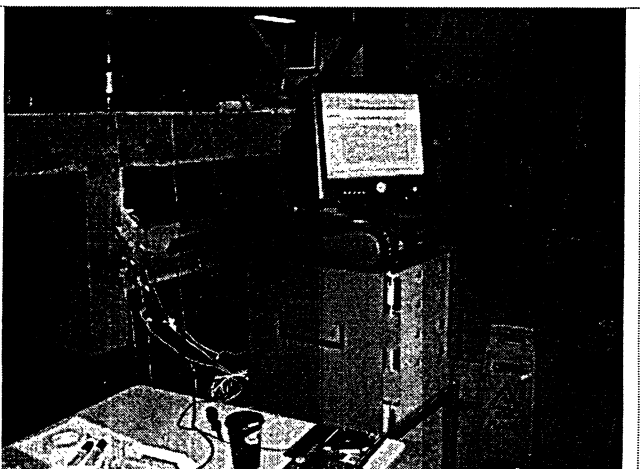
(d) Data Acquisition System

Figure D.1 Views of Testing Setup
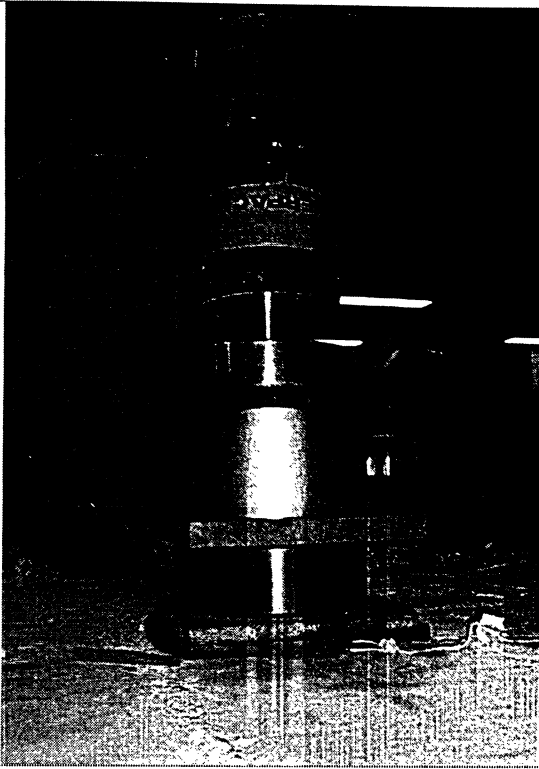
(a) Load Cell and Hydraulic Jack   (b) LVDT's Setup
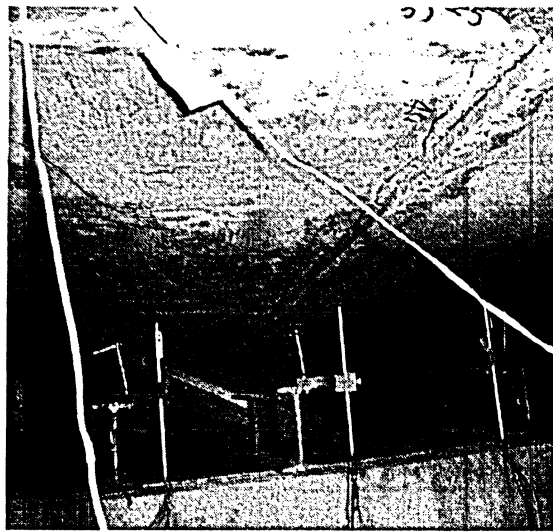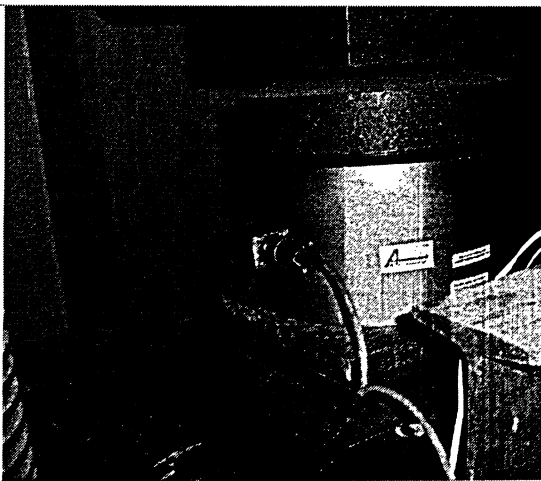
(c) Testing of Elastomeric
     Bearing Pad
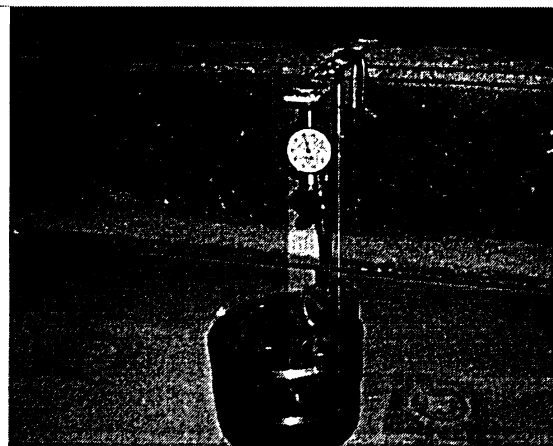
(d) Dial Gauge To Measure The
     The Deflection of Frame During
     Testing

Figure D.2 Views of Testing Setup
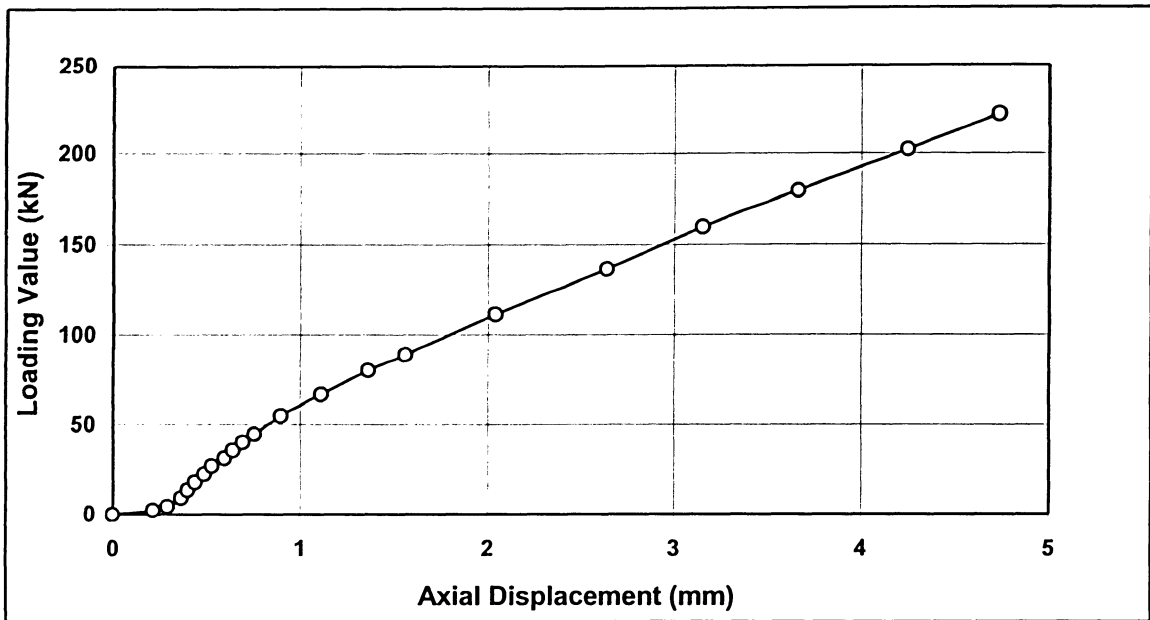
Figure D.3 Stress-Displacement Curves of the Elastomeric Bearing Pads
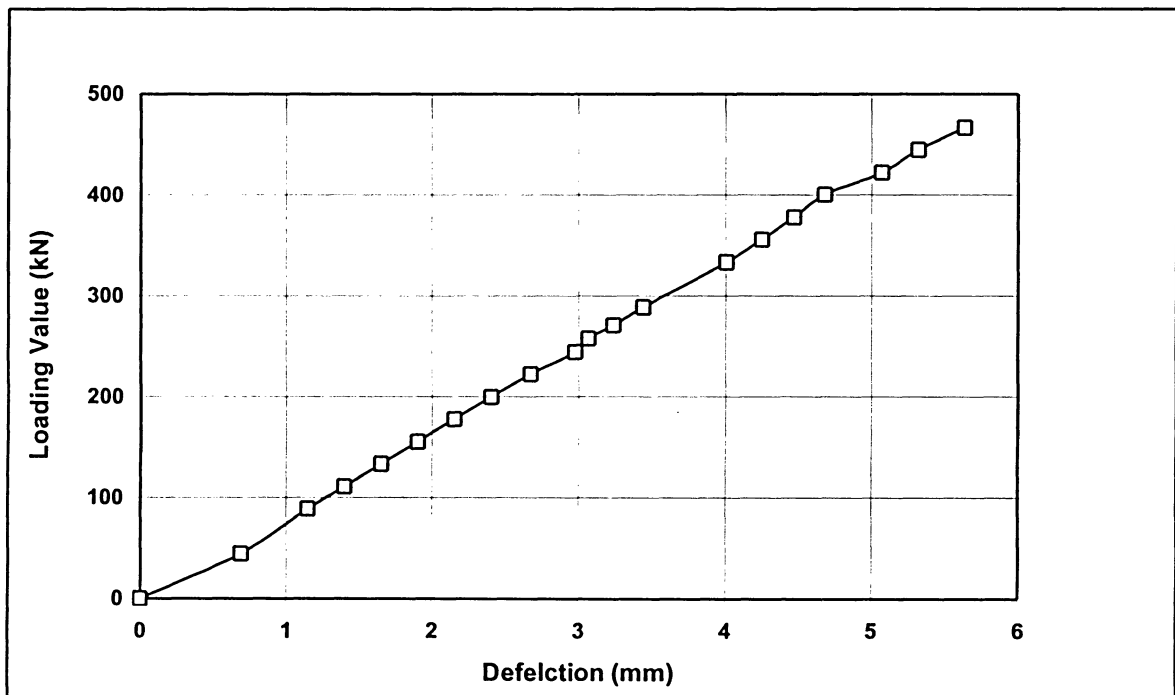
Figure D.4 Loading-Deflection Curves of Steel Frame

179
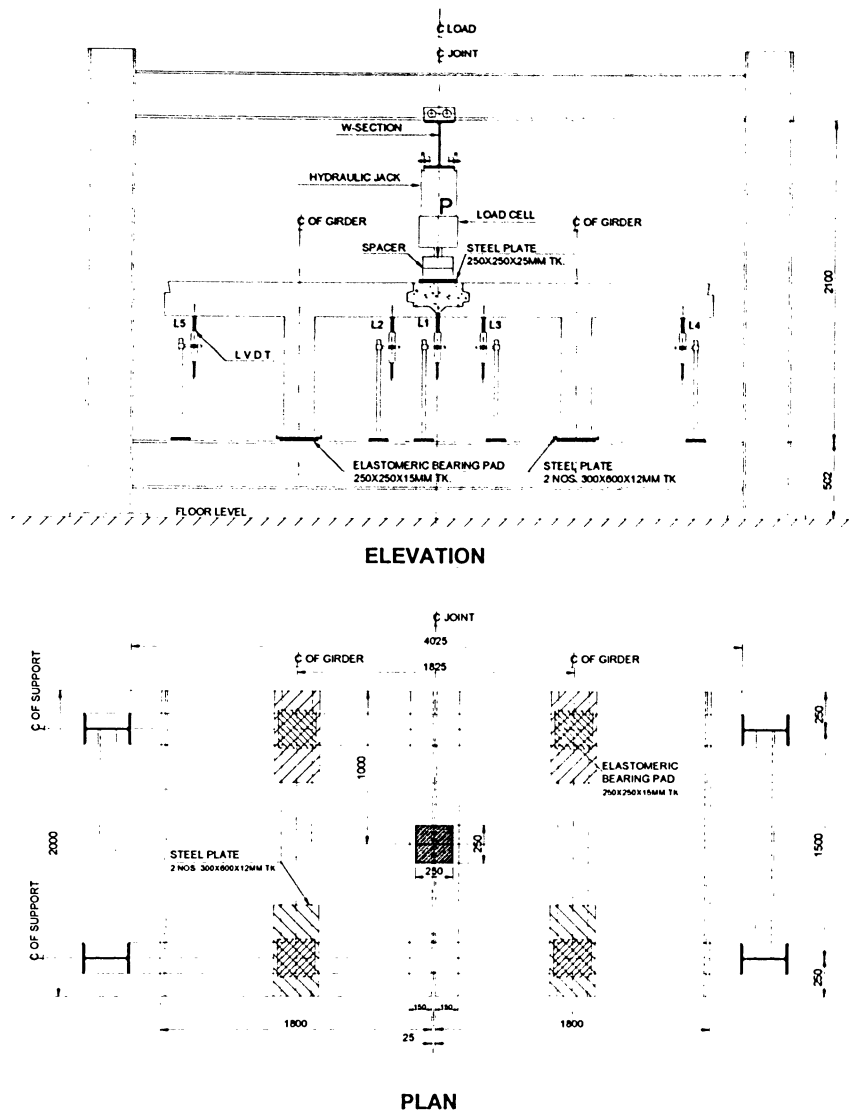
Figure D.5 Test Setup for Model M1

180
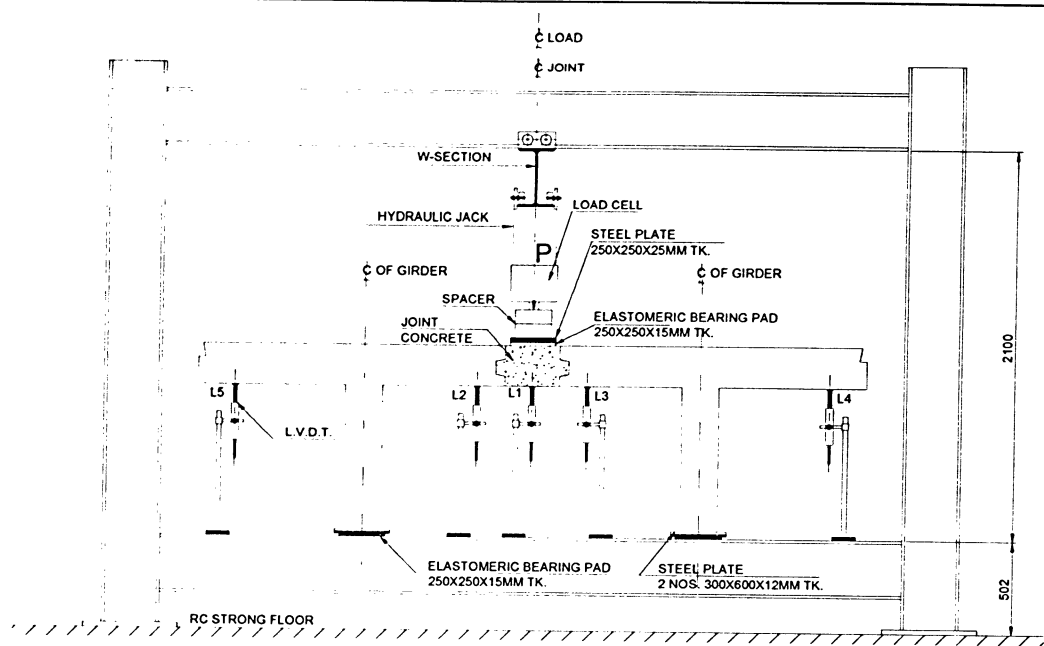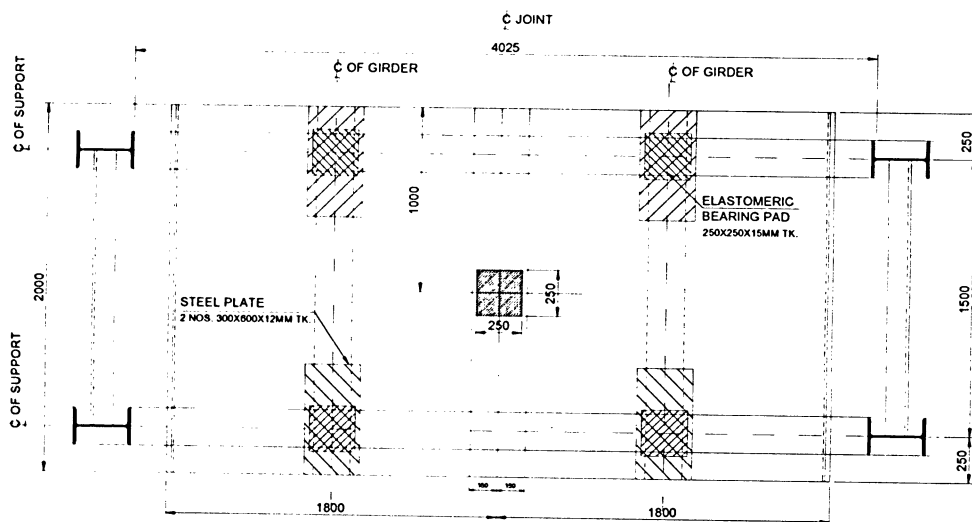
ELEVATION

PLAN

Note: All Dimension in mm.

Figure D.6 Test Setup for Model M2

181
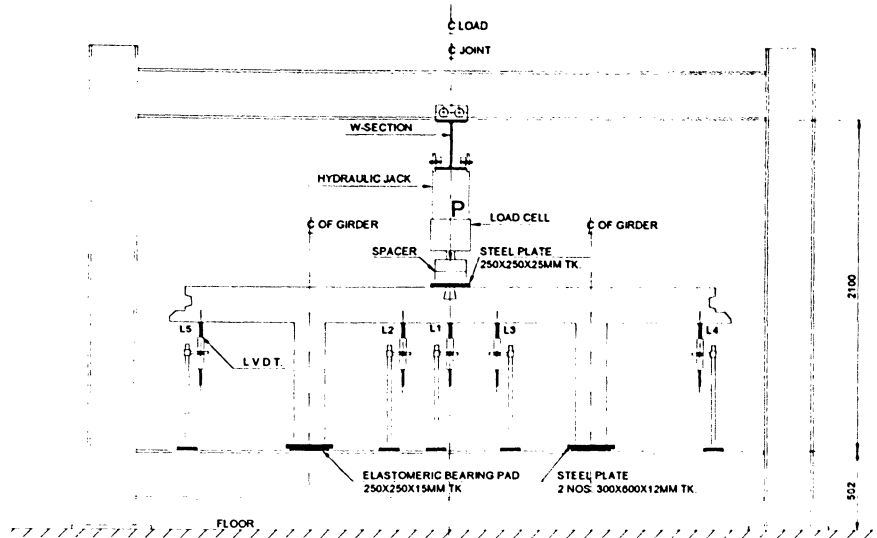
ELEVATION
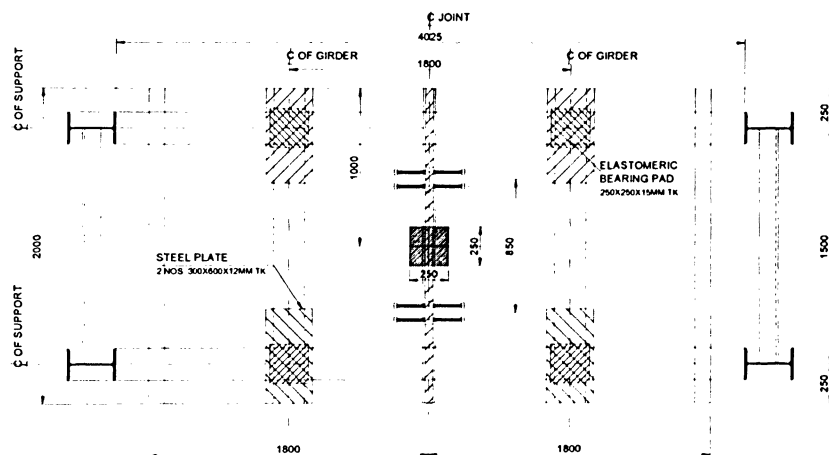
PLAN

Note: All Dimension in mm.

Figure D.7 Test Setup for Model M3

182

Figure D.8 Test Setup for Model M4

APPENDIX E

RECORD OF GAUGES READING

Table E.1 Record of Steel Strain Gauges of M1

Load kN	TS1	TS2	TS3	BS1	BS2	BS3	BS4	BS5	BS6	BS7	BS8	BS9	REMARK
							STRAIN (um/m)						
0.0	0	0	0	0	0	0	0	0	0	0	0	0	
13.5	0	2	8	-1	4	9	3	1	-1	6	2	1	
26.7	0	5	14	-2	6	26	15	1	-2	19	3	2	
36.0	0	7	19	-4	7	35	25	1	-2	27	3	4	
53.4	0	11	32	-6	8	53	41	1	-3	44	5	6	
62.2	0	16	39	-8	8	65	48	2	-3	52	5	8	
89.0	1	18	51	-10	9	105	76	3	-4	83	7	9	
107.0	1	21	64	-12	12	149	115	5	-4	120	9	10	
115.7	1	24	71	-13	13	233	165	5	-4	195	8	12	
133.7	2	29	75	-14	15	471	341	11	-5	445	9	15	
142.7	2	30	76	-15	20	512	373	12	-5	480	9	18	
160.1	3	33	81	-15	29	783	717	16	-6	809	14	19	
169.4	3	35	88	-16	30	836	763	18	-6	862	14	20	
186.8	4	36	93	-16	40	1022	1001	26	-6	1156	24	24	
195.5	5	36	98	-17	41	1070	1049	29	-7	1220	26	25	
204.8	8	37	101	-17	59	1120	1185	54	-7	1461	46	26	
222.4	10	39	104	-18	67	1191	1307	89	-8	1662	66	29	
236.1	12	43	171	-20	100	1221	1379	146	-8	1838	214	29	
244.6	12	43	235	-20	139	Failed	1443	203	-8	1975	277	30	
262.5	15	45	262	-22	141		1520	268	-9	2119	371	31	
271.1	17	48	294	-22	150		1563	394	-9	2311	457	31	
289.3	18	50	332	-23	157		1649	488	-10	2539	533	32	
298.4	19	53	356	-28	188		1697	602	-12	2728	635	33	
315.9	23	56	407	-31	274		1814	781	-18	3007	764	36	
324.7	25	61	425	-32	290		1863	816	-18	3115	793	36	
342.7	31	66	460	-34	395		2082	1046	-21	4927	950	37	
351.5	34	93	476	-36	423		2244	1151	-23	5682	1021	38	
360.4	35	231	479	-37	546		2893	1352	-26	Failed	1224	38	
369.2	39	263	489	-38	573		3059	1513	-27		1268	39	
373.7	41	290	497	-39	595		3175	1558	-28		1304	39	
378.4	41	309	501	-40	611		3256	1588	-29		1330	40	

185

Table E.2 Record of Concrete Strain Gauges of M1

Load	STRAIN (um/m)						REMARK
kN	C1	C2	C3	C4	C5	C6	
0.0	0	0	0	0	0	0	
13.5	-6	-12	-5	-3	-16	-5	
26.7	-10	-29	-16	-8	-48	-8	
36.0	-14	-42	-19	-11	-63	-12	
53.4	-21	-16	-26	-18	-104	-16	
62.2	-24	-32	-29	-20	-119	-20	
89.0	-36	-57	-42	-32	-162	-33	
107.0	-42	-98	-62	-40	-198	-43	
115.7	-48	-122	-67	-44	-236	-49	
133.7	-49	-217	-74	-51	-341	-53	
142.7	-53	-238	-78	-54	-362	-57	
160.1	-59	-349	-83	-63	-495	-37	
169.4	-65	-375	-86	-66	-524	-41	
186.8	-75	-494	-99	-78	-648	-60	
195.5	-85	-524	-102	-83	-676	-74	
204.8	-96	-581	-107	-96	-778	-91	
222.4	-113	-661	-118	-110	-855	-135	
236.1	-129	-746	-128	-127	-951	-165	
244.6	-143	-803	-137	-132	-1019	-189	
262.5	-150	-860	-141	-141	-1082	-201	
271.1	-155	-909	-144	-151	-1157	-212	
289.3	-162	-978	-148	-168	-1261	-224	
298.4	-170	-1047	-154	-189	-1368	-229	
315.9	-181	-1183	-186	-226	-1530	-250	
324.7	-184	-1220	-190	-234	-1572	-257	
342.7	-190	-1358	-191	-265	-1759	-290	
351.5	-203	-1411	-192	-276	-1843	-302	.
360.4	-216	-1514	-194	-311	-2026	-341	
369.2	-221	-1551	-196	-318	-2068	-351	
373.7	-225	-1574	-197	-323	-2104	-358	
378.4	-229	-1587	-199	-328	-2132	-363	

TableE.3 Record of LVDT's Readings of M1

Load	DEFLECTION (mm)					REMARK
kN	LVDT-1	LVDT-2	LVDT-3	LVDT-4	LVDT-5	
0.0	0.00	0.00	0.00	0.00	0.00	
13.5	0.04	0.10	0.03	-0.17	-0.01	
26.7	0.14	0.25	0.10	-0.31	-0.02	
36.0	0.18	0.30	0.12	-0.41	-0.03	
53.4	0.28	0.39	0.17	-0.59	-0.08	
62.2	0.30	0.40	0.19	-0.67	-0.11	
89.0	0.37	0.48	0.23	-0.97	-0.23	
107.0	0.44	0.53	0.26	-1.18	-0.33	
115.7	0.52	0.61	0.30	-1.30	-0.38	
133.7	0.69	0.76	0.41	-1.60	-0.59	
142.7	0.78	0.84	0.45	-1.73	-0.67	
160.1	1.25	1.07	0.75	-2.14	-0.96	
169.4	1.37	1.22	0.83	-2.28	-1.06	
186.8	1.85	1.65	1.15	-2.68	-1.33	
195.5	1.98	1.78	1.20	-2.83	-1.44	
204.8	2.42	2.14	1.49	-3.15	-1.68	
222.4	2.86	2.52	1.77	-3.54	-1.95	
236.1	3.65	3.14	2.28	-4.11	-2.39	
244.6	4.40	3.65	2.71	-4.56	-2.76	
262.5	4.80	4.01	2.94	-4.92	-3.03	
271.1	5.42	4.43	3.30	-5.32	-3.33	
289.3	6.08	4.93	3.67	-5.81	-3.73	
298.4	6.85	5.46	4.13	-6.29	-4.10	
315.9	8.10	6.41	4.89	-7.15	-4.83	
324.7	8.42	6.65	5.09	-7.40	-5.03	
342.7	10.07	7.81	6.11	-8.49	-5.96	
351.5	10.80	8.32	6.54	-8.97	-6.38	
360.4	13.16	9.85	8.08	-10.56	-8.04	
369.2	13.81	10.30	8.48	-11.01	-8.48	
373.7	14.31	10.63	8.80	-11.35	-8.82	
378.4	14.69	10.91	9.04	-11.61	-9.08	

Table E.4 Record of Steel Strain Gauges of M2

Load kN	TS1	TS2	TS3	BS1	BS2	BS3	BS4	BS5	BS6	BS7	BS8	BS9	REMARK
									STRAIN (um/m)				
0	0	0	0	0	0	0	0	0	0	0	0	0	
13.4	N.A.	1	2	0	1	7	0	4	6	-1	0	5	
26.8		4	4	0	3	16	0	7	10	0	0	9	
40.3		7	6	0	5	21	0	10	16	-1	0	13	
54.4		10	9	0	6	28	0	15	22	-1	0	20	
68.1		13	11	0	7	33	0	19	27	0	0	24	
83.6		16	14	0	8	33	0	23	35	0	0	32	
93.8		19	16	0	9	42	0	27	41	0	0	38	
108.7		22	17	0	10	59	0	32	51	0	0	45	
121.0		25	19	0	11	88	0	38	62	0	0	53	
134.0		28	20	0	12	168	0	50	118	0	0	80	
147.0		31	42	0	13	223	0	63	169	0	0	107	
160.5		34	69	0	15	302	0	98	250	0	24	157	
175.1		37	83	0	16	360	0	124	294	-1	65	184	
190.4		41	110	0	17	445	0	188	369	0	129	233	
200.2		45	126	0	42	488	0	230	415	0	171	256	
215.7		49	144	0	80	614	0	376	577	1	284	318	
222.9		53	156	0	106	668	0	427	641	1	342	342	
231.4		57	172	0	146	768	0	486	752	2	439	385	
246.9		62	230	0	245	1091	0	661	1086	2	635	458	
258.4		66	247	0	260	1165	0	707	1156	1	717	473	
271.7		70	332	0	369	1612	0	1016	1407	1	1133	609	
288.7		74	376	0	437	1916	0	1165	1604	1	1294	705	
301.1		78	396	0	526	2155	0	1266	1884	1	1453	790	
311.3		80	413	0	649	2365	0	1341	2131	1	1544	925	
329.1		97	430	0	970	2602	0	1616	2688	0	1787	1297	
342.5		166	461	0	1347	2923	0	1769	3317	0	2000	1717	
351.5		181	477	0	1420	3085	0	1810	3541	-1	2086	1792	

Table E.4 Record of Steel Strain Gauges of M2 (Continued)

Load				STRAIN (um/m)									REMARK
kN	TS1	TS2	TS3	BS1	BS2	BS3	BS4	BS5	BS6	BS7	BS8	BS9	
364.8		226	503	0	1541	3466	0	1884	3921	-1	2306	1996	
378.1		275	550	0	1630	3713	0	1955	4265	0	2440	2100	
395.3		339	585	0	1785	4004	0	2048	4828	-2	2591	2252	
405.7		425	585	0	1890	4408	0	2137	5487	0	2774	2384	
418.1		454	609	0	1969	4682	0	2201	5898	-2	2924	2453	
431.7		531	649	0	2154	5289	0	2408	6567	-2	4091	2721	
445.1		596	686	0	2328	5888	0	2612	7095	-3	6130	2962	
458.2		853	704	0	Failed	7128	0	2865	8395	-6	7945	3437	
470.7		1081	N.A.	0		8340	0	Failed	9881	-7	10468	6119	
479.3		1127	N.A.	0		9832	0		11309	-8	11296	11345	

189

Table E.5 Record of Concrete Strain Gauges of M2

LOAD	STRAIN (um/m)						REMARK
kN	C1	C2	C3	C4	C5	C6	
0	0	0	0	0	0	0	
13.4	0	-13	-12	0	-4	0	
26.8	0	-24	-13	0	-4	-3	
40.3	0	-35	-13	0	-4	-8	
54.4	0	-38	-13	-1	-4	-14	
68.1	0	-38	-13	-7	-4	-20	
83.6	0	-38	-13	-15	-4	-27	
93.8	0	-38	-13	-23	-4	-30	
108.7	0	-38	-13	-31	-7	-38	
121.0	0	-38	-13	-22	-24	-44	
134.0	-6	-59	-13	-33	-55	-47	
147.0	-15	-82	-13	-36	-78	-55	
160.5	-28	-108	-13	-42	-108	-64	
175.1	-39	-127	-13	-49	-130	-70	
190.4	-53	-156	-14	-65	-158	-79	
200.2	-60	-172	-20	-71	-175	-84	
215.7	-90	-201	-22	-98	-216	-90	
222.9	-102	-215	-26	-108	-232	-95	
231.4	-350	-227	-27	80	-268	-104	
246.9	-696	-159	-28	74	-312	-175	
258.4	-710	-182	-29	65	-332	-183	
271.7	-763	-253	-31	12	-385	-202	
288.7	-797	-309	-33	0	-437	-215	
301.1	-810	-378	-69	0	-489	-227	
311.3	-818	-443	-85	0	-533	-242	
329.1	-837	-557	-113	0	-645	-268	
342.5	-835	-644	-133	0	-798	-285	
351.5	-838	-732	-137	0	-865	-289	
364.8	-966	-1031	-174	-4	-1067	-303	
378.1	-980	-1300	-188	-15	-1344	-310	
395.3	-1004	-1621	-275	-37	-1733	-326	
405.7	-1021	-1901	-315	-54	-2050	-335	
418.1	-1029	-2061	-320	-62	-2170	-338	
431.7	-590	-2670	254	-139	-2473	-354	
445.1	-599	-2995	179	-134	-2823	-360	
458.2	-617	-3718	32	-84	-3565	-363	
470.7	-341	-3700	209	-41	Failed	-354	
479.3	-339	Failed	224	0		-305	

Table E.6 Record of LVDT's Readings of M2

Load	DEFLECTION (mm)					REMARK
kN	LVDT-1	LVDT-2	LVDT-3	LVDT-4	LVDT-5	
0	0	0	0	0	0	
13.4	0.02	0.02	0.03	0.01	-0.09	
26.8	0.00	0.00	0.03	0.00	-0.18	
40.3	-0.01	-0.01	0.04	-0.02	-0.27	
54.4	-0.01	-0.01	0.04	-0.04	-0.36	
68.1	-0.04	-0.04	0.03	-0.09	-0.44	
83.6	-0.02	-0.03	0.03	-0.14	-0.53	
93.8	0.00	-0.01	0.07	-0.16	-0.58	
108.7	0.00	-0.02	0.06	-0.24	-0.68	
121.0	0.06	0.03	0.13	-0.26	-0.76	
134.0	0.24	0.18	0.26	-0.46	-0.99	
147.0	0.40	0.30	0.41	-0.56	-1.15	
160.5	0.62	0.39	0.61	-0.69	-1.33	
175.1	0.68	0.36	0.66	-0.84	-1.50	
190.4	0.87	0.52	0.82	-0.96	-1.70	
200.2	0.95	0.60	0.89	-1.08	-1.85	
215.7	1.21	0.66	1.11	-1.23	-2.11	
222.9	1.31	0.62	1.19	-1.33	-2.24	
231.4	1.81	0.74	1.54	-1.32	-2.33	
246.9	2.46	0.87	2.08	-1.61	-2.64	
258.4	2.56	1.01	2.16	-1.77	-2.81	
271.7	3.35	1.15	2.73	-2.13	-3.25	
288.7	3.74	1.28	3.03	-2.38	-3.54	
301.1	4.17	1.49	3.38	-2.58	-3.80	
311.3	4.48	1.70	3.60	-2.84	-4.07	
329.1	5.29	2.38	4.24	-3.29	-4.60	
342.5	6.23	3.13	4.97	-3.79	-5.10	
351.5	6.52	3.31	5.18	-4.05	-5.36	
364.8	7.55	4.45	5.97	-4.60	-5.92	
378.1	8.49	5.13	6.64	-5.21	-6.57	
395.3	9.77	6.07	7.57	-5.97	-7.36	
405.7	11.06	6.95	8.46	-6.66	-8.12	
418.1	11.74	7.40	8.91	-7.18	-8.66	
431.7	13.84	8.87	10.36	-8.38	-9.97	
445.1	15.52	10.01	11.50	-9.48	-11.10	
458.2	19.20	12.49	13.92	-11.73	-13.41	
470.7	24.90	16.33	17.34	-15.17	-17.09	
479.3	28.75	19.22	19.81	-17.92	-20.01	

Table E.7 Record of Steel Strain Gauges of M3

Load	STRAIN (um/m)							REMARK
kN	TS1	TS2	BS2	BS5	BS6	BS8	BS9	
0.0	0	0	0	0	0	0	0	
8.9	0	-5	0	1	0	14	0	
17.8	1	-24	-1	2	0	23	0	
26.8	2	-39	-2	4	0	32	-1	
35.6	2	-61	-3	5	0	38	-1	
44.6	3	-78	-3	6	-1	45	-2	
53.7	3	-81	-3	8	-1	55	-2	
62.4	4	-86	-3	9	-1	66	-3	
71.2	4	-95	-4	10	-1	78	-3	
80.1	5	-98	-4	10	-2	93	-4	
89.2	6	-105	-4	11	-2	105	-4	
98.0	7	-115	-5	14	-2	127	-5	
106.8	7	-121	-5	15	-2	136	-5	
115.7	8	-132	-5	18	-3	141	-6	
124.7	9	-143	-10	19	-3	150	-6	
133.8	9	-252	-20	20	-3	160	-7	
142.3	10	-292	-23	21	-4	298	-7	
151.2	12	-298	-28	21	-4	381	-8	
160.1	15	-300	-30	23	-5	382	-8	
169.1	17	-304	-35	24	-5	399	-10	
178.3	19	-310	-41	24	-5	410	-10	
186.9	22	-312	-46	25	-6	425	-11	
191.3	26	-318	-47	25	-7	459	-12	
195.8	26	-325	-47	26	-7	470	-12	
200.2	27	-326	-48	26	-7	486	-12	
205.2	28	-330	-49	28	-8	501	-14	
209.4	28	-334	-49	28	-8	524	-15	
214.6	29	-385	-50	28	-9	544	-17	

Table E.8 Record of Concrete Strain Gauges of M3

Load	STRAIN (um/m)						REMARK
kN	C1	C2	C3	C4	C5	C6	
0.0	0	0	0	0	0	0	
8.9	-4	-22	-2	-1	-24	-2	
17.8	-8	-49	-6	-4	-51	-5	
26.8	-11	-77	-18	-11	-78	-7	
35.6	-16	-108	-19	-13	-107	-8	
44.6	-19	-142	-22	-15	-137	-10	
53.7	-23	-181	-25	-17	-172	-12	
62.4	-26	-223	-28	-19	-209	-14	
71.2	-31	-281	-32	-20	-255	-16	
80.1	-35	-360	-33	-20	-310	-18	
89.2	-39	-445	-34	-21	-359	-20	
98.0	-42	-522	-40	-23	-417	-25	
106.8	-46	-589	-42	-24	-480	-26	
115.7	-47	-661	-43	-25	-562	-27	
124.7	-48	-718	-44	-26	-651	-28	
133.8	-49	-791	-46	-28	-669	-30	
142.3	-49	-861	-46	-29	-689	-32	
151.2	-50	-930	-47	-30	-703	-34	
160.1	-50	-1045	-47	-32	-712	-36	
169.1	-51	-1119	-48	-32	-729	-37	
178.3	-52	-1227	-49	-34	-740	-38	
186.9	-53	-1367	-49	-34	-759	-39	
191.3	-53	-1406	-50	-35	-785	-39	
195.8	-55	-1461	-50	-36	-812	-41	
200.2	-55	-1492	-51	-36	-827	-42	
205.2	-56	-1665	-52	-37	-835	-45	
209.4	-56	-1712	-53	-38	-840	-47	
214.6	-58	-1820	-54	-39	-924	-48	

Table E.9 Record of LVDT's Readings of M3

LOAD	DEFLECTION (mm)					REMARK
kN	LVDT-1	LVDT-2	LVDT-3	LVDT-4	LVDT-5	
0.0	0	0	0	0	0	
8.9	0.01	0.03	0.01	-0.01	-0.04	
17.8	0.06	0.08	0.02	-0.02	-0.08	
26.8	0.08	0.10	0.04	-0.03	-0.15	
35.6	0.12	0.16	0.05	-0.04	-0.19	
44.6	0.17	0.20	0.07	-0.38	-0.23	
53.7	0.25	0.28	0.10	-0.44	-0.28	
62.4	0.32	0.36	0.12	-0.55	-0.35	
71.2	0.43	0.47	0.17	-0.65	-0.44	
80.1	0.60	0.62	0.27	-0.78	-0.53	
89.2	0.79	0.77	0.38	-0.94	-0.67	CRACK
98.0	1.10	1.09	0.55	-1.13	-0.79	
106.8	1.29	1.24	0.67	-1.32	-0.93	
115.7	1.60	1.50	0.89	-1.57	-1.14	
124.7	1.82	1.68	1.01	-1.76	-1.32	
133.8	2.18	1.99	1.22	-2.01	-1.57	
142.3	2.57	2.30	1.50	-2.29	-1.81	
151.2	2.92	2.61	1.72	-2.54	-2.06	
160.1	3.60	3.19	2.18	-2.96	-2.48	
169.1	3.94	3.49	2.37	-3.20	-2.71	
178.3	4.47	3.95	2.73	-3.58	-3.10	
186.9	5.19	4.51	3.22	-4.06	-3.57	
191.3	5.35	4.63	3.33	-4.18	-3.71	
195.8	5.62	4.83	3.52	-4.38	-3.90	
200.2	5.73	4.91	3.57	-4.49	-4.02	
205.2	6.77	5.69	4.31	-5.22	-4.72	
209.4	6.97	5.84	4.47	-5.40	-4.90	
214.6	7.50	6.21	4.83	-5.84	-5.32	

Table E.10 Record of Steel Strain Gauges of M4

Load	STRAIN (um/m)								REMARK
kN	TS1	TS2	BS1	BS2	BS5	BS6	BS8	BS9	
0.0	0	0	0	0	-1	0	0	0	
5.0	0	0	0	1	0	0	1	0	
9.7	0	0	0	2	1	0	2	0	
15.2	0	-1	1	3	3	0	3	0	
19.8	1	-2	2	4	4	0	4	0	
25.3	1	-2	3	6	6	0	5	0	
34.4	1	-3	4	7	8	-1	8	0	
43.9	2	-4	4	7	11	-1	11	0	
52.2	2	-5	5	7	13	-1	13	0	
63.4	3	-6	6	8	16	-1	17	0	
72.2	4	-9	6	9	19	-1	21	0	
81.6	5	-9	7	9	22	-2	23	0	
90.8	6	-11	7	9	31	-2	31	0	
100.3	7	-13	8	9	34	-2	33	0	
109.9	7	-15	8	9	39	-3	36	0	
118.3	9	-19	9	10	51	-3	40	0	
127.6	9	-22	10	10	60	-3	46	-1	
136.4	9	-24	11	10	63	-3	51	-1	
145.1	10	-26	11	10	67	-3	57	-1	
156.5	11	-29	12	13	153	-3	115	-1	
167.7	12	-31	14	14	203	-4	164	-1	
177.6	13	-33	17	17	396	-4	540	-1	
190.5	14	-34	18	18	539	-4	686	-2	
203.8	18	-45	18	19	1035	-4	1028	-2	
215.1	19	-48	19	19	1319	-4	1275	-2	
224.7	21	-52	21	20	1465	-4	1419	-2	
233.2	22	-48	22	21	1621	-4	1570	-3	
248.5	25	-51	23	22	1906	-4	1845	-3	
257.3	27	-64	25	23	2100	-4	2088	-3	
261.9	27	-64	26	24	2195	-4	2183	-3	
265.6	29	-64	27	24	2233	-4	2212	-3	

Table E.11 Record of Concrete Strain Gauges of M4

Load	STRAIN (um/m)						REMARK
kN	C1	C2	C3	C4	C5	C6	
0.0	0	0	0	0	0	0	
5.0	-4	-15	-4	-4	-10	-2	
9.7	-6	-26	-6	-6	-21	-3	
15.2	-6	-43	-9	-4	-37	-6	
19.8	-8	-56	-10	-7	-50	-7	
25.3	-10	-75	-12	-8	-67	-8	
34.4	-14	-113	-16	-10	-101	-11	
43.9	-18	-178	-18	-14	-161	-14	
52.2	-21	-308	-20	-18	-290	-17	
63.4	-23	-491	-24	-25	-475	-18	
72.2	-26	-637	-27	-27	-645	-19	
81.6	-29	-727	-29	-30	-751	-21	
90.8	-41	-849	-35	-30	-859	-27	
100.3	-44	-923	-38	-31	-936	-29	
109.9	-48	-998	-39	-34	-1024	-33	
118.3	-57	-1075	-48	-47	-1176	-39	
127.6	-65	-1207	-50	-53	-1245	-46	
136.4	-70	-1277	-54	-56	-1302	-49	
145.1	-73	-1344	-55	-57	-1359	-52	
156.5	-78	-1483	-58	-60	-1473	-60	
167.7	-82	-1561	-62	-66	-1550	-63	
177.6	-89	-1737	-63	-73	-1630	-70	
190.5	-93	-1836	-65	-78	-1726	-68	
203.8	-95	-1951	-68	-81	-2184	-72	
215.1	-105	-2114	-70	-86	-2325	-78	
224.7	-110	-2233	-73	-89	-2420	-81	
233.2	-120	-2310	-76	-93	-2519	-83	
248.5	-125	-2474	-77	-99	-2683	-83	
257.3	-130	-2623	-80	-104	-3242	-86	
261.9	-136	-2722	-93	-111	-3338	-93	
265.6	-141	-2779	-95	-121	-3385	-93	

Table E.12 Record of LVDT's Readings of M4

Load	DEFLECTION (mm)					REMARK
kN	LVDT-1	LVDT-2	LVDT-3	LVDT-4	LVDT-5	
0.0	0.00	0.00	0.00	0.00	0.00	
5.0	-0.02	-0.04	0.01	-0.01	-0.01	
9.7	-0.03	-0.08	0.03	-0.02	-0.03	
15.2	-0.04	-0.15	0.06	-0.03	-0.05	
19.8	-0.04	-0.20	0.10	-0.04	-0.06	
25.3	-0.07	-0.22	0.15	-0.05	-0.09	
34.4	-0.08	-0.16	0.23	-0.08	-0.11	
43.9	-0.07	-0.04	0.34	-0.13	-0.16	
52.2	0.00	0.13	0.53	-0.23	-0.27	
63.4	0.09	0.38	0.81	-0.44	-0.48	
72.2	0.23	0.69	1.13	-0.70	-0.70	
81.6	0.33	0.93	1.39	-0.91	-0.92	
90.8	0.55	1.39	1.86	-1.21	-1.20	
100.3	0.63	1.59	2.06	-1.42	-1.37	
109.9	0.74	1.87	2.33	-1.67	-1.59	
118.3	0.95	2.28	2.77	-1.94	-1.83	
127.6	1.22	2.85	3.33	-2.32	-2.17	
136.4	1.29	3.02	3.49	-2.51	-2.31	
145.1	1.38	3.21	3.71	-2.72	-2.49	
156.5	1.73	3.85	4.36	-3.21	-2.92	
167.7	1.88	4.18	4.68	-3.54	-3.19	
177.6	2.36	5.05	5.56	-4.15	-3.75	
190.5	2.62	5.51	6.02	-4.57	-4.13	
203.8	3.28	6.48	6.96	-5.27	-4.81	
215.1	3.90	7.35	7.84	-5.92	-5.46	
224.7	4.40	7.92	8.43	-6.40	-5.90	
233.2	4.89	8.48	8.99	-6.86	-6.33	
248.5	5.69	9.44	9.93	-7.71	-7.12	
257.3	6.61	10.36	10.85	-8.49	-7.86	
261.9	7.16	11.04	11.56	-9.12	-8.42	
265.6	7.49	11.35	11.88	-9.43	-8.70	